ANALYSIS OF ANTI-RESONANT REFLECTING OPTICAL WAVEGUIDE GRATING USING THE METHOD OF LINES

by

MUHAMMAD NADEEM AKRAM

A Thesis Presented to the
DEANSHIP OF GRADUATE STUDIES

In Partial Fulfillment of the Requirements
for the Degree

MASTER OF SCIENCE

IN

ELECTRICAL ENGINEERING

KING FAHD UNIVERSITY
OF PETROLEUM AND MINERALS

Dhahran, Saudi Arabia

April 2000

KING FAHD UNIVERSITY OF PETROLEUM AND MINERALS

DHAHRAN 31261, SAUDI ARABIA

DEANSHIP OF GRADUATE STUDIES

This thesis, written by

MUHAMMAD NADEEM AKRAM

under the direction of his Thesis Advisor and approved by his Thesis Committee, has been presented to and accepted by the Dean of Graduate Studies, in partial fulfillment of the requirements for the degree of

MASTER OF SCIENCE IN ELECTRICAL ENGINEERING

Thesis Committee

Dr. H. A. AL – JAMID (Chairman)

Dr. MAHMOUD M. DAWOUD (Member)

Dr. HUSAIN M. MASOUDI (Member)

Department Chairman

Dean of Graduate Studies

Date

To

my parents,

my wife Dr. Sameera and,

our beloved son Usama.

Acknowledgements

I am thankful to King Fahd University of Petroleum and Minerals, Dhahran, Saudi Arabia for supporting my M.Sc studies and this research work.

I am thankful to my thesis advisor Dr. Hussain A. Al-Jamid for formulating and supervising my thesis research work. He has been very helpful and supportive during this research. His constant guidance and deep insight into the field of integrated optics made it very easy for me to understand the necessary mathematics and produce effective results. His management skills are no less than his technical skills from which I specially benefited. I am also grateful to him for providing me some of his own computer programs. At the later stages, he helped me a lot in writing my thesis. I am also thankful to my committee member Dr S. J. Al-Bader for giving thought provoking comments on the results. The efforts of other committee members Dr. Husain M. Masoudi and Dr. Mahmoud M. Dawoud are also appreciated.

I am thankful to Dr. Sameer A. Al-Baiyat, Chairman Electrical Engineering Department for establishing an excellent graduate research laboratory in our department.

I am also thankful to Dr R. Pregla and Dr. Stefen Helfert, Fern University, Hagen, Germany, for providing me results of their research paper for comparison and sending some literature.

Thanks are due to my friend, Mr. Zainul-Abideen Khurram for introducing me to LaTeX, Unix and Linux. His voluntary efforts to maintain the graduate laboratory are highly acknowledged and appreciated.

I am thankful to my parents for their love, guidance and support.

Finally, I am thankful to my wife for her love and patience during my Master's studies.

Contents

List of Tables

List of Figures

Nomenclature

English Symbols

$\mathbf{E}$	electric field vector, volts/meter
$\mathbf{H}$	magnetic field vector, amperes/meter
N	diagonal matrix of refractive-index squared at mesh grids
I	identity matrix
P	time-averaged power per unit length in the y-direction, watts/m
Q	matrix of the eigen-value equation
n	refractive index
k_o	free space wavenumber, radians/meter
h	mesh size, meter
d	thickness of a layer, meter
j	$\sqrt{-1}$
t	times, sec
$\mathbf{A} \cdot \mathbf{B}$	scalar (dot) product of vectors $\mathbf{A}$ and $\mathbf{B}$
$\mathbf{A} \times \mathbf{B}$	vector (cross) product of vectors $\mathbf{A}$ and $\mathbf{B}$

Greek Symbols

ψ	general field component of the **E** or **H** field
Ψ	general field component of the **E** or **H** sampled field, column vector
ϵ_o	free space permittivity, $4\pi \cdot 10^{-7}$ Vs/Am
ϵ_r	relative permittivity
μ_o	free space permeability, $8.8541 \cdot 10^{-12}$ As/Vm
μ_r	relative permeability
$\omega = 2\pi f$	angular frequency, rad/sec
α_m	mth modal field expansion coefficient
β	propagation constant. radians/meter
λ	wavelength, meter
∇	nabla operator, $\frac{\partial}{\partial x}\hat{a_x} + \frac{\partial}{\partial y}\hat{a_y} + \frac{\partial}{\partial z}\hat{a_z}$
∇^2	Laplace operator, $\frac{\partial^2}{\partial x^2} + \frac{\partial^2}{\partial y^2} + \frac{\partial^2}{\partial z^2}$

Abbreviations

TE	Transverse Electric Mode
TM	Transverse Magnetic Mode
MoL	Method of Lines
PML	Perfectly Matched Layer
ARROW	Anti-Resonant Reflecting Optical Waveguide
BPM	Beam Propagation Method
ABC	Absorbing Boundary Condition

n_{eff}	Effective Index of a Multilayer Structure
λ_B	Bragg Wavelength
Re	Real part of a complex number

Subscripts

A_x, A_y, A_z	x, y, z components of a vector $\mathbf{A}$
$\psi_0, \psi_{\pm 1}, \psi_{\pm 2}$	sample number of field ψ
$\psi_{0\pm}, \psi_{1\pm}, \psi_{2\pm}$	field immediately to the left or to the right of a sample point

Superscript

ψ'	first derivative of ψ
ψ''	second derivative of ψ
ψ'''	third derivative of ψ
ψ''''	fourth derivative of ψ
A^*	complex conjugate of A

THESIS ABSTRACT

Name: MUHAMMAD NADEEM AKRAM

Title: ANALYSIS OF ANTI-RESONANT REFLECTING OPTICAL WAVEGUIDE GRATING USING THE METHOD OF LINES

Degree: MASTER OF SCIENCE

Major Field: ELECTRICAL ENGINEERING

Date of Degree: APRIL 2000

This research work is related to the modeling of integrated optical waveguides, waveguide discontinuities and gratings using the Method of Lines (MoL). The basic three-point central-difference approximation of the $\partial^2/\partial x^2$ operator used in the MoL is extended to five-point and seven-point approximations with appropriate interface conditions for the E and H fields. This gives us improved numerical accuracy and reduced matrix size. It is applied to find the modal field and effective indices of the TE and TM Modes in different multi-layer optical waveguides. Single and multiple waveguide discontinuity problems are solved using the MoL. The Perfectly Matched Layer (PML) absorber is used to absorb the radiated fields from discontinuities. The MoL is applied to periodic waveguide gratings and their reflection and transmission spectra are calculated. A fast and stable Cascading and Doubling Algorithm is used to model long gratings having thousands of periods. The MoL is applied to model a multi-layer ARROW structure. Periodic corrugations are introduced on the top surface of ARROW for possible optical filtering applications. The reflection and transmission spectra of the resulting ARROW Grating are calculated for different amount of loss in the ARROW with different number of grating periods and different groove depths.

Keywords: Optical Waveguides, Waveguide Discontinuities, Waveguide Gratings, Method of Lines (MoL), Higher-Order Approximations, Perfectly Matched Layer (PML), ARROW Waveguide, ARROW Grating.

Master of Science Degree

King Fahd University of Petroleum and Minerals, Dhahran.
April 2000

Chapter 1

Introduction

1.1 Integrated Optics

An Optical Integrated Circuit (OIC) is a thin-film type of optical circuit designed to perform a certain function. Integrated optics is the name given to a new generation of opto-electronic systems in which the familiar wires and cables are replaced by light guiding optical fibers, and conventional integrated circuits are replaced by optical integrated circuits. OIC research started when S.E. Miller of Bell Labs proposed the concept of integrated optics in 1969. In an OIC, the signal is carried by means of beams of light rather than by electric current, and the various circuit elements are interconnected on the substrate wafer by optical waveguides. Some advantages of integrated optic systems are reduced weight, increased bandwidth or multiplexing capability, resistance to electro-magnetic interference and low loss signal transmission. When the basic components : source, waveguide and detector are

all integrated on a single substrate, the device is called a monolithic OIC. Compound semiconductors such as Gallium Arsenide ($GaAs$) and Indium Phosphide (InP) are the candidate substrates for this type of IC. When the components are made of different materials, the device is called hybrid OIC. For example, the source and detector are made of compound semiconductors such as Silicon (Si) and the waveguide is made of dielectric materials such as Lithium Niobate ($LiNbO_3$) or Silicon Oxide (SiO_2).

1.2 Optical Waveguides

An optical waveguide is an arrangement or a device which can confine electromagnetic energy and transport it from one region of space to another region without any considerable power loss. A famous example of an optical waveguide is the optical fiber which is a cylindrical waveguide. Usually, the total-internal-reflection (TIR) phenomenon is utilized to design such an arrangement. A dielectric slab waveguide has a middle layer of high refractive index surrounded by layers of low refractive indices on both sides . Thus, electro-magnetic energy can be trapped inside the high index layer by the TIR phenomenon on both sides and can be transported over a long distance. These waveguides could also have a multi-layer structure with more than three layers including metallic layers. The refractive index profile may be constant or continuously varying in each layer.

1.3 Waveguide Gratings

Periodic structures (i.e. gratings) fabricated in optical waveguide structures are one of the most important elements for OIC construction. They can be used as various passive components (e.g. couplers, deflectors, reflectors, wavelength filters, and mode converters), and they have many applications to functional devices for optical wave control. The operation of devices based on gratings depends on electromagnetic wave coupling through phase matching of different propagating modes by the grating region. Figure 1.1 shows a waveguide grating structure, with grating period T and height h. This structure is typically composed of hundreds or thousands of periods. Each discontinuity or period causes a small reflection of the field and the total reflected field is the phasor sum of individual reflections. The grating parameters T, h and total number of grating periods affect the power reflection and transmission spectra of the structure.

1.4 ARROW Waveguide

Anti-Resonant Reflecting Optical Waveguides have received much attention due to their attractive features such as low transmission loss, high polarization selectivity, compatibility with mono-mode optical fibers [5] due to the large core size and small refractive index mismatch. They can be easily integrated monolithically with electronics components as they use SiO_2/Si material system [6]. This makes it a

favorable candidate for designing complete integrated optics circuits having all the necessary components, that is: source, waveguide and detector on a single wafer of Silicon. These devices are used in optical communication networks, wavelength selective filters, directional coupler, power splitter, modulator, semiconductor laser sources, detectors and optical sensors.

Unlike conventional waveguides that depend on total internal reflection (TIR) phenomenon for guidance of the optical field in a region of high refractive index surrounded by regions of lower refractive index, the ARROW structure partially depends on anti-resonant reflection [7] for guidance in a medium of low refractive index surrounded by a medium of high refractive index. Since TIR at the core-cladding interface may not be realized in this situation, the ARROW structure is essentially a leaky waveguide [8] and thus ARROW modes have a complex propagation constant. The radiation losses of the leaky waves are reduced by the high reflectivity of an anti-resonant cladding layer.

A typical ARROW waveguide is shown in the figure 1.2. The ARROW structure is characterized by the presence of a high index layer n_2 which provides the high reflectivity required to achieve low loss operation of the waveguide. It is also noted that TE modes of the ARROW waveguide are generally low loss while the TM modes are of high loss [4, 9], since TM reflections are always lower by the same phenomenon which gives rise to the Brewster angle. This device also behaves as a TE pass polarizer.

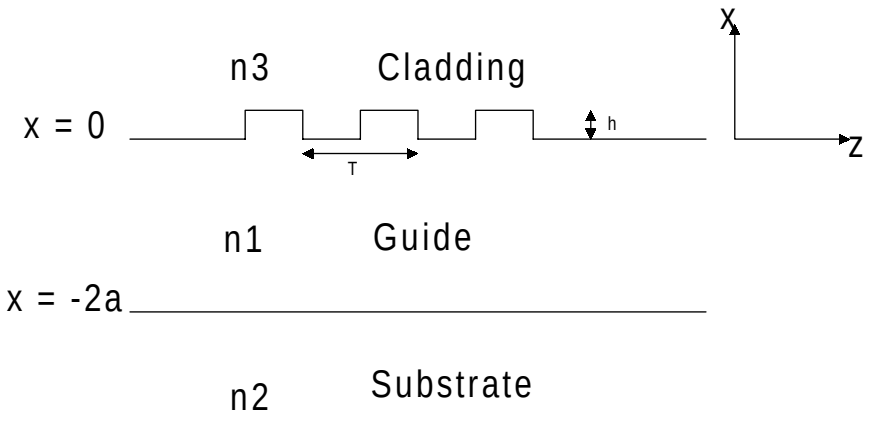

Figure 1.1: A Waveguide Grating Structure

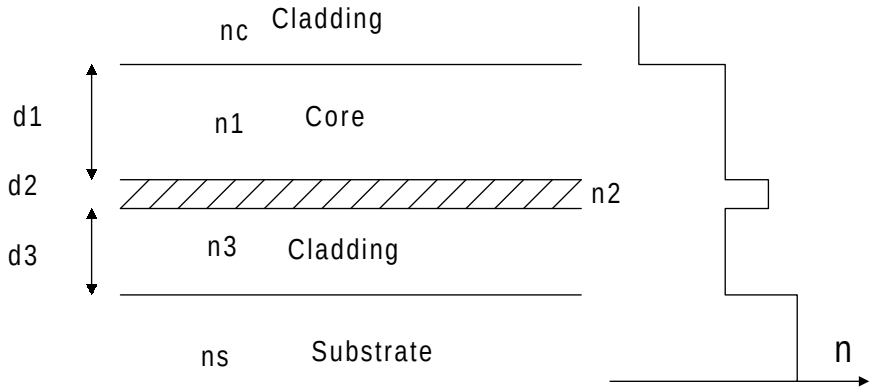

Figure 1.2: Refractive Index Profile in an ARROW Waveguide

1.5 Method of Lines and other Numerical Methods

Optical waveguide problems that can be analytically solved are limited to simple structures and devices. For complicated devices, either analytical solutions do not exist in closed form or even if they exist, they are difficult to solve. Several numerical methods have been developed to model longitudinally-dependent effects in these waveguide structures. Among these methods are the Beam Propagation Method (BPM) [10, 11], Finite Difference Time Domain (FDTD) method [12], Collocation Method [13], Mode Matching Method (MMM) [3] and Method of Lines (MoL) [14, 15]. A good review of these and some other numerical methods is given in [16, 17].

The basic BPM can't be used to model waveguide discontinuities due to its inability to account for backwards reflected waves at a discontinuity. It is an approximate method requiring the wave to be paraxial [3]. The FFT-BPM version is also known to be inefficient in problems having large index discontinuities. Hence, it is good only for low contrast and gradual bends in optical waveguides.

The FDTD method can be used to model discontinuity problems but it requires the whole structure to be discretized and stored in computer memory. Hence to model long gratings, it will take excessively large memory. Also this is a time-domain method and the algorithm should be run for considerable amount of time to get steady state response and some post-processing is necessary. Anyway this method is gaining popularity due to its ease of understanding and implementation.

The Collocation Method is based on Helmholtz equation and does not require the Fresnel approximation for its implementation [18]. In this method, the field is expanded into a set of suitable orthogonal basis functions $\phi_n(x)$ in the transverse direction. The choice of basis functions depend on the problem geometry. Since these basis are not the exact ones for the problem, we need a larger number of basis to achieve accurate results.

The Mode Matching Method (MMM) or Eigenmode Propagation Method (EPM) employs eigen-mode expansion of the field, in which the discrete guided modes, the continuous radiation modes and continuous evanescent modes are taken as basis [19]. The choice of these basis functions is problem dependent. The reflection and transmission coefficients are solved through a mode matching procedure.

The Method of Lines (MoL) is a semi-analytical technique used to solve partial differential equations (PDE). For an n-independent variable PDE, only (n-1) variables are discretized to obtain a system of ordinary differential equations (ODE) [20] in the remaining independent variable. This results in a higher numerical accuracy due to less discretized variables, less computational time due to the analyticity in the remaining independent variable and smaller memory requirements as we do not need to discretize in the analytical direction. Instead of approximating the field by a series expansion of basis functions (as done in Mode Matching Methods), the second-derivative operator is approximated by a finite-difference scheme. The resulting matrix ODE is solved to find the eigenmodes of the structure. This method can account for backward reflected field due to longitudinally inhomogenous structures,

which permits the analysis of planar waveguides having longitudinal discontinuities, steps or periodic structures. It has been used to analyze a single discontinuity [21, 22] and multiple discontinuities in optical waveguides [23, 24, 25, 1].

1.6 Statement of the Problem

The Method of Lines is chosen for this analysis because it is a rigorous method and it can model high-contrast waveguides including metals. It can account for the reflected field at sharp waveguide discontinuities, junctions and bends. The basic three-point central-difference approximation of $\frac{\partial^2}{\partial x^2}$ operator used in the Method of Lines gives relatively poor estimate of the modal fields and effective indices of a multi-layer waveguide structure. Thus to get an accurate value of these quantities, we need to have many discretization lines with a small discretization distance. This gives us large matrices, thus increasing calculation time and memory requirements. Our first objective is to use higher-order approximations of $\frac{\partial^2}{\partial x^2}$ operator with appropriate interface conditions to improve the accuracy while using fewer discretization lines to sample the problem space. This helps to reduce the computational time in stationary as well as multiple discontinuity problems. Another improvement is to use a non-uniform meshing scheme to reduce the number of sampling points. When radiative fields are involved in the problem, we have to terminate the problem geometry with appropriate absorbing boundary conditions to model an infinite space. In this thesis, Perfectly-Matched-Layer (PML) is used as an absorbing layer. To

model a grating having many periods, the basic method is to match the tangential fields at each discontinuity and express unknown field coefficients in each region in terms of the known incident field. This layer-by-layer procedure is very slow and the memory requirement is also large as we need to store the intermediate results. Our objective is to develop a fast and memory efficient algorithm to model long periodic gratings taking advantage of the periodic nature of the grating. MoL will be used to find modal fields and effective indices of the ARROW structure. The ARROW is a relatively new device and there is much interest in its applications in integrated optics. The ARROW Grating is a brand new structure proposed in this thesis and our focus is on analyzing its performance for different configurations. The spectral response of this device will be calculated for different amount of loss in ARROW, different number of grating periods and different groove depths. A logical conclusion will be drawn about the performance of the device. In this work, both TE and TM modes will be analyzed and a general purpose software will be developed to model multi-layer waveguides with gratings.

1.7 Thesis Organization

This thesis is organized into eight chapters. In chapter 1, a basic overview of Integrated Optics, Method of Lines, Optical Waveguides, Waveguide Gratings, ARROW Waveguide and ARROW Gratings is given. In chapter 2, the eigen-value equation of a basic three-layer dielectric slab waveguide is derived for the TE and TM modes.

In chapter 3, the numerical Method of Lines is explained and applied to solve the scalar Helmholtz equation. The necessary interface conditions are derived to model multi-layer structures. The basic three-point central-difference approximation of $\frac{\partial^2}{\partial x^2}$ operator is extended to five-point and seven-point approximations with appropriate interface conditions. This gives us improved accuracy in determining effective-indices and modal field profile of a waveguide. We may reduce the total number of discretization lines in the problem space, thus reducing the matrix size and overall computational time to model multiple waveguide discontinuities. In chapter 4, the Method of Lines is used to model single and multiple waveguide discontinuities or junctions. The Perfectly-Matched-Layer (PML) absorber is used to absorb radiated fields and simulate an infinite space at the mesh termination. In chapter 5, a Cascading and Doubling Algorithm is described to model long gratings having thousands of periods. This algorithm finds the equivalent reflection and transmission matrices of two discontinuities joined together from their individual reflection and transmission matrices. This procedure is repeated to find the total reflection and transmission matrices of a grating. Thus we can model 2^n periods in n calculational steps. This algorithm gives us improved speed and smaller memory requirement as compared to other methods. In chapter 6, the Anti-Resonant Reflecting Optical Waveguide (ARROW) is described and the Method of Lines is used to model this multi-layer structure. The effective indices and modal fields for the ARROW structure are calculated and compared with analytical results. In chapter 7, periodic corrugations are introduced on the top surface of ARROW and this device is named ARROW

Grating. This structure is modeled using the MoL with the Cascading and Doubling Algorithm. The modal spectral reflectivity and transmissivity of the ARROW Grating is calculated for different number of grating periods and grating depths. The amount of radiation or leakage loss of the ARROW grating is varied and its effect on the spectral response is determined. In the last chapter, the work done is summarized with conclusions and some possible future extensions are proposed.

Chapter 2

Three-Layer Dielectric Slab Waveguide

2.1 Basic Formulation

In this chapter, we will be concerned with finding the guided modes of the basic three-layer dielectric slab waveguide directly from Maxwell's equations. We consider the lossless asymmetric dielectric slab shown in figure 2.1. We shall assume that $n_1 > n_2 \geq n_3$ so that total internal reflection (TIR) can occur at each interface. Writing Maxwell's equations in terms of the refractive index n_i $(i = 1, 2, 3)$ of the three layers and assuming that the material of each layer is non-magnetic and isotropic (these assumptions are valid throughout this thesis), that is $\mu = \mu_o$ and ϵ is a scalar, we have [26]:

$$\nabla \times \mathbf{H} = n_i^2 \epsilon_o \frac{\partial \mathbf{E}}{\partial t} \tag{2.1}$$

$$\nabla \times \mathbf{E} = -\mu_o \frac{\partial \mathbf{H}}{\partial t} \tag{2.2}$$

$$\nabla \cdot \mathbf{E} = 0 \tag{2.3}$$

$$\nabla \cdot \mathbf{H} = 0 \tag{2.4}$$

[1] If we apply the curl operator to equation 2.2, we get:

$$\nabla \times \nabla \times \mathbf{E} = -\mu_o \nabla \times \frac{\partial \mathbf{H}}{\partial t} \tag{2.5}$$

$$= -\mu_o n_i^2 \epsilon_o \frac{\partial^2 \mathbf{E}}{\partial t^2} \tag{2.6}$$

where equation 2.1 has been used to eliminate $\mathbf{H}$. To simplify further, we use the identity

$$\nabla \times \nabla \times \mathbf{A} = \nabla(\nabla.\mathbf{A}) - \nabla^2 \mathbf{A} \tag{2.7}$$

where $\mathbf{A}$ is any vector. We obtain:

$$\nabla^2 \mathbf{E} = \mu_o \epsilon_o n_i^2 \frac{\partial^2 \mathbf{E}}{\partial t^2} \tag{2.8}$$

Writing the last equation in phasor notation (assuming a time-harmonic field of the form $e^{-j\omega t}$) we obtain [26]:

$$\nabla^2 \mathbf{E} + k_o^2 n_i^2 \mathbf{E} = 0 \tag{2.9}$$

[1] Here $\mathbf{E}$ and $\mathbf{H}$ are vectorial fields, that is $\mathbf{E} \equiv (E_x, E_y, E_z)$ and $\mathbf{H} \equiv (H_x, H_y, H_z)$. Each scalar component is a function of the space co-ordinates x, y, z and the time co-ordinate t, that is $E_x(x, y, z, t)$, $E_y(x, y, z, t)$, $E_z(x, y, z, t)$ and $H_x(x, y, z, t)$, $H_y(x, y, z, t)$, $H_z(x, y, z, t)$.

which is the familiar vector wave equation for a uniform dielectric with refractive index n_i. Here k_o is the free-space wavenumber given by $k_o = \omega\sqrt{\mu_o \epsilon_o}$. The electric field vector $\mathbf{E}$ in equation 2.9 is now complex having both magnitude and phase. It is now a function of space co-ordinates x, y, z and angular frequency ω since the time dependence is taken out by the phasor transformation. We may simplify this result by assuming that the structure is uniform in the y-direction (see figure 2.2) and extends to infinity, so that the field distribution of the modes is uniform in the y-direction. Thus $\frac{\partial}{\partial y} = 0$. If we further assume a z-dependence of the form $e^{j\beta z}$, with β as the longitudinal propagation constant, equation 2.9 may be written for the three regions of the guide as follows [26]:

$$\frac{d^2\mathbf{E}_1}{dx^2} + q^2\mathbf{E}_1 = 0 \quad , \quad -2a \leq x \leq 0 \tag{2.10}$$

$$\frac{d^2\mathbf{E}_2}{dx^2} - p^2\mathbf{E}_2 = 0 \quad , \quad -2a \geq x \tag{2.11}$$

$$\frac{d^2\mathbf{E}_3}{dx^2} - r^2\mathbf{E}_3 = 0 \quad , \quad x \geq 0 \tag{2.12}$$

where $q^2 = n_1^2k^2 - \beta^2$, $p^2 = \beta^2 - n_2^2k^2$ and $r^2 = \beta^2 - n_3^2k^2$. Similar forms of the wave equation in the three regions may easily be derived for the magnetic field $\mathbf{H}$ from Maxwell's equations. These are second-order ordinary homogenous differential equations with constant coefficients which can be easily solved. The solution is either sinosoidal or exponential depending upon the sign of the coefficients q^2, p^2 and r^2.

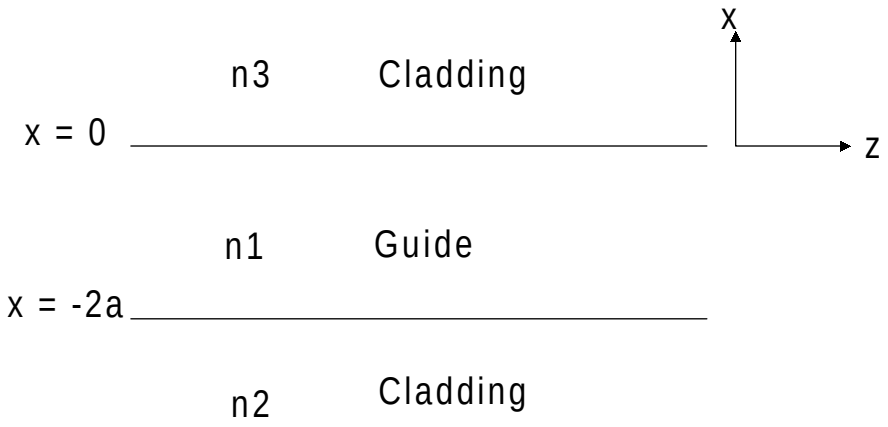

Figure 2.1: Three Layer Slab Waveguide, 2-D View

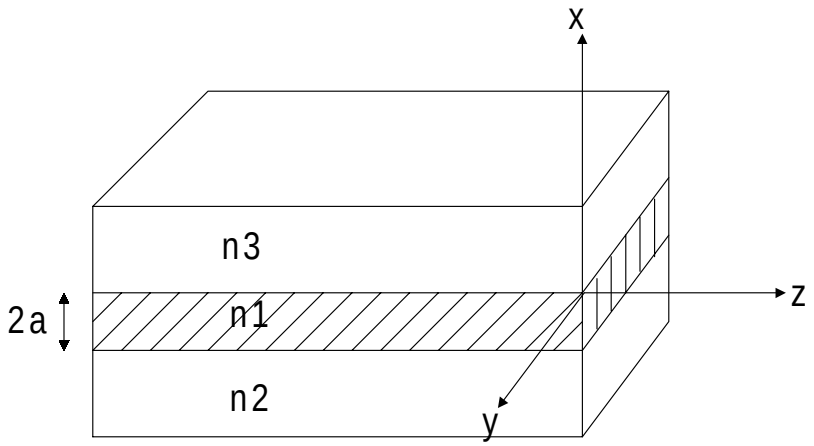

Figure 2.2: Three Layer Slab Waveguide, 3-D View

2.2 Transverse Electric (TE) Guided Modes

Our assumption $\frac{\partial}{\partial y} = 0$ implies that the only non-zero field components for TE modes are E_y, H_x and H_z [26]. From Maxwell's equations we get:

$$H_x = -\frac{\beta}{\omega\mu_o} E_y \tag{2.13}$$

$$H_z = -\frac{j}{\omega\mu_o} \frac{\partial E_y}{\partial x} \tag{2.14}$$

Equations 2.13 and 2.14 express two nonzero magnetic field components in terms of the single nonzero electric field component E_y, which itself is given by the solution of the wave equations in each region. The other requirements to be satisfied by these field components is that the tangential components E_y and H_z should be continuous at the $n_1 - n_2$ and $n_1 - n_3$ interfaces of the dielectric waveguide. Let us choose the origin of the x-axis at the $n_1 - n_3$ interface, so that the $n_1 - n_2$ interface is at $x = -2a$ (see figure 2.1). For guided modes, we require that the power to be confined largely to the central region of the guide and no power escapes from the structure. The form of equations 2.12, 2.10 and 2.11 then implies that this requirement will be satisfied for an oscillatory solution in region 1 ($q^2 \geq 0$) with evanescent tails in the cladding region 2 and 3 ($r^2, p^2 \geq 0$) (see figure 2.3) . Assuming $n_1 > n_2 \geq n_3$ and combining these conditions on β, we can derive the possible range of β, that is $n_1 k \geq \beta \geq n_2 k \geq n_3 k$. Thus, the solution of E_y in the three regions for the guided modes is [26]:

$$E_y = \begin{cases} Ae^{-rx} & , x \geq 0 \\ A\cos(qx) + B\sin(qx) & , 0 \geq x \geq -2a \\ \left(A\cos(2aq) - B\sin(2aq)\right)e^{p(x+2a)} & , x \leq -2a \end{cases} \tag{2.15}$$

The form of equation has been chosen so that the requirement of the continuity of E_y at $x = 0$ and $x = -2a$ is automatically satisfied. To complete the boundary requirements, it remains to ensure continuity of H_z. This component is given by:

$$H_z = \frac{-j}{\omega\mu_o} \begin{cases} -rAe^{-rx} & , x \geq 0 \\ q\left(-A\sin(qx) + B\cos(qx)\right) & , 0 \geq x \geq -2a \\ p\left(A\cos(2aq) - B\sin(2aq)\right)e^{p(x+2a)} & , x \leq -2a \end{cases} \tag{2.16}$$

The continuity condition yields two equations. One at $x = 0$ and the second at $x = -2a$, that is:

$$-rA = qB \tag{2.17}$$

and

$$q\left(A\sin(2aq) + B\cos(2aq)\right) = p\left(A\cos(2aq) - B\sin(2aq)\right) \tag{2.18}$$

Eliminating the ratio A/B from these equations yields [26]:

$$\tan(2aq) = \frac{q(p+r)}{q^2 - pr} \tag{2.19}$$

This is the eigenvalue equation for the TE modes of asymmetric slab waveguide. It can be shown that only certain discrete values of β can satisfy it, so this guide will

only *support* a discrete set of guided modes with no power loss factor. This is an implicit relationship which involves the wavelength, refractive indices of the layers and core thickness as known quantities, and the propagation constant β as the only unknown quantity. Thus β can be found from this equation using numerical or graphical methods. Then using this value of β, the previous equations are used to obtain the modal field in each layer. It is easiest to do this for a symmetric guide, which can only support modes with symmetric or anti-symmetric field patterns. In this case it can be easily shown that the eigen-value equation 2.19 reduces to:

$$\tan(2aq) = \frac{2pq}{q^2 - p^2} \tag{2.20}$$

An example of the TE modes for a three-layer slab waveguide is given in figure 2.3.

2.3 Transverse Magnetic (TM) Guided Modes

For this polarization, the only non-zero field components are H_y, E_x and E_z [26]. Also from Maxwell's equations, we have:

$$E_x = -\frac{\beta}{\omega n_i^2 \epsilon_o} H_y \tag{2.21}$$

$$E_z = -\frac{j}{\omega n_i^2 \epsilon_o} \frac{\partial H_y}{\partial x} \tag{2.22}$$

These equations relate the electric field components E_x and E_z to the only nonzero magnetic field component H_y which itself is a solution of wave equations in the three regions. The solution of the H_y may be written as [26]:

$$H_y = \begin{cases} Ce^{-rx} & , x \geq 0 \\ C\cos(qx) + D\sin(qx) & , 0 \geq x \geq -2a \\ \left(C\cos(2aq) - D\sin(2aq)\right)e^{p(x+2a)} & , x \leq -2a \end{cases} \tag{2.23}$$

and E_z is given by:

$$E_z = \frac{j}{\omega\epsilon_o} \begin{cases} -\frac{rC}{n_3^2}e^{-rx} & , x \geq 0 \\ \frac{q}{n_1^2}\left(-C\sin(qx) + D\cos(qx)\right) & , 0 \geq x \geq -2a \\ \frac{p}{n_2^2}\left(C\cos(2aq) - D\sin(2aq)\right)e^{p(x+2a)} & , x \leq -2a \end{cases} \tag{2.24}$$

continuity of E_z at $x = 0$ and $x = -2a$ gives:

$$-\frac{rC}{n_3^2} = \frac{qD}{n_1^2} \tag{2.25}$$

and

$$\frac{q}{n_1^2}\left(C\sin(2aq) + D\cos(2aq)\right) = \frac{p}{n_2^2}\left(C\cos(2aq) - D\sin(2aq)\right) \tag{2.26}$$

Eliminating the ratio C/D from these equation results in [26]:

$$\tan(2aq) = \frac{qn_1^2\left(n_3^2p + n_2^2r\right)}{n_2^3n_3^2q^2 - n_1^4pr} \tag{2.27}$$

which is the eigenvalue equation for the TM modes of a slab waveguide. An example of the TM modes is given in figure 2.4. As evident from the figure, the H_y field is continuous across a layer interface but its first derivative is discontinuous causing a kink in the mode profile.

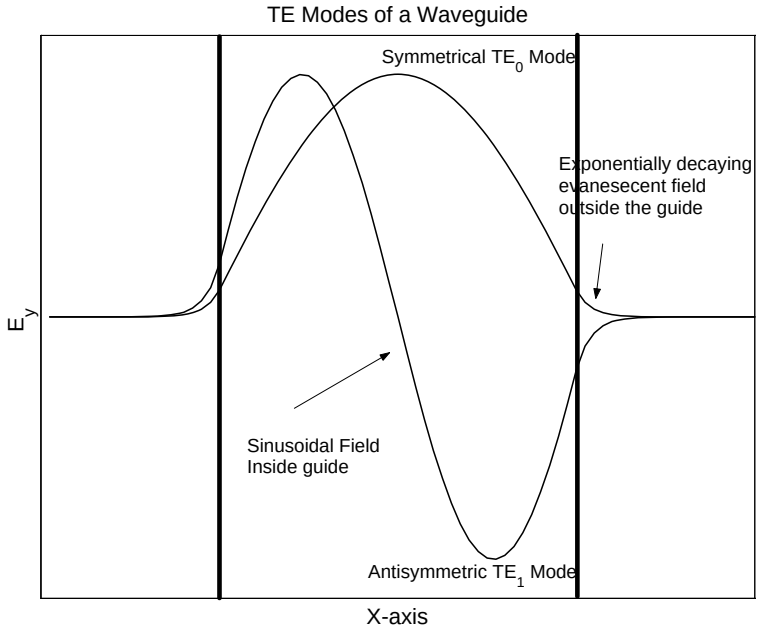

Figure 2.3: *TE* Mode Patterns of a Slab Waveguide

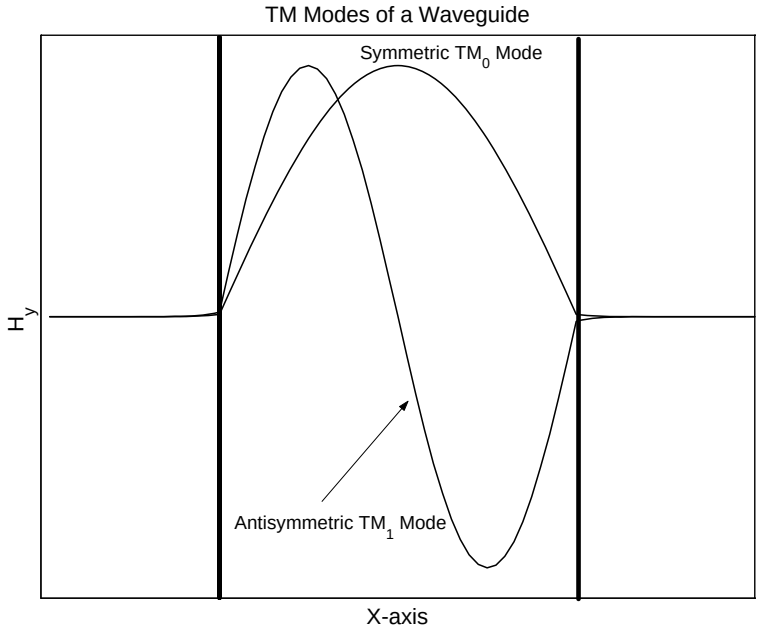

Figure 2.4: *TM* Mode Patterns of a Slab Waveguide

2.4 Other Types of Modes

The modal solutions found so far are, of course, descriptive of light confined inside the guide. However, further solutions should exist to account for light propagation *outside* the guide. These are known as radiation modes and they correspond to leakage of energy from the guide into the open space [27]. We solved equations 2.12, 2.10 and 2.11 to find the TE modes of a slab waveguide. This is, of course, a general second-order differential equation, which can be written in the form:

$$\frac{d^2E_i}{dx^2} - C_i^2 E_i = 0 \tag{2.28}$$

In our previous analysis the form of the solution was exponential or sinosoidal, depending upon the *sign* of the term $C_i^2 = n_i^2 k_o^2 - \beta^2$. if we consider all possible values of β, it turns out that a wider range of solutions can be found. If we again take $n_1 > n_2 \geq n_3$, the complete set can be represented as a diagram in β-space [27] as shown in figure 2.5. The essential features of the diagram are [27]:

1. For $\beta > k_o n_1$, the solutions are exponential in all three layers. Since this implies infinite field amplitudes at large distances from the guide, these are unrealistic solutions.

2. For $k_o n_1 > \beta > k_o n_2$, there are a discrete number of bound or *guided modes*, which are the solutions already found. They vary sinosoidally inside the guide core and decay exponentially outside the guide.

3. For $k_o n_2 > \beta > k_o n_3$, the solutions vary exponentially in the top layer and

sinosoidally in both the guide and bottom layer. Since these fully penetrate the bottom layer, they are called *substrate modes*. Any value of β is allowed between the two limits given above , so the set forms a continuum.

4. For $k_o n_3 > \beta$, solutions vary sinosoidally in all three layers. These particular field patterns are known as *radiation modes*. Once again any value of β is allowed in the range above, so the set forms another continuum.

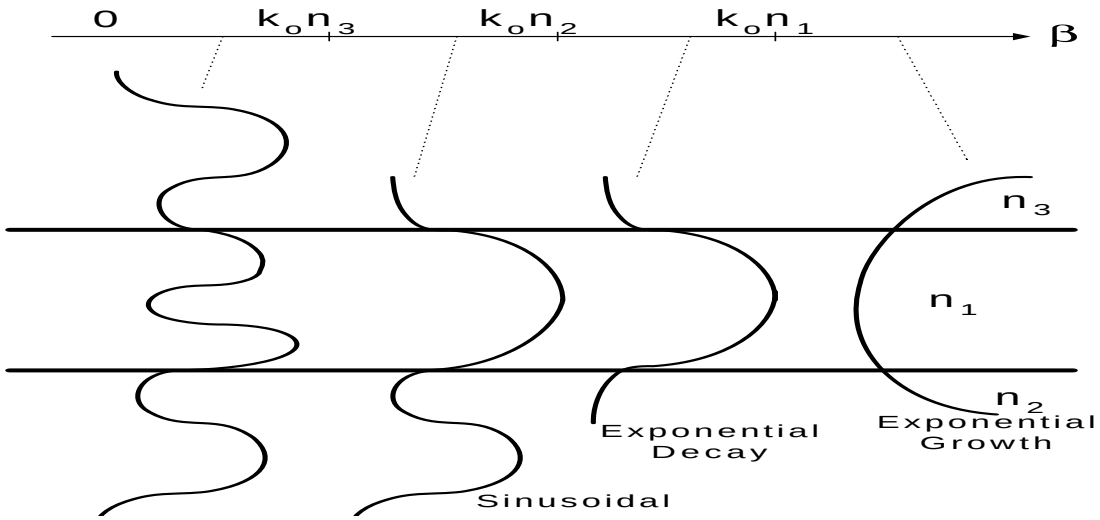

Figure 2.5: Modal Solutions represented in the β-Space

2.5 Modal Power in an Arbitrary Field

Every lossless optical waveguide supports a finite number of field patterns or *modes* which can propagate in the waveguide without attenuation. So any general field $\psi(x, z)$ can be represented as a linear summation of a complete finite set of or-

thonormal modes, that is [20]:

$$\begin{aligned}\psi(x,z) &= \alpha_0 f_0(x)e^{j\beta_0 z} + \alpha_1 f_1(x)e^{j\beta_1 z} + \alpha_2 f_2(x)e^{j\beta_2 z} + \cdots + \alpha_m f_m(x)e^{j\beta_m z} + \cdots \\ &\quad + \int_v \alpha_v f_v(x)e^{j\beta_v z}dv \end{aligned} \tag{2.29}$$

where α_m = mth-mode excitation coefficient, β_m = mth-mode propagation coefficient and $\int_v \alpha_v f_v(x)e^{j\beta_v z}dv$ represents an integration over the continuum of all radiation modes. The integer m represents the highest possible order of the guided modes. The modal transverse profiles $\{f_m(x)\}$ describe a set of orthonormal functions over the transverse coordinate. The modal coefficient α_m is given by [20]:

$$\alpha_m = \frac{\int_{-\infty}^{+\infty} \psi(x,0)f_m(x)dx}{\int_{-\infty}^{+\infty} f_m^*(x)f_m(x)dx} \tag{2.30}$$

The power per unit y-length flowing in the z direction per unit length of y direction is given by [27]:

$$P_z = \frac{1}{2}\int_{-\infty}^{+\infty} Re(\mathbf{E}\times\mathbf{H}^*)_z dx \tag{2.31}$$

Chapter 3

The Method of Lines (MoL) : Higher-Order Approximations

3.1 Introduction

Method of Lines is a semi-analytical technique used to solve a system of partial differential equations (PDE). For an n-independent variable PDE system, only (n-1) variables are discretized to obtain a system of ordinary differential equations (ODE) in the remaining independent variable [20, 28]. This results in a higher numerical accuracy due to reduced discretization error, less computational time as the solution is analytical in the remaining variable and smaller memory requirement as we do not need to discretize and store the analytical direction. This method can account for the backwards reflected field due to longitudinally inhomogenous structures, which permits the analysis of planar waveguides having longitudinal discontinuities, steps

or periodic structures. It has been used to analyze single discontinuity [21, 22] and multiple discontinuities in optical waveguides [14, 23, 24, 25, 29, 1]. It has also been applied to solve non-linear waveguide problems [30] as well as diffraction problem from waveguide ends [31]. This method has been used to model 3-D problems [32, 33] for both optical and microwave waveguides. The method in general has been applied in other branches of science as well.

3.2 Basic Algorithm

For the waveguide structure under investigation, the waveguide geometry is discretized in the transverse direction. Figure 3.1 shows a planar waveguide structure in which the interfaces of layers are parallel to the z-axis. Consequently, discretization is done in the x-direction. The structure is bounded by an electric wall where $E_y = 0$ or a magnetic wall where $H_y = 0$ as appropriate. Consider the two dimensional wave equation:

$$\frac{\partial^2 \psi(x,z)}{\partial x^2} + \frac{\partial^2 \psi(x,z)}{\partial z^2} + k_o^2 n^2 \psi(x,z) = 0 \tag{3.1}$$

Here both the field $\psi(x,z)$ and the refractive index $n(x)$ are discretized along the x-axis. The $\frac{\partial^2}{\partial x^2}$ term in equation 3.1 is replaced by a three-point central difference approximation of the form:

$$\frac{\partial^2 \psi_i}{\partial x^2} = \frac{\psi_{i+1} - 2\psi_i + \psi_{i-1}}{(\Delta x)^2} \tag{3.2}$$

So at the *ith* grid we get

$$\frac{\psi_{i+1}(z) - 2\psi_i(z) + \psi_{i-1}(z)}{(\Delta x)^2} + \frac{d^2\psi_i(z)}{dz^2} + k_o^2 n_i^2 \psi_i(z) = 0 \tag{3.3}$$

When this equation is applied at each of the M discrete points, we get M distinct equations, which can be put together in a single matrix equation of the form:

$$\frac{1}{(\Delta x)^2}\begin{bmatrix} -2 & 1 & & & & & \\ 1 & -2 & 1 & & & \mathcal{O} & \\ & 1 & -2 & 1 & & & \\ & & \ddots & \ddots & \ddots & & \\ & \mathcal{O} & & & 1 & -2 & 1 \\ & & & & & 1 & -2 \end{bmatrix}\begin{bmatrix} \psi_1(z) \\ \psi_2(z) \\ \psi_3(z) \\ \vdots \\ \vdots \\ \psi_M(z) \end{bmatrix} + \frac{d^2}{dz^2}\begin{bmatrix} \psi_1(z) \\ \psi_2(z) \\ \psi_3(z) \\ \vdots \\ \vdots \\ \psi_M(z) \end{bmatrix}$$

$$+k_o^2\begin{bmatrix} n_1^2 & & & & & \\ & n_2^2 & & & \mathcal{O} & \\ & & n_3^2 & & & \\ & & & \ddots & & \\ & \mathcal{O} & & & \ddots & \\ & & & & & n_M^2 \end{bmatrix}\begin{bmatrix} \psi_1(z) \\ \psi_2(z) \\ \psi_3(z) \\ \vdots \\ \vdots \\ \psi_M(z) \end{bmatrix} = \begin{bmatrix} 0 \\ 0 \\ 0 \\ \vdots \\ \vdots \\ 0 \end{bmatrix}$$

written in a compact notation, we get:

$$\frac{1}{(\Delta x)^2} C\Psi + \frac{d^2}{dz^2}\Psi + k_o^2 N\Psi = 0 \tag{3.4}$$

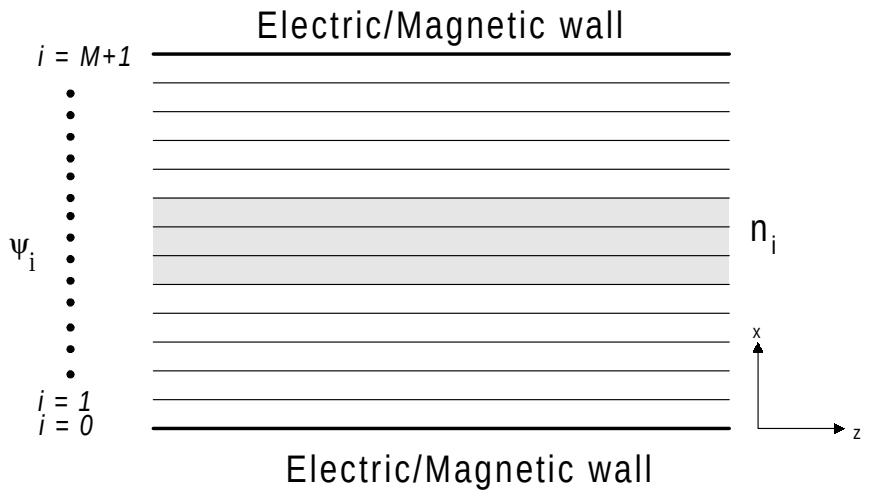

Figure 3.1: Mesh Discretization used in the MoL

where C is a tri-diagonal second-order central-difference matrix , N is a diagonal matrix whose elements are $n_1^2, n_2^2, ..., n_M^2$ and $\Psi = [\psi_1(z), \psi_2(z), ..., \psi_M(z)]^t$ is the discretized field vector. The above equation may then be written in the form:

$$\frac{d^2}{dz^2}\Psi + Q\Psi = 0 \tag{3.5}$$

where

$$Q = \frac{1}{(\Delta x)^2}C + k_o^2 N \tag{3.6}$$

The solution of this 2nd-order ordinary matrix differential equation is formally given by [14]:

$$\Psi = e^{j\sqrt{Q}z}A + e^{-j\sqrt{Q}z}B \tag{3.7}$$

where $e^{j\sqrt{Q}z}$ represents field propagation in the $+z$ direction and $e^{-j\sqrt{Q}z}$ represents field propagation in $-z$ direction. The matrices $e^{j\sqrt{Q}z}$ and $e^{-j\sqrt{Q}z}$ are calculated by

diagonalizing the matrix Q to find the eigenvalues and eigenvectors. The matrix Q may be written in the form:

$$Q = UVU^{-1} \tag{3.8}$$

where U is the eigenvector matrix and V is a diagonal matrix containing the eigenvalues of Q. The matrix exponent is then calculated using the following well known relation of linear algebra:

$$e^{j\sqrt{Q}z} = Ue^{j\sqrt{V}z}U^{-1} \tag{3.9}$$

3.3 Calculation of Power and Modal Coefficients in the MoL

For TM modes, the incident magnetic field is:

$$H_y = e^{+jS_0z}A_0 \tag{3.10}$$

where the $M \times 1$ column matrix A_0 represents the incident field at $z = 0$ and $M \times M$ matrix $S_0 = \sqrt{Q_0}$ and Q_0 is defined in the previous section. Using Maxwell's equations, x component of the incident electric field is given by:

$$E_x = \frac{j}{\omega\epsilon_o n_i^2}\frac{\partial H_y}{\partial z} \tag{3.11}$$

where n_i is the sampled refractive index at the ith discretization line. Substituting equation 3.10 into equation 3.11, we have:

$$E_x = \frac{j}{\omega\epsilon_o N}\frac{\partial}{\partial z}(e^{+jS_0z}A_0) \tag{3.12}$$

$$= -\frac{1}{\omega\epsilon_o N} S_0 e^{+jS_0 z} A_0 \tag{3.13}$$

and hence, the incident electric field component E_x at $z = 0$ is given by:

$$E_x|_{z=0} = -\frac{1}{\omega\epsilon_o N} S_0 A_0 \tag{3.14}$$

The average power flow in the z direction is given by:

$$P_z = \frac{1}{2} Re \int_{-\infty}^{\infty} E_x H_y^* dx \tag{3.15}$$

For discrete samples, integration is replaced by summation over the index of the array.

$$P_z = \frac{1}{2} Re \left[\sum_{m=1}^{M} E_{xm} H_{ym}^* \Delta x \right] \tag{3.16}$$

$$= \frac{1}{2\omega\epsilon_o} Re \left[N^{-1} S_0 A_0 A_0^* \right] \Delta x \tag{3.17}$$

[1]where N matrix is defined in the section 3.2. Using the modal coefficient formula 2.30, we can calculate the modal expansion coefficient α_m, that is:

$$\alpha_m = \frac{A^t N^{-1} F_m}{F_m^t N^{-1} F_m} \tag{3.18}$$

where the $M \times 1$ vector F_m represents the discretized modal field distribution of the mth mode, A is the discretized general field and the superscript t represents transpose of a vector. Note that the formulas presented in this section become valid for the TE modes by replacing the N matrix with the identity matrix I.

[1]for a uniform mesh, Δx is constant for all layers but for a non-uniform mesh, Δx is different for each layer.

3.4 Interface Conditions

In order to correctly model the electric and magnetic fields behaviour at an interface, the interface conditions (I.Cs.) should be appropriately accounted for in the Method of Lines formulation. In this thesis, we are mainly concerned with multi-layer structures in which the material properties are constant within each layer and change *abruptly* from one layer to the next (see figure 2.1). The tangential electric field E_y and its first derivative are continuous across an interface. The tangential magnetic field H_y is continuous but its first derivative is discontinuous at an interface. All the higher order derivatives of both E_y and H_y are discontinuous at an interface. We can derive these relations using Maxwell equations. For TE polarization, from equation 2.14

$$H_z = -\frac{j}{\omega\mu_o}\frac{\partial E_y}{\partial x} \tag{3.19}$$

at an interface, the H_z field is continuous, that is $H_z^{0^+} = H_z^{0^-}$, so the equation 3.19 becomes:

$$-\frac{j}{\omega\mu_o}\frac{\partial E_y^{0^+}}{\partial x} = -\frac{j}{\omega\mu_o}\frac{\partial E_y^{0^-}}{\partial x} \tag{3.20}$$

that is

$$\frac{\partial E_y^{0^+}}{\partial x} = \frac{\partial E_y^{0^-}}{\partial x} \tag{3.21}$$

Similarly for TM polarization, from equation 2.22

$$E_z = -\frac{j}{\omega n_j^2\epsilon_o}\frac{\partial H_y}{\partial x} \tag{3.22}$$

at an interface, E_z is continuous, that is $E_z^{0^+} = E_z^{0^-}$, so

$$\frac{j}{\omega n_2^2 \epsilon_o}\frac{\partial H_y^{0^+}}{\partial x} = \frac{j}{\omega n_1^2 \epsilon_o}\frac{\partial H_y^{0^-}}{\partial x} \tag{3.23}$$

that is:

$$\frac{1}{n_2^2}\frac{\partial H_y^{0^+}}{\partial x} = \frac{1}{n_1^2}\frac{\partial H_y^{0^-}}{\partial x} \tag{3.24}$$

3.5 Improved Three-Point Approximation of the $\frac{\partial^2}{\partial x^2}$ Operator

Now a general formula to approximate the $\frac{\partial^2}{\partial x^2}$ operator for TE and TM polarizations will be derived using Taylor's series expansion of the field. We shall use the symbol ψ to represent either E_y or H_y depending upon the polarization. The field is sampled or discretized in a way that there is *always* a sample point at an interface. Within a certain layer i, the refractive index n_i and discretization distance h_i are constant. From one layer to the next, either the refractive index n_i or the mesh size h_i or both may change. The refractive index chosen at the interface sampling point is either the left layer refractive index or the right layer refractive index, and this choice should be consistent throughout the whole structure. In this way, we can correctly model the layer thickness and abrupt refractive index discontinuity. With reference to figure 3.2, the field on either side of the interface is expanded in terms of the field at the interface using Taylor's series expansion, that is:

$$\psi_{-1} \;=\; \psi_{0^-} - h_1\psi'_{0^-} + \frac{h_1^2}{2!}\psi''_{0^-} + ... \tag{3.25}$$

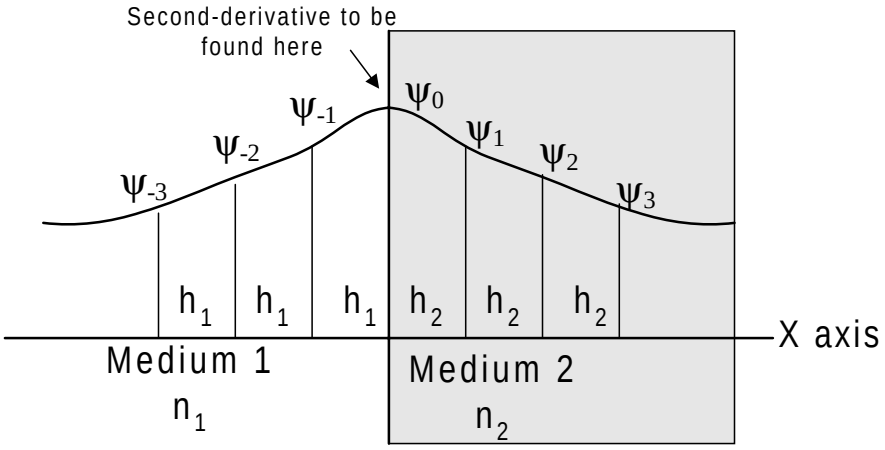

Figure 3.2: Discretized Field in the Transverse Direction

$$\psi_{+1} \quad = \quad \psi_{0^+} + h_2\psi'_{0^+} + \frac{h_2^2}{2!}\psi''_{0^+} + ... \tag{3.26}$$

Here ψ_{0^+} and ψ_{0^-} represent the field at $x = 0^+$ and $x = 0^-$ of the interface respectively. The $\frac{d}{dx}$ operator is represented by a *prime* on top of the symbol. Using the interface conditions, $\psi_{0^+} = \psi_{0^-}$ and $\psi'_{0^+} = \rho_{21}\psi'_{0^-}$ where $\rho_{21} = 1$ for the TE case and $\rho_{21} = \frac{n_2^2}{n_1^2}$ for the TM case, from equation 2.9 and the assumption that $\frac{\partial}{\partial y} = 0$, we get:

$$\frac{\partial^2\psi}{\partial z^2} + \frac{\partial^2\psi}{\partial x^2} + k_o^2 n_i^2 \psi = 0 \tag{3.27}$$

applying this equation at $x = 0^+$ and $x = 0^-$ of the interface and subtracting, we get:

$$\frac{\partial^2\psi_{0^+}}{\partial z^2} - \frac{\partial^2\psi_{0^-}}{\partial z^2} + \frac{\partial^2\psi_{0^+}}{\partial x^2} - \frac{\partial^2\psi_{0^-}}{\partial x^2} + k_o^2 n_2^2 \psi_{0^+} - k_o^2 n_1^2 \psi_{0^-} = 0 \tag{3.28}$$

that is:

$$\frac{\partial^2\psi_{0^+}}{\partial x^2} = \frac{\partial^2\psi_{0^-}}{\partial x^2} + k_o^2(n_1^2 - n_2^2)\psi_0 \tag{3.29}$$

where $\psi_{0+} = \psi_{0-} = \psi_0$. Equation 3.29 represents the discontinuity in second derivative at the interface. Expressing all ψ_{0+} in terms of ψ_{0-} in equation 3.26, we get

$$\psi_{+1} = \left[1 + 0.5h_2^2 k_o^2 (n_1^2 - n_2^2)\right] \psi_o + h_2 \rho_{21} \psi'_{0-} + 0.5h_2^2 \psi''_{0-} \tag{3.30}$$

eliminating ψ'_{0-} from equations 3.30 and 3.25, we get:

$$\psi''_{0-} = \frac{\psi_{+1} - \left[\tau_{21}\rho_{21} + 1 + 0.5h_2^2 k_o^2 (n_1^2 - n_2^2)\right]\psi_0 + \tau_{21}\rho_{21}\psi_{-1}}{0.5h_2(h_1\rho_{21} + h_2)} \tag{3.31}$$

where $\tau_{21} = \frac{h_2}{h_1}$. This relation approximates the $\frac{\partial^2}{\partial x^2}$ operator at any sampling point i in terms of the field values at $i+1$, i and $i-1$ sampling points. So this is a better three-point central-difference approximation of $\frac{\partial^2}{\partial x^2}$ operator with the inclusion of interface boundary conditions. Note that in a region of uniform refractive index and uniform mesh size i.e. $n_1 = n_2$ and $h_1 = h_2$, this reduces to the regular three-point central-difference approximation, that is:

$$\psi''_{0-} \approx \frac{\psi_{+1} - 2\psi_0 + \psi_{-1}}{h^2} \tag{3.32}$$

3.6 Higher-Order Approximation of the $\frac{\partial^2}{\partial x^2}$ Operator

The improved formula 3.31 for the second derivative approximation has an accuracy of $\mathcal{O}(h^2)$ at regions of uniform index and mesh size. Its accuracy decreases at mesh

or index discontinuities. In integrated optical waveguide modeling, the required accuracy in estimating the effective index is fairly high. So we need to use a relatively large number of discretization lines to reduce numerical errors. This leads to larger matrices and longer computational time. We can improve numerical accuracy without having excessive number of discretization lines using higher-order approximation of the second derivative operator. In this section, we derive the necessary formulas with appropriate interface conditions for the five-point and seven-point approximations.

3.6.1 Five-Point Approximation

Refer to the figure 3.2, assuming there exists an index discontinuity and mesh discontinuity at the interface $x = 0$ of two layers. We expand the field on either sides of the interface in terms of the field at the interface using Taylor's series expansion, that is:

$$\psi_{+1} = \psi_{0+} + h_2\psi'_{0+} + \frac{h_2^2}{2!}\psi''_{0+} + \frac{h_2^3}{3!}\psi'''_{0+} + \frac{h_2^4}{4!}\psi''''_{0+} + ... \tag{3.33}$$

$$\psi_{-1} = \psi_{0-} - h_1\psi'_{0-} + \frac{h_1^2}{2!}\psi''_{0-} - \frac{h_1^3}{3!}\psi'''_{0-} + \frac{h_1^4}{4!}\psi''''_{0-} - +... \tag{3.34}$$

$$\psi_{+2} = \psi_{0+} + 2h_2\psi'_{0+} + \frac{(2h_2)^2}{2!}\psi''_{0+} + \frac{(2h_2)^3}{3!}\psi'''_{0+} + \frac{(2h_2)^4}{4!}\psi''''_{0+} + ... \tag{3.35}$$

$$\psi_{-2} = \psi_{0-} - 2h_1\psi'_{0-} + \frac{(2h_1)^2}{2!}\psi''_{0-} - \frac{(2h_1)^3}{3!}\psi'''_{0-} + \frac{(2h_1)^4}{4!}\psi''''_{0-} - +... \tag{3.36}$$

The interface conditions for TE and TM Polarization are:

$$\psi_{0+} = \psi_{0-} \tag{3.37}$$

$$\psi_{0+}^{'} = \rho_{21}\psi_{0-}^{'} \tag{3.38}$$

$$\psi_{0+}^{''} = \psi_{0-}^{''} + k_o^2(n_1^2 - n_2^2)\psi_0 \tag{3.39}$$

where $\rho_{21} = \frac{n_2^2}{n_1^2}$ for the TM case and $\rho_{21} = 1$ for the TE case. In this case, we have to account for the discontinuity of the third and fourth derivatives at the interface. Differentiating equation 3.27 with respect to x, we get:

$$\frac{\partial^2\psi^{'}}{\partial z^2} + \psi^{'''} + k_o^2 n_i^2 \psi^{'} = 0 \tag{3.40}$$

where the *prime* on top of a symbol shows derivative with respect to x. Applying this equation at $x = 0^+$ and $x = 0^-$ of the interface and subtracting, we get:

$$\frac{\partial^2\psi_{0+}^{'}}{\partial z^2} + \psi_{0+}^{'''} + k_o^2 n_2^2 \psi_{0+}^{'} - \frac{\partial^2\psi_{0-}^{'}}{\partial z^2} - \psi_{0-}^{'''} - k_o^2 n_1^2 \psi_{0-}^{'} = 0 \tag{3.41}$$

From equations 3.37, 3.38, 3.39 expressing the 0^+ side derivatives in terms of 0^- side derivative in the above equation and simplifying, we get:

$$\psi_{0+}^{'''} = \rho_{21}\left[\psi_{0-}^{'''} + k_o^2(n_1^2 - n_2^2)\psi_{0-}^{'}\right] \tag{3.42}$$

This relation accounts for the discontinuity in the third derivative of the field with respect to x at an index or mesh discontinuity. Similarly differentiating equation 3.27 twice with respect to x, we get:

$$\frac{\partial^2\psi^{''}}{\partial z^2} + \psi^{''''} + k_o^2 n_i^2 \psi^{''} = 0 \tag{3.43}$$

$$\frac{\partial^2}{\partial z^2}(-\frac{\partial^2\psi}{\partial z^2} - k_o^2 n_i^2 \psi) + \psi^{''''} + k_o^2 n_i^2 \psi^{''} = 0 \tag{3.44}$$

$$\frac{\partial^4\psi}{\partial z^4} + k_o^2 n_i^2 \frac{\partial^2\psi}{\partial z^2} - \psi^{''''} - k_o^2 n_i^2 \psi^{''} = 0 \tag{3.45}$$

$$\frac{\partial^4\psi}{\partial z^4} + k_o^2 n_i^2(-\psi^{''} - k_o^2 n_i^2\psi) - \psi^{''''} - k_o^2 n_i^2\psi^{''} = 0 \tag{3.46}$$

$$\frac{\partial^4\psi}{\partial z^4} - 2k_o^2 n_i^2\psi^{''} - \psi^{''''} - k_o^4 n_i^4\psi = 0 \tag{3.47}$$

where equation 3.27 is used to replace $\psi^{''}$ in equation 3.43 and $\frac{\partial^2\psi}{\partial z^2}$ in equation 3.45. Evaluating equation 3.47 on both sides of the interface and subtracting:

$$\begin{aligned}(-\frac{\partial^4\psi_{0^+}}{\partial z^4} + 2k_o^2 n_2^2\psi_{0^+}^{''} + \psi_{0^+}^{''''} + k_o^4 n_2^4\psi_{0^+}) - \\ (-\frac{\partial^4\psi_{0^-}}{\partial z^4} + 2k_o^2 n_1^2\psi_{0^-}^{''} + \psi_{0^-}^{''''} + k_o^4 n_1^4\psi_{0^-}) = 0\end{aligned} \tag{3.48}$$

$$\psi_{0^+}^{''''} = \psi_{0^-}^{''''} - 2k_o^2 n_2^2\psi_{0^+}^{''} + 2k_o^2 n_1^2\psi_{0^-}^{''} - k_o^4(n_2^4 - n_1^4)\psi_{0^-} \tag{3.49}$$

expressing $\psi_{0^+}^{''}$ in terms of $\psi_{0^-}^{''}$ and simplifying, we get

$$\psi_{0^+}^{''''} = \psi_{0^-}^{''''} + 2k_o^2(n_1^2 - n_2^2)\psi_{0^-}^{''} + k_o^4(n_1^2 - n_2^2)^2\psi_0 \tag{3.50}$$

This relation accounts for the discontinuity in $\psi^{''''}$ at an index or mesh discontinuity for both TE and TM modes. Now we have expressed the 0^- side derivatives of ψ in terms of 0^+ side derivatives at the interface. Putting these values in equations 3.33 and 3.35 we get

$$\begin{aligned}\psi_{+1} = \quad & \left(1 + \frac{h_2^2}{2}k_o^2(n_1^2 - n_2^2) + \frac{h_2^4}{24}k_o^4(n_1^2 - n_2^2)^2\right)\psi_0 + \rho_{21}\left(h_2 + \frac{h_2^3}{6}k_o^2(n_1^2 - n_2^2)\right)\psi_{0^-}^{'} \\ & + \left(\frac{h_2^2}{2} + \frac{h_2^4}{12}k_o^2(n_1^2 - n_2^2)\right)\psi_{0^-}^{''} + \frac{h_2^3}{6}\rho_{21}\psi_{0^-}^{'''} + \frac{h_2^4}{24}\psi_{0^-}^{''''} + ...\end{aligned} \tag{3.51}$$

$$\begin{aligned}\psi_{+2} = \quad & \left(1 + 2h_2^2k_o^2(n_1^2 - n_2^2) + \frac{2h_2^4}{3}k_o^4(n_1^2 - n_2^2)^2\right)\psi_0 + \rho_{21}\left(2h_2 + \frac{4h_2^3}{3}k_o^2(n_1^2 - n_2^2)\right)\psi_{0^-}^{'} \\ & + \left(2h_2^2 + \frac{4h_2^4}{3}k_o^2(n_1^2 - n_2^2)\right)\psi_{0^-}^{''} + \frac{4h_2^3}{3}\rho_{21}\psi_{0^-}^{'''} + \frac{2h_2^4}{3}\psi_{0^-}^{''''} + ...\end{aligned} \tag{3.52}$$

Equations 3.34 and 3.36 remain unchanged. Equations 3.51, 3.52, 3.34 and 3.36 can be put in the matrix form, that is:

$$\begin{bmatrix} \psi_{+1} - a \cdot \psi_0 \\ \psi_{+2} - b \cdot \psi_0 \\ \psi_{-1} - c \cdot \psi_0 \\ \psi_{-2} - d \cdot \psi_0 \end{bmatrix} = \begin{bmatrix} a_{11} & a_{12} & a_{13} & a_{14} \\ a_{21} & a_{22} & a_{23} & a_{24} \\ a_{31} & a_{32} & a_{33} & a_{34} \\ a_{41} & a_{42} & a_{43} & a_{44} \end{bmatrix} \begin{bmatrix} \psi'_{0-} \\ \psi''_{0-} \\ \psi'''_{0-} \\ \psi''''_{0-} \end{bmatrix}$$

where a, b, c and d are the coefficients of ψ_0 in the previous equations. Inverting the matrix equation to find the unknowns, we get:

$$\begin{bmatrix} \psi'_{0-} \\ \psi''_{0-} \\ \psi'''_{0-} \\ \psi''''_{0-} \end{bmatrix} = \begin{bmatrix} b_{11} & b_{12} & b_{13} & b_{14} \\ b_{21} & b_{22} & b_{23} & b_{24} \\ b_{31} & b_{32} & b_{33} & b_{34} \\ b_{41} & b_{42} & b_{43} & b_{44} \end{bmatrix} \begin{bmatrix} \psi_{+1} - a \cdot \psi_0 \\ \psi_{+2} - b \cdot \psi_0 \\ \psi_{-1} - c \cdot \psi_0 \\ \psi_{-2} - d \cdot \psi_0 \end{bmatrix}$$

From which we find:

$$\begin{aligned} \psi''_{0-} \quad = \quad & b_{22}\psi_{+2} + b_{21}\psi_{+1} - (a \cdot b_{21} + b \cdot b_{22} + c \cdot b_{23} + d \cdot b_{24})\psi_0 + \\ & b_{23}\psi_{-1} + b_{24}\psi_{-2} \end{aligned} \tag{3.53}$$

This relation gives ψ''_i approximation at an *interface* in terms of the field samples ψ_{i+2} , ψ_{i+1} , ψ_i , ψ_{i-1} and ψ_{i-2}. In this relation, the discontinuity in ψ , ψ' , ψ'' , ψ''' and ψ'''' at an index or mesh discontinuity are appropriately included. In regions of

uniform index and mesh, this reduces to the regular 5-point approximation, that is:

$$\psi''_{0^-} \approx \frac{1}{12h^2}(-\psi_{+2} + 16\psi_{+1} - 30\psi_0 + 16\psi_{-1} - \psi_{-2}) \tag{3.54}$$

Note that by using this five-point approximations , we get a penta-diagonal matrix of the form:

$$\frac{1}{12h^2}\begin{bmatrix} -30 & 16 & -1 & & & & & \\ 16 & -30 & 16 & -1 & & & \mathcal{O} & \\ -1 & 16 & -30 & 16 & -1 & & & \\ & \ddots & \ddots & \ddots & \ddots & \ddots & & \\ & & & -1 & 16 & -30 & 16 & -1 \\ & \mathcal{O} & & & -1 & 16 & -30 & 16 \\ & & & & & -1 & 16 & -30 \end{bmatrix}$$

Now we have to find the 5-point second-derivative formula at one sampling point *ahead* and one sampling point *before* the interface. In this derivation, it is assumed that minimum number of samples in one layer are 4. Refer to the figure 3.3, there is an index and a mesh discontinuity at ψ_{-1}. So we need to match the boundary conditions at ψ_{-1} while ψ''_0 is to be expressed in terms of ψ_{-2} , ψ_{-1} , ψ_0 , ψ_{+1} and ψ_{+2}. Expand the field samples on either side of the interface in terms of field value ψ_{-1} at the interface:

$$\psi_0 \;=\; \psi_{-1^+} + h_2\psi'_{-1^+} + \frac{h_2^2}{2!}\psi''_{-1^+} + \frac{h_2^3}{3!}\psi'''_{-1^+} + \frac{h_2^4}{4!}\psi''''_{-1^+} + ... \tag{3.55}$$

$$\psi_{+1} = \psi_{-1^+} + 2h_2\psi'_{-1^+} + 2h_2^2\psi''_{-1^+} + \frac{4h_2^3}{3}\psi'''_{-1^+} + \frac{2h_2^4}{3}\psi''''_{-1^+} + ... \quad (3.56)$$

$$\psi_{+2} = \psi_{-1^+} + 3h_2\psi'_{-1^+} + \frac{9h_2^2}{2}\psi''_{-1^+} + \frac{9h_2^3}{2}\psi'''_{-1^+} + \frac{27h_2^4}{8}\psi''''_{-1^+} + ... \quad (3.57)$$

$$\psi_{-2} = \psi_{-1^-} - h_1\psi'_{-1^-} + \frac{h_1^2}{2!}\psi''_{-1^-} - \frac{h_1^3}{3!}\psi'''_{-1^-} + \frac{h_1^4}{4!}\psi''''_{-1^-} - + ... \quad (3.58)$$

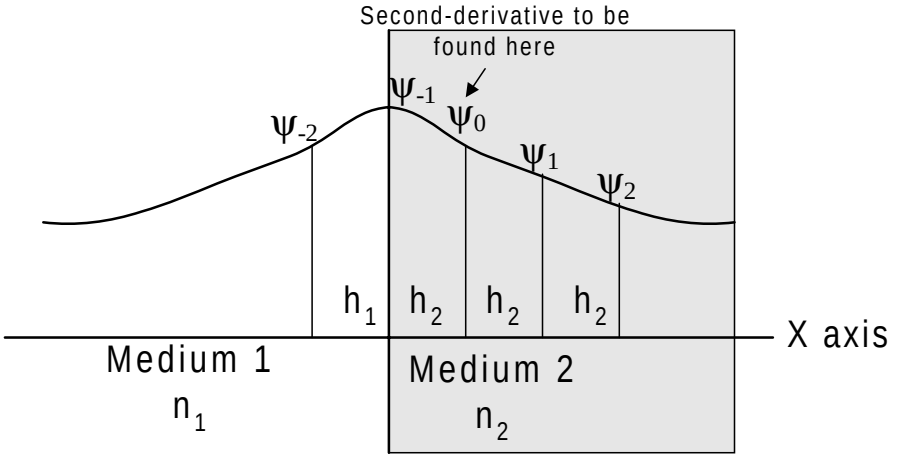

Figure 3.3: At one Point Ahead of the Interface

Using the interface conditions 3.37, 3.38, 3.39, 3.42 and 3.50, we express ψ_{-1^-} derivatives in terms of ψ_{-1^+} derivatives in the previous equation. After simplification, we get:

$$\psi_{-2} = \psi_{-1}\left(1 - \frac{h_1^2}{2}k_o^2(n_1^2 - n_2^2) + \frac{h_1^4}{24}k_o^4(n_1^2 - n_2^2)^2\right) + \frac{1}{\rho_{21}}\psi'_{-1^+}\left(-h_1 + \frac{h_1^3}{6}k_o^2(n_1^2 - n_2^2)\right)$$
$$+\psi''_{-1^+}\left(\frac{h_1^2}{2} - \frac{h_1^4}{12}k_o^2(n_1^2 - n_2^2)\right) + \psi'''_{-1^+}(-\frac{h_1^3}{6\rho_{21}}) + \psi''''_{-1^+}(\frac{h_1^4}{24}) \quad (3.59)$$

Other equations remain the same. Putting in the matrix notation :

$$\begin{bmatrix} \psi_0 - \psi_{-1} \\ \psi_{+1} - \psi_{-1} \\ \psi_{+2} - \psi_{-1} \\ \psi_{-2} - a \cdot \psi_{-1} \end{bmatrix} = \begin{bmatrix} a_{11} & a_{12} & a_{13} & a_{14} \\ a_{21} & a_{22} & a_{23} & a_{24} \\ a_{31} & a_{32} & a_{33} & a_{34} \\ a_{41} & a_{42} & a_{43} & a_{44} \end{bmatrix} \begin{bmatrix} \psi'_{-1^+} \\ \psi''_{-1^+} \\ \psi'''_{-1^+} \\ \psi''''_{-1^+} \end{bmatrix}$$

where a is the coefficient of ψ_{-1} in equation 3.59. Inverting the matrix equation to find the unknowns, we get:

$$\begin{bmatrix} \psi'_{-1^+} \\ \psi''_{-1^+} \\ \psi'''_{-1^+} \\ \psi''''_{-1^+} \end{bmatrix} = \begin{bmatrix} b_{11} & b_{12} & b_{13} & b_{14} \\ b_{21} & b_{22} & b_{23} & b_{24} \\ b_{31} & b_{32} & b_{33} & b_{34} \\ b_{41} & b_{42} & b_{43} & b_{44} \end{bmatrix} \begin{bmatrix} \psi_0 - \psi_{-1} \\ \psi_{+1} - \psi_{-1} \\ \psi_{+2} - \psi_{-2} \\ \psi_{-2} - a \cdot \psi_{-1} \end{bmatrix}$$

From this we can find ψ'_{-1^+},ψ''_{-1^+},ψ'''_{-1^+} and ψ''''_{-1^+}. Differentiating equation 3.55 with respect to x, we get:

$$\psi''_0 = \psi''_{-1^+} + h_2\psi'''_{-1^+} + \frac{h_2^2}{2}\psi''''_{-1^+} + ... \tag{3.60}$$

Putting the values of ψ''_{-1^+},ψ'''_{-1^+} and ψ''''_{-1^+} in the above equation and simplifying, we get :

$$\begin{aligned} \psi''_0 = \quad & \psi_{+2}(b_{23} + h_2 b_{33} + 0.5h_2^2 b_{43}) + \psi_{+1}(b_{22} + h_2 b_{32} + 0.5h_2^2 b_{42}) + \\ & \psi_0(b_{21} + h_2 b_{31} + 0.5h_2^2 b_{41}) + \psi_{-2}(b_{24} + h_2 b_{34} + 0.5h_2^2 b_{44}) - \\ & \psi_{-1}(p_1 + h_2 p_2 + 0.5h_2^2 p_3) \end{aligned} \tag{3.61}$$

where $p_1 = b_{21}+b_{22}+b_{23}+a\cdot b_{24}$, $p_2 = b_{31}+b_{32}+b_{33}+a\cdot b_{34}$ and $p_3 = b_{41}+b_{42}+b_{43}+a\cdot b_{44}$. This relation gives the five-point second-derivative approximation at one sample point *ahead* of the index or mesh discontinuity. The relation at one sample point *before* the interface can obtained by interchanging $h_2 \rightleftharpoons -h_1$, $\psi_{+1} \rightleftharpoons \psi_{-1}$, $\psi_{+2} \rightleftharpoons \psi_{-2}$ and $n_1^2 \rightleftharpoons n_2^2$.

3.6.2 Seven-Point Approximation

A similar procedure is adapted to find the 7-point second-derivative approximation with appropriate interface conditions. With reference to the figure 3.2, to find at $\psi_0^{''}$, expanding the sampled field on either sides of the interface in terms of ψ_0:

$$\begin{aligned}
\psi_{+1} &= \psi_{0+} + h_2\psi_{0+}^{'} + \frac{h_2^2}{2!}\psi_{0+}^{''} + \frac{h_2^3}{3!}\psi_{0+}^{'''} + \frac{h_2^4}{4!}\psi_{0+}^{''''} + \\
&\quad \frac{h_5^4}{5!}\psi_{0+}^{''''} + \frac{h_2^6}{6!}\psi_{0+}^{''''''} + ... \qquad (3.62)\\
\psi_{+2} &= \psi_{0+} + 2h_2\psi_{0+}^{'} + \frac{(2h_2)^2}{2!}\psi_{0+}^{''} + \frac{(2h_2)^3}{3!}\psi_{0+}^{'''} + \frac{(2h_2)^4}{4!}\psi_{0+}^{''''} \\
&\quad + \frac{(2h_2)^5}{5!}\psi_{0+}^{''''} + \frac{(2h_2)^6}{6!}\psi_{0+}^{''''''} + ... \qquad (3.63)\\
\psi_{+3} &= \psi_{0+} + 3h_2\psi_{0+}^{'} + \frac{(3h_2)^2}{2!}\psi_{0+}^{''} + \frac{(3h_2)^3}{3!}\psi_{0+}^{'''} + \frac{(3h_2)^4}{4!}\psi_{0+}^{''''} \\
&\quad + \frac{(3h_2)^5}{5!}\psi_{0+}^{''''} + \frac{(3h_2)^6}{6!}\psi_{0+}^{''''''} + ... \qquad (3.64)\\
\psi_{-1} &= \psi_{0-} - h_1\psi_{0-}^{'} + \frac{h_1^2}{2!}\psi_{0-}^{''} - \frac{h_1^3}{3!}\psi_{0-}^{'''} + \frac{h_1^4}{4!}\psi_{0-}^{''''} \\
&\quad - \frac{h_1^5}{5!}\psi_{0-}^{''''} + \frac{h_1^6}{6!}\psi_{0-}^{''''''} - +... \qquad (3.65)\\
\psi_{-2} &= \psi_{0-} - 2h_1\psi_{0-}^{'} + \frac{(2h_1)^2}{2!}\psi_{0-}^{''} - \frac{(2h_1)^3}{3!}\psi_{0-}^{'''} + \frac{(2h_1)^4}{4!}\psi_{0-}^{''''}
\end{aligned}$$

$$-\frac{(2h_1)^5}{5!}\psi^{'''''}_{0-} + \frac{(2h_1)^6}{6!}\psi^{'''''}_{0-} - + ... \tag{3.66}$$

$$\psi_{-3} = \psi_{0-} - 3h_1\psi^{'}_{0-} + \frac{(3h_1)^2}{2!}\psi^{''}_{0-} - \frac{(3h_1)^3}{3!}\psi^{'''}_{0-} + \frac{(3h_1)^4}{4!}\psi^{''''}_{0-}$$
$$-\frac{(3h_1)^5}{5!}\psi^{'''''}_{0-} + \frac{(3h_1)^6}{6!}\psi^{'''''}_{0-} - + ... \tag{3.67}$$

We have derived the interface conditions (Equations 3.37, 3.38, 3.39, 3.42, 3.50) to account for the discontinuity in field derivatives on both sides of an interface. Following a similar procedure , we can derive the discontinuity in $\psi^{''''}$ and $\psi^{'''''}$ at an index or a mesh discontinuity. The final relations for both TE and TM polarization are given below:

$$\psi^{'''''}_{0+} = \rho_{21}\left(\psi^{'''''}_{0-} + 2k_o^2(n_1^2 - n_2^2)\psi^{'''}_{0-} + k_o^4(n_1^2 - n_2^2)^2\psi^{'}_{0-}\right) \tag{3.68}$$

$$\psi^{'''''}_{0+} = \psi^{'''''}_{0-} + 3k_o^2(n_1^2 - n_2^2)\psi^{''''}_{0-} + 3k_o^4(n_1^2 - n_2^2)^2\psi^{''}_{0-} + k_o^6(n_1^2 - n_2^2)^3\psi_0 \tag{3.69}$$

Now express the 0^+ side derivatives in terms of the 0^- side derivatives in Taylor series expansion 3.62. We get the simplified expression:

$$\psi_{+1} = \psi_0\left(1 + \frac{\zeta_{12}h_2^2}{2!} + \frac{\zeta_{12}^2h_2^4}{4!} + \frac{\zeta_{12}^3h_2^6}{6!}\right) + \rho_{21}\psi^{'}_{0-}\left(h_2 + \frac{\zeta_{12}h_2^3}{3!} + \frac{\zeta_{12}^2h_2^5}{5!}\right)$$
$$+\psi^{''}_{0-}\left(\frac{h_2^2}{2!} + \frac{2\zeta_{12}h_2^4}{4!} + \frac{3\zeta_{12}^2h_2^6}{6!}\right) + \rho_{21}\psi^{'''}_{0-}\left(\frac{h_2^3}{3!} + \frac{2\zeta_{12}h_2^5}{5!}\right)$$
$$+\psi^{''''}_{0-}\left(\frac{h_2^4}{4!} + \frac{3\zeta_{12}h_2^6}{6!}\right) + \rho_{21}\frac{h_2^5}{5!}\psi^{'''''}_{0-} + \frac{h_2^6}{6!}\psi^{'''''}_{0-} \tag{3.70}$$

where $\zeta_{12} = k_o^2(n_1^2 - n_2^2)$ in the above equation. Expressions for ψ_{+2} and ψ_{+3} are obtained by replacing h_2 by $2h_2$ and $3h_2$ in the equation 3.70 respectively. For ψ_{-1}, ψ_{-2} and ψ_{-3}, Taylor series is unchanged. Assimilate the final results in a matrix form :

$$\begin{bmatrix} \psi_{+1} - a \cdot \psi_0 \\ \psi_{+2} - b \cdot \psi_0 \\ \psi_{+3} - c \cdot \psi_0 \\ \psi_{-1} - \psi_0 \\ \psi_{-2} - \psi_0 \\ \psi_{-3} - \psi_0 \end{bmatrix} = \begin{bmatrix} . & . & . & . & . & . \\ . & . & . & . & . & . \\ . & . & . & . & . & . \\ . & . & . & . & . & . \\ . & . & . & . & . & . \\ . & . & . & . & . & . \end{bmatrix} \begin{bmatrix} \psi'_{0-} \\ \psi''_{0-} \\ \psi'''_{0-} \\ \psi''''_{0-} \\ \psi'''''_{0-} \\ \psi''''''_{0-} \end{bmatrix}$$

where a, b and c are the coefficients of corresponding ψ_0 terms in the previous equation. Inverting the matrix equation to find the unknowns, we get:

$$\begin{bmatrix} \psi'_{0-} \\ \psi''_{0-} \\ \psi'''_{0-} \\ \psi''''_{0-} \\ \psi'''''_{0-} \\ \psi''''''_{0-} \end{bmatrix} = \begin{bmatrix} b_{11} & b_{12} & b_{13} & b_{14} & b_{15} & b_{16} \\ b_{21} & b_{22} & b_{23} & b_{24} & b_{25} & b_{26} \\ b_{31} & b_{32} & b_{33} & b_{34} & b_{35} & b_{36} \\ b_{41} & b_{42} & b_{43} & b_{44} & b_{45} & b_{46} \\ b_{51} & b_{52} & b_{53} & b_{54} & b_{55} & b_{56} \\ b_{61} & b_{62} & b_{63} & b_{64} & b_{65} & b_{66} \end{bmatrix} \begin{bmatrix} \psi_{+1} - a \cdot \psi_0 \\ \psi_{+2} - b \cdot \psi_0 \\ \psi_{+3} - c \cdot \psi_0 \\ \psi_{-1} - \psi_0 \\ \psi_{-2} - \psi_0 \\ \psi_{-3} - \psi_0 \end{bmatrix}$$

From which we find:

$$\begin{aligned} \psi''_{0-} &= b_{23}\psi_{+3} + b_{22}\psi_{+2} + b_{21}\psi_{+1} - (a \cdot b_{21} + b \cdot b_{22} + c \cdot b_{23} + b_{24} + b_{25} + b_{26})\psi_0 \\ &\quad + b_{24}\psi_{-1} + b_{25}\psi_{-2} + b_{26}\psi_{-3} \end{aligned} \tag{3.71}$$

This relation gives approximation of ψ''_i at an interface point in terms of the field samples ψ_{i+3} , ψ_{i+2} , ψ_{i+1} , ψ_i , ψ_{i-1} , ψ_{i-2} and ψ_{i-3} on either sides of the interface.

In this relation, the discontinuities in ψ , $\psi^{'}$, $\psi^{''}$, $\psi^{'''}$, $\psi^{''''}$, $\psi^{'''''}$ and $\psi^{''''''}$ at an index or a mesh discontinuity are appropriately included. In the regions of uniform index and uniform mesh, this relation reduces to the regular 7-point approximation of the form:

$$\psi_{0-}^{''} \approx \frac{1}{180h^2}(2\psi_{+3} - 27\psi_{+2} + 270\psi_{+1} - 490\psi_0 + 270\psi_{-1} - 27\psi_{-2} + 2\psi_{-3}) \quad (3.72)$$

Note that by using this seven-point approximations , we get a hepta-diagonal matrix of the form:

$$\frac{1}{180h^2}\begin{bmatrix} -490 & 270 & -27 & 2 & & & & & & \\ 270 & -490 & 270 & -27 & 2 & & & & \mathcal{O} & \\ -27 & 270 & -490 & 270 & -27 & 2 & & & & \\ 2 & -27 & 270 & -490 & 270 & -27 & 2 & & & \\ & \ddots & \ddots & \ddots & \ddots & \ddots & \ddots & \ddots & & \\ & & & 2 & -27 & 270 & -490 & 270 & -27 & 2 \\ & & & & 2 & -27 & 270 & -490 & 270 & -27 \\ & \mathcal{O} & & & & 2 & -27 & 270 & -490 & 270 \\ & & & & & & 2 & -27 & 270 & -490 \end{bmatrix}$$

To find the second-derivative formula at one sampling point before the interface, the procedure is similar to that followed in the previous section. Refer to the figure 3.4, there is a mesh and an index discontinuity at ψ_{+1} and we have to express $\psi_0^{''}$

in terms of ψ_{-3} , ψ_{-2} , ψ_{-1} , ψ_0 , ψ_{+1} , ψ_{+2} and ψ_{+3}. Expanding the field on either sides of the interface in terms of ψ_{+1}, that is:

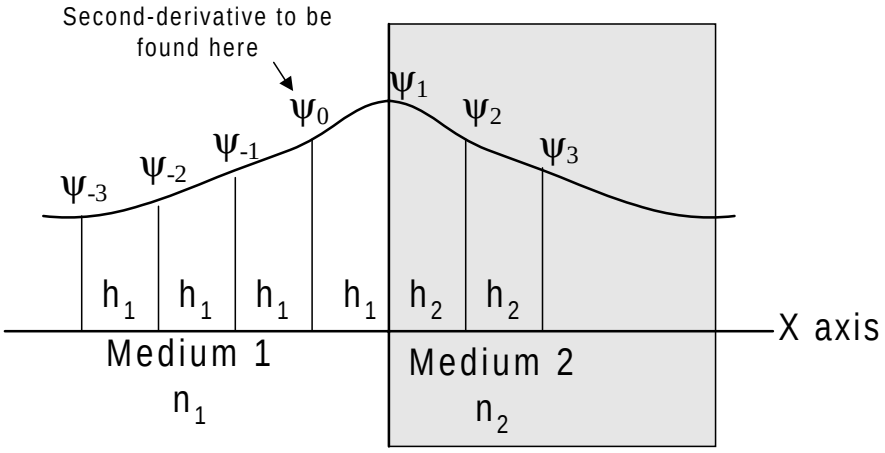

Figure 3.4: At one Point Before the Interface

$$\psi_0 = \psi_{+1^-} + h_2\psi'_{+1^-} + ... + \frac{h_2^6}{6!}\psi^{''''''}_{+1^-} + ... \tag{3.73}$$

$$\psi_{-1} = \psi_{+1^-} - 2h_1\psi'_{+1^-} + ... + \frac{(-2h_1)^6}{6!}\psi^{''''''}_{+1^-} + ... \tag{3.74}$$

$$\psi_{-2} = \psi_{+1^-} - 3h_1\psi'_{+1^-} + ... + \frac{(3h_1)^6}{6!}\psi^{''''''}_{+1^-} + ... \tag{3.75}$$

$$\psi_{-3} = \psi_{+1^-} - 4h_1\psi'_{+1^-} + ... + \frac{(4h_1)^6}{6!}\psi^{''''''}_{+1^-} + ... \tag{3.76}$$

$$\psi_{+2} = \psi_{+1^+} + h_2\psi'_{+1^+} + ... + \frac{h_2^6}{6!}\psi^{''''''}_{+1^+} + ... \tag{3.77}$$

$$\psi_{+3} = \psi_{+1^+} + 2h_2\psi'_{+1^+} + ... + \frac{(2h_2)^6}{6!}\psi^{''''''}_{+1^+} + ... \tag{3.78}$$

replace all $\psi^{(n)}_{+1^+}$ derivatives with $\psi^{(n)}_{+1^-}$ derivatives in the above equations. After simplifying, we get:

$$\begin{aligned}\psi_{+2} = \quad & \psi_{+1}\left(1 + \frac{\zeta_{12}h_2^2}{2!} + \frac{\zeta_{12}^2h_2^4}{4!} + \frac{\zeta_{12}^3h_2^6}{6!}\right) + \rho_{21}\psi'_{+1^-}\left(h_2 + \frac{\zeta_{12}h_2^3}{3!} + \frac{\zeta_{12}^2h_2^5}{5!}\right) \\ & + \psi''_{+1^-}\left(\frac{h_2^2}{2!} + \frac{2\zeta_{12}h_2^4}{4!} + \frac{3\zeta_{12}^2h_2^6}{6!}\right) + \rho_{21}\psi'''_{+1^-}\left(\frac{h_2^3}{3!} + \frac{2\zeta_{12}h_2^5}{5!}\right)\end{aligned}$$

$$+\psi^{''''}_{+1^-}\left(\frac{h_2^4}{4!}+\frac{3\zeta_{12}h_2^6}{6!}\right)+\rho_{21}\psi^{'''''}_{+1^-}\frac{h_2^5}{5!}+\psi^{''''''}_{+1^-}\frac{h_2^6}{6!} \tag{3.79}$$

For ψ_{+3}, replace h_2 by $2h_2$ in equation 3.79. The remaining equations are unchanged. Putting the above equations in the matrix form:

$$\begin{bmatrix} \psi_{+2}-a\cdot\psi_{+1} \\ \psi_{+3}-b\cdot\psi_{+1} \\ \psi_0-\psi_{+1} \\ \psi_{-1}-\psi_{+1} \\ \psi_{-2}-\psi_{+1} \\ \psi_{-3}-\psi_{+1} \end{bmatrix} = \begin{bmatrix} . & . & . & . & . & . \\ . & . & . & . & . & . \\ . & . & . & . & . & . \\ . & . & . & . & . & . \\ . & . & . & . & . & . \\ . & . & . & . & . & . \end{bmatrix} \begin{bmatrix} \psi^{'}_{+1^-} \\ \psi^{''}_{+1^-} \\ \psi^{'''}_{+1^-} \\ \psi^{''''}_{+1^-} \\ \psi^{'''''}_{+1^-} \\ \psi^{''''''}_{+1^-} \end{bmatrix}$$

where a and b are the coefficients of the corresponding ψ_{+1} terms. Inverting the above matrix equation to find the unknowns, we get:

$$\begin{bmatrix} \psi^{'}_{+1^-} \\ \psi^{''}_{+1^-} \\ \psi^{'''}_{+1^-} \\ \psi^{''''}_{+1^-} \\ \psi^{'''''}_{+1^-} \\ \psi^{''''''}_{+1^-} \end{bmatrix} = \begin{bmatrix} b_{11} & b_{12} & b_{13} & b_{14} & b_{15} & b_{16} \\ b_{21} & b_{22} & b_{23} & b_{24} & b_{25} & b_{26} \\ b_{31} & b_{32} & b_{33} & b_{34} & b_{35} & b_{36} \\ b_{41} & b_{42} & b_{43} & b_{44} & b_{45} & b_{46} \\ b_{51} & b_{52} & b_{53} & b_{54} & b_{55} & b_{56} \\ b_{61} & b_{62} & b_{63} & b_{64} & b_{65} & b_{66} \end{bmatrix} \begin{bmatrix} \psi_{+2}-a\cdot\psi_{+1} \\ \psi_{+3}-b\cdot\psi_{+1} \\ \psi_0-\psi_{+1} \\ \psi_{-1}-\psi_{+1} \\ \psi_{-2}-\psi_{+1} \\ \psi_{-3}-\psi_{+1} \end{bmatrix}$$

From this equation, we can find $\psi^{'}_{+1^-}$, $\psi^{''}_{+1^-}$, $\psi^{'''}_{+1^-}$, $\psi^{''''}_{+1^-}$, $\psi^{'''''}_{+1^-}$ and $\psi^{''''''}_{+1^-}$.

Differentiating Taylor's series expansion 3.73 of ψ_0 twice with respect to x, we get:

$$\psi_0^{''} = \psi_{+1^-}^{''} - h_1\psi_{+1^-}^{'''} + \frac{h_1^2}{2!}\psi_{+1^-}^{''''} - \frac{h_1^3}{3!}\psi_{+1^-}^{'''''} + \frac{h_1^4}{4!}\psi_{+1^-}^{''''''} - +... \tag{3.80}$$

Putting the values of $\psi_{+1^-}^{''}$, $\psi_{+1^-}^{'''}$, $\psi_{+1^-}^{''''}$, $\psi_{+1^-}^{'''''}$ and $\psi_{+1^-}^{''''''}$ in equation 3.80 and simplifying, we get the final relationship:

$$\begin{aligned}
\psi_0^{''} = \quad & \psi_{-3}\left(b_{26} - h_1 b_{36} + \frac{h_1^2}{2!}b_{46} - \frac{h_1^3}{3!}b_{56} + \frac{h_1^4}{4!}b_{66}\right) + \\
& \psi_{-2}\left(b_{25} - h_1 b_{35} + \frac{h_1^2}{2!}b_{45} - \frac{h_1^3}{3!}b_{55} + \frac{h_1^4}{4!}b_{65}\right) + \\
& \psi_{-1}\left(b_{24} - h_1 b_{34} + \frac{h_1^2}{2!}b_{44} - \frac{h_1^3}{3!}b_{54} + \frac{h_1^4}{4!}b_{64}\right) + \\
& \psi_{+1}\left(p_1 - h_1 p_2 + \frac{h_1^2}{2!}p_3 - \frac{h_1^3}{3!}p_4 + \frac{h_1^4}{4!}p_5\right) + \\
& \psi_{+2}\left(b_{21} - h_1 b_{31} + \frac{h_1^2}{2!}b_{41} - \frac{h_1^3}{3!}b_{51} + \frac{h_1^4}{4!}b_{61}\right) + \\
& \psi_{+3}\left(b_{22} - h_1 b_{32} + \frac{h_1^2}{2!}b_{42} - \frac{h_1^3}{3!}b_{52} + \frac{h_1^4}{4!}b_{62}\right) + \\
& \psi_{0}\left(b_{23} - h_1 b_{33} + \frac{h_1^2}{2!}b_{43} - \frac{h_1^3}{3!}b_{53} + \frac{h_1^4}{4!}b_{63}\right)
\end{aligned} \tag{3.81}$$

where $p_1 = a\cdot b_{21} + b\cdot b_{22} + b_{23} + b_{24} + b_{25} + b_{26}$, $p_2 = a\cdot b_{31} + b\cdot b_{32} + b_{33} + b_{34} + b_{35} + b_{36}$, $p_3 = a\cdot b_{41} + b\cdot b_{42} + b_{43} + b_{44} + b_{45} + b_{46}$, $p_4 = a\cdot b_{51} + b\cdot b_{52} + b_{53} + b_{54} + b_{55} + b_{56}$ and $p_5 = a\cdot b_{61} + b\cdot b_{62} + b_{63} + b_{64} + b_{65} + b_{66}$. This relation gives the seven-point second derivative approximation at one sample point before the interface. The relation at one sample point ahead of the interface is obtained by interchanging $h_2 \rightleftharpoons -h_1$, $\psi_{+1} \rightleftharpoons \psi_{-1}$, $\psi_{+2} \rightleftharpoons \psi_{-2}$, $\psi_{+3} \rightleftharpoons \psi_{-3}$ and $n_1^2 \rightleftharpoons n_2^2$. A similar procedure is followed to find the second-derivative formula at two sample points away from the interface. In this derivation, it is assumed that the minimum number of sample points in one

layer is 6. Refer to the figure 3.5, there is an index and a mesh discontinuity at ψ_{+2}. Expanding the field on either sides of the interface in terms of ψ_{+2}, we get:

$$\psi_0 = \psi_{+2^-} - 2h_1\psi'_{+2^-} + ... + \frac{(-2h_1)^6}{6!}\psi'''''_{+2^-} + ... \quad (3.82)$$

$$\psi_{-1} = \psi_{+2^-} - 3h_1\psi'_{+2^-} + ... + \frac{(-3h_1)^6}{6!}\psi'''''_{+2^-} + ... \quad (3.83)$$

$$\psi_{-2} = \psi_{+2^-} - 4h_1\psi'_{+2^-} + ... + \frac{(4h_1)^6}{6!}\psi'''''_{+2^-} + ... \quad (3.84)$$

$$\psi_{-3} = \psi_{+2^-} - 5h_1\psi'_{+2^-} + ... + \frac{(5h_1)^6}{6!}\psi'''''_{+2^-} + ... \quad (3.85)$$

$$\psi_{+1} = \psi_{+2^-} - h_1\psi'_{+2^-} + ... + \frac{h_1^6}{6!}\psi'''''_{+2^-} + ... \quad (3.86)$$

$$\psi_{+3} = \psi_{+2^+} + h_2\psi'_{+2^+} + ... + \frac{(h_2)^6}{6!}\psi'''''_{+2^+} + ... \quad (3.87)$$

replacing all $\psi^{(n)}_{+2^+}$ derivatives with $\psi^{(n)}_{+2^-}$ derivatives in above equations and simplifying, we get:

$$\begin{aligned}\psi_{+3} = \quad & \psi_{+2^-}\left(1 + \frac{\zeta_{12}h_2^2}{2!} + \frac{\zeta_{12}^2h_2^4}{4!} + \frac{\zeta_{12}^3h_2^6}{6!}\right) + \rho_{21}\psi'_{+2^-}\left(h_2 + \frac{\zeta_{12}h_2^3}{3!} + \frac{\zeta_{12}^2h_2^5}{5!}\right) \\ & + \psi''_{+2^-}\left(\frac{h_2^2}{2!} + \frac{2\zeta_{12}h_2^4}{4!} + \frac{3\zeta_{12}^2h_2^6}{6!}\right) + \rho_{21}\psi'''_{+2^-}\left(\frac{h_2^3}{3!} + \frac{2\zeta_{12}h_2^5}{5!}\right) \\ & + \psi''''_{+2^-}\left(\frac{h_2^4}{4!} + \frac{3\zeta_{12}h_2^6}{6!}\right) + \rho_{21}\psi'''''_{+2^-}\frac{h_2^5}{5!} + \psi'''''_{+2^-}\frac{h_2^6}{6!} \end{aligned} \quad (3.88)$$

while other equations (3.85, 3.86, 3.87) remain unchanged. From Taylor's series expansion of ψ_0, that is equation 3.82, differentiating twice with respect to x, we get:

$$\psi''_0 = \psi''_{+2^-} - 2h_1\psi'''_{+2^-} + \frac{(2h_1)^2}{2!}\psi''''_{+2^-} - \frac{(2h_1)^3}{3!}\psi'''''_{+2^-} + \frac{(2h_1)^4}{4!}\psi'''''_{+2^-} - + ... \quad (3.89)$$

Following the intermediate steps, we get the final relation:

$$\psi''_0 = \quad \psi_{-3}\left(b_{26} - 2h_1b_{36} + \frac{(2h_1)^2}{2!}b_{46} - \frac{(2h_1)^3}{3!}b_{56} + \frac{(2h_1)^4}{4!}b_{66}\right) +$$

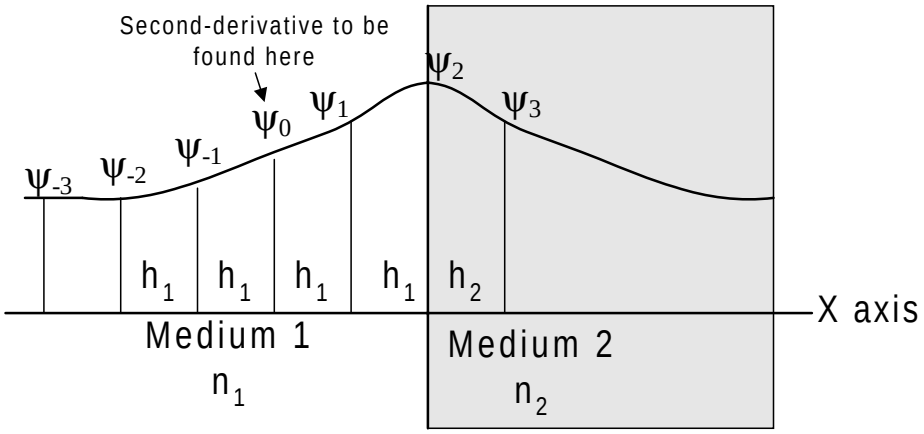

Figure 3.5: At two Points Before the Interface

$$
\begin{aligned}
&\psi_{-2}\left(b_{25}-2h_1b_{35}+\frac{(2h_1)^2}{2!}b_{45}-\frac{(2h_1)^3}{3!}b_{55}+\frac{(2h_1)^4}{4!}b_{65}\right)+\\
&\psi_{-1}\left(b_{24}-2h_1b_{34}+\frac{(2h_1)^2}{2!}b_{44}-\frac{(2h_1)^3}{3!}b_{54}+\frac{(2h_1)^4}{4!}b_{64}\right)+\\
&\psi_{+1}\left(p_1-2h_1p_2+\frac{(2h_1)^2}{2!}p_3-\frac{(2h_1)^3}{3!}p_4+\frac{(2h_1)^4}{4!}p_5\right)+\\
&\psi_{+2}\left(b_{21}-2h_1b_{31}+\frac{(2h_1)^2}{2!}b_{41}-\frac{(2h_1)^3}{3!}b_{51}+\frac{(2h_1)^4}{4!}b_{61}\right)+\\
&\psi_{+3}\left(b_{22}-2h_1b_{32}+\frac{(2h_1)^2}{2!}b_{42}-\frac{(2h_1)^3}{3!}b_{52}+\frac{(2h_1)^4}{4!}b_{62}\right)+\\
&\psi_{0}\left(b_{23}-2h_1b_{33}+\frac{(2h_1)^2}{2!}b_{43}-\frac{(2h_1)^3}{3!}b_{53}+\frac{(2h_1)^4}{4!}b_{63}\right)
\end{aligned}
\tag{3.90}
$$

where $p_1 = a \cdot b_{21} + b_{22} + b_{23} + b_{24} + b_{25} + b_{26}$, $p_2 = a \cdot b_{31} + b_{32} + b_{33} + b_{34} + b_{35} + b_{36}$, $p_3 = a \cdot b_{41} + b_{42} + b_{43} + b_{44} + b_{45} + b_{46}$, $p_4 = a \cdot b_{51} + b_{52} + b_{53} + b_{54} + b_{55} + b_{56}$ and $p_5 = a \cdot b_{61} + b_{62} + b_{63} + b_{64} + b_{65} + b_{66}$. This relation gives the seven-point second derivative approximation at two sample points before the interface. The relation at two sample points ahead of the interface is obtained by interchanging $h_2 \rightleftharpoons -h_1$, $\psi_{+1} \rightleftharpoons \psi_{-1}$, $\psi_{+2} \rightleftharpoons \psi_{-2}$, $\psi_{+3} \rightleftharpoons \psi_{-3}$ and $n_1^2 \rightleftharpoons n_2^2$.

3.7 Results

In this section, the previously developed formulae for 3-point, 5-point and 7-point approximation of the $\frac{\partial^2}{\partial x^2}$ operator are used to model a high-contrast waveguide, a low-contrast waveguide and a metal/dielectric single interface. The effective index n_{eff} and modal field of the fundamental TE and TM modes are calculated using the MoL. These MoL results are compared with analytical results and their convergence behaviour is studied by increasing the number of discretization points in the problem space. It is found that the 7-point formula gives a better estimate of n_{eff} and modal field with relatively few sample points as compared to the 5-point and the 3-point formula. The basic 3-point formula without interface conditions can not distinguish between the TE and TM polarizations and these modes appear to become degenerate. The minimum sample points in a layer are 1,3 and 5 for the 3-point, 5-point and 7-point formulations, respectively.

3.7.1 Air/GaAs/Air Symmetrical Waveguide

The waveguide structure considered is given in the inset of figure 3.6. A uniform mesh is used to model the waveguide and the number of sample points are varied while keeping the outer layer thickness sufficiently large so that the modal field decays sufficiently to a small value $\approx 10^{-5}$ as compared to its value at the $Air/GaAs$ interface. If the mesh is prematurely terminated by an electric/magnetic wall boundary condition, it interacts with the exponentially decaying field and affects the re-

sults. The phase parameter is defined as $B_o = \frac{n_{eff}^2 - 1^2}{3.6^2 - 1^2}$. The analytical values of the TE_0 mode are $n_{eff} = 3.54396160934$ and $B_o = 0.96652708097$, and for the TM mode are $n_{eff} = 3.5294344200389$ and $B_o = 0.95793539509$ (see Appendix A). The error $B_{MoL} - B_o$ is plotted against the number of sample points in the middle layer. The normalized error between the analytical mode and the MoL results is also plotted in figure 3.8. The results show the superiority of the 5-point and the 7-point formulation to find n_{eff} and modal field for both the TE and TM polarization as compared to the 3-point formulation. The monotonic convergence behaviour of the MoL is also evident from the results and an extrapolation to the analytical value can be made.

3.7.2 GaAlAs/GaAs/GaAlAs Symmetrical Waveguide

The waveguide structure considered here is given in the inset of figure 3.9 and is taken from [34]. The phase parameter is defined as $B_o = \frac{n_{eff}^2 - 3.4^2}{3.6^2 - 3.4^2}$. The analytical values for the TE mode are $n_{eff} = 3.42438294476$ and $B_o = 0.60818184356$, and for the TM mode are $n_{eff} = 3.424171841369$ and $B_o = 0.602897658$. The phase parameter B_{MoL} is plotted against the number of sample points in the middle layer. The modeling scheme is same as described in the previous section. In [34], the problem space is prematurely terminated close to the interface where the field has not sufficiently decayed. Thus our results are not directly comparable with those of [34]. Nevertheless, the 5-point and the 7-point formulations give better results

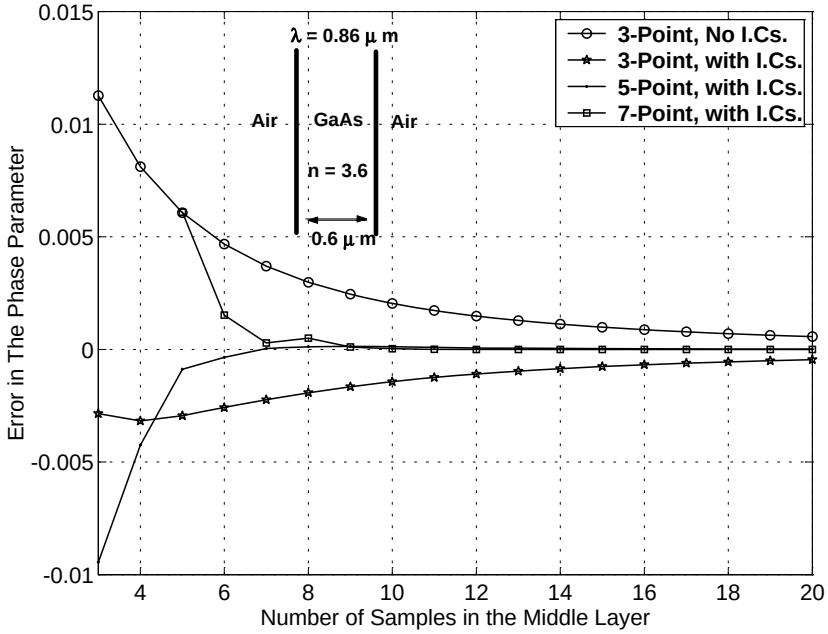

Figure 3.6: Error in Phase Parameter ($B_{MoL} - B_o$) for the TE_0 Mode

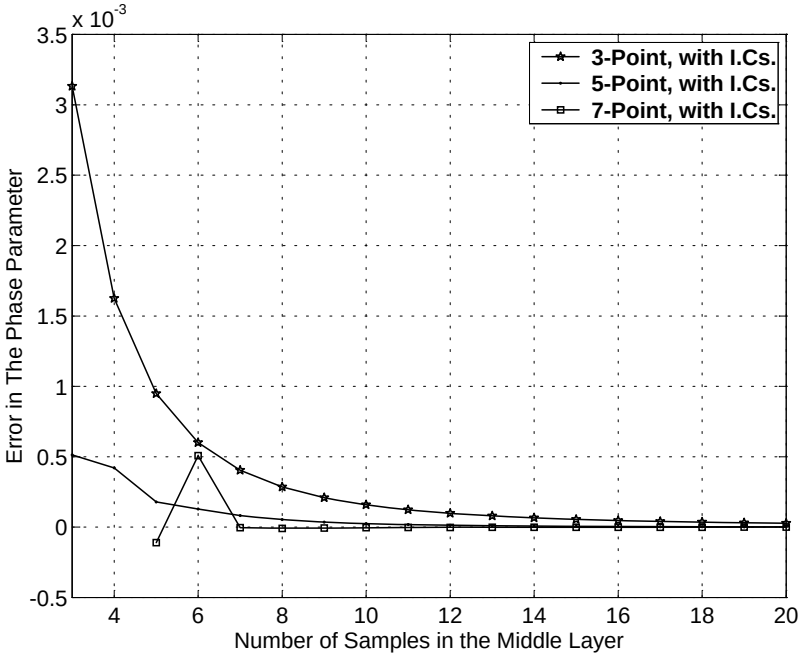

Figure 3.7: Error in Phase Parameter ($B_{MoL} - B_o$) for the TM_0 Mode

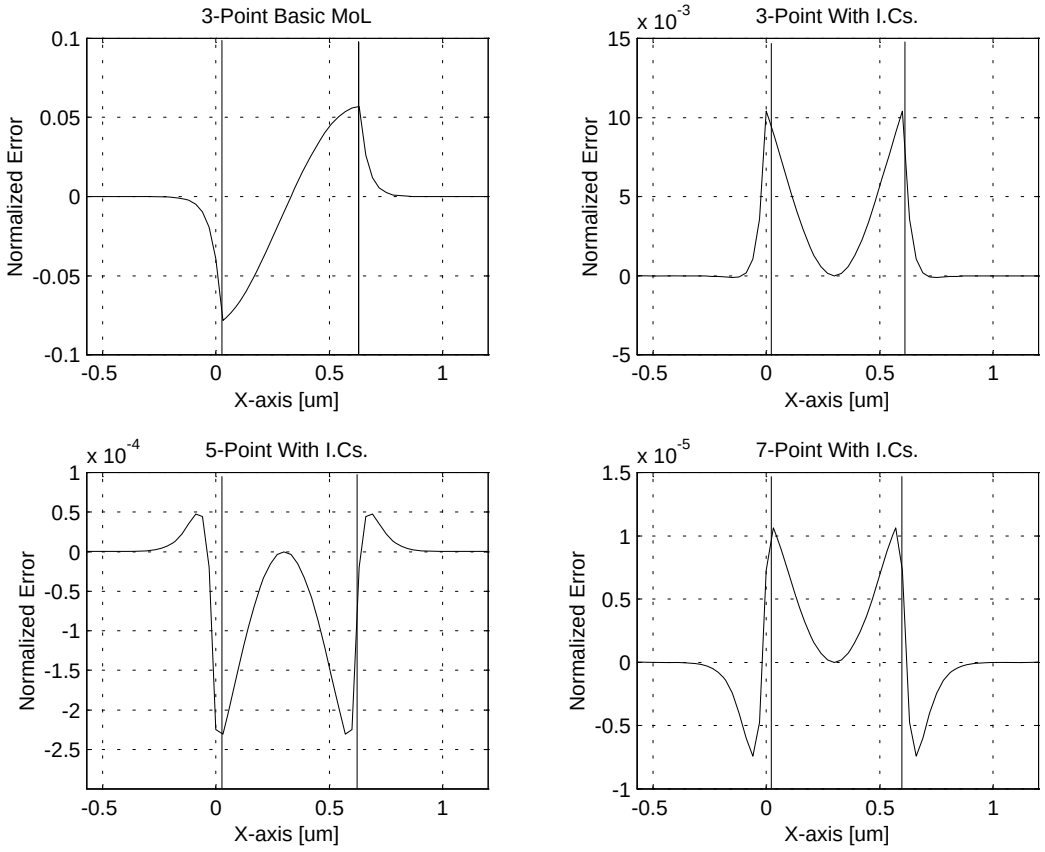

Figure 3.8: Error in the TE_0 Modal Field, (Analytical - Numerical)

than the formulation used in reference [34] and the 3-point formulation gives similar accuracy. In [35, 36, 37] higher-order approximations for the MoL is developed. Our scheme is different from them as we *always* place a mesh point on the interface and account for the necessary discontinuity in both the E or H field including their higher derivatives in Taylor's series expansion. In other schemes [29], the interface is placed somewhere in between the mesh points and its position has to be optimized for different waveguides. Moreover, they ignore the discontinuity in higher-order derivatives of the E or H field while using Taylor's series expansion. Some schemes are based on taking the *average* of the right and left layer refractive indices at an interface. We always take the refractive index at an interface point to be either of the left layer index at $x = 0^-$ or the right layer index at $x = 0^+$.

3.7.3 Metal/Dielectric Surface Plasmon Mode

The single interface between a metal (most often, silver or gold) and a dielectric, as shown in the inset of figure 3.11, supports surface plasmon modes. These modes are TM polarized and are characterised by a field, called *evanescent* field, that decays exponentially on both sides of the interface. The field decays very fast inside the metal while its decay in the dielectric layer is much slower. Surface plasmon modes are known to be lossy with a complex propagation constant [27]. They can only exist as surface waves at a metal/dielectric interface when the complex dielectric constant of the metal has a negative real part. An analytic expression exist to find

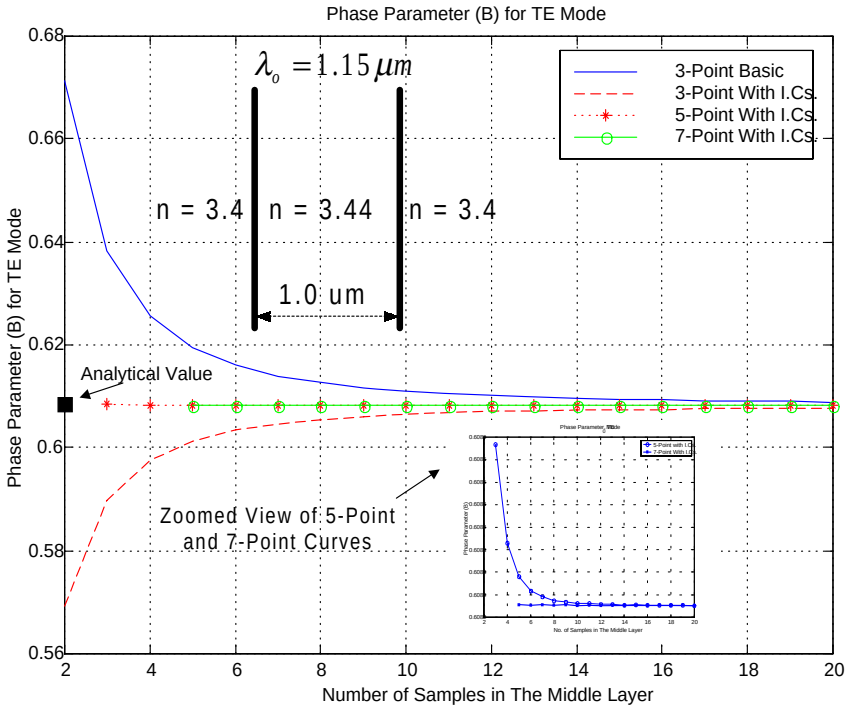

Figure 3.9: Convergence of Phase Parameter B_{MoL} for the TE_0 Mode

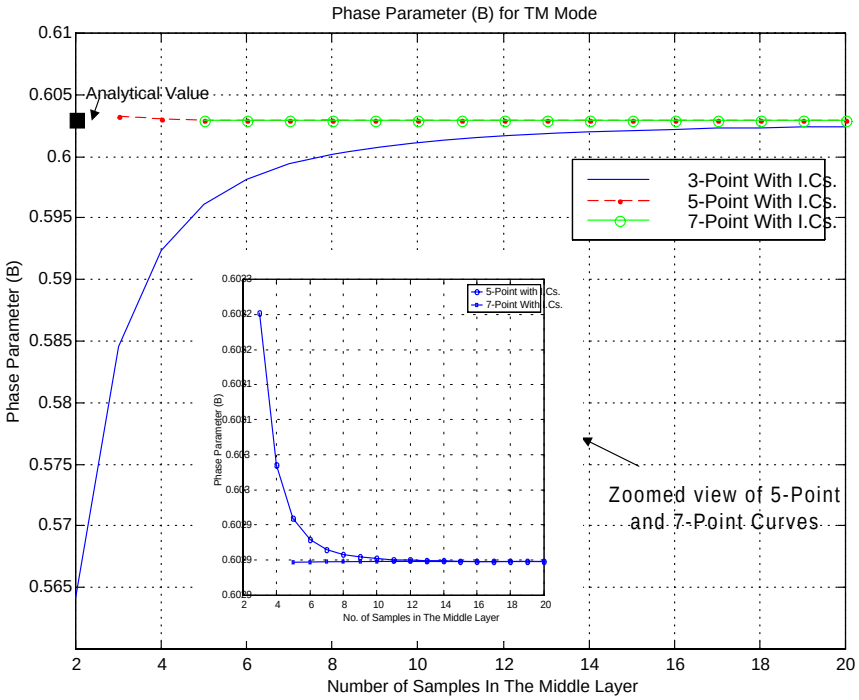

Figure 3.10: Convergence of Phase Parameter B_{MoL} for the TM_0 Mode

the propagation constant β and the effective index of the structure, that is:

$$n_{eff} = \sqrt{\frac{\epsilon_{r1}\epsilon_{r2}}{\epsilon_{r1} + \epsilon_{r2}}} \tag{3.91}$$

In this example, the operating wavelength is $\lambda = 0.6328\mu m$. The problem space is divided into many *artificial* layers and a non-uniform discretization scheme is used to sample the waveguide effectively. A fine mesh is used in regions of fast field decay and a coarse mesh is employed in regions of slow field decay. This decreases the total sampling points considerably as compared to a uniform sampling scheme. The mesh scheme is kept same and effective index is calculated and compared against analytical value for the 3-point, the 5-point and the 7-point formulations. The results are given in table 3.1. It is found that the 7-point formulation gives better results than the 5-point or the 3-point schemes. The basic 3-point formulation without inclusion of interface conditions can not be used to model this problem. Our scheme can include materials having *complex* refractive index (e.g. metals and lossy dielectric materials) into the MoL in a unified way while others [38, 39] have to use specialized finite-difference formulation to model such materials.

Total number of Lines	3-Point	5-Point	7-Point
40	1.2777e-3	1.3884e-4	1.1763e-5
50	3.6511e-4	5.5902e-6	1.6812e-8
70	1.8689e-4	1.4497e-6	1.1039e-8
100	9.1737e-5	3.3788e-7	1.1815e-8

Table 3.1: Absolute Error in the real part of n_{eff} for the Surface Plasmon mode, Analytical $n_{eff} = 1.0326549624$

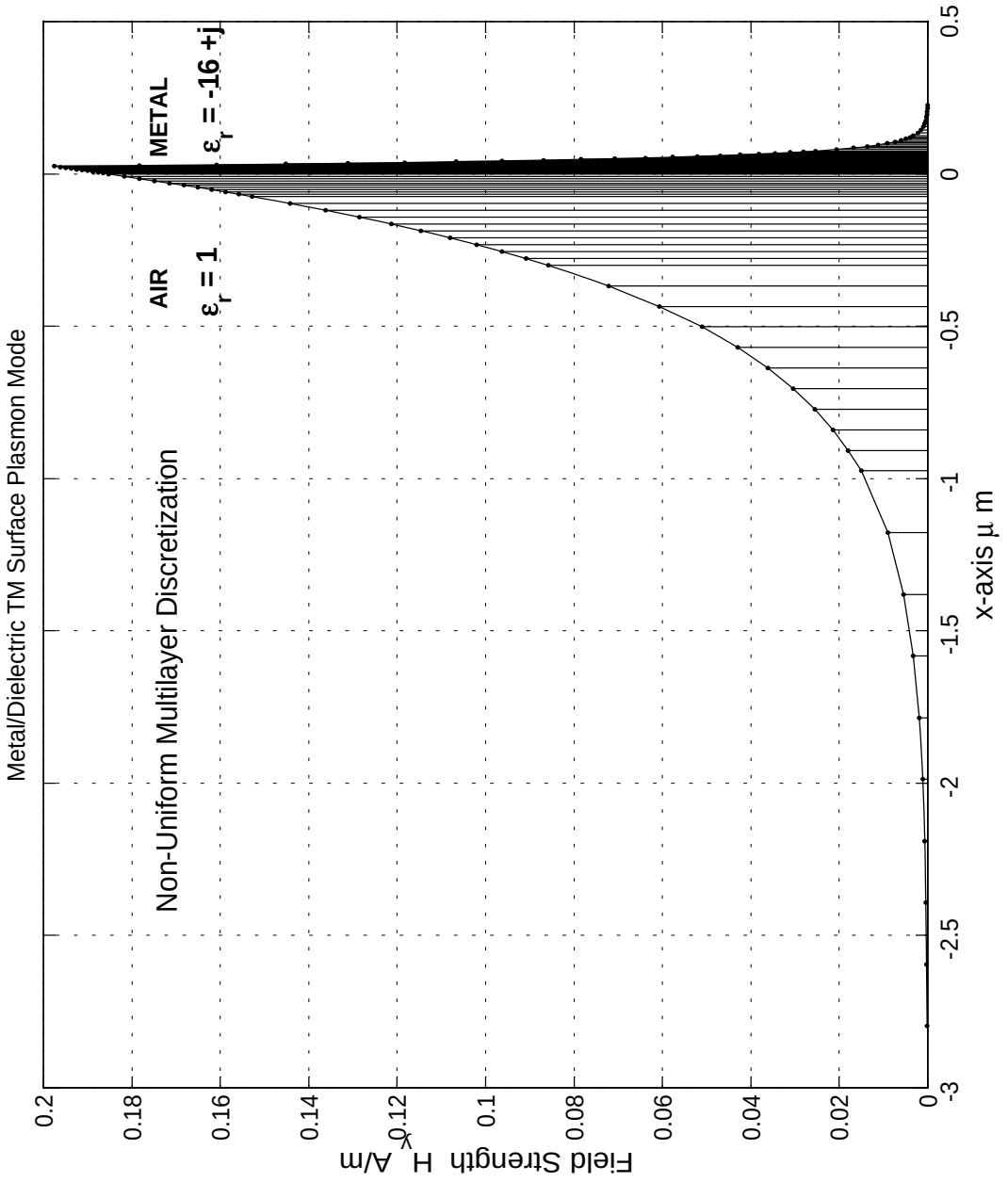

Figure 3.11: A Metal-Dielectric Surface Plasmon Mode

3.7.4 Field Propagation using the MoL

A high-contrast $Air/GaAs/Air$ waveguide (see figure 3.6) is modeled and the *analytical* TM_o mode is propagated in the z direction using the MoL. The modal field propagates without changing its shape and without any power loss even for a long distance as shown is figure 3.12. When a Gaussian shaped mode is launched in the waveguide, its shape changes considerably as it propagates along the waveguide. The energy *outside* the TM_o mode leaks from the waveguide as it correspond to a continuous spectrum of radiation modes. The problem space is terminated with a magnetic wall boundary condition where $H_y = 0$. So the energy reflects back from the wall and the ripples are evident as seen in figure 3.13. This depicts that we are not simulating an open-space at the mesh termination. This necessitates the need of an appropriate method to model open-space at mesh boundary, so that the radiated waves do not reflect back from the mesh boundary and enter the problem space thus corrupting the computational results. Such schemes, called Absorbing Boundary Conditions, do exist and are discussed in the next chapter.

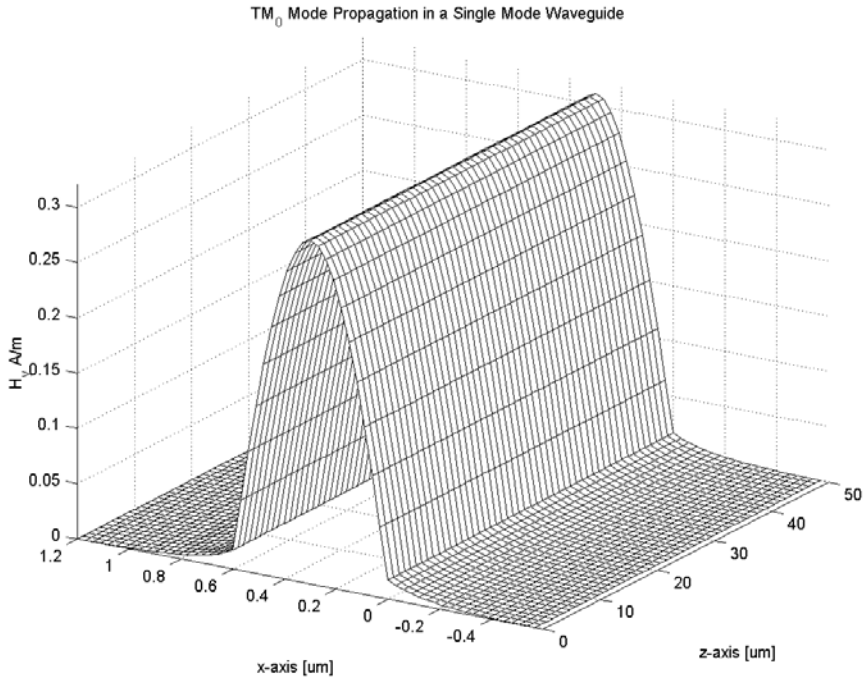

Figure 3.12: The TM_0 Modal Field Propagation in a Slab Waveguide

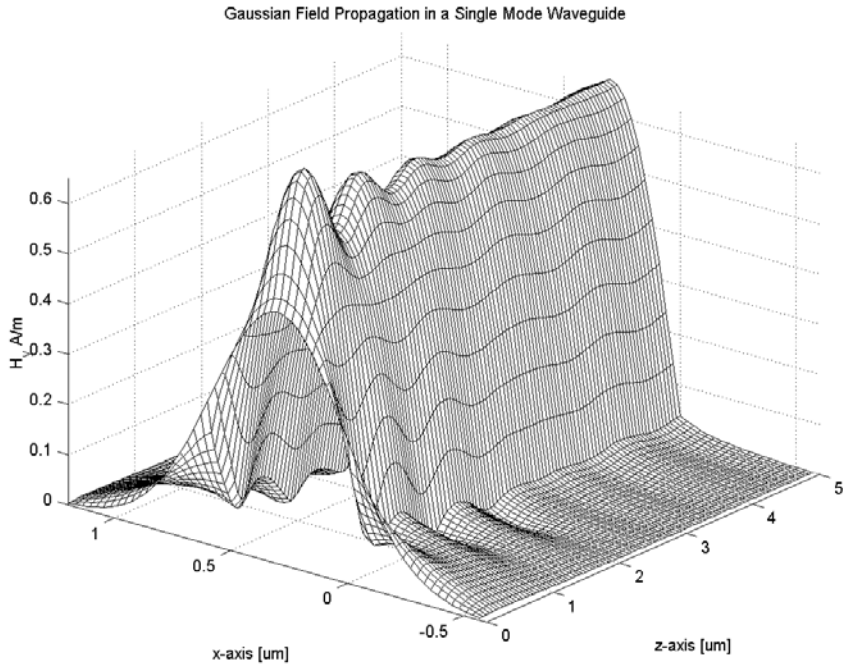

Figure 3.13: Gaussian Field Propagation in a Slab Waveguide

Chapter 4

Analysis of Single and Multiple Waveguide Discontinuities

4.1 Introduction

Discontinuity problems are important in the investigation of optical devices, such as laser facets, gratings, waveguide ends, and connections of different waveguide sections. The classic problem to model scattering from single and multiple discontinuities has been solved by many researchers using different analytical and numerical methods such as the Mode Matching Method [3], the Method of Lines [21, 23, 40, 24] and the Equivalent Transmission-Line Network Method [41]. A good reference to these methods is given in [3][42]. The MoL has been applied to solve a non-linear scattering problem from single discontinuity [43] and surface-plasmon mode scattering problems [44, 45]. In this chapter, the necessary mathematical formulation

to model this structure using the Method of Lines will be explained. A recursive algorithm based on the MoL will be explained. This scheme can be used to model multiple discontinuities and gratings.

4.2 Absorbing Boundary Conditions

In order to model *free space* at the boundaries of the problem space, absorbing boundary conditions are required to terminate the problem space. If we use electric/magnetic wall boundary condition with either $E_y = 0$ or $H_y = 0$, it will reflect back the radiative waves into the problem space and hence corrupt the computed results. The use of an appropriate numerical absorbing boundary conditions in the finite-difference simulation of wave equation in an open space region is necessary because it will limit the computational domain width and absorb the outgoing waves.

4.2.1 Mur's ABC Absorber

One such absorbing boundary condition is based on factorizing the two-way wave equation and approximate a one-way wave equation [46]. The scalar wave equation for the TE waves in two-dimensional rectangular coordinate system is:

$$\frac{\partial^2 \psi}{\partial x^2} + \frac{\partial^2 \psi}{\partial z^2} - \frac{1}{c^2}\frac{\partial^2 \psi}{\partial t^2} = 0 \tag{4.1}$$

Using the operator notation, the above equation can be expressed as:

$$\hat{L}\psi \equiv D_x^2 \psi + D_z^2 \psi - \frac{1}{c^2} D_t^2 \psi = 0 \tag{4.2}$$

where Ψ represents E_y and $\hat{L}$ is the two-way wave operator. By factorizing the wave operator, we get:

$$\hat{L}\psi = \hat{L}^{+}\hat{L}^{-}\psi = 0 \tag{4.3}$$

where

$$\hat{L}^{+} \equiv D_x + \frac{D_t}{c}\sqrt{1 - \frac{c^2 D_z^2}{D_t^2}} \quad \text{and} \quad \hat{L}^{-} \equiv D_x - \frac{D_t}{c}\sqrt{1 - \frac{c^2 D_z^2}{D_t^2}} \tag{4.4}$$

The $\hat{L}^{+}$ operator represents the wave propagating in the $+x$ direction and $\hat{L}^{-}$ represents the wave propagating in the $-x$ direction. Each operator represents the one-way wave equation. With reference to figure 3.1, the application of $\hat{L}^{+}$ operator at the top of the problem space will absorb waves propagating in the $+x$ direction. Similarly application of $\hat{L}^{-}$ operator at the bottom of the problem space will absorb waves propagating in the $-x$ direction. The radical function in the one-way wave equation can be approximated by a Taylor's series expansion. Taking the first two terms of the expansion only:

$$\hat{L}^{-} = D_x - \frac{1}{c}D_t + \frac{c}{2}\frac{D_z^2}{D_t} \tag{4.5}$$

To prevent the reflections from the bottom , we consider:

$$\hat{L}^{-}\psi_1 = \left[D_t^{-1}(D_x D_t - \frac{1}{c}D_t^2 + \frac{c}{2}D_z^2)\right]\psi_1 = 0 \tag{4.6}$$

since $D_t^{-1}\psi_1 \neq 0$, we get:

$$\frac{\partial^2\psi_1}{\partial x \partial t} - \frac{1}{c}\frac{\partial^2\psi_1}{\partial t^2} + \frac{c}{2}\frac{\partial^2\psi_1}{\partial z^2} = 0 \tag{4.7}$$

we have assumed a time dependence of the form $e^{-j\omega t}$, so :

$$-j\omega\frac{\partial\psi_1}{\partial x}+\frac{\omega^2}{c}\psi_1+\frac{c}{2}\frac{\partial^2\psi_1}{\partial z^2}=0 \tag{4.8}$$

the finite-difference approximation of $\frac{\partial}{\partial x}$ operator using Taylor's series expansion 3.25, 3.26 and the interface conditions 3.37, 3.38, 3.39, we get:

$$\psi_{0-}^{'}=\frac{\psi_{+1}-\tau_{21}^2\psi_{-1}+\psi_0(\tau_{21}^2-1-0.5h_2^2\zeta_{12})}{\tau_{21}^2h_1+h_2\rho_{21}} \tag{4.9}$$

where $\tau_{21}=\frac{h_2}{h_1}$ and $\zeta_{12}=k_o^2(n_1^2-n_2^2)$. Note that in region of uniform refractive index and uniform mesh, equation 4.9 reduces to the regular formula $\frac{1}{2h}(\psi_{+1}-\psi_{-1})$ which is applicable in our case. From equation 4.8, we get:

$$\frac{\partial^2\psi_1}{\partial z^2}=\frac{2j\omega}{c}\left[\frac{\psi_2-\psi_0}{2\Delta x}+\frac{j\omega\psi_1}{c}\right] \tag{4.10}$$

where $c=c_o/n$ and $k_o=\omega/c_o$, c_o is the speed of light in free space and n is the refractive index of the material. The incorporation of equation 4.10 into wave equation 3.27 at the bottom of problem space at the grid line $i=1$, we get:

$$2jk_on\left[\frac{\psi_2-\psi_0}{2\Delta x}+jk_on\psi_1\right]+\frac{\psi_2-2\psi_1+\psi_0}{(\Delta x)^2}+k_o^2n^2\psi_1=0 \tag{4.11}$$

simplifying:

$$\psi_0=\left[\frac{2+k_o^2n^2(\Delta x)^2}{1-jk_on\Delta x}\right]\psi_1-\left[\frac{1+jk_on\Delta x}{1-jk_on\Delta x}\right]\psi_2 \tag{4.12}$$

A similar procedure can be adopted at the top of the problem space to express ψ_{m+1} in terms of ψ_m and ψ_{m-1}. So :

$$\psi_0 = -a_{bot}\psi_1+b_{bot}\psi_2 \tag{4.13}$$

$$\psi_{m+1} = b_{top}\psi_{m-1}-a_{top}\psi_m \tag{4.14}$$

where:

$$a = -\frac{2 + k_o^2 n^2 (\Delta x)^2}{1 - jk_o n \Delta x} \quad \text{and} \quad b = -\frac{1 + jk_o n \Delta x}{1 - jk_o n \Delta x} \tag{4.15}$$

By incorporating this into the MoL matrix C, we get:

$$C = \frac{1}{(\Delta x)^2} \begin{bmatrix} -(2 + a_{bot}) & (1 + b_{bot}) & & & & & \\ 1 & -2 & 1 & & \mathcal{O} & & \\ & 1 & -2 & 1 & & & \\ & & & \ddots & & & \\ & & \mathcal{O} & 1 & -2 & 1 & \\ & & & & (1 + b_{top}) & -(2 + a_{top}) & \end{bmatrix}$$

Field Propagation in a Slab Waveguide:

A slab waveguide with refractive index distribution 1/3.6/1 and core width $0.3\,\mu m$ is modeled. The operating wavelength is chosen to be $0.86\,\mu m$. The mesh boundary is terminated with Mur's ABC on both sides of the problem space. A TM polarized fundamental mode field added with some random noise is impressed at the input end of the waveguide and its propagation along the z direction is observed. The results are plotted in the figures 4.1-4.6. After propagating a certain distance, The field in the guide layer is seen to develop to the fundamental TM_o mode of the waveguide. The field in the outer layers has some energy which corresponds to the TM_0 mode.

This residual energy does not vanish even after propagating a long distance. This shows that the Mur's ABC used causes considerable reflection and is not perfectly absorbing the radiative field. This shows the poor absorption characteristics of this ABC in this case.

4.2.2 Perfectly Matched Layer PML Absorber

The PML absorbing scheme based on complex distance approach was first incorporated into the MoL By Dr. Al-Bader and Dr. Al-Jamid [47]. It has been shown in the literature that the PML can absorb propagating waves over a wide range of incident angles [47] and the reflected field is extremely small. The absorbtion of the *radiative* wave is done by changing the distance x from *real* to *imaginary*. This introduces an numerical attenuation factor in the radiative field and hence causes decay of the radiative field in the PML region. The last mesh point is terminated by an electric/magnetic wall boundary condition. The *real* distance is transformed to a *complex* one according to:

$$x \rightarrow x(1 + j\sigma) \tag{4.16}$$

$$dx \rightarrow dx(1 + j\sigma) \tag{4.17}$$

here σ is the decay factor constant. The wave e^{+jkx} propagating in $+x$ direction in the real space will be converted to

$$e^{+jkx(1+j\sigma)} = e^{+jkx}e^{-k\sigma x} \tag{4.18}$$

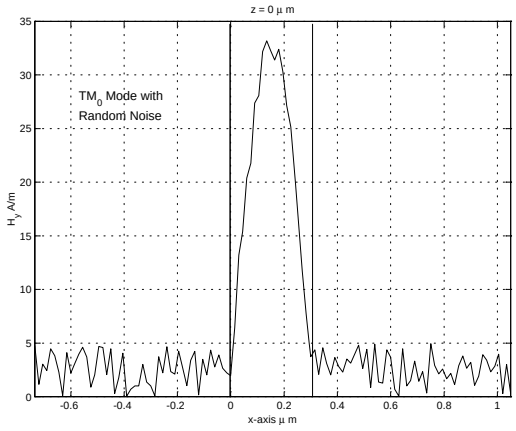

Figure 4.1: Input TM_0 Field, z = 0 μm

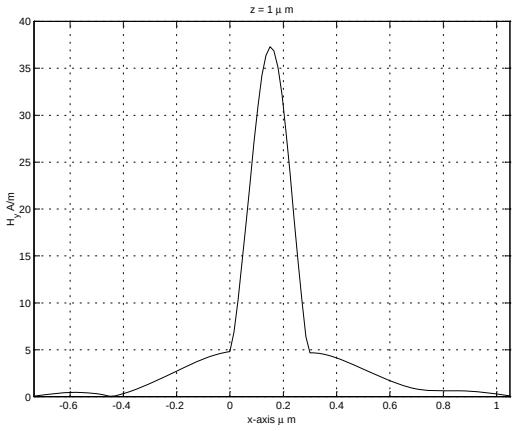

Figure 4.2: Transmitted Field, z = 1 μm

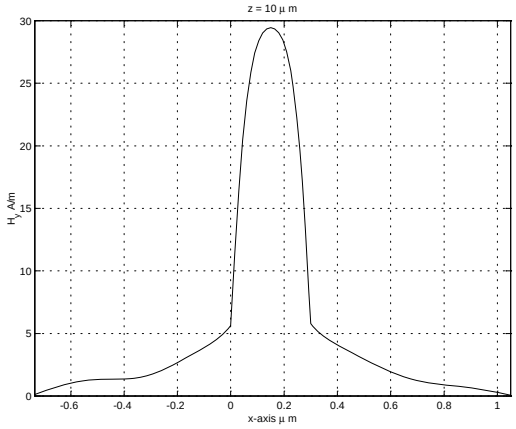

Figure 4.3: Field at z = 10 μm

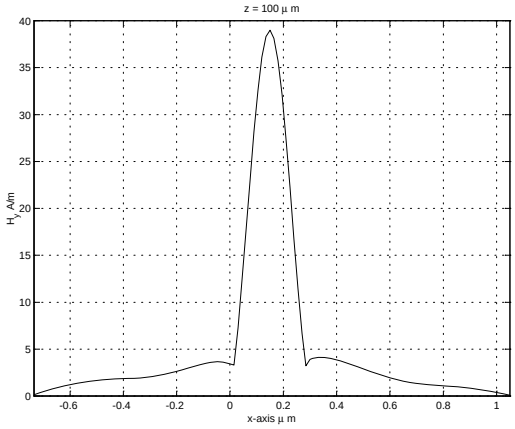

Figure 4.4: Field at z = 100 μm

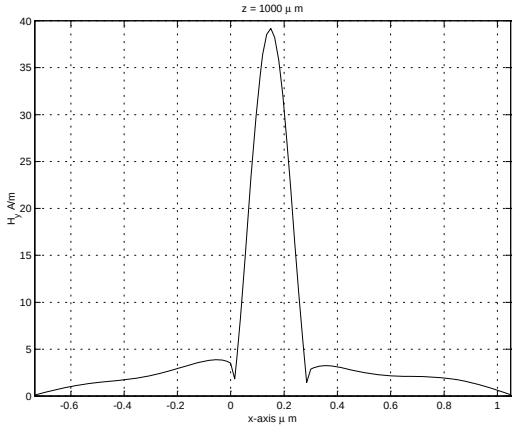

Figure 4.5: Field at z = 1000 μm

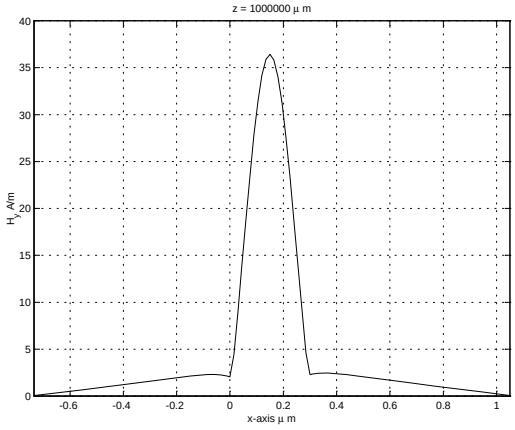

Figure 4.6: Field at z = 1000000 μm

in complex space. The factor $e^{-k\sigma x}$ causes the decay of the field in the $+x$ direction in the complex space. The value of σ is set arbitrarily and the number of samples in the PML absorber is chosen to cause a significant decay in the field so that it is not reflected by the electric/magnetic wall. This absorbing scheme is incorporated into the MoL and used throughout this thesis.

Gaussian Field Propagation in Air:

The performance of PML is analyzed by modeling free-space surrounded by PML layers on both sides. A Gaussian field is launched in air and its propagation along the z direction is observed (see figures 4.8-4.16). An analytical expression based on scalar diffraction theory is used to calculate the spread of Gaussian field [27] as it propagates in a medium. The MoL propagated field is compared against the analytically propagated field over a large distance. Each PML layer has 5 points with $\sigma = 1$. A non-uniform double layer scheme as shown in figure 4.17 is used to model a relatively *thicker* PML. Thus, the field magnitude at the last mesh point drops considerably due to the $e^{-k\sigma x}$ factor appearing in equation 4.18 . The problem space is finally terminated by an electric/magnetic wall. The visual comparison of the analytical field and the MoL computed field shows that the two fields are almost identical over a long propagation distance. This shows the superior performance of the PML as compared to Mur's ABC in absorbing radiative fields and correctly modeling open-space.

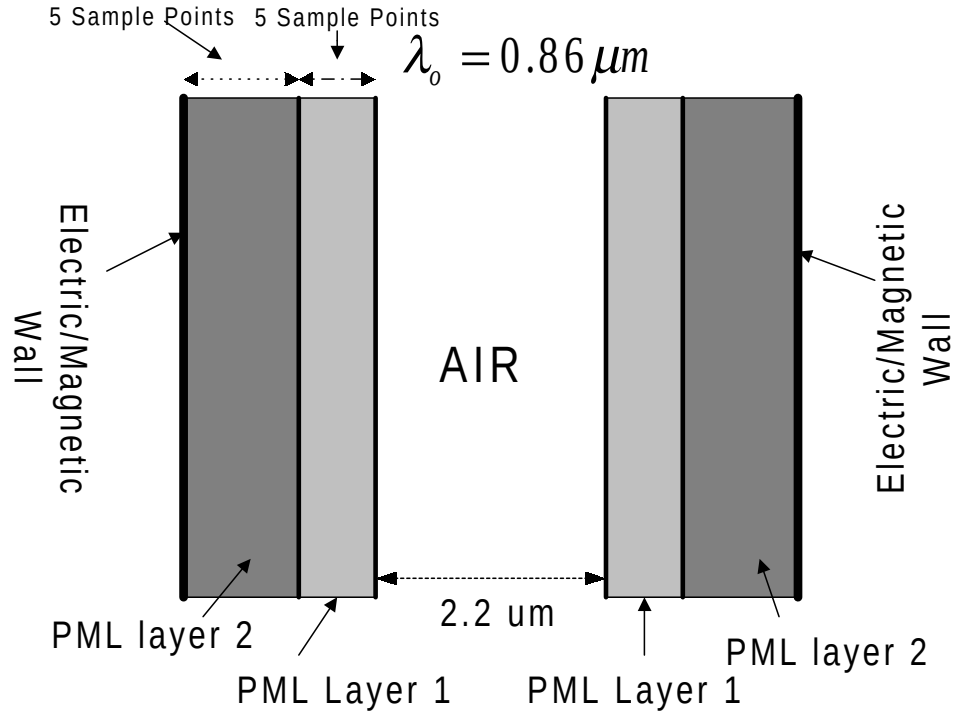

Figure 4.7: A Perfectly Matched Layer (PML) Scheme

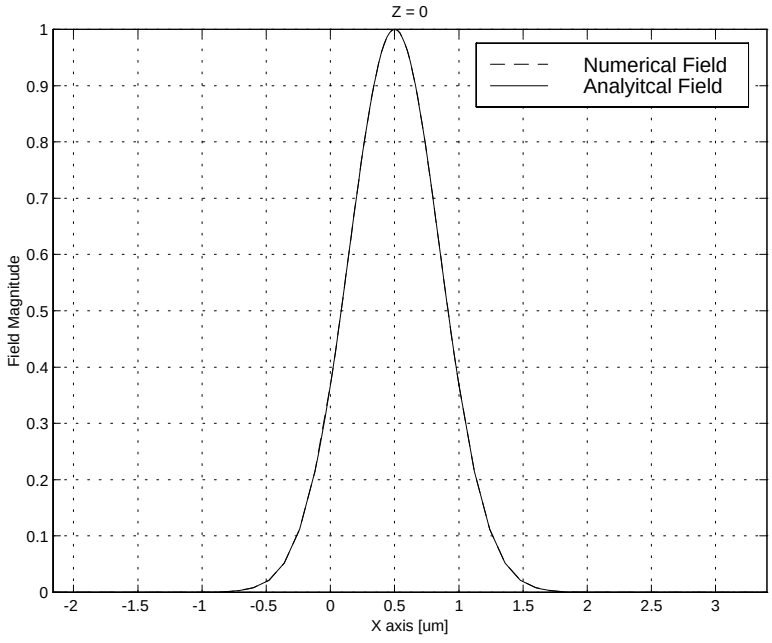

Figure 4.8: Incident Gaussian Field at z = 0

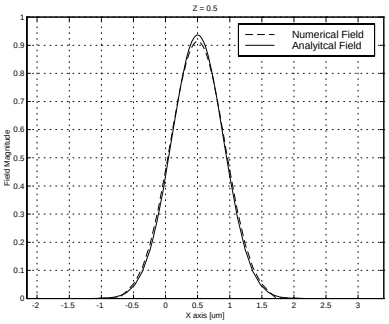

Figure 4.9: Field at z = 0.5 μm

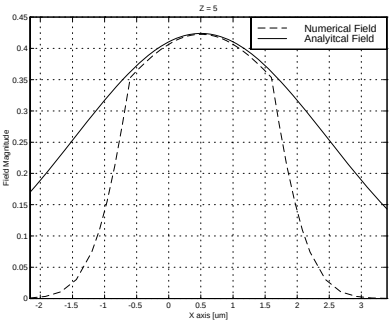

Figure 4.10: Field at z = 5.0 μm

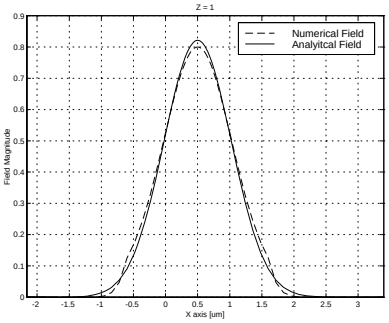

Figure 4.11: Field at z = 1.0 μm

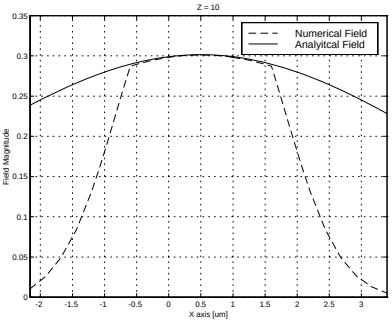

Figure 4.12: Field at z = 10.0 μm

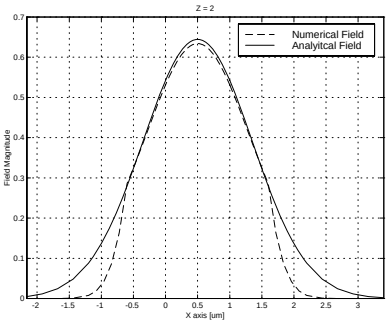

Figure 4.13: Field at z = 2.0 μm

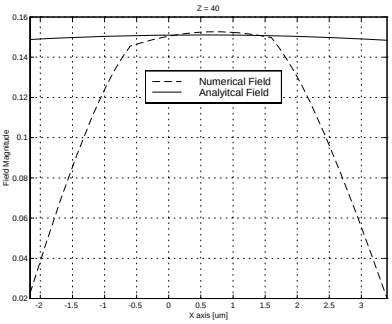

Figure 4.14: Field at z = 40.0 μm

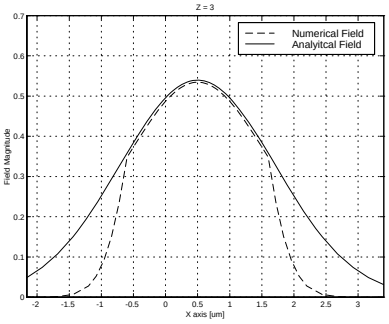

Figure 4.15: Field at z = 3.0 μm

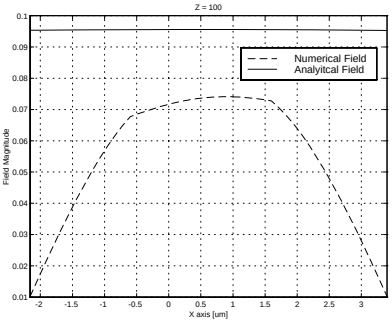

Figure 4.16: Field at z = 100.0 μm

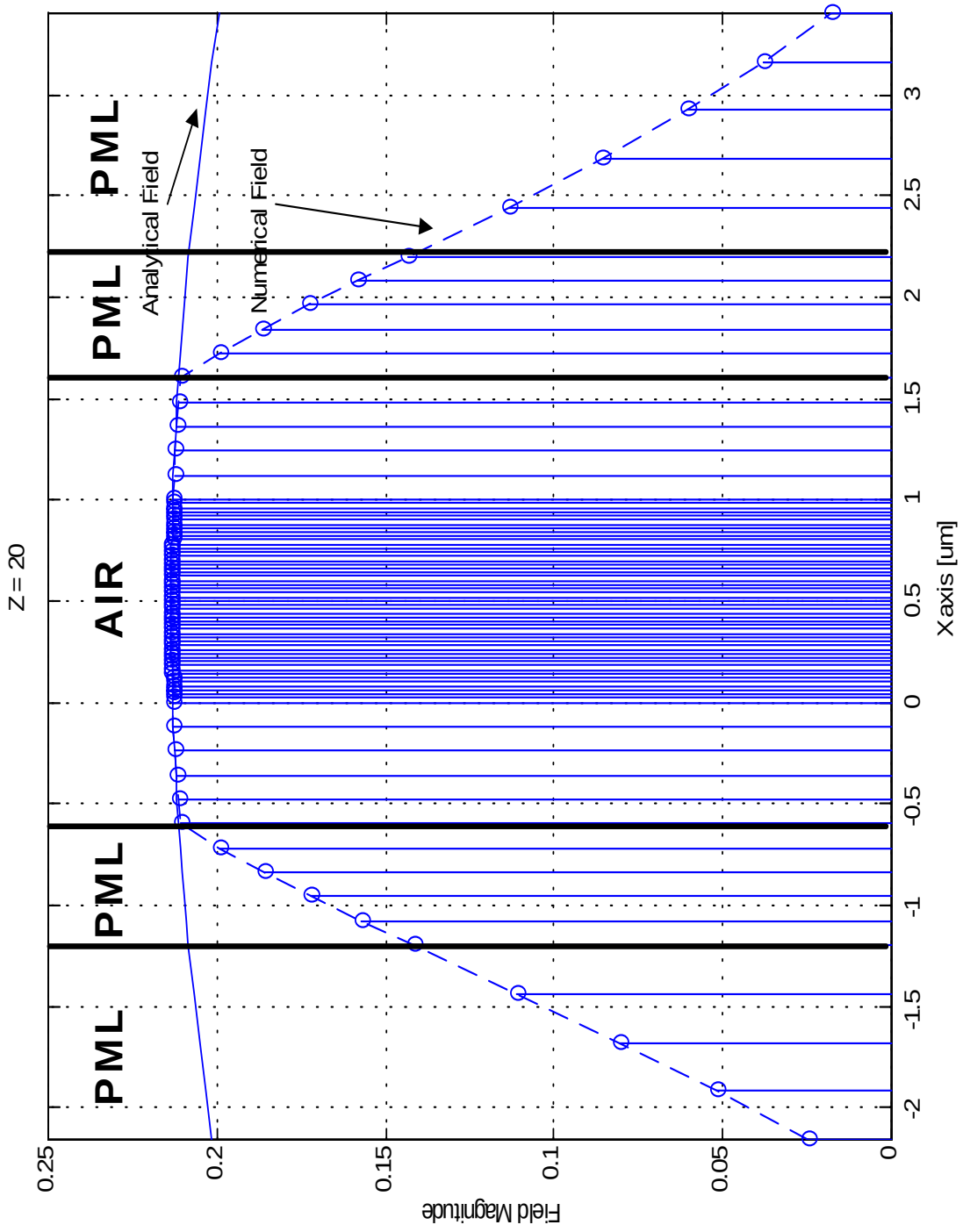

Figure 4.17: Non-Uniform Mesh Scheme, Field at z = 20 μm

Field Propagation in a Slab Waveguide:

A slab waveguide with refractive index distribution 1/3.6/1 and guide layer width $0.3\,\mu m$ is surrounded by a single layer PML with $\sigma = 1$. A uniform mesh is employed and operating wavelength is $0.86\,\mu m$ with TM polarization. The TM_o mode with some random noise added (see figure 4.18) is launched in the waveguide and its propagation observed. As shown in figures 4.19, 4.20 and 4.21, the noisy field develops into the TM_o mode and the radiative energy *outside* the fundamental mode leaks out from the device. There are no ripples is the field showing that the PML reflects little power back into the problem space.

In another test, a very sharp Gaussian pulse in launched into the waveguide and its propagation observed. As shown in figure 4.22, the pulse develops into the TM_o mode after propagating some distance and the energy outside the fundamental mode leaks. This shows the excellent performance of the PML over a wide range of incident angles as the sharp pulse has a broad angular spectrum.

4.3 Single Discontinuity

With reference to figure 4.23, the problem space is divided into two regions, region (0) and region (1). The field is incident from region (0). After reflection from the discontinuity, there is a reflected field in region (0) and a transmitted field in region (1). The total field in each region is the sum of the forward and the backward

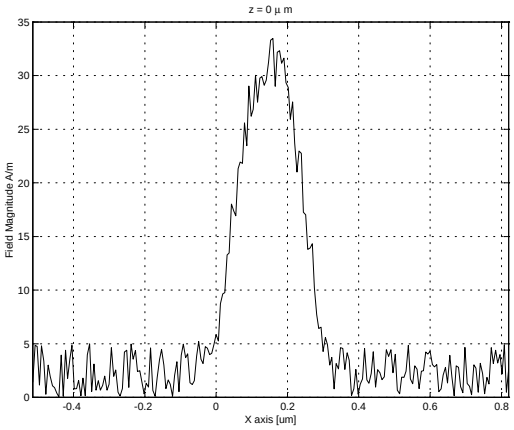

Figure 4.18: TM_0 Field with Noise

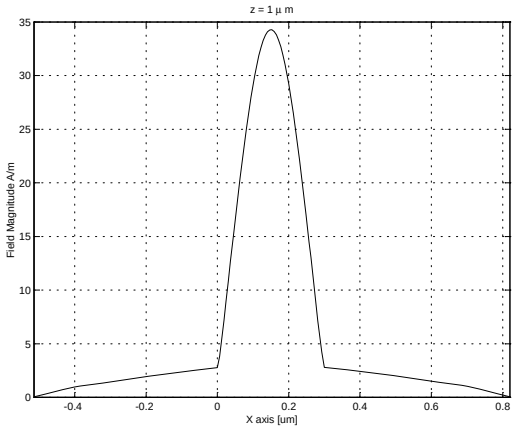

Figure 4.19: Field at z = 1 μm

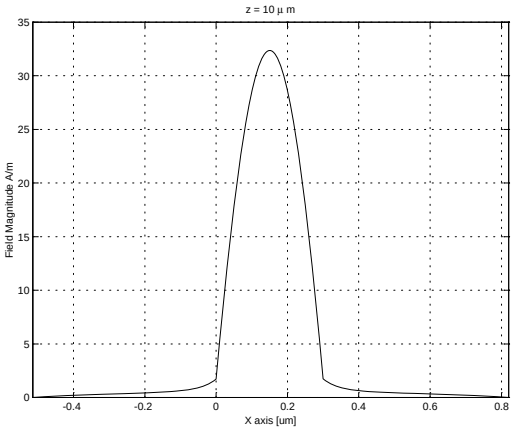

Figure 4.20: Field at z = 10 μm

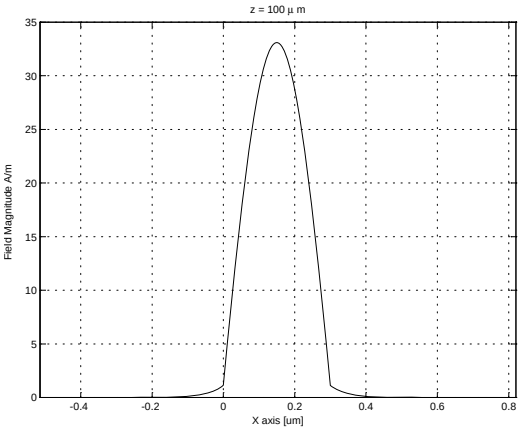

Figure 4.21: Field at z = 100 μm

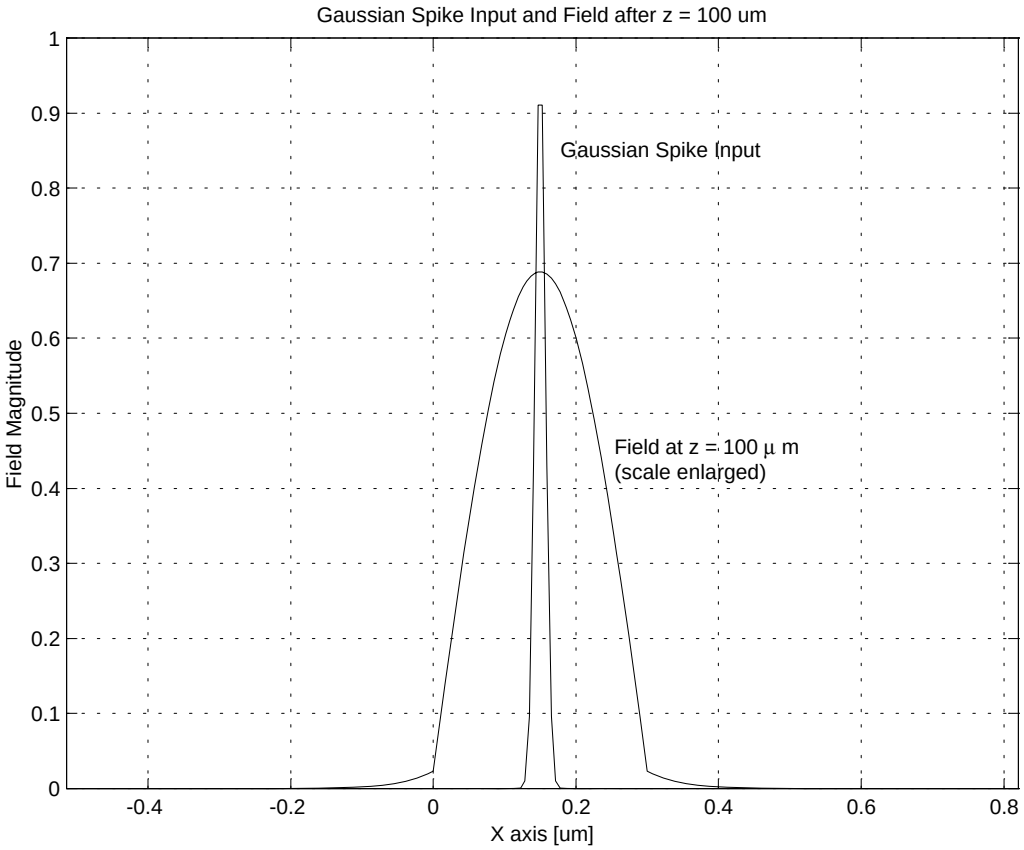

Figure 4.22: A Gaussian Spike Input and its Propagation

traveling field: [1]

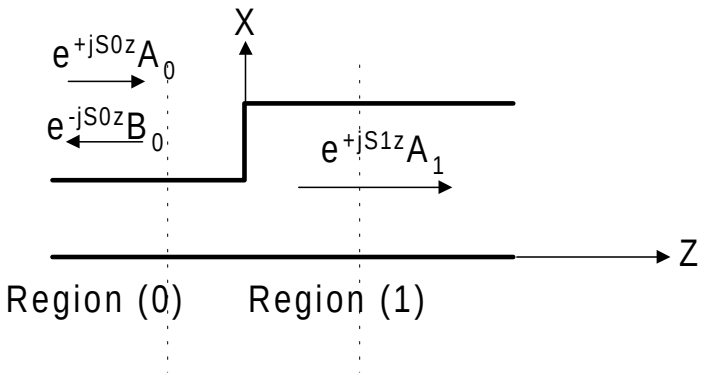

Figure 4.23: A Single Waveguide Discontinuity

$$\Psi_0 = e^{+jS_0z}A_0 + e^{-jS_0z}B_0 \tag{4.19}$$

$$\Psi_1 = e^{+jS_1z}A_1 \tag{4.20}$$

where Ψ is a column vector representing the field at the sample points, A_0, B_0, A_1 are constant vectors, $S = \sqrt{Q}$ and Q is defined in chapter 3. For TM polarization, Ψ is continuous at the interface at $z = 0$, thus $\Psi_0|_{z=0} = \Psi_1|_{z=0}$. From equation 4.19

$$A_0 + B_0 = A_1 \tag{4.21}$$

from the interface condition equation 3.24, at the *ith* discretization line, the field on either side of the discontinuity at $z = 0$ is related by

$$\frac{\psi'_{iz-}}{n^2_{iz-}} = \frac{\psi'_{iz+}}{n^2_{iz+}} \tag{4.22}$$

The *prime* superscript represents derivative with respect to z, normal to the interface. For all the discretization lines, the set of equations 4.22 can be put together

[1] It is emphasized that these field variables represent the steady-state values at a single frequency after all the transients have died away.

in one matrix equation of the form:

$$N_0^{-1}\Psi_0^{'} = (N_1)^{-1}\Psi_1^{'} \tag{4.23}$$

where the matrix N is a diagonal matrix of refractive index squared n_i^2 at each sample point. From equation 4.19, differentiating with respect to z, we have:

$$\Psi_0^{'} = jS_0e^{jS_0z}A_0 - jS_0e^{-jS_0z}B_0 \tag{4.24}$$

at the interface:

$$\Psi_0^{'}|_{z=0} = jS_0(A_0 - B_0) \tag{4.25}$$

similarly:

$$\Psi_1^{'}|_{z=0} = jS_1A_1 \tag{4.26}$$

substitute the last two equations in equation 4.23, and simplifying:

$$(N_0)^{-1}S_0(A_0 - B_0) = (N_1)^{-1}S_1A_1 \tag{4.27}$$

$$(A_0 - B_0) = S_0^{-1}(N_0)(N_1)^{-1}S_1A_1 \tag{4.28}$$

Eliminating B_0 and simplifying, we get the transmitted field A_1 in terms of A_0:

$$A_1 = 2(I + S_0^{-1}N_0N_1^{-1}S_1)^{-1}A_0 \tag{4.29}$$

Eliminating A_0 and simplifying, we get the reflected field at $z = 0$:

$$B_0 = (I - S_0^{-1}N_0N_1^{-1}S_1)(I + S_0^{-1}N_0N_1^{-1}S_1)^{-1}A_0 \tag{4.30}$$

Putting the above two equations in words:

$$\begin{bmatrix} Transmitted \\ Field \\ Vector \end{bmatrix} = \begin{bmatrix} Transmission \\ Coefficient \\ Matrix \end{bmatrix} \begin{bmatrix} Incident \\ Field \\ Vector \end{bmatrix}$$

$$\begin{bmatrix} Reflected \\ Field \\ Vector \end{bmatrix} = \begin{bmatrix} Reflection \\ Coefficient \\ Matrix \end{bmatrix} \begin{bmatrix} Incident \\ Field \\ Vector \end{bmatrix}$$

For the TE polarization, both field and its z derivatives are continuous across an interface. Following a similar procedure, we derive the *Transmission* and *Reflection* matrices for the TE case.

$$A_1 = 2(I + S_0^{-1}S_1)^{-1}A_0 \tag{4.31}$$

$$B_0 = (I - S_0^{-1}S_1)(I + S_0^{-1}S_1)^{-1}A_0 \tag{4.32}$$

where the last two equations were obtained from equation 4.29 and 4.30 by replacing N_0 and N_1 by the identity matrix I. The transmission matrix T and the reflection matrix R are related by:

$$A_1 = B_0 + A_0 \tag{4.33}$$

$$= RA_0 + A_0 \tag{4.34}$$

$$= (R + I)A_0 = TA_0 \tag{4.35}$$

4.3.1 Results: Scattering of the Modal Field

A single waveguide discontinuity is modeled as shown in figure 4.24 at $\lambda = 0.86\,\mu m$. The TM_o mode of the narrow waveguide is incident from the left on the junction. The reflected and transmitted fields are calculated and propagated backwards and forward in the respective waveguides. The problem space is terminated with a single layer PML on both sides. The results are shown in figures 4.24, 4.25 and 4.26. The power should be conserved at the junction, that is $P_{incident} = P_{reflected} + P_{transmitted}$. This condition is checked and verified during the simulation. The reflected field conforms to the TM_o mode of the narrow waveguide after propagating backwards a long distance as the energy outside the fundamental mode leaks out. This shows that the PML absorbs the radiative fields effectively. Similarly, the transmitted field gradually develops into the TM_o mode of the thick waveguide.

4.4 Double Discontinuity

Refer to figure 4.27, the problem space is divided into three regions. In general, the total field in each regions is composed of forward traveling field e^{+jSz} and backwards traveling field e^{-jSz}.

$$\Psi_0 = e^{+jS_0 z} A_0 + e^{-jS_0 z} B_0 \tag{4.36}$$

$$\Psi_1 = e^{+jS_1 z} A_1 + e^{-jS_1 (z-d)} B_1 \tag{4.37}$$

$$\Psi_2 = e^{+jS_2 (z-d)} A_2 \tag{4.38}$$

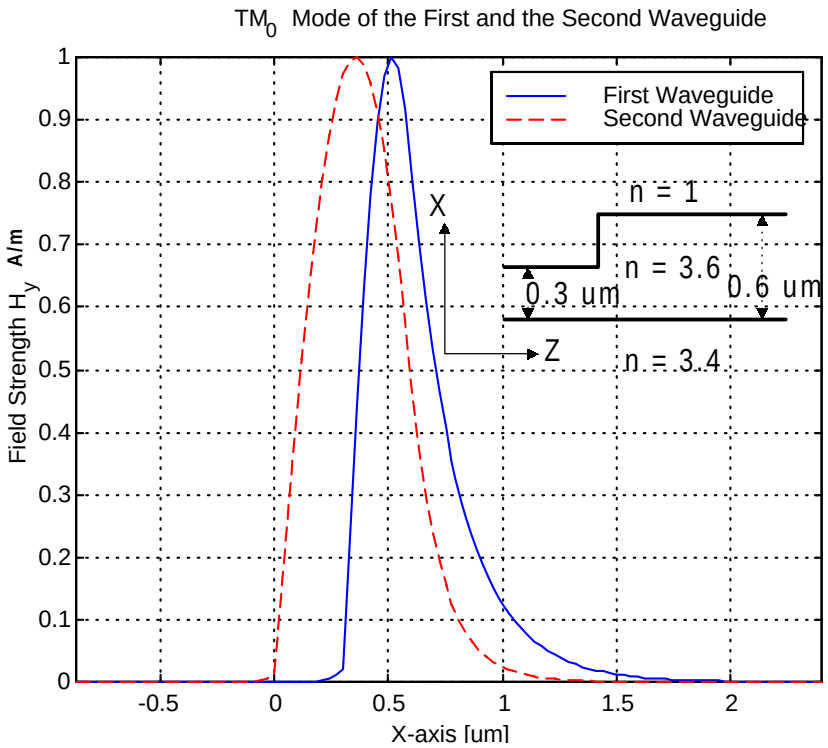

Figure 4.24: Waveguide TM_0 Modal Field

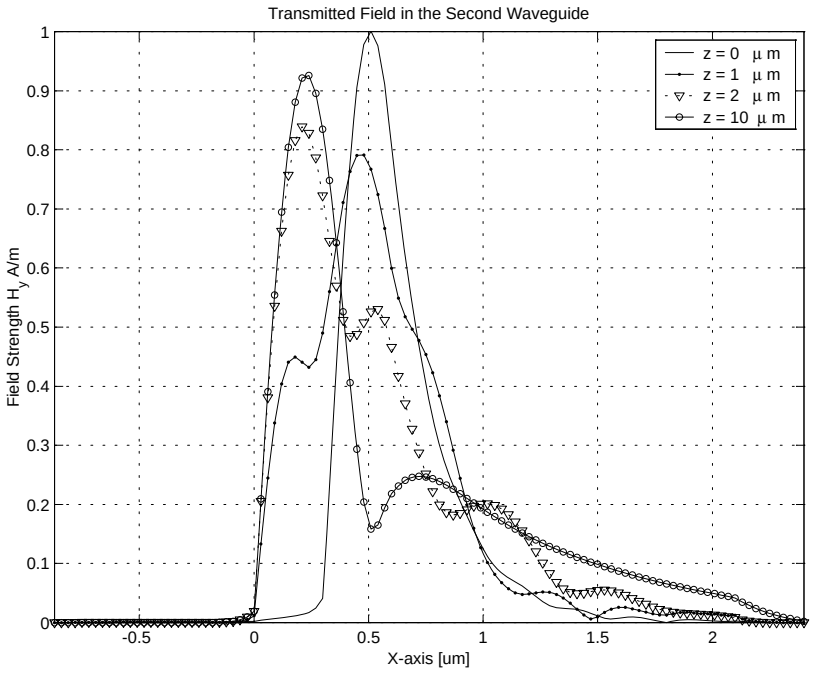

Figure 4.25: Transmitted Field after the discontinuity

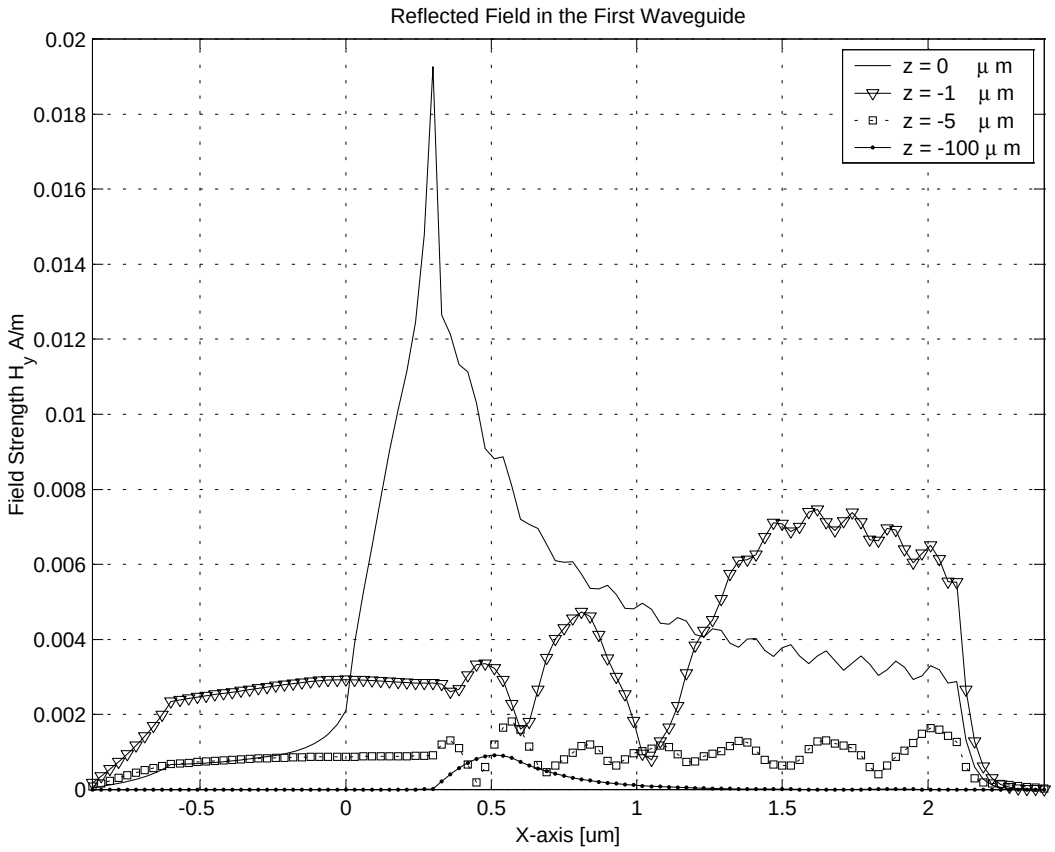

Figure 4.26: Reflected Field Backwards from the Discontinuity

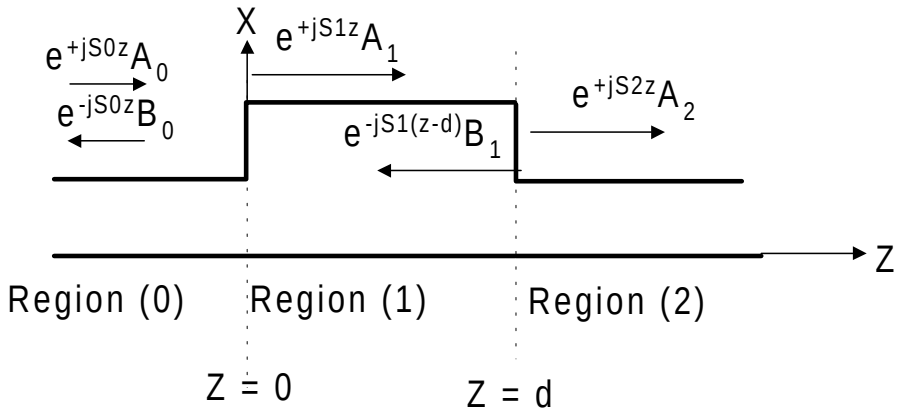

Figure 4.27: A Double Waveguide Discontinuity

[1] For the TE polarization, the field vector Ψ and its derivative Ψ' with respect to z are continuous at a discontinuity. Applying the interface conditions at $z = 0$ and simplifying , we get:

$$A_0 + B_0 = A_1 + e^{+jS_1 d} B_1 \tag{4.39}$$

$$T_1(A_0 - B_0) = A_1 - e^{+jS_1 d} B_1 \quad \text{, where} \quad T_1 = S_1^{-1} S_0 \tag{4.40}$$

Applying the interface conditions at $z = d$ and simplifying , we get:

$$e^{+jS_1 d} A_1 + B_1 = A_2 \tag{4.41}$$

$$T_2(e^{+jS_1 d} A_1 - B_1) = A_2 \quad \text{, where} \quad T_2 = S_2^{-1} S_1 \tag{4.42}$$

We end up with four equations with five unknowns A_0, B_0, A_1, B_1 and A_2. We can solve for the unknowns in terms of the incident field A_0. The procedure is similar

[1] Note that this particular form of equations 4.37 and 4.38 is chosen to avoid numerical instabilities in the MoL. An alternate form of equation 4.37, that is $\Psi_1 = e^{+jS_1 z} A_1 + e^{-jS_1 z} B_1$, may also be chosen. This results in a factor $\left[e^{jS_1 d}\right]^{-1}$ in the resulting formulas. Unfortunately, this factor turns out to be ill-conditioned or singular during simulation and its inverse can not be calculated.

to that followed in the single discontinuity section. The final results are:

$$A_2 = (I + T_2)^{-1} T_2 e^{+jS_1 d} K_4 A_0 \quad (4.43)$$

$$B_0 = K_3 A_0 \quad (4.44)$$

where:

$$K_4 = (I + T_1) + (I - T_1) K_3 \quad \text{, and} \quad (4.45)$$

$$K_3 = (S_1 + S_2)^{-1} (S_2 - S_1) \quad (4.46)$$

The results for the TM polarization are similar but with $T_1 = S_1^{-1} N_1 N_0^{-1} S_0$ and $T_2 = S_2^{-1} N_2 N_1^{-1} S_1$.

4.4.1 Results: Scattering of the Modal Field

A double waveguide discontinuity is modeled as shown in figure 4.28 at $\lambda = 0.86\,\mu m$. The TM_o mode of the narrow waveguide is incident from the left on the junction. The reflected and transmitted fields are calculated and propagated backwards and forward in the respective waveguides. The results are shown in figures 4.28, 4.29, 4.33 and 4.30. The reflected field conforms to the TM_o mode of the narrow waveguide after propagating backwards a long distance as the energy outside the fundamental mode leaks out. Similarly, the transmitted field gradually develops into the TM_o mode of the thin waveguide.

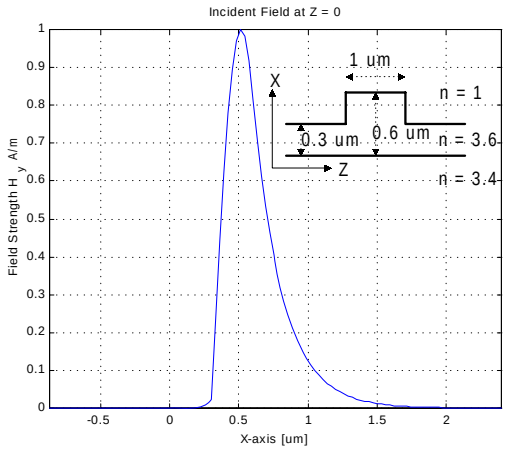

Figure 4.28: Incident Modal Field at the First Discontinuity

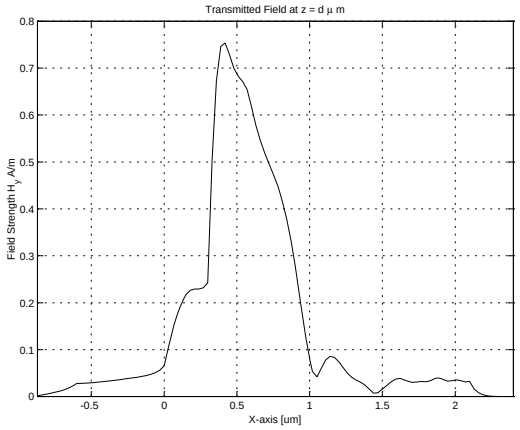

Figure 4.29: Transmitted Field after the Second Discontinuity, z = d

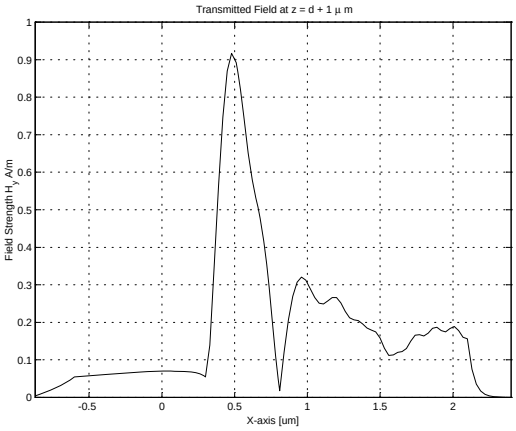

Figure 4.30: Transmitted Field at z = d + 1

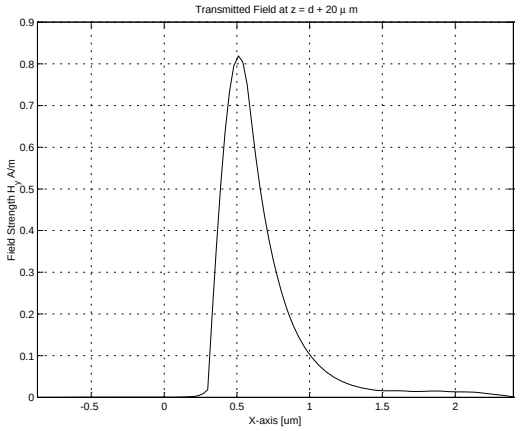

Figure 4.31: Transmitted Field at z = d + 5

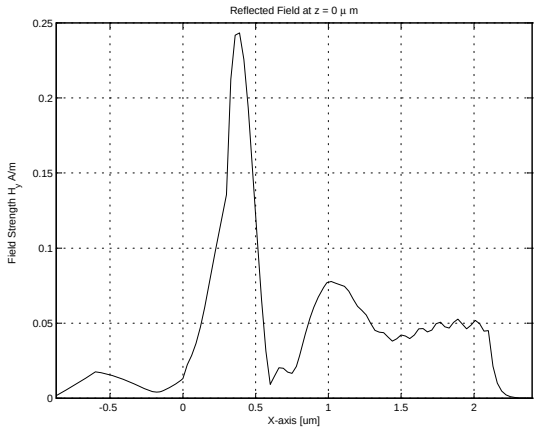

Figure 4.32: Backwards Reflected Field at z = 0

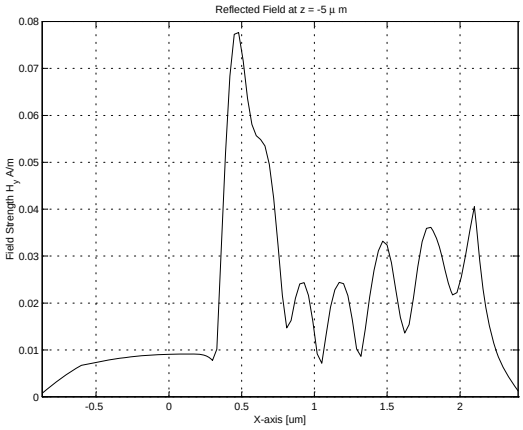

Figure 4.33: Backwards Reflected Field at z = -5 μm

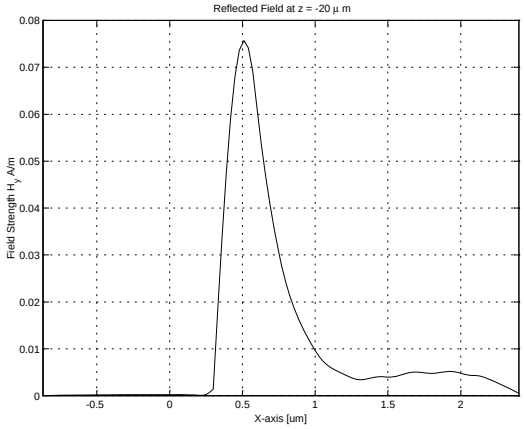

Figure 4.34: Reflected Field, z = -20 μm

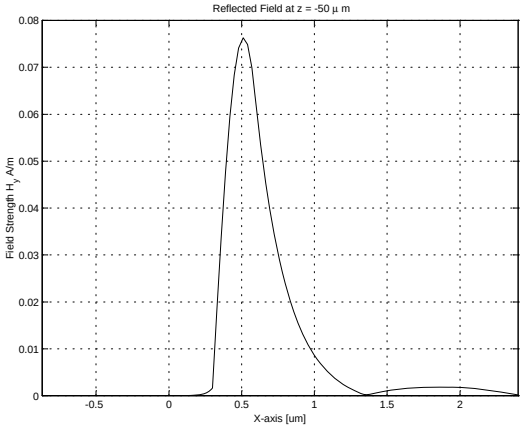

Figure 4.35: Reflected Field, z = -50 μm

4.5 Multiple Discontinuities

Consider the multi-layer structure in figure 4.36. The total field in each layer is the sum of the forward and the backwards traveling wave, that is:

$$\Psi_0 = e^{+jS_0z}A_0 + e^{-jS_0z}B_0 \tag{4.47}$$

$$\Psi_1 = e^{+jS_1z}A_1 + e^{-jS_1(z-d_1)}B_1 \tag{4.48}$$

$$\vdots$$

$$\Psi_k = e^{+jS_k(z-d_{k-1})}A_k + e^{-jS_k(z-d_k)}B_k \tag{4.49}$$

$$\vdots$$

$$\Psi_{N+1} = e^{+jS_{N+1}(z-d_N)}A_{N+1} \tag{4.50}$$

The wave is incident on the interface $z = 0$ from the left. In the region $N + 1$, the wave is assumed to propagate without reflection in the $+z$ direction. At each discontinuity, the boundary condition requires the continuity of the tangential field E_y and H_x. In other words, the continuity of Ψ and $\frac{d\Psi}{dz}$ must be satisfied. Application of these conditions results in the following recursive relationship [1]:

$$e^{jS_k(d_k-d_{k-1})}A_k = \frac{1}{2}(I + S_k^{-1}S_{k+1})A_{k+1} + \frac{1}{2}(I - S_k^{-1}S_{k+1})e^{jS_{k+1}(d_{k+1}-d_k)}B_{k+1} \tag{4.51}$$

$$B_k = \frac{1}{2}(I - S_k^{-1}S_{k+1})A_{k+1} + \frac{1}{2}(I + S_k^{-1}S_{k+1})e^{jS_{k+1}(d_{k+1}-d_k)}B_{k+1} \tag{4.52}$$

where $k = 0, 1, 2, ..., N$, For $k = 0$, $d_0 = d_{-1} = 0$ and for $k = N$, $B_{N+1} = 0$. This is a recursive relationship which express the field in layer k in terms of the field in layer $k + 1$. We start from the last layer, in which there is only a forward

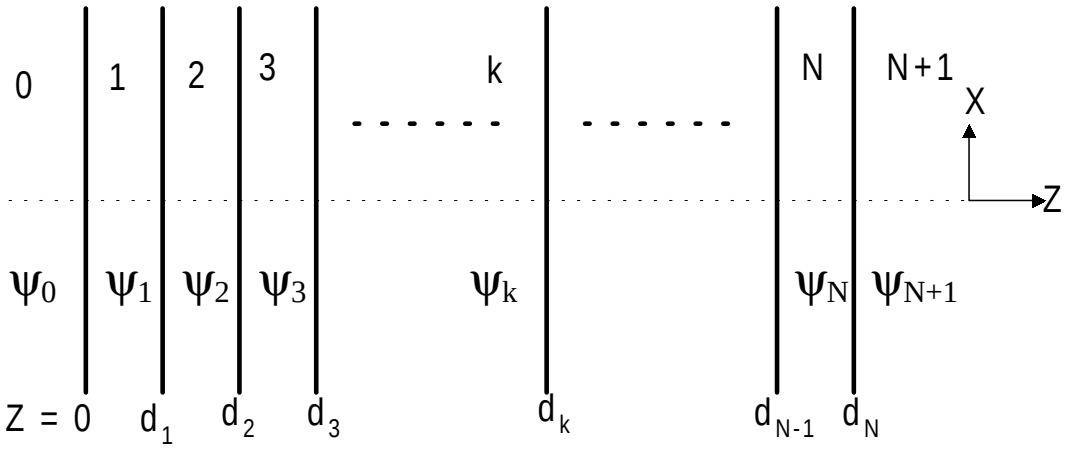

Figure 4.36: Multiple Waveguide Discontinuities [1]

propagating wave, and work backwards, layer by layer, until we reach the first layer. Thus the field in last layer is expressed in terms of the field in first layer. From this, we can find the reflection and transmission matrices and hence the reflected and transmitted fields. The field in the intermediate layers can also be calculated if required.

Chapter 5

The Cascading and Doubling Algorithm

5.1 Introduction

Periodically corrugated optical waveguides or gratings have played an important role in the design and operation of many integrated optical devices such as in wavelength filtering, coupling, Distributed Bragg Reflector (DBR) and Distributed Feedback (DFB) semiconductor laser. A number of theoretical analysis have been done on waveguides with periodic corrugations. Marcuse [48] used coupled-mode theory to analyze a slab waveguide with sinosoidal deformation of one interface. The spectral response of a grating filter using coupled-mode theory was calculated and compared with experimental work in [49]. In reference [50], the Effective-Index method was used to model a waveguide grating and the results compared with coupled-mode

theory. A major limitation of the coupled-mode theory is that it can only model small perturbations due to its approximate formulation. The Method of Lines is suited to model such problems as it does not have any approximation except for the approximation of the central-difference second-derivative operator. So to model a long grating with deep corrugations, a fast and stable algorithm within the Method of Lines framework is developed. This method, named Cascading and Doubling Algorithm [51] can model gratings with thousands of periods in relatively fewer steps as compared to the layer-by-layer algorithm given in the last chapter. In this chapter, the derivation of this algorithm is explained and comparisons are made with published results.

5.2 The Cascading and Doubling Algorithm

With reference to figure 5.1, two discontinuities 'A' and 'B' are attached together. Their individual reflection and transmission matrices are assumed to be known. We will next develop the scheme to find the reflection and transmission matrices of the combined structure. R_A and T_A are reflection and transmission matrices of the isolated structure 'A'. For an asymmterical discontinuity $R_{A1} \neq R_{A2}$ and $T_{A1} \neq T_{A2}$. [1] The same comments apply to discontinuity 'B'. If the two discontinuities are not identical then $R_A \neq R_B$ and $T_A \neq T_B$. The reflection and transmission matrices of the combined structure are denoted by R_0 and T_0 respectively. These matrices

[1] $R_{A1}, T_{A2}(R_{A2}, T_{A1})$ are the reflection and transmission matrices of the discontinuity 'A' when the field is incident from left(right) of the discontinuity.

are obtained by adding the successive reflections and transmissions of the incident field as the two structures interact with each other. The field propagation in the unperturbed waveguide section of length 'd' is described by $e^{\pm jSz}$. The field vector a_0 is assumed to be incident from the left on the first discontinuity (see figure 5.2). We can express the net reflected field in terms of the summation of forward and backwards traveling waves after multiple reflections from the two discontinuities.

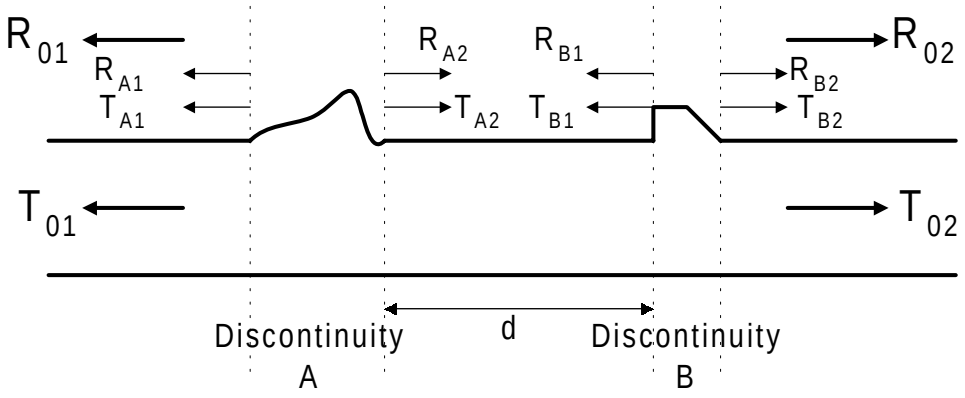

Figure 5.1: Two Waveguide Structures Cascaded Together

$$\begin{aligned} R_{01}a_0 &= R_{A1}a_0 + T_{A1}e^{jSd}R_{B1}e^{jSd}T_{A2}a_0 + T_{A1}\left(e^{jSd}R_{B1}e^{jSd}R_{A2}\right)e^{jSd}R_{B1}e^{jSd}T_{A2}a_0 + \\ &\quad T_{A1}\left(e^{jSd}R_{B1}e^{jSd}R_{A2}\right)^2 e^{jSd}R_{B1}e^{jSd}T_{A2}a_0 + \\ &\quad T_{A1}(e^{jSd}R_{B1}e^{jSd}R_{A2})^3 e^{jSd}R_{B1}e^{jSd}T_{A2}a_0 + ... \qquad (5.1) \end{aligned}$$

$$R_{01}a_0 = R_{A1}a_0 + T_{A1}\left[\sum_{n=0}^{\infty}\left(e^{jSd}R_{B1}e^{jSd}R_{A2}\right)^n\right]e^{jSd}R_{B1}e^{jSd}T_{A2}a_0 \qquad (5.2)$$

$$R_{01} = R_{A1} + T_{A1}\left[\sum_{n=0}^{\infty}\left(e^{jSd}R_{B1}e^{jSd}R_{A2}\right)^n\right]e^{jSd}R_{B1}e^{jSd}T_{A2} \qquad (5.3)$$

$$R_{01} = R_{A1} + T_{A1}\left(I - e^{jSd}R_{B1}e^{jSd}R_{A2}\right)^{-1}e^{jSd}R_{B1}e^{jSd}T_{A2} \qquad (5.4)$$

where the infinite geometric series in 5.3 is assumed to be convergent and is replaced by an equivalent quotient term. The transmission matrix T_0 of the combined structure is obtained in a similar fashion.

$$\begin{aligned} T_{02}a_0 &= T_{B2}e^{jSd}T_{A2}a_0 + T_{B2}\left(e^{jSd}R_{A2}e^{jSd}R_{B1}\right)a_0 + \\ &\quad T_{B2}\left(e^{jSd}R_{A2}e^{jSd}R_{B1}\right)^2 e^{jSd}T_{A2}a_0 + ... \qquad (5.5) \end{aligned}$$

$$T_{02}a_0 = T_{B2}\left[\sum_{n=0}^{\infty}\left(e^{jSd}R_{A2}e^{jSd}R_{B1}\right)^n\right]e^{jSd}T_{A2}a_0 \qquad (5.6)$$

$$T_{02} = T_{B2}\left[\sum_{n=0}^{\infty}\left(e^{jSd}R_{A1}e^{jSd}R_{B1}\right)^n\right]e^{jSd}T_{A2} \qquad (5.7)$$

$$T_{02} = T_{B2}\left(I - e^{jSd}R_{A2}e^{jSd}R_{B1}\right)^{-1}e^{jSd}T_{A2} \qquad (5.8)$$

The quotients appearing in equations 5.4 and 5.8 are different. In order to make the computation of R_{01} and T_{02} more efficient, equation 5.1 is modified such that the quotient terms become identical. That is:

$$\begin{aligned} R_{01}a_0 &= R_{A1}a_0 + T_{A1}e^{jSd}R_{B1}e^{jSd}T_{A2}a_0 + T_{A1}e^{jSd}R_{B1}\left(e^{jSd}R_{A2}e^{jSd}R_{B1}\right)e^{jSd}T_{A2}a_0 + \\ &\quad T_{A1}e^{jSd}R_{B1}(e^{jSd}R_{A2}e^{jSd}R_{B1}e^{jSd}R_{A2}e^{jSd}R_{B1})e^{jSd}T_{A2}a_0 + ... \qquad (5.9) \end{aligned}$$

$$R_{01} = R_{A1} + T_{A1}e^{jSd}R_{B1}\left[\sum_{n=0}^{\infty}\left(e^{jSd}R_{A2}e^{jSd}R_{B1}\right)^n\right]e^{jSd}T_{A2}a_0 \qquad (5.10)$$

$$R_{01} = R_{A1} + T_{A1}e^{jSd}R_{B1}\left(I - e^{jSd}R_{A2}e^{jSd}R_{B1}\right)^{-1}e^{jSd}T_{A2} \qquad (5.11)$$

Thus equations 5.8 and 5.11 are very similar to each other with a common quotient factor $\left(I - e^{jSd}R_{A2}e^{jSd}R_{B1}\right)^{-1}e^{jSd}T_{A2}$. This is the Cascading Algorithm which gives net reflection and transmission matrices of a cascaded structure composed of two

sub-structures in terms of their individual reflection and transmission matrices.

5.2.1 Symmetrical and Periodic Structures

For a symmetric structures, $R_1 = R_2 = R$ and $T_1 = T_2 = T$. Thus equations 5.8 and 5.11 reduce to :

$$R_{01} = R_A + T_A e^{jSd} R_B \left(I - e^{jSd} R_A e^{jSd} R_B\right)^{-1} e^{jSd} T_A \tag{5.12}$$

$$T_{02} = T_B \left(I - e^{jSd} R_A e^{jSd} R_B\right)^{-1} e^{jSd} T_A \tag{5.13}$$

If structures 'A' and 'B' are identical and symmetric, then $R_A = R_B$ and $T_A = T_B$. So the relations are further simplified to:

$$R_{01} = R + T e^{jSd} R \left(I - e^{jSd} R e^{jSd} R\right)^{-1} e^{jSd} T \tag{5.14}$$

$$T_{02} = T \left(I - e^{jSd} R e^{jSd} R\right)^{-1} e^{jSd} T \tag{5.15}$$

If two identical structures are also connected to each other directly, such that $d = 0$, then:

$$R_{01} = R + TR \left(I - R^2\right)^{-1} T \tag{5.16}$$

$$T_{02} = T \left(I - R^2\right)^{-1} T \tag{5.17}$$

It is important to note that R_{01} and T_{02} are reflection and transmission matrices as *seen* from left of the waveguide. The relations for R_{02} and T_{01} as *seen* from the right are easily obtained from 5.8 and 5.11 by interchanging $A \rightleftharpoons B$ and $1 \rightleftharpoons 2$.

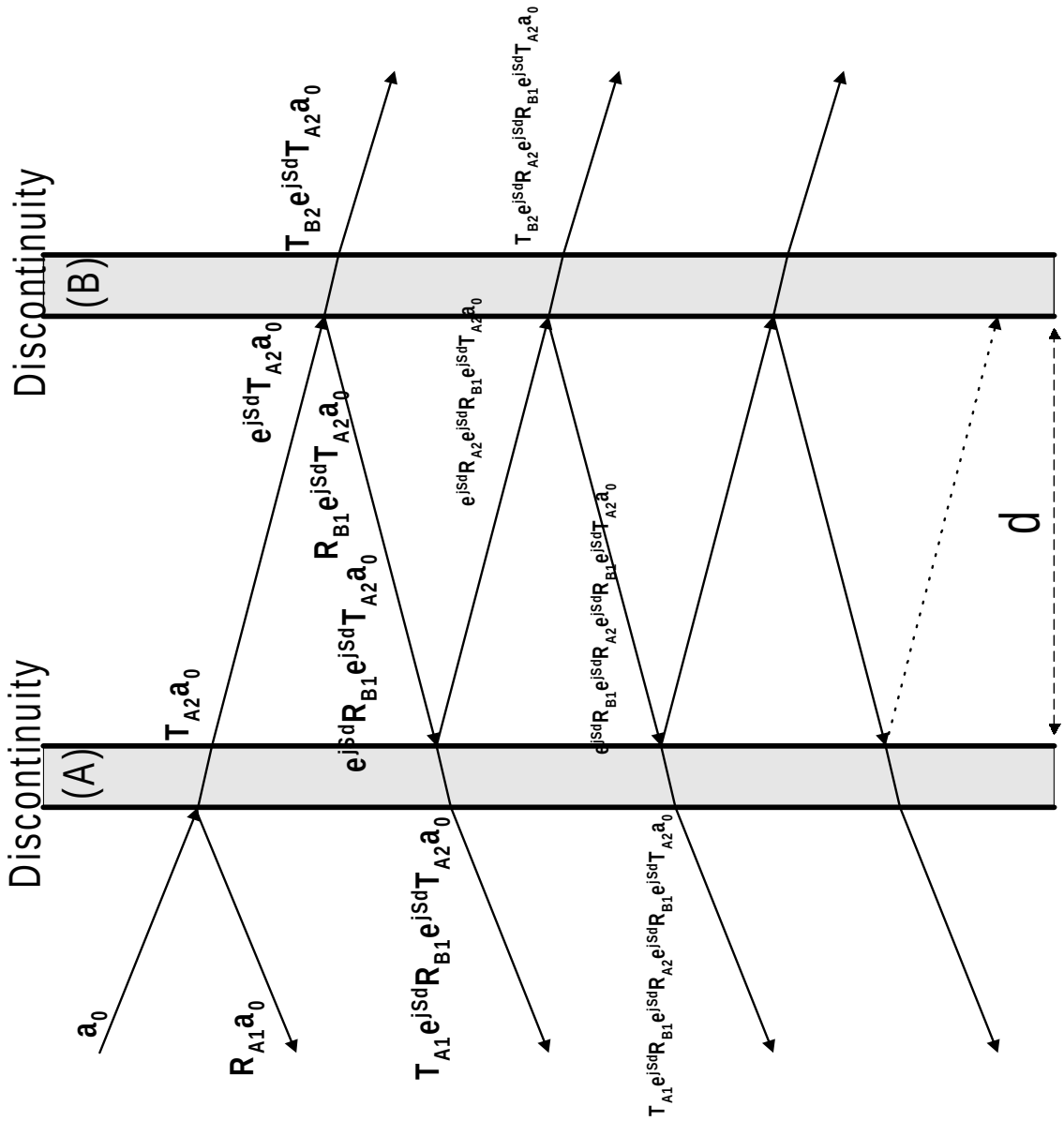

Figure 5.2: Multiple Reflections from two Cascaded Discontinuities

That is:

$$R_{02} = R_{B2} + T_{B2}e^{jSd}R_{A2}\left(I - e^{jSd}R_{B1}e^{jSd}R_{A2}\right)^{-1}e^{jSd}T_{B1} \tag{5.18}$$

$$T_{01} = T_{A1}\left(I - e^{jSd}R_{B1}e^{jSd}R_{A2}\right)^{-1}e^{jSd}T_{B1} \tag{5.19}$$

5.2.2 Case Study: Rectangular Gratings

The rectangular grating is a classic example of a symmetrical periodic structure. With reference to figure 5.3, this problem can be solved by considering the first discontinuity as shown in figure 5.4. The reflection matrix for the TM polarized field is given by:

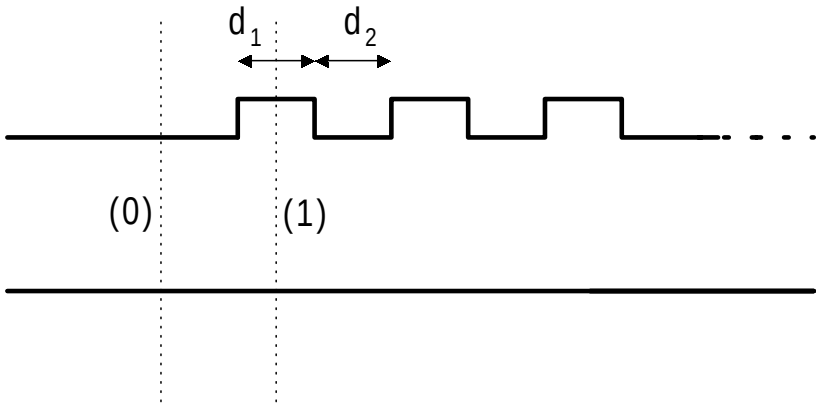

Figure 5.3: A Rectangular Waveguide Grating

$$R_{A1} = \left[I - S_0^{-1}N_0N_1^{-1}S_1\right]\left[I + S_0^{-1}N_0N_1^{-1}S_1\right]^{-1} \tag{5.20}$$

$$= \left[\left(S_0^{-1}N_0N_1^{-1}S_1\right)^{-1} - I\right]S_0^{-1}N_0N_1^{-1}S_1 \cdot$$

$$\cdot \left[\left(\left(S_0^{-1}N_0N_1^{-1}S_1\right)^{-1} + I\right)S_0^{-1}N_0N_1^{-1}S_1\right]^{-1} \tag{5.21}$$

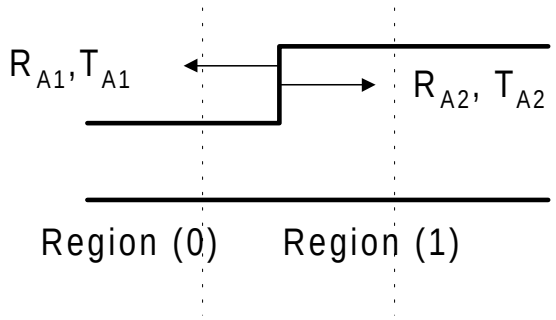

Figure 5.4: A Single Step Discontinuity

$$= \left[\left(S_0^{-1}N_0N_1^{-1}S_1\right)^{-1} - I\right] S_0^{-1}N_0N_1^{-1}S_1 \cdot$$
$$\cdot \left(S_0^{-1}N_0N_1^{-1}S_1\right)^{-1} \left[\left(S_0^{-1}N_0N_1^{-1}S_1\right)^{-1} + I\right]^{-1} \quad (5.22)$$

$$= \left[\left(S_0^{-1}N_0N_1^{-1}S_1\right)^{-1} - I\right] \left[\left(S_0^{-1}N_0N_1^{-1}S_1\right)^{-1} + I\right]^{-1} \quad (5.23)$$

$$= -\left[I - \left(S_0^{-1}N_0N_1^{-1}S_1\right)^{-1}\right] \left[I + \left(S_0^{-1}N_0N_1^{-1}S_1\right)^{-1}\right]^{-1} \quad (5.24)$$

$$= -\left[I - S_1^{-1}N_1N_0^{-1}S_0\right] \left[I + S_1^{-1}N_1N_0^{-1}S_0\right]^{-1} \quad (5.25)$$

$$= -R_{A2} \quad (5.26)$$

Thus for the above case $R_{A1} = -R_{A2}$, $T_{A2} = I + R_{A1}$ (refer to equation 4.35) and $T_{A1} = I + R_{A2}$. The results are valid for both TE and TM cases. The next step is to treat the double discontinuity shown in figure 5.5. All Rs and Ts appearing in figure 5.5 can be expressed in terms of R_{A1}.

$$R_{A2} = -R_{A1} \quad (5.27)$$

$$T_{A1} = I + R_{A2} = I - R_{A1} \quad (5.28)$$

$$T_{A2} = I + R_{A1} \tag{5.29}$$

$$R_{B1} = R_{A2} = -R_{A1} \tag{5.30}$$

$$R_{B2} = R_{A1} \tag{5.31}$$

$$T_{B1} = T_{A2} = I + R_{A1} \tag{5.32}$$

$$T_{B2} = T_{A1} = I - R_{A1} \tag{5.33}$$

Since the structure of figure 5.5 is symmetric, we need only to define R and T for the structure. Using equations 5.8 and 5.11 we obtain:

$$R = R_{A1} + (I - R_{A1})\, e^{jS_1d_1}\, (-R_{A1}) \left[I - \left(e^{jS_1d_1} R_{A1}\right)^2\right]^{-1} \cdot e^{jS_1d_1}\, (I + R_{A1}) \tag{5.34}$$

$$T = (I - R_{A1}) \left[I - \left(e^{jS_1d_1} R_{A1}\right)^2\right]^{-1} e^{jS_1d_1}\, (I + R_{A1}) \tag{5.35}$$

The final step is to model the whole structure iteratively. It starts by combining two symmetric identical structures as shown in figure 5.6. Using the equations 5.14 and 5.15, the new reflection and transmission matrices for the combined structure is expressed in terms of the old reflection and transmission matrices of the individual structure, that is:

$$R_{new} \leftarrow R_{old} + T_{old} e^{jS_0d_0} R_{old} \left[I - \left(e^{jS_0d_0} R_{old}\right)^2\right]^{-1} e^{jS_0d_0} T_{old} \tag{5.36}$$

$$T_{new} \leftarrow T_{old} \left[I - \left(e^{jS_0d_0} R_{old}\right)^2\right]^{-1} e^{jS_0d_0} T_{old} \tag{5.37}$$

These two equations are the basis of so called Doubling Algorithm. The factor $\left[I - \left(e^{jS_0d_0} R\right)^2\right]^{-1} e^{jS_0d_0} T$ is common in both equations which makes the algorithm

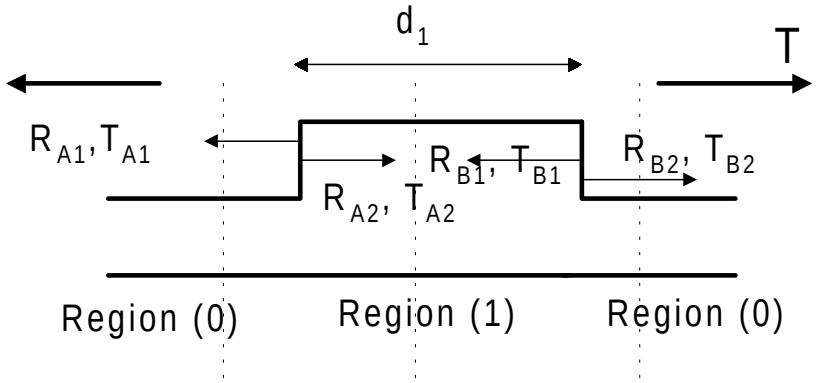

Figure 5.5: A Double Waveguide Discontinuity

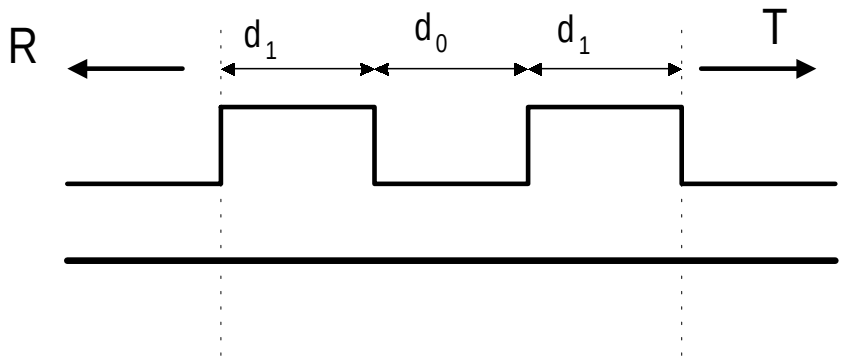

Figure 5.6: Two Identical Structures Cascaded Together

very fast. At each iteration, the number of grating periods simulated is doubled, that is 1, 2, 4, 8, 16, 32 and so on. This works in power of 2 only but we can model any number of periods by attaching the appropriate number of sections each having periods in power of 2. For example we can model 10 periods by attaching 8 and 2 periods. Note that the reflection and transmission matrix for 2 periods is already computed while computing reflection and transmission matrix of 8 periods. So it is saved in a temporary location and used in the attaching algorithm. For N discretization lines, this algorithm works on an $N \times N$ matrix for storage and eigen-value calculation. Some other algorithms [40, 24], based on raising a matrix to a certain power to model a certain number of periods, operate upon $2N \times 2N$ matrices. It becomes computationally expensive to find eigen-values and eigen-vectors of a $2N \times 2N$ matrix if the number of discretization lines N in a given problem space is larger. So our algorithm has this extra advantage of modeling waveguides with wider cross-sections efficiently.

5.3 Results

In this section, the algorithm developed is applied to find the spectral response of different waveguide gratings. The results obtained are in close agreement with published results, thus establishing the validity of this algorithm.

5.3.1 Air/GaAs/Air Waveguide Grating

A shallow waveguide grating having 256 periods as shown in the inset of figure 5.7 is modeled using a uniform mesh scheme. The TE_o mode is launched in the waveguide and the reflected and transmitted field calculated. The fundamental-mode coefficient α_0 from the reflected field is calculated and the TE_o mode power in the reflected field is determined. The modal power reflectivity is plotted against the wavelength. It has a central main lobe and several side lobes. The calculation are done for the 3-point, 5-point and 7-point formulation to show the advantage in using higher-order approximations in the MoL. The results are shown in Table 5.1. For the 3-point formulation, the number of sample points in the middle layer is 30 and the width of cladding layers is chosen thick enough (0.3 μm) to give a substantial field decay at the PML interface. A single layer PML is used with 7 sample points on each side. The resulting absolute error in n_{eff} (Mol vs. Analytical) is 4.869e-4. The time required to simulate one wavelength for 256 periods is around 10 seconds (using a Pentium II machine at 233 MHz with 64 MB RAM running MATLAB 5.2 under Windows 98). For the 5-point formulation, the number of sample points in the middle layer is 15 and the PML has 7 points on each side. The resulting absolute error in n_{eff} is 3.085e-5. The time required to simulate one wavelength for 256 periods is around 2.2 seconds. For the 7-point formulation, the number of sample points in the middle layer is 10 and the PML has 7 points on each side. The resulting absolute error in n_{eff} is 1.761e-6. The time required to simulate one

wavelength for 256 periods is around 1.2 seconds. This analysis clearly shows that higher-order approximations gives us more accurate n_{eff} prediction and the matrix size is also reduced. This results in smaller computational time to model multiple-discontinuity problems and gratings.

	3-Point	5-Point	7-Point
No. of Samples in the Middle Layer	30	15	10
No. of PML Samples on each Side	7	7	7
Total No. of Sample Points	104	59	44
Absolute Error in n_{eff}	4.869e-4	3.085e-5	1.761e-6
Time per Wavelength (sec)	10	2.2	1.2

Table 5.1: Calculational Time for Higher-Order Approximations

In figure 5.8, the waveguide width is increased to $0.4\,\mu m$ and a groove depth of $0.01\,\mu m$ is used with 8192 periods. The modal reflectivity plot has many closely packed side lobes and and flat central lobe. The [dB] scale is used to show the fine details in the reflectivity plot.

5.3.2 Comparison 1: Asymmetrical Deep Waveguide Grating

A deep grating from reference [2] is modeled using the Cascading and Doubling Algorithm, and its modal spectral reflectivity is calculated for different number of periods. A non-uniform mesh with single layer PML is used to model the device as shown in figure 5.10. The 5-point second-derivative approximation is used with

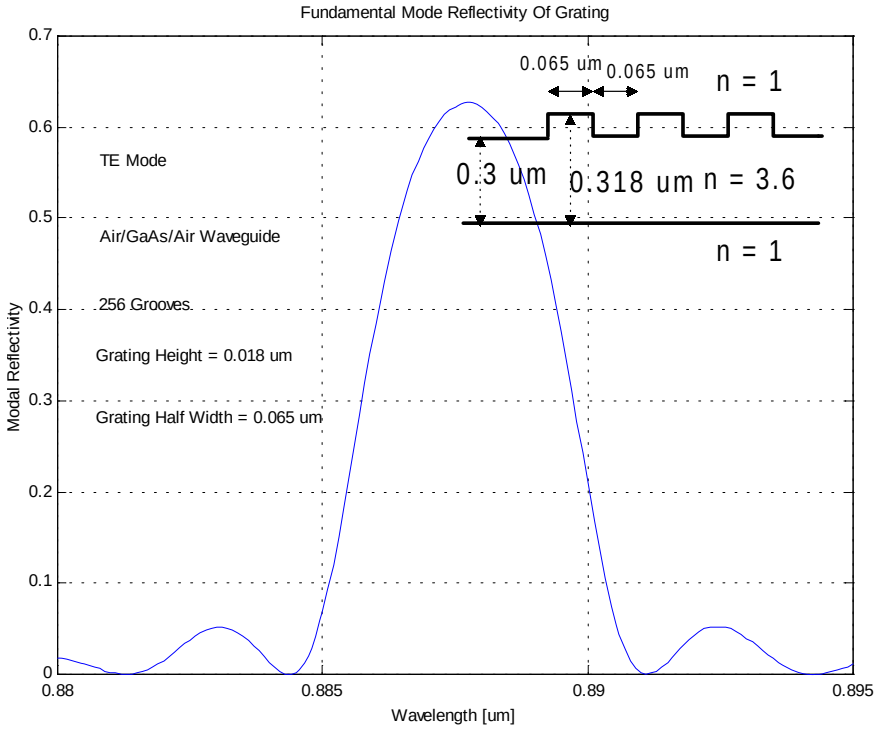

Figure 5.7: Modal Reflectivity of a Short Grating

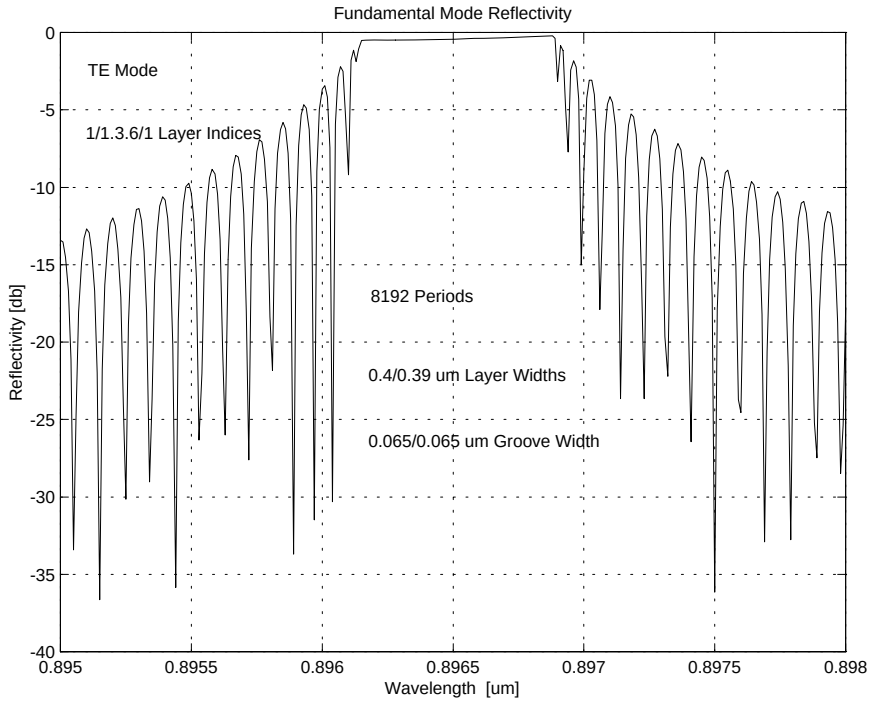

Figure 5.8: Modal Reflectivity of a Long Grating

appropriate interface conditions in the MoL . The total number of 77 sample points are used in the problem space. As shown in figure 5.11, our results are in close agreement with those from [2] and [52], establishing the accuracy of our algorithm. As the number of periods is increased, the spectral reflectivity plot becomes asymmetric and the side lobes become densely packed. Results for a semi-infinite grating with 262114 grooves is given in figure 5.14 showing that the algorithm is stable for a long grating having thousands of periods. It took approximately 6 seconds per wavelength to calculate the reflectivity and transmissivity for this semi-infinite case. The relative ease of the Doubling Algorithm to model long gratings is also evident as at each iteration, the number of periods modeled is doubled. The results for the TM polarization are also plotted in figure 5.15. They are quite different from the TE results in terms of main lobe width and peak reflectivity. The peak reflectivity has increased and the width of main lobe has almost doubled.

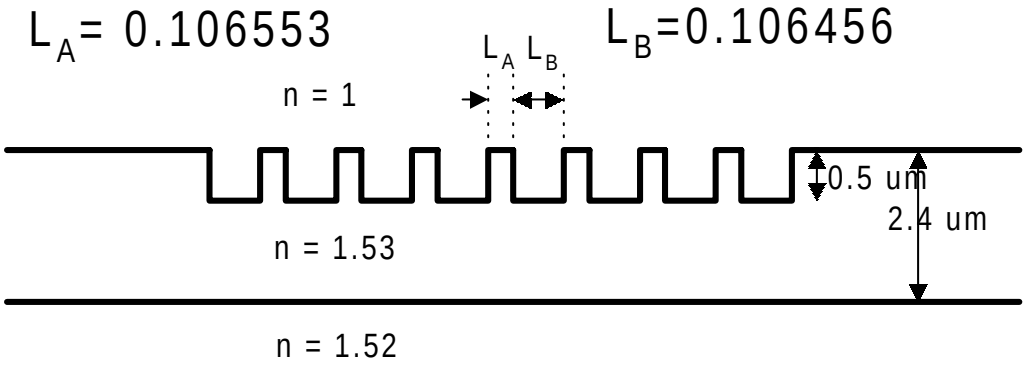

Figure 5.9: A Deep Waveguide Grating Structure from [2]

In another simulation of the same device, The groove depth is reduced considerably and the spectral response recalculated. In figure 5.17, the groove depth is 0.42% with 65536 periods and in figure 5.18, the groove depth is 2.9% with 32768 periods. The results show that main lobe width and side lobe level depend on the groove depth. For shallow grating, the main lobe width is small and the side lobes are low, while for deep grating, the main lobe is wide and asymmetric with higher side lobes. The peak reflectivity is low for shallow grating and we need to use more periods to get a higher reflection at the resonance wavelength.

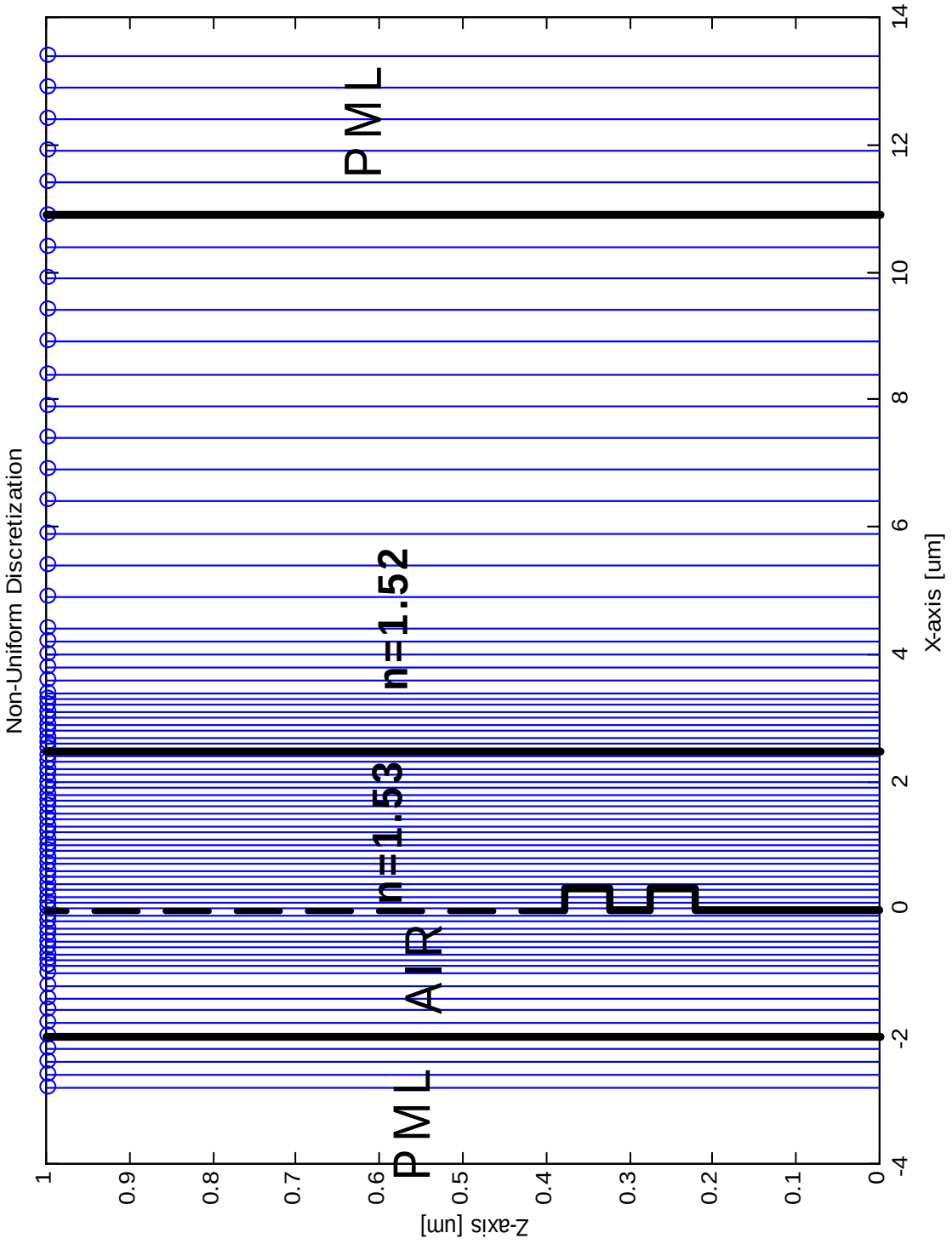

Figure 5.10: The Non-Uniform Mesh used to Model Deep Waveguide Grating

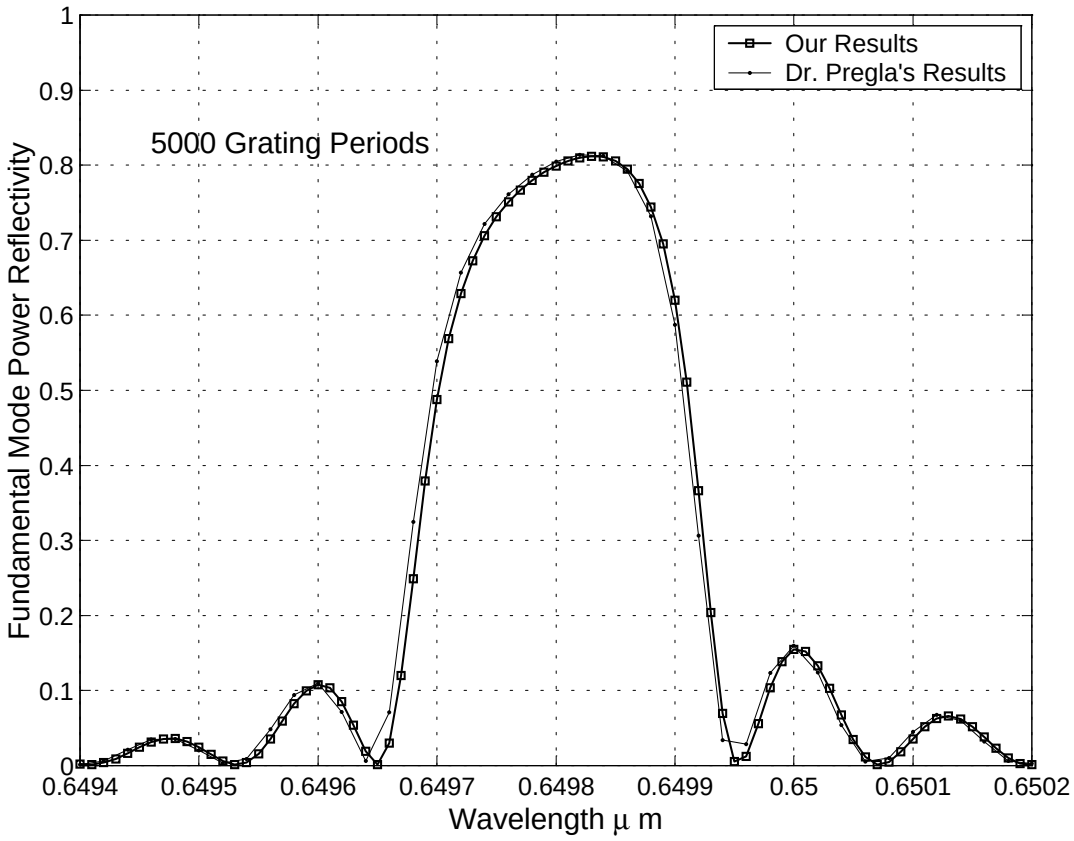

Figure 5.11: Deep Grating Modal Reflectivity

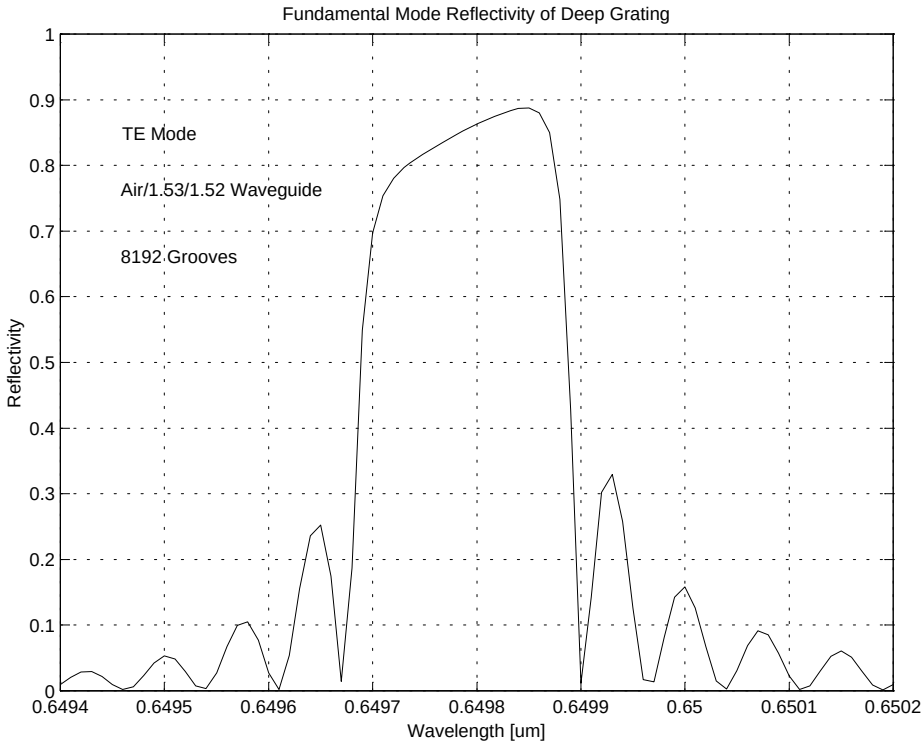

Figure 5.12: Deep Grating Modal Reflectivity, 8192 Periods

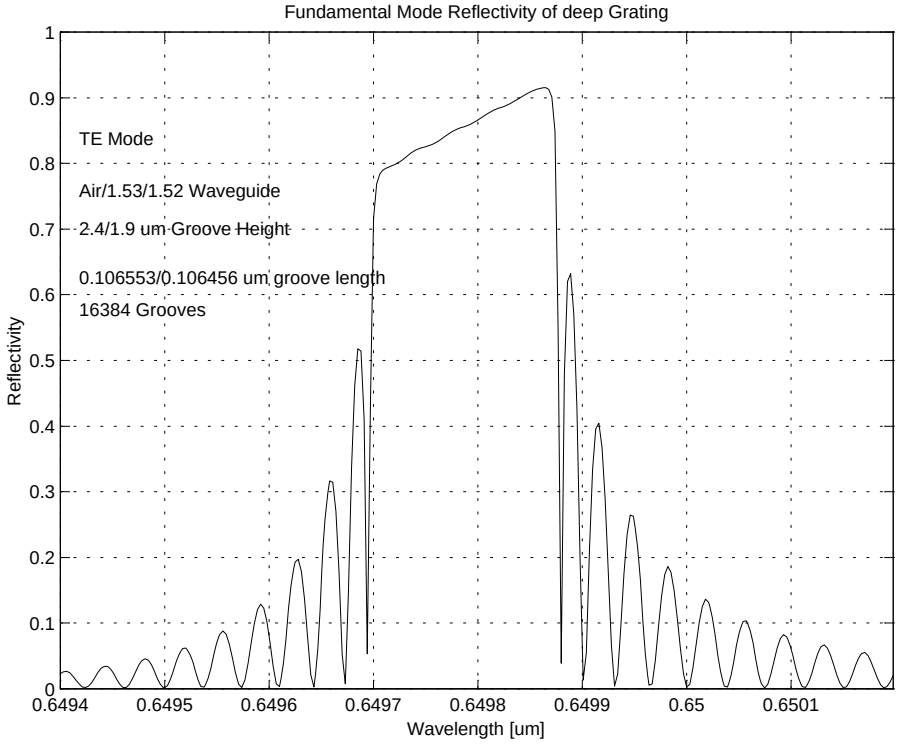

Figure 5.13: Deep Grating Modal Reflectivity, 16384 periods

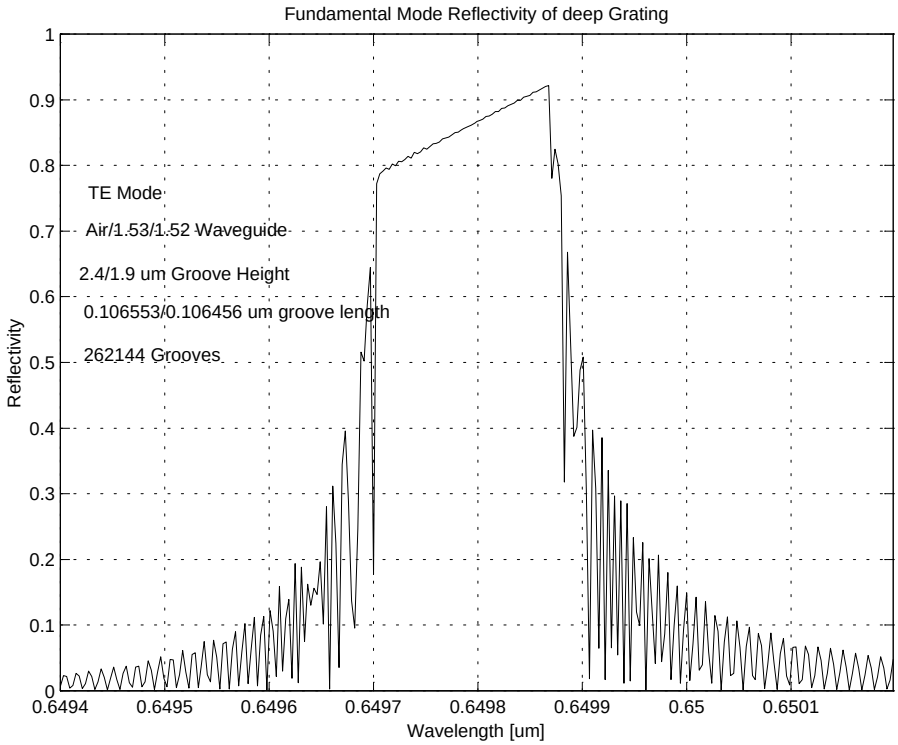

Figure 5.14: Deep Grating Modal Reflectivity, Semi-Infinite

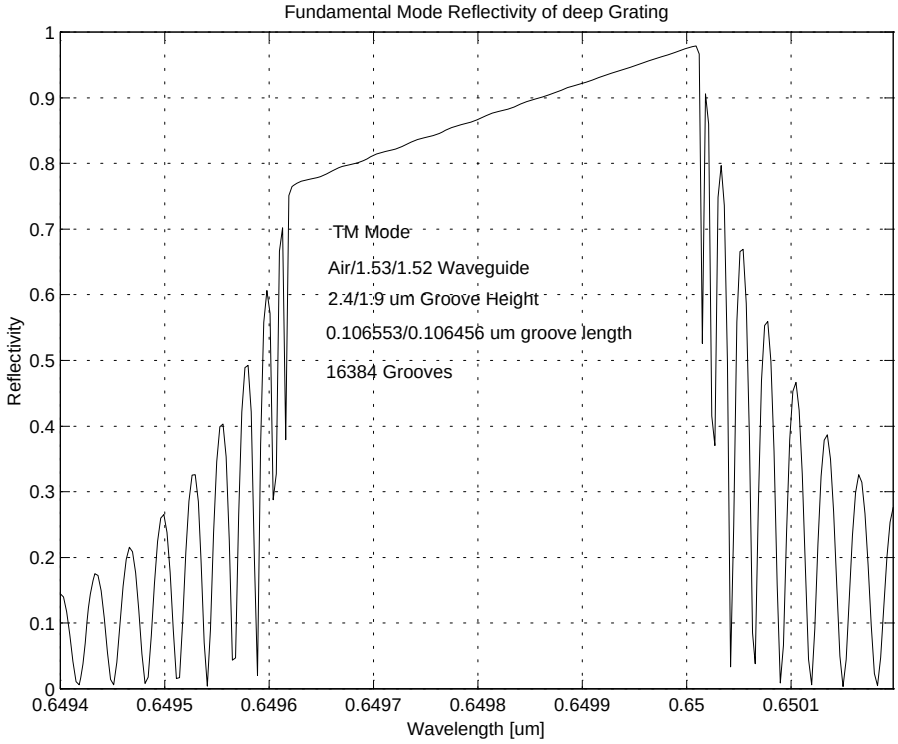

Figure 5.15: Deep Grating Modal Reflectivity, TM Mode

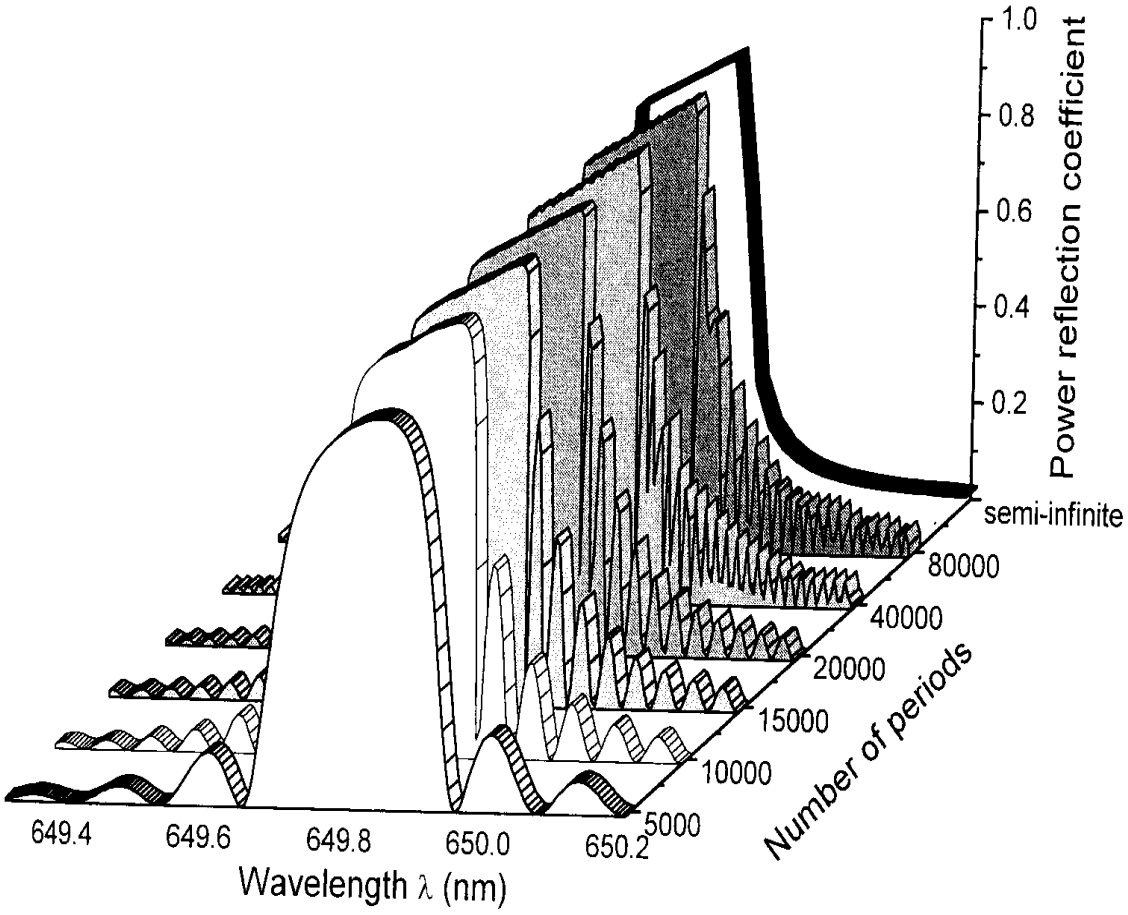

Figure 5.16: Deep Grating Modal Spectral Reflectivity, from [2]

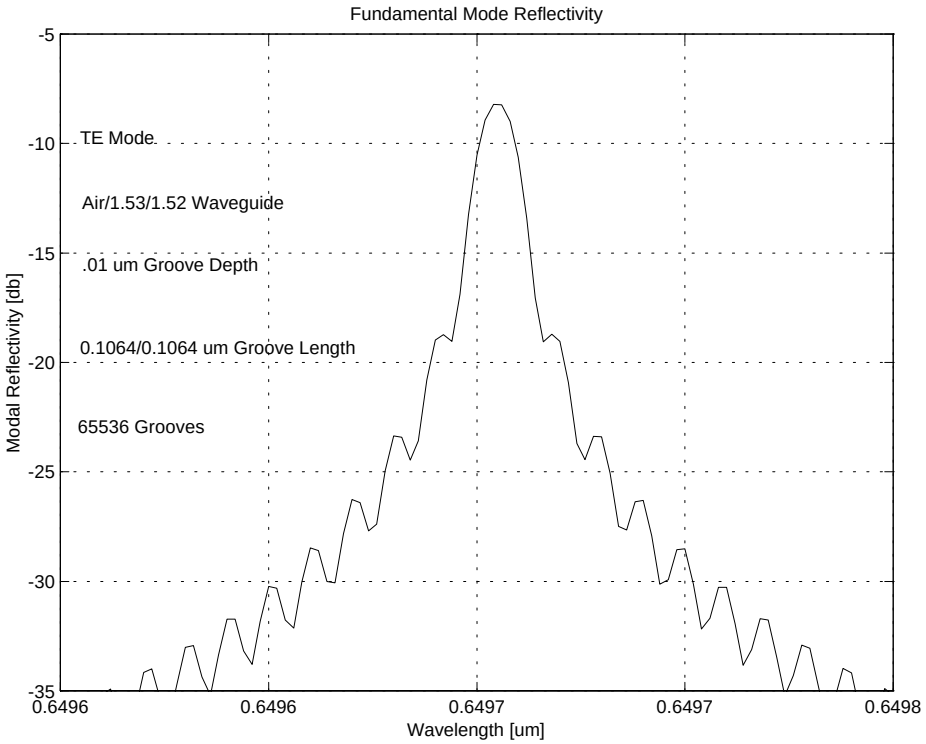

Figure 5.17: Shallow Grating Modal Reflectivity, 0.42% Depth

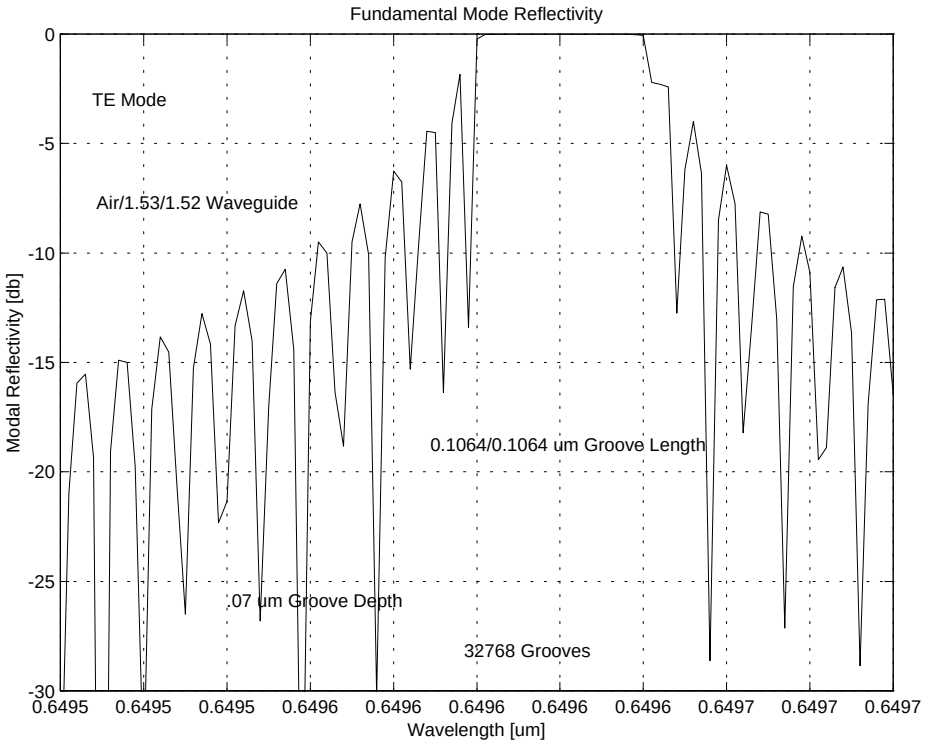

Figure 5.18: Shallow Grating Modal Reflectivity, 2.9% Depth

5.3.3 Comparison 2: Symmetrical Deep Waveguide Grating

A deep grating from reference [3] is modeled and the calculated results are compared for both the TE and TM cases. A non-uniform mesh scheme with a single layer PML is used to model the device. The wavelength is normalized to '1' and the normalized grating period $2d$ is varied. The waveguide thickness parameter 't' is $1/3\pi$. Our results, as shown in figures 5.20, 5.22, 5.24 and 5.26 for modal spectral reflectivity and transmissivity, are in close agreement with those from [3]. This structure is modeled by attaching sections of '8' and '2' periods to get the '10' period device. This shows the versatility of the Cascading and Doubling Algorithm in modeling any number of waveguide discontinuities in a stable and elegant way.

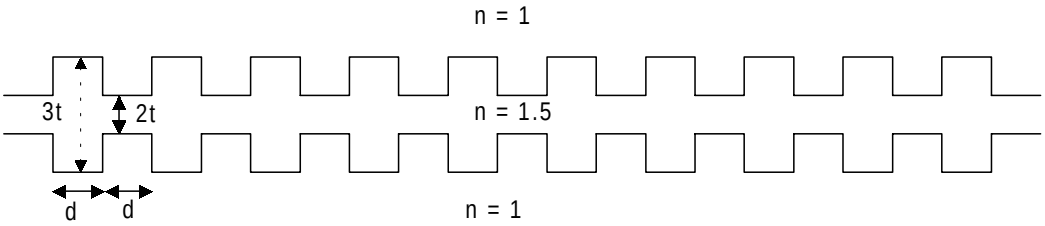

Figure 5.19: A Symmetrical Waveguide Grating from [3], $\lambda = 1\mu m$, $k = 2\pi(\mu m)^{-1}$, $kt = 2/3$

5.3.4 Effect of Changing the Groove Depth

A waveguide grating with 256 periods as shown in the inset of figure 5.28 is modeled for TE_0 mode. The spectral responses for 10%, 20% and 26% groove depths are calculated and plotted in figures 5.28,5.29 and 5.30 respectively. As the groove

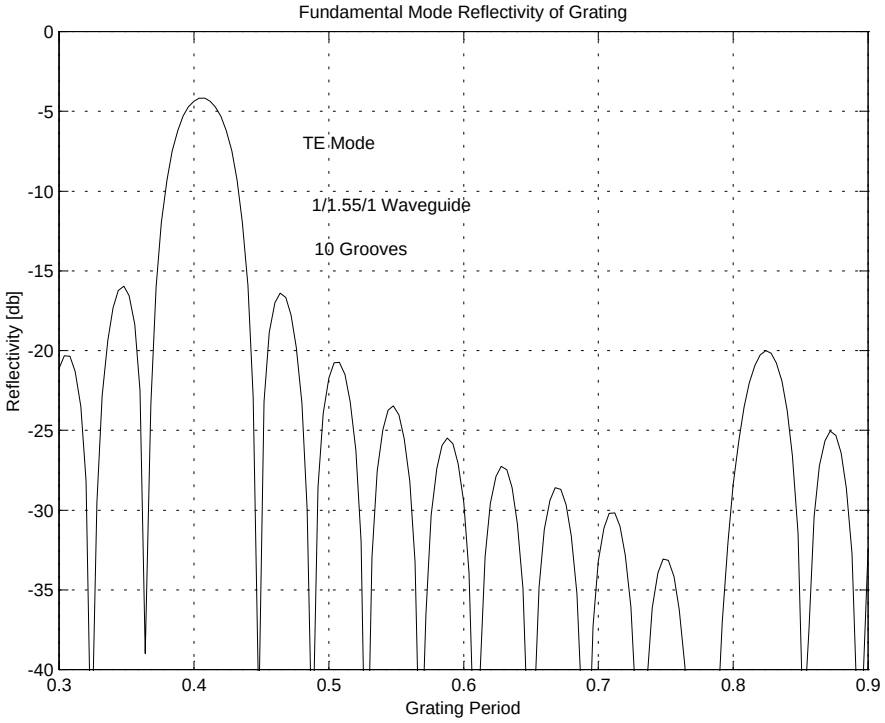

Figure 5.20: Modal Reflectivity, TE_0 Case, Our Results

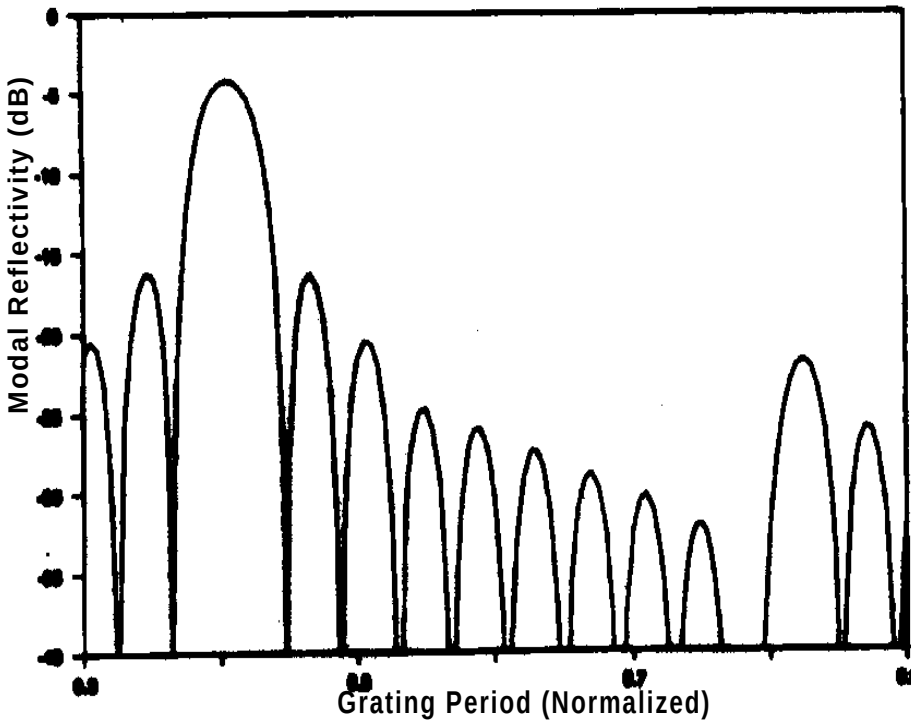

Figure 5.21: Modal Reflectivity, TE_0 Case, from [3]

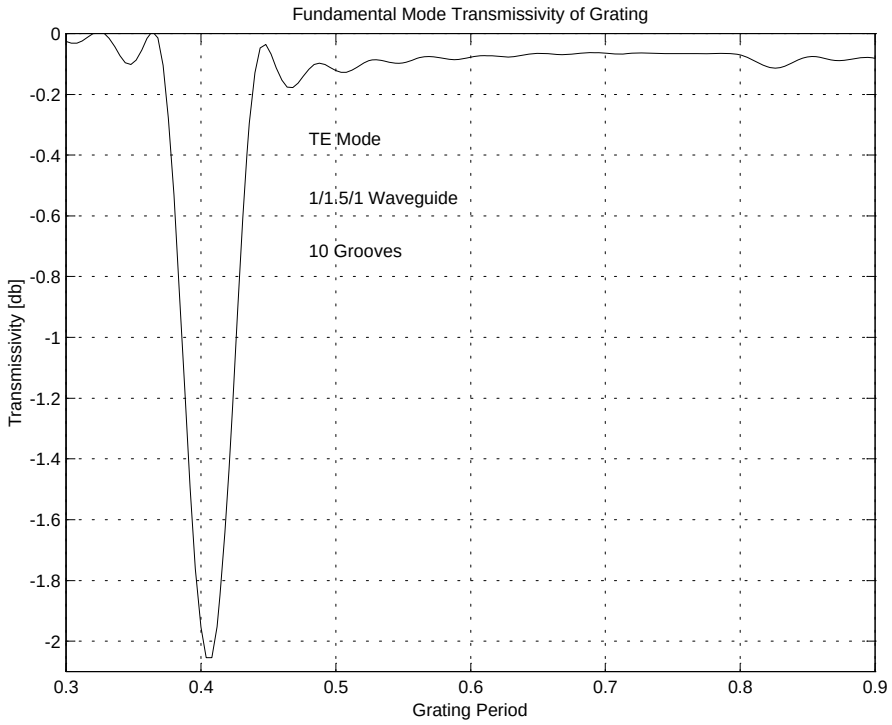

Figure 5.22: Modal Transmissivity, TE_0 Case, Our Results

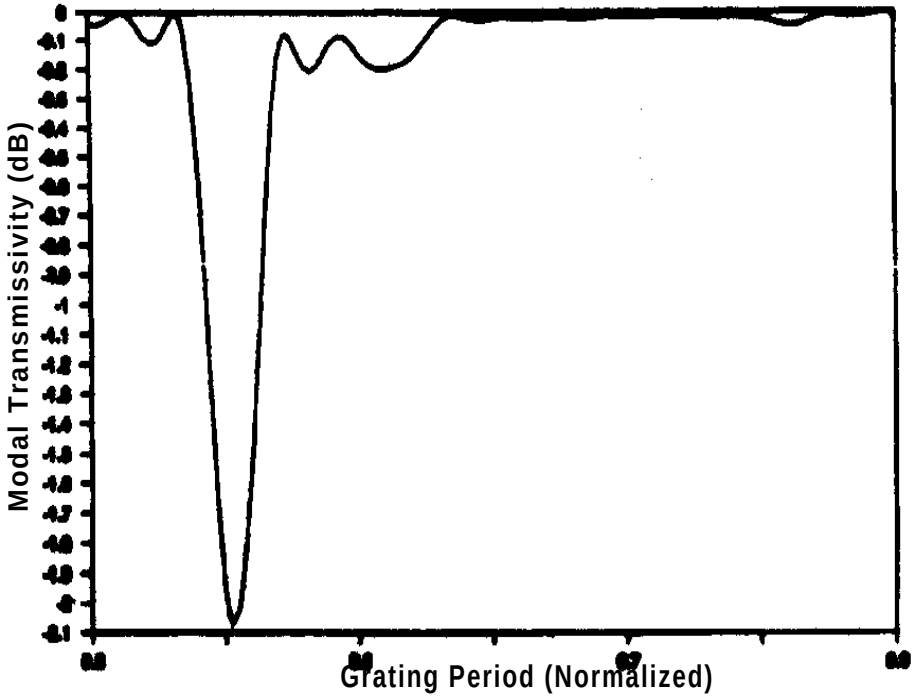

Figure 5.23: Modal Transmissivity, TE_0 Case, from [3]

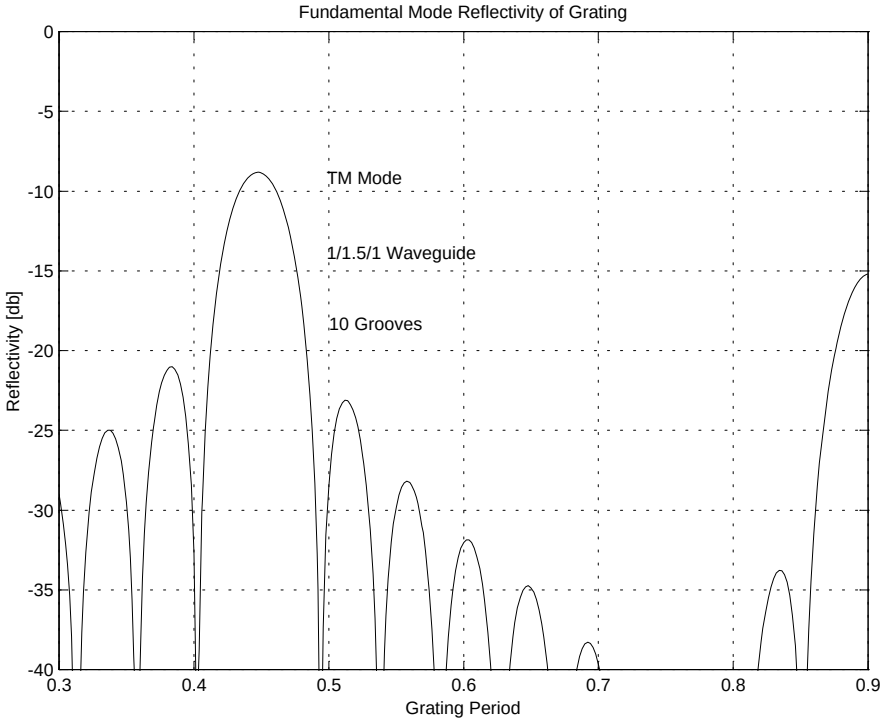

Figure 5.24: Modal Reflectivity, TM_0 Case, Our Results

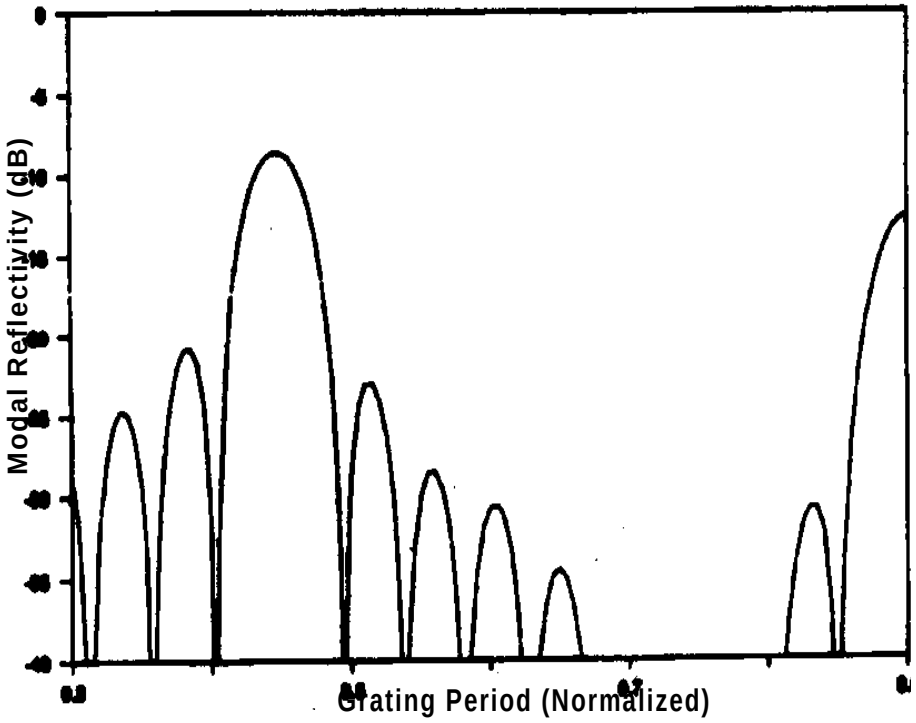

Figure 5.25: Modal Reflectivity, TM_0 Case, from [3]

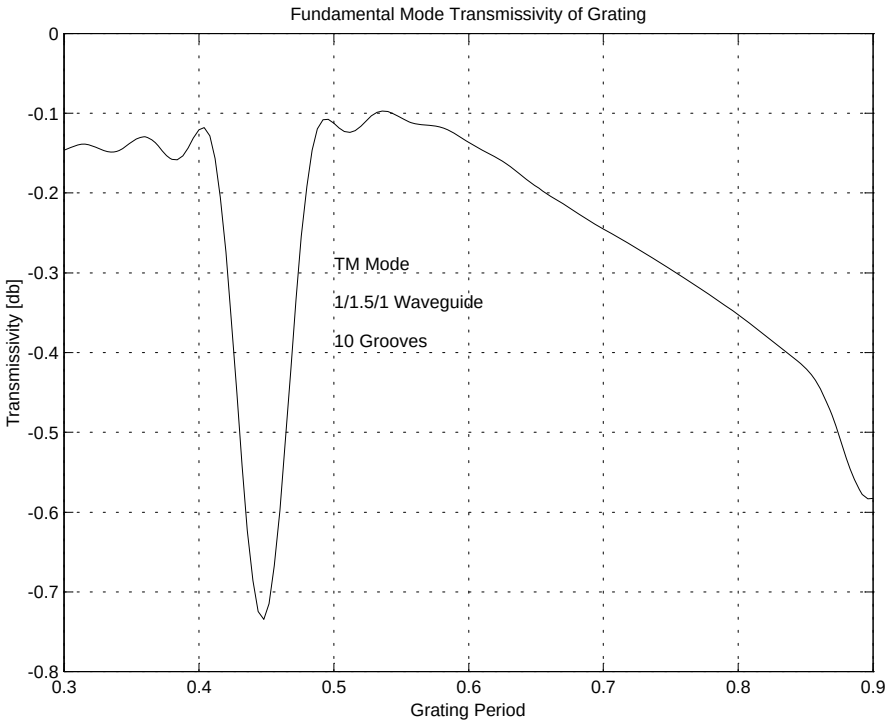

Figure 5.26: Modal Transmissivity, TM_0 Case, Our Results

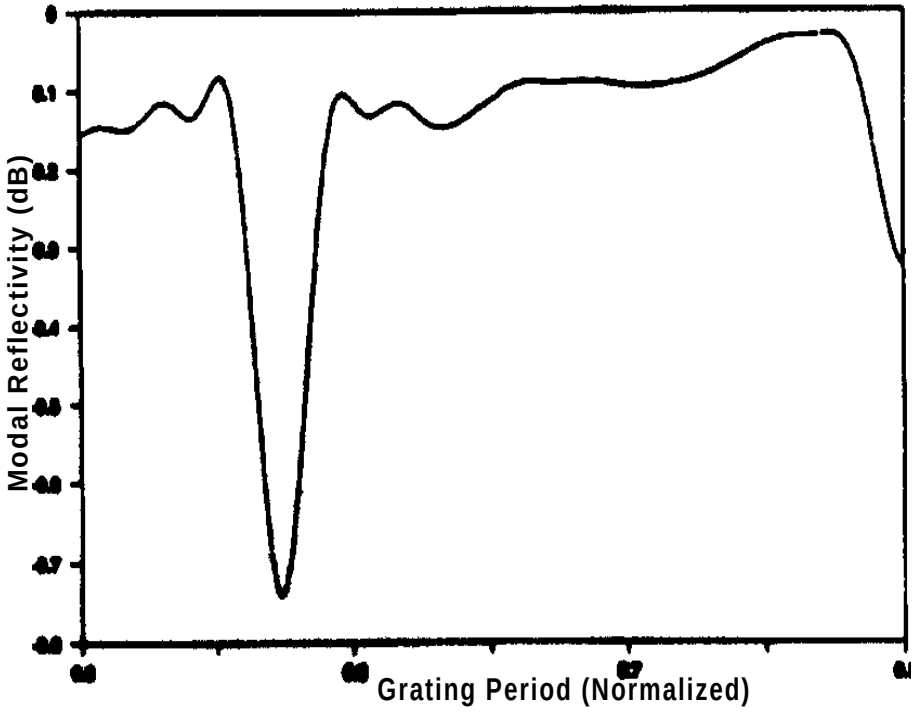

Figure 5.27: Modal Transmissivity, TM_0 Case, from [3]

depth is increased, the main lobe becomes wider and asymmetric. The wavelength for peak reflectivity, often called Bragg Wavelength λ_B shifts towards the shorter wavelength and the side lobe level also increases.

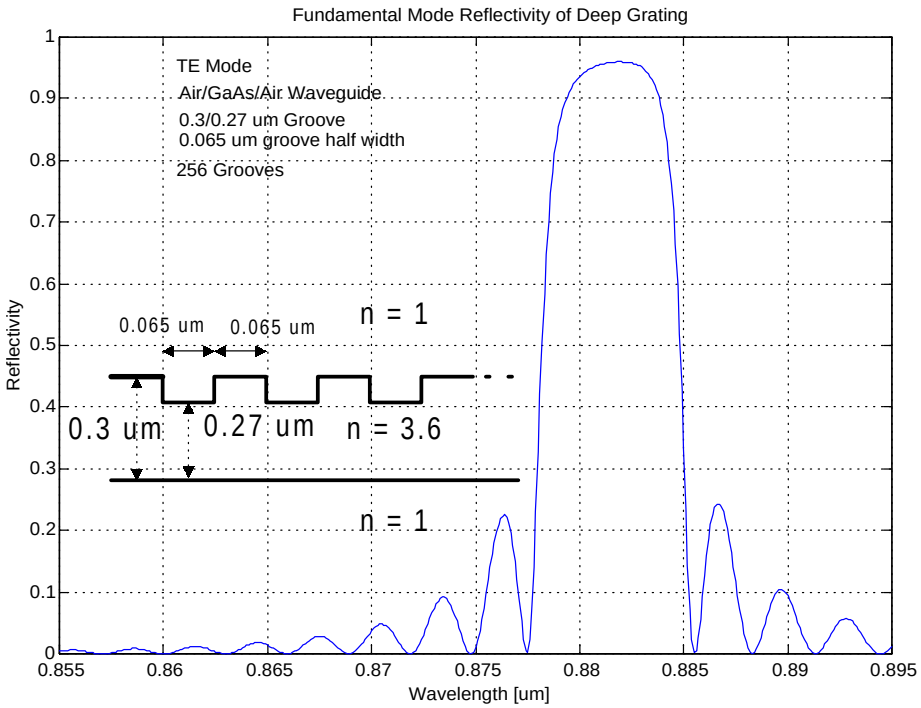

Figure 5.28: Modal Reflectivity, 10% Groove Depth

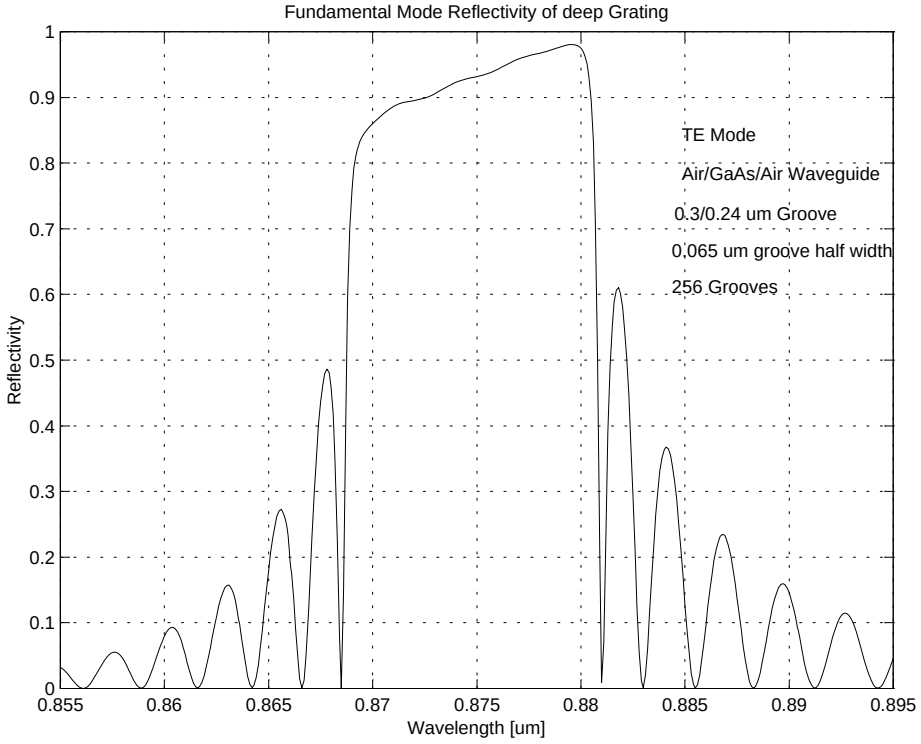

Figure 5.29: Modal Reflectivity, 20% Groove Depth

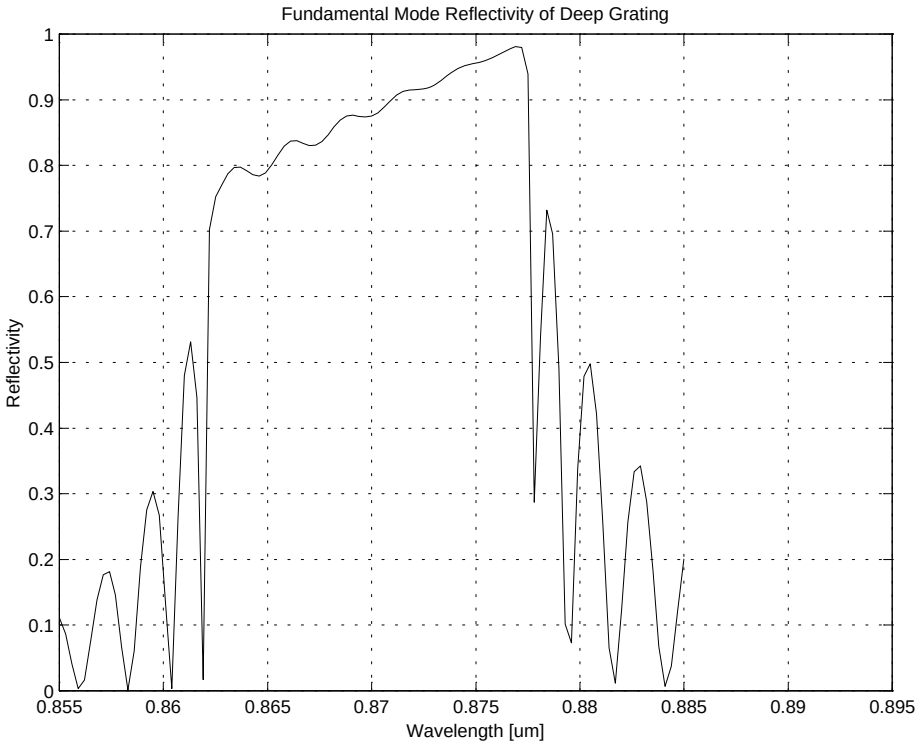

Figure 5.30: Modal Reflectivity, 26% Groove Depth

Chapter 6

Analysis of Anti-Resonant Reflecting Optical Waveguide (ARROW) Modes

6.1 Introduction

The Anti-Resonance Reflecting Optical Waveguides ARROW (see figure 1.2), which utilize the high reflectivity of two interference cladding layers deposited on the high index substrate can play an important role in integrated optics devices. Such a structure may be used as an excellent integrated optics polarizer [4]. Its large mode diameter allows excellent coupling to external elements such as single-mode optical fibers. Moreover, the ARROW waveguides seem to be promising for integrating vari-

ous electronic and topical devices on a single semiconductor chip. In order to design integrated optical devices, it is necessary to know very precisely the propagation constant or effective index of the leaky modes of this structure.

The idea of ARROW waveguide was first proposed by M. A. Duguay and co-workers [4]. The formulae to calculate the thickness of each layer are given in his paper. The modal characteristics of the ARROW waveguide are studied by many authors [53, 6, 54, 5]. In these papers, the ARROW waveguide is analyzed using equivalent transmission-line and transverse-resonance methods. In the previous work, much attention has been paid to the calculation of TE and TM mode losses of the ARROW Waveguide. In [8], the author describes loss calculation for ARROW waveguides using leaky mode solutions of the vector wave equation. General analytical expressions have been reported in the literature for TE, TM, HE and EH modes of multi-layer ARROW waveguides. In [6], standard-transfer matrix method is applied to ARROW waveguide and dispersion plots are given.

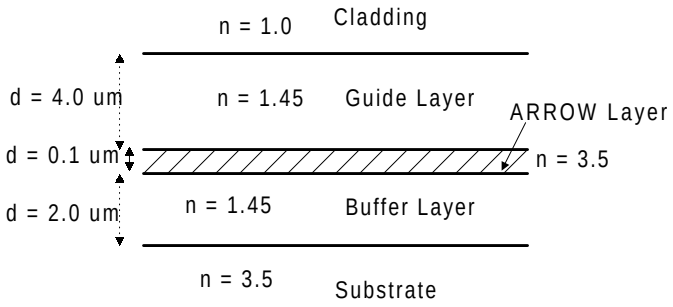

Figure 6.1: An ARROW Waveguide [4]

6.2 ARROW Eigenmodes

In this section, the Method of Lines is applied to model an ARROW structure taken from reference [4], and the results are compared with published as well as analytical results. A close agreement is found between the MoL calculation of the effective index (real and imaginary parts) and the modal field with those available in the literature. A non-uniform mesh scheme is used in the MoL to model the device effectively. A double layer PML is used as an absorbing boundary condition. It effectively absorbs the radiation and leaky modes [53] [6] of the ARROW giving excellent open-space approximation. It is found during the simulation that the performance of the PML depends upon the mesh size and the total thickness of the PML. If the sampling period is large, the PML does not absorb the leaky modes effectively giving *reflections* of the leaky mode from the PML. The same effect is observed if the PML thickness is small and if it is prematurely terminated by E/M wall. In this case, the modal field has not decayed to a sufficiently small value and reflection from the E/M wall occurs. The first layer of the PML has dense discretization lines, and the second layer has a coarse mesh to model a larger distance with relatively lesser sample points.

6.2.1 TE Modes

The ARROW structure is shown in figure 6.1. The ARROW modes have complex effective indices. The real part of the effective index lies between that of the cladding

layer index and the guide layer index, that is $1.0 < Re(n_{eff}) < 1.45$. The imaginary-part of effective index is converted into power loss per unit distance, that is in terms of dB/cm. The results for TE polarization are plotted in figures 6.2, 6.5, 6.3 and 6.4. The real-part of the effective index and power loss per unit distance are also given and found to be in close agreement with those in [4]. Note from Table 6.1 that only the lowest-order TE_0 mode has a small power loss of 0.25 dB/cm, while all higher-order modes have much higher loss factor (at least 100 times higher). On the other hand, all TM mode of ARROW are highly lossy. This makes this device effectively a single-mode waveguide and a TE-pass polarizer. All higher-order modes will decay significantly within a short propagation distance due to their high loss factor.

6.2.2 TM Modes

The simulations are repeated for the TM polarization and the results are shown in figures 6.6 and 6.7. The TM modes have much higher loss factor and they decay quickly within a short propagation distance.

6.2.3 Cladding Modes

The ARROW layer has a high refractive index $n = 3.5$ and the surrounding layers are of lower refractive-index $n = 1.45$. This shows that the high index layer can support at least one conventional mode based on the TIR principle. This is called

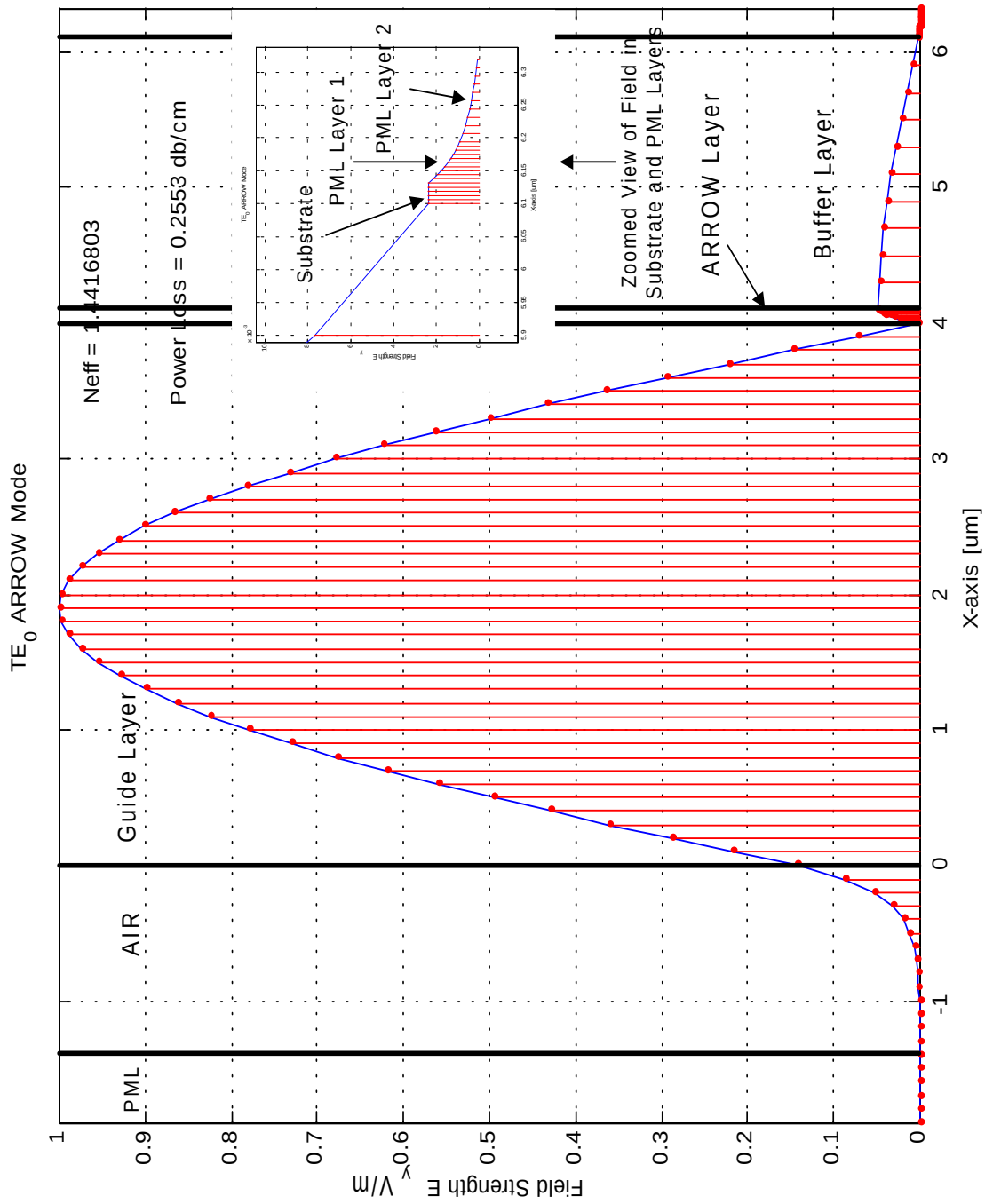

Figure 6.2: TE_0 Modal Field of the ARROW, Non-Uniform Mesh

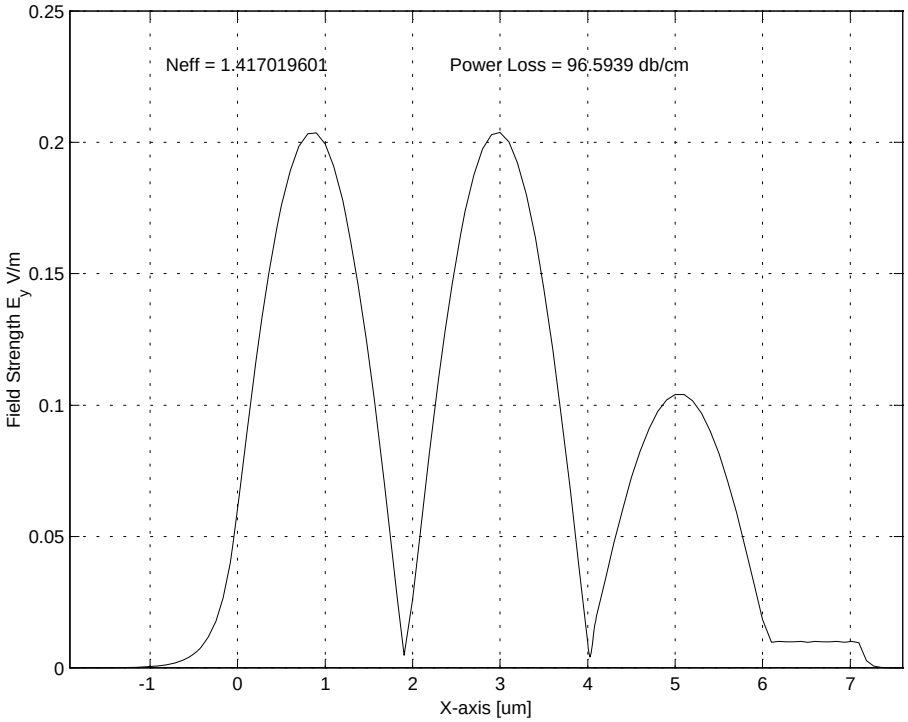

Figure 6.3: TE_1 Modal Field of the ARROW

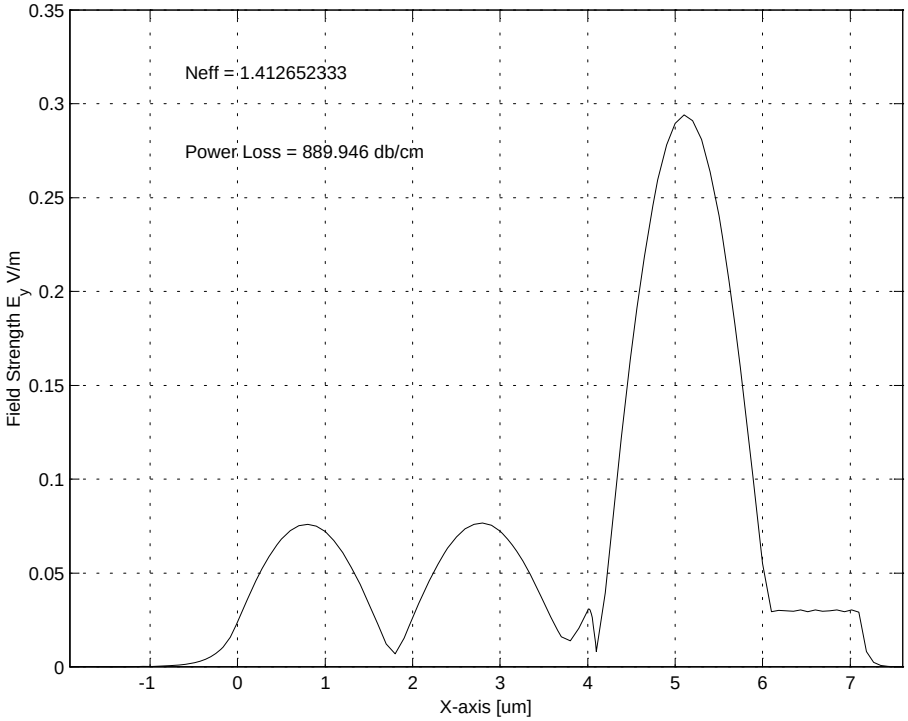

Figure 6.4: TE_2 Modal Field of the ARROW

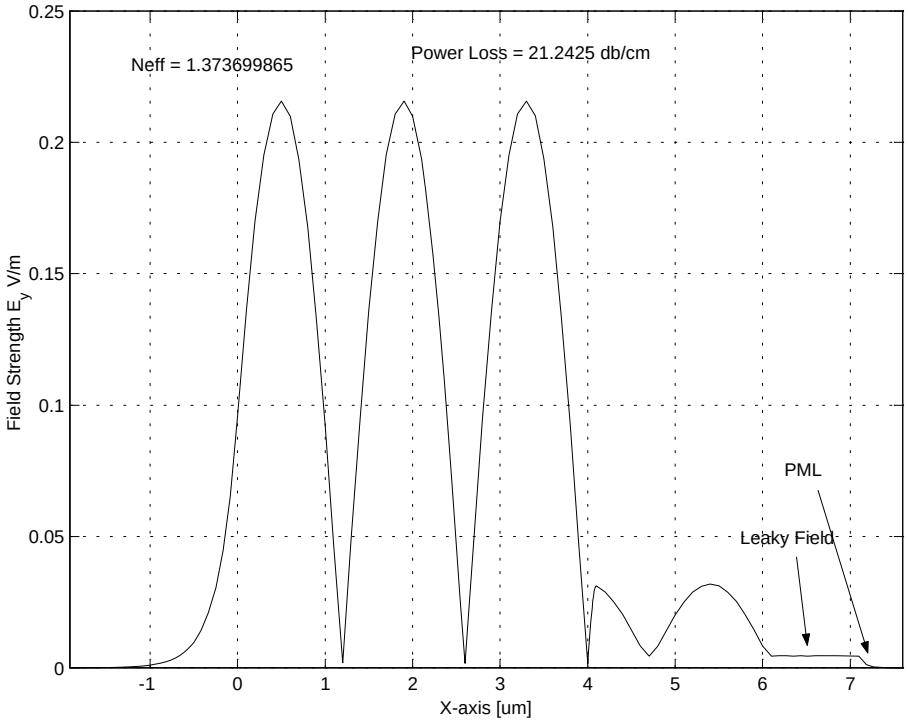

Figure 6.5: TE_3 Modal Field of the ARROW

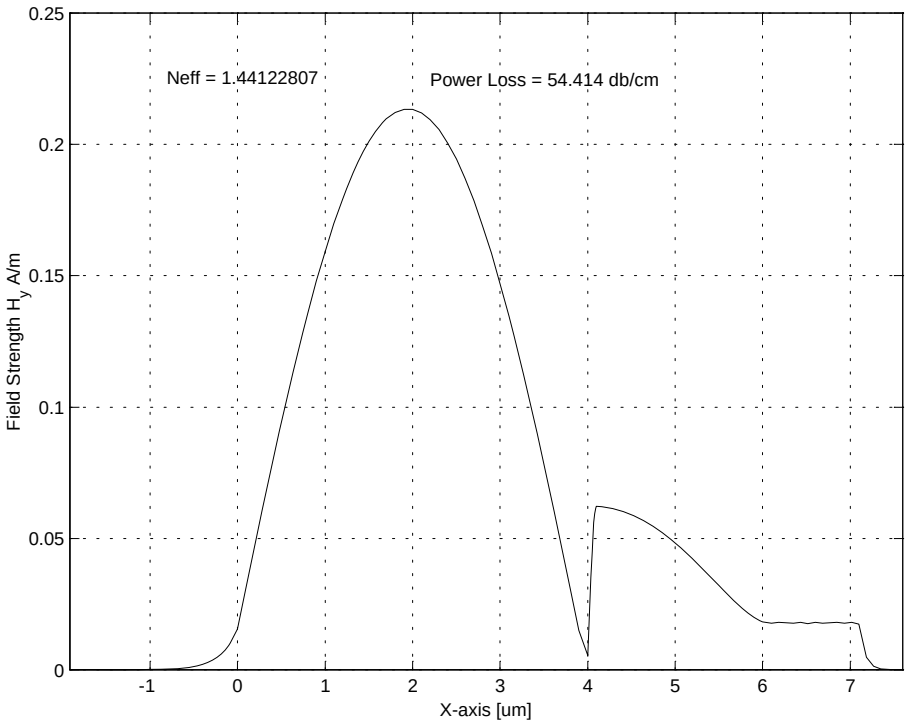

Figure 6.6: TM_0 Modal Field of the ARROW

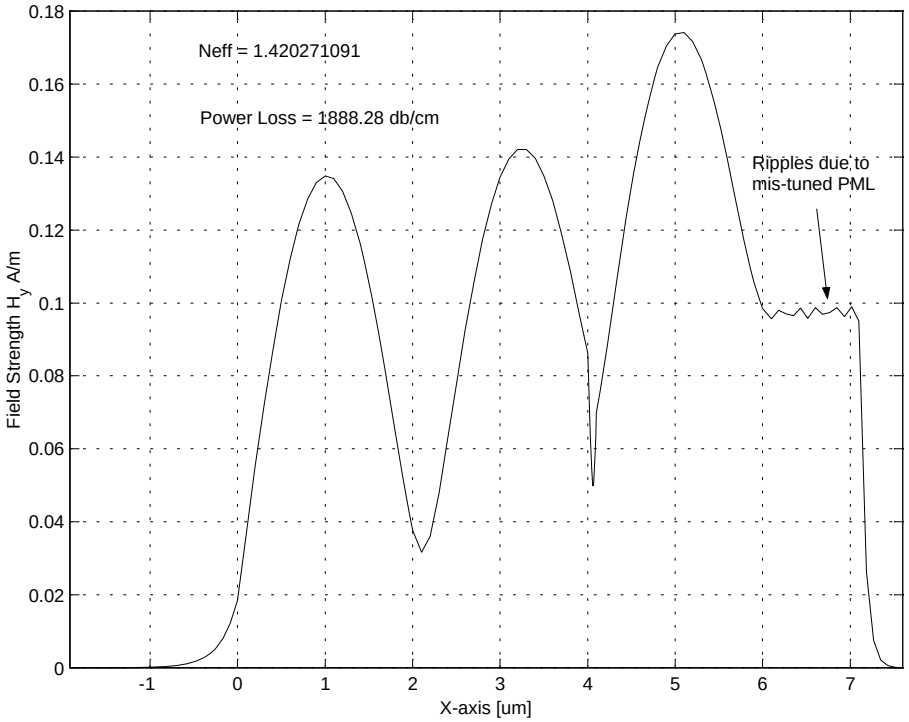

Figure 6.7: TM_1 Modal Field of the ARROW

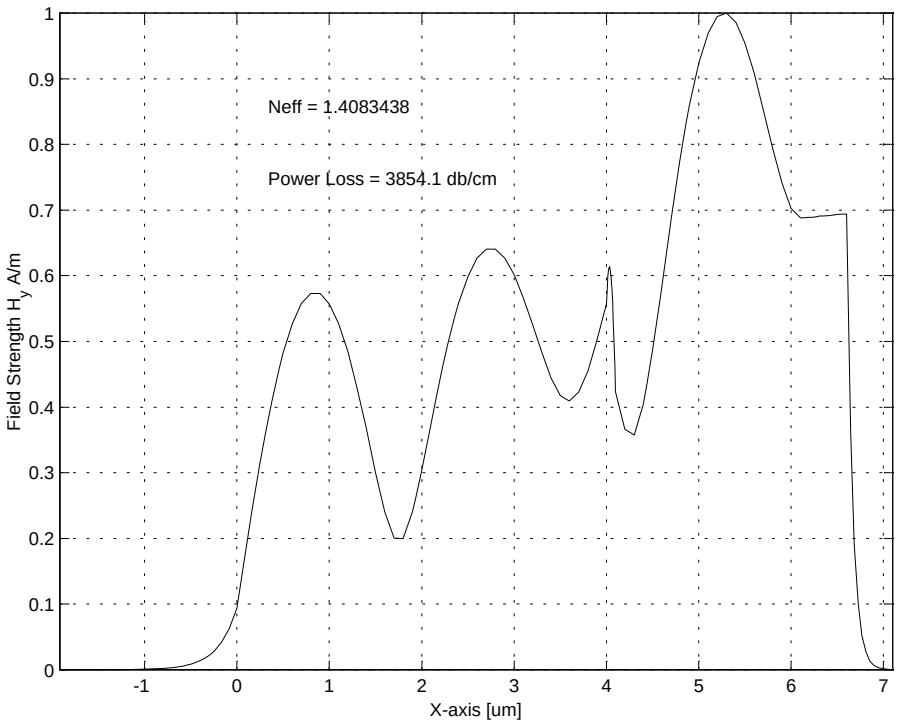

Figure 6.8: TM_2 Modal Field of the ARROW

the cladding mode and one such mode is shown in figure 6.9. The effective index of the cladding mode lies between the high and the low refractive indices, that is $1.45 < n_{eff} < 3.5$. This mode has *zero* power loss factor associated with its propagation constant due to the TIR guidance on both sides of the guiding layer.

Mode	N_{eff} $(real - part)$	Power Loss (dB/cm)
TE_0	1.441680	0.255
TE_1	1.417019	96.60
TE_2	1.412652	889.95
TE_3	1.373699	21.24
TE_4	1.313734	396.84
TE_5	1.228132	186.99
TM_0	1.441228	54.41
TM_1	1.420271	1888.28
TM_2	1.408343	3854.10
TE_{C0}	2.360204	0.000

Table 6.1: Effective-Indices of different ARROW Modes

6.2.4 Effect of Varying ARROW Parameters

Varying the Guide Layer Thickness:

The design of ARROW waveguide layer thickness and refractive- indices for single-mode low-loss operation is based on the formulae derived in many references [55][4]. If we deviate from these optimized values, the power loss associated with ARROW modes will increase. In this section, the guide layer thickness is varied to see its effect on the power loss of the TE_0 mode. The modal field profiles for different guide layer thickness are plotted in figure 6.10. The power loss factor associated

with each case is given in the inset of the figure. This figure shows that if the guide layer thickness is decreased while keeping all other parameters constant, the power loss of the fundamental ARROW TE mode increases. If the guide layer thickness is decreased from 4 μm to 2 μm, the power loss increases form 0.25 dB/cm to 58.3 dB/cm. As evident from the modal profile, for narrow waveguide the TE_0 mode profile has more energy in the buffer layer. This increases its leakage loss into the substrate layer causing the mode to attenuate quickly. The higher-order ARROW modes (TE_1, TE_2 etc.) are usually highly lossy by a factor of 100 or so as compared to the TE_0 fundamental ARROW mode.

Varying the ARROW Layer Thickness:

If the ARROW layer thickness is varied from its optimized value, the waveguide becomes lossy as shown in figure 6.11. The ARROW layer does not work in anti-resonance mode to suppress the radiation into substrate, rather, it resonates and increases the leakage into the substrate layer causing considerable power loss.

Varying the Buffer Layer Thickness:

The effect of varying buffer layer thickness is to increase the power loss of the fundamental ARROW mode as shown in figure 6.12. There is more energy in the buffer layer which leaks into the higher index substrate layer.

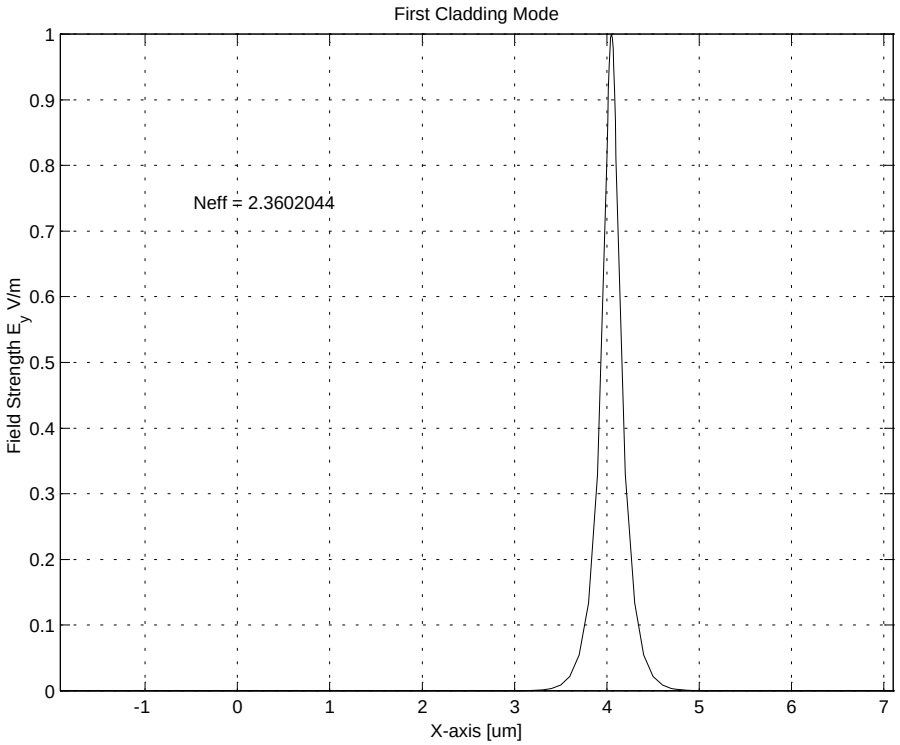

Figure 6.9: TE_{C0} First Cladding Mode of the ARROW

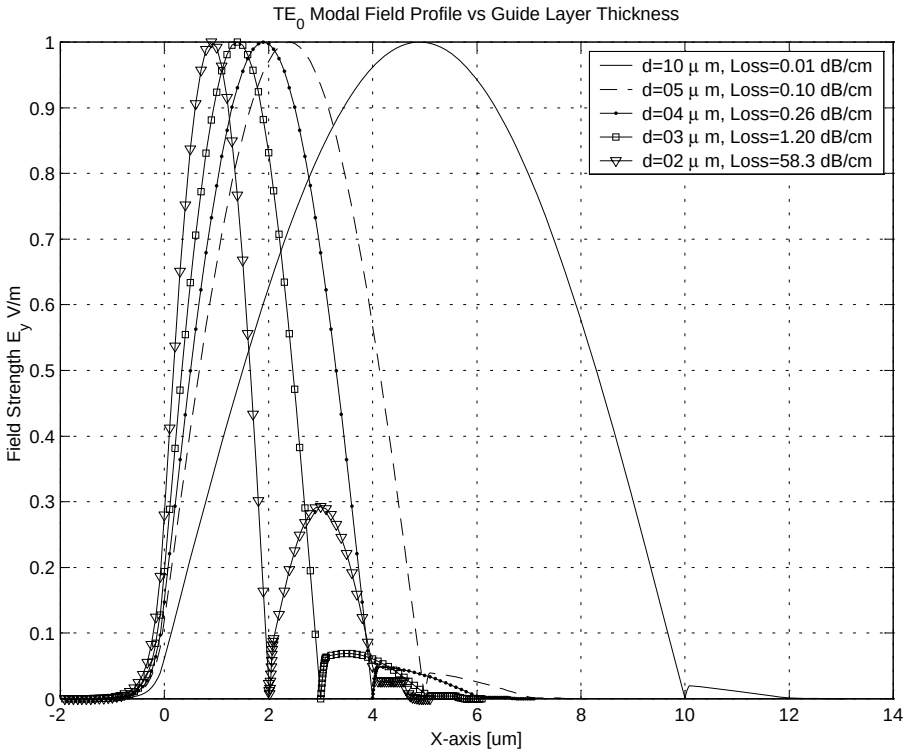

Figure 6.10: TE_0 Mode Profile vs Guide Layer Thickness

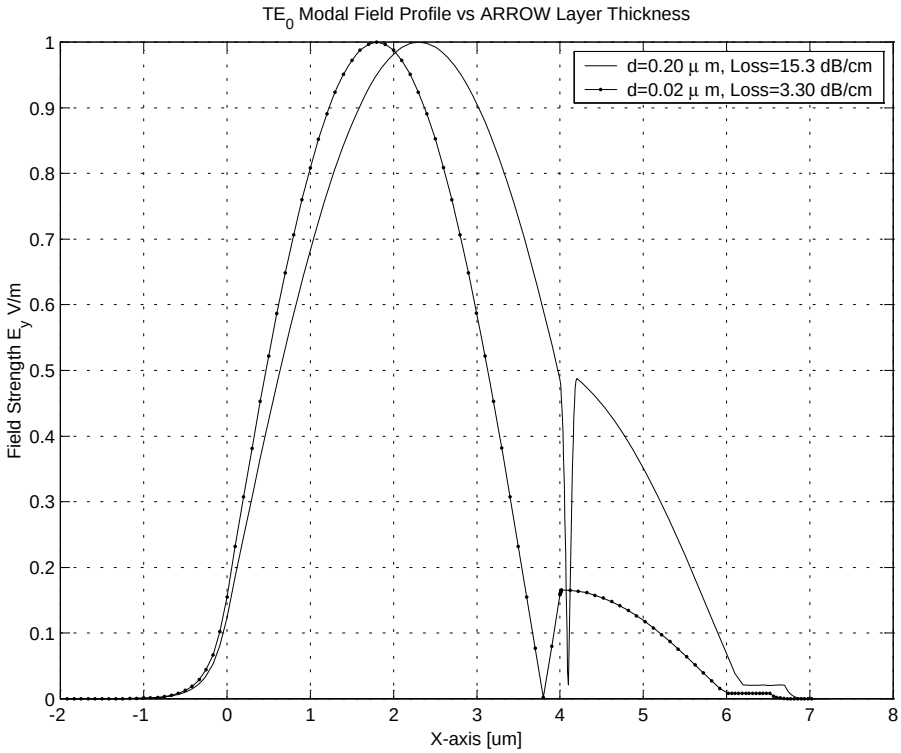

Figure 6.11: TE_0 Mode Profile vs ARROW Layer Thickness

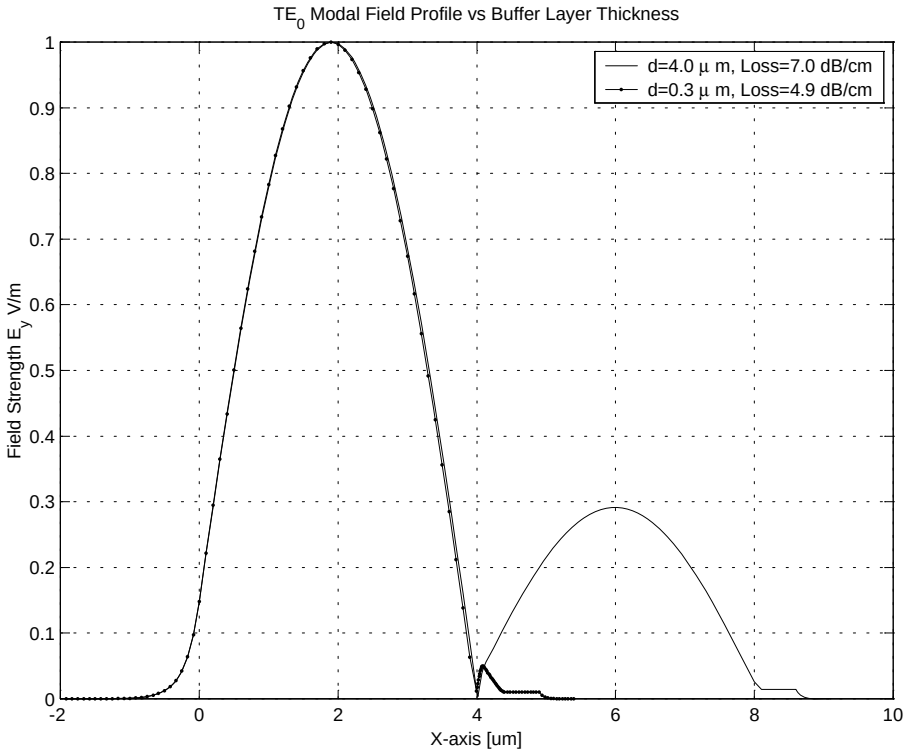

Figure 6.12: TE_0 Mode Profile vs Buffer Layer Thickness

Varying the Guide Layer Refractive-Index:

If the guide-layer refractive-index is decreased, the leakage loss of ARROW mode increases as shown in figure 6.13. If on the other hand, the refractive-index is increased, the modal field is more confined in the guide layer and leakage loss decreases. If the guide layer index is higher than that of the ARROW and buffer layer, it will behave as a regular waveguide with TIR confined mode.

6.3 Comparison of the Analytical and the MoL Results

To establish the accuracy of the MoL results, the power-loss of the fundamental ARROW mode is plotted against wavelength and the results are compared with the analytical values. The MoL results are in close agreement with those obtained from analytical calculation as shown in figure 6.14. This result shows that the ARROW waveguide has relatively low-loss over a wide wavelength range. There is a peak at about $0.65\,\mu m$ which is due to the resonance transmission of the ARROW layer. The anti-resonance condition of ARROW layer is fulfilled in a wide wavelength region and the device has low power loss in this region.

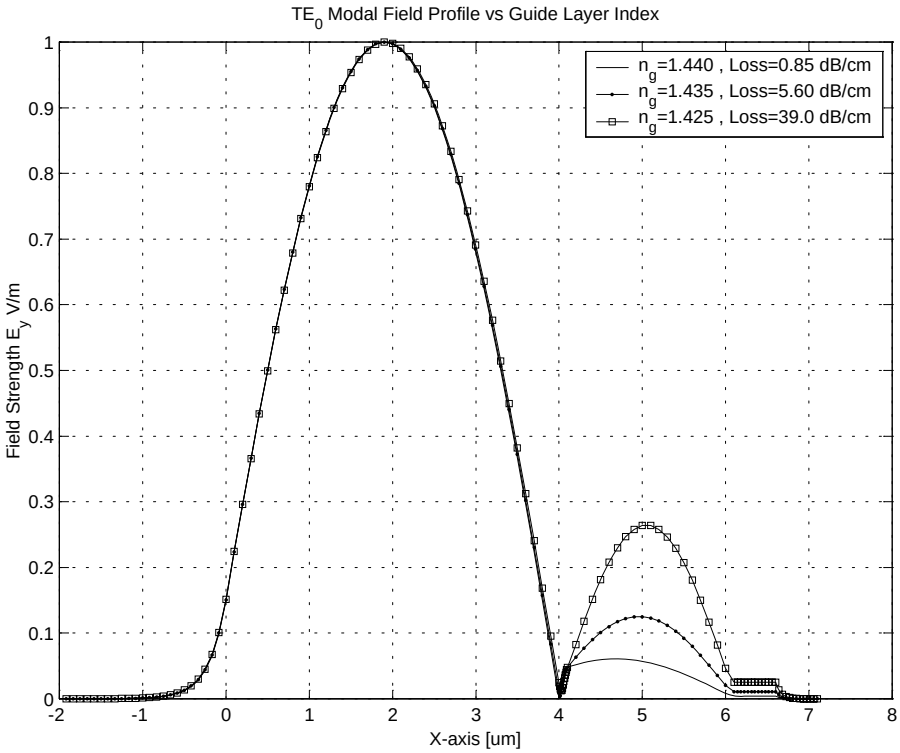

Figure 6.13: TE_0 Mode Profile vs Guide Layer Refractive Index

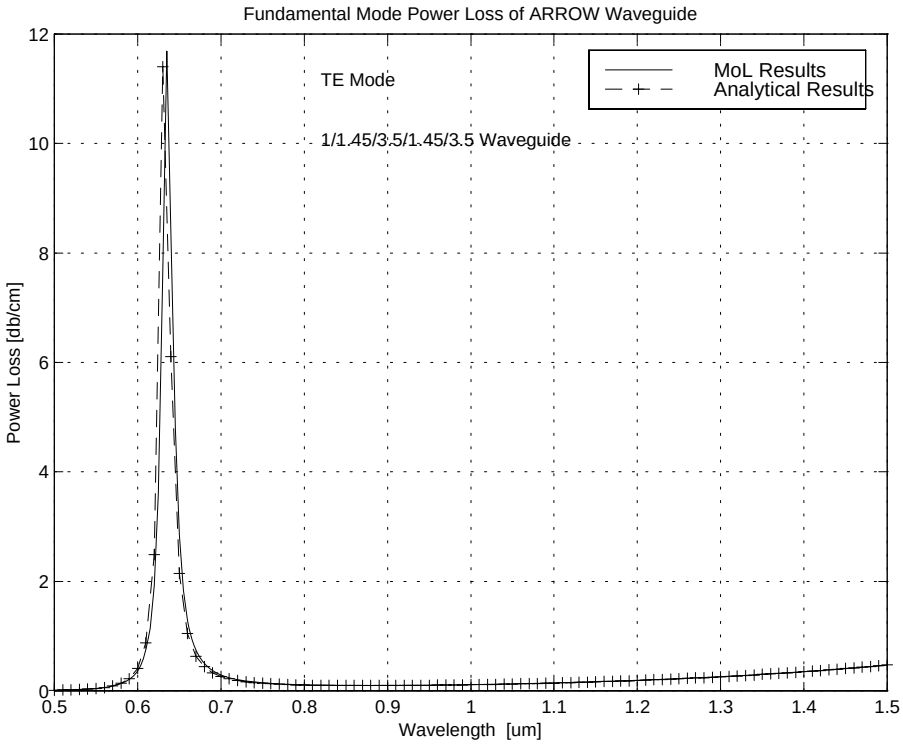

Figure 6.14: TE_0 Mode Power Loss vs Wavelength

6.4 Modal Field Propagation in an ARROW

The propagation characteristics of the ARROW waveguide and performance of the PML is studied by launching a TE_0 ARROW mode with some random noise in the waveguide and observing its development over a large propagation distance. As shown in figure 6.15, the field develops into the TE_0 ARROW mode plus a cladding mode. All higher-order modes are highly lossy and therefore decay quickly. Note that the cladding mode has a lower-loss than the first ARROW mode 6.1. So, after propagating a very large distance along the axis of the waveguide, the first ARROW mode will eventually decay and only the cladding mode will survive without suffering any power loss.

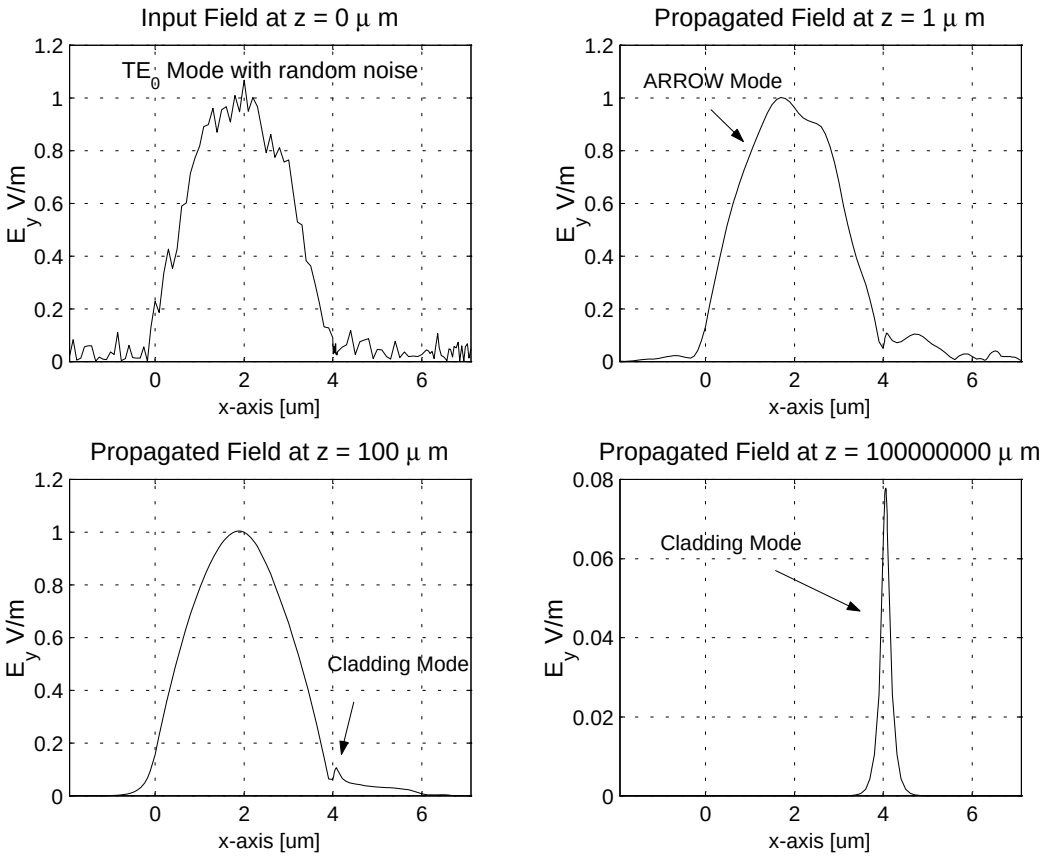

Figure 6.15: Propagation of the TE_0 ARROW Mode with Noise

Chapter 7

Analysis of ARROW Gratings

7.1 Introduction

ARROW waveguides can be used for wavelength filtering. The structure itself is wavelength selective as the anti-resonance condition is satisfied only in a certain wavelength range. So for wavelengths above or below the design wavelength, the modes will have higher loss. However, the ARROW has low-loss over a wide wavelength range as shown in the last chapter. In [56, 57, 58, 59], the authors describe an ARROW-based optical wavelength filter. These filters are based on a directional coupler arrangement using two adjacent ARROW waveguides. Due to different core diameters, the two waveguides have different propagation constant for the fundamental ARROW mode and are phase-matched only at a central wavelength. In [60], an ARROW-based directional coupler acousto-optic filter is designed.

In this chapter, periodic corrugations are introduced on the top surface of the

ARROW (see figure 7.1) resulting in an **ARROW Grating**. This device behaves as a wavelength selective filter due to multiple reflections from each discontinuity and their interaction with each other to cause resonance or anti-resonance in the propagation direction. In this chapter, modal spectral response of the ARROW

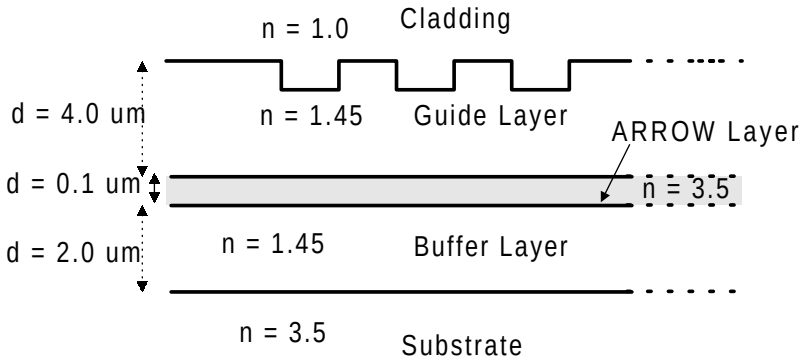

Figure 7.1: An ARROW Grating Structure

grating will be analyzed using the Method of Lines for different groove depths, different number of periods and different loss of the ARROW. Our main focus will be on fundamental ARROW mode with TE polarization. As found in the last chapter, the ARROW has very high loss for higher TE modes and all TM modes, so these modes will not be analyzed for ARROW grating in this thesis. It is found that the ARROW grating behaves as conventional waveguide grating when the basic ARROW is optimized for low-loss operation. However, when the ARROW loss is increased, either by changing the refractive-index of guide layer or by varying layer thickness of a certain layer, the ARROW grating behaviour is changed. As the loss of ARROW increases, the ripples in the modal spectral reflectivity curve are smoothed

out and the peak reflectivity decreases. The ARROW grating filter bandwidth can be made very narrow by making the grating shallow while increasing the number of periods to achieve a higher peak reflectivity. If the grating is made deeper, its response becomes irregular and its bandwidth is increased.

7.2 Results

In this section, the modal spectral response of the ARROW grating is presented for different configurations of the basic ARROW structure from [4].

7.2.1 Low Loss Grating: 10% Groove Depth

In figure 7.2, the modal spectral reflectivity and transmissivity of the ARROW grating with 10% groove depth and 1024 periods is plotted. The 3-db bandwidth of the reflectivity curve is approximately 1.5 nm. There is little loss in the transmission curve due to a smaller number of periods. In figure 7.3, the response of the same structure with 32768 periods is given. For more periods, the peak reflectivity increases and main lobe becomes flatter with higher and closely packed side lobes. The modal transmissivity plot has a deep notch in the stop band. Its transmission is good in the pass band with small ripples. The 3-db reflection bandwidth shrinks to approximately 1.0 nm. This behaviour of the low-loss ARROW grating is typical of the uniform gratings and is similar to that of the conventional waveguide gratings.

7.2.2 Low Loss and Lossy Grating: 5% Groove Depth

In this section, the effect of introducing loss into the ARROW waveguide is analyzed for different number of grating periods. In figure 7.4, the response of the low-loss ARROW grating with 1024 periods is shown. It has a 3-db bandwidth of about 1.0 nm. A power loss of 5.6 db/cm is then introduced in the ARROW waveguide by lowering the guide layer refractive-index from 1.45 to 1.43, and the spectral response is shown in figure 7.5. There is little difference between the two graphs except that the peak reflectivity has slightly dropped for the lossy ARROW. In addition, there is a shift in the Bragg wavelength (resonance wavelength) to the lower wavelengths due to the change in the effective index of the basic ARROW. This behaviour is similar for all other cases discussed below. An approximate relation between the Bragg wavelength λ_B, the grating period $2d$ and the effective index is given by $\lambda_B = 2dn_{eff}$ [2].

In figure 7.6, the response of the low-loss grating with 8192 periods is given. It has a 3-db reflection bandwidth of 0.5 nm and the peak reflectivity is very close to 0.0 db. The behaviour of the lossy grating is similar to the low-loss case except that the reflectivity drops slightly below 0.0 db. The side lobe ripples are slightly suppressed and transmissivity also drops to about 4.0 db in the pass band (see figure 7.7). This suggests that the lossy ARROW grating may be useful only in the

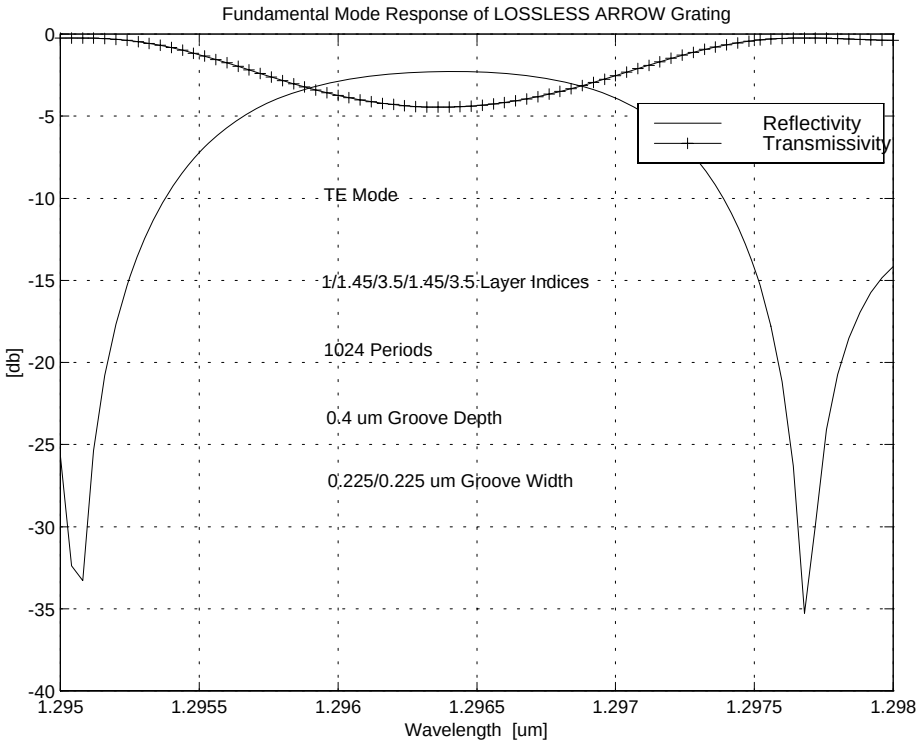

Figure 7.2: Low Loss ARROW Grating, 10% Groove Depth, 1024 Periods

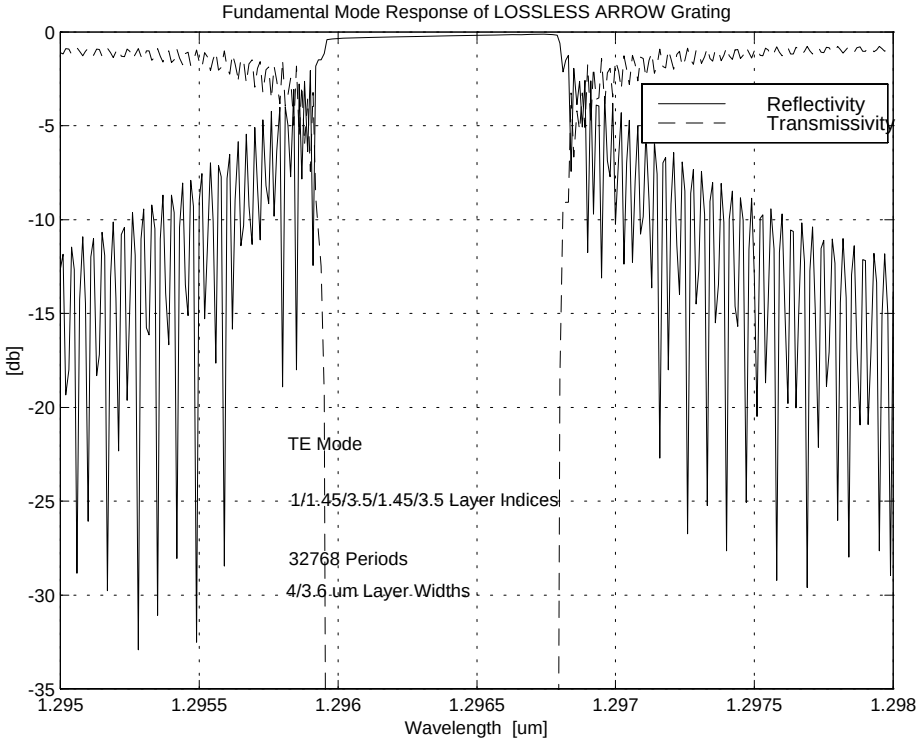

Figure 7.3: Low Loss ARROW Grating, 10% Groove Depth, 32768 Periods

reflection case and for the transmission case, the device insertion loss is very high.

If the number of periods is further increased to 32768, the low-loss grating has higher side lobes and a flatter main lobe (figure 7.8). The 3-db bandwidth is about 0.5 nm. The spectral response of the corresponding lossy structure has suppressed ripples and its peak reflectivity also drops slightly as compared to the low-loss case (see figure 7.9). The grating transmission is very poor and the pass-band loss increases to about 15.0 db. In figure 7.10, the number of periods is increased to 131072 for the same configuration. The side lobes are seen to be completely suppressed in the reflection mode while 3-db bandwidth is almost the same (0.5 nm). Comparing figures 7.9 and 7.10, we see that the only difference between the two curves is in terms of lower ripples in the side lobes for the longer grating while peak reflectivity, bandwidth and Bragg wavelength are the same as that of the short grating. This shows that after a certain number of periods of the grating, adding extra periods will not affect the modal spectral reflectivity.

If loss is introduced by some other mechanism, for example by changing the ARROW layer thickness from $0.1\,\mu m$ to $0.19\,\mu m$, the response of the grating is unchanged for the same number of periods (figure 7.11). In figure 7.12, a loss of 4.9 db is introduce by decreasing the buffer layer thickness from $2.0\,\mu m$ to $0.3\,\mu m$. The modal reflectivity has similar characteristics with suppressed side lobes. If a small conductivity is introduced into the guide layer, thus making the material lossy, the behaviour of the ARROW grating is similar to the previous case. In figure 7.13, an imaginary factor of 10^{-5} is added in the guide layer refractive index to make it

lossy (introducing about 4.5 dB/cm power loss). We observe no change in the 3-db bandwidth or the peak reflectivity. In figure 7.14, a power loss of 30.0 db/cm is introduced by lowering the refractive-index of the guide layer from 1.45 to 1.425. The pass band in this case is no longer flat, its peak reflectivity drops to -7.0 db and the overall curve becomes broader.

7.2.3 Shallow Gratings

In figure 7.15, the modal spectral reflectivity of the low-loss ARROW grating with 0.5% groove depth and 131072 periods is plotted. It has a very narrow 3-db bandwidth of about 0.05 nm and low side lobes level (about 20 db). In the companion figure 7.16, the ARROW is deliberately made lossy (power loss = 3.0 db/cm) by increasing ARROW layer thickness from $0.1\,\mu m$ to $0.19\,\mu m$. The peak reflectivity decreases from 0 db for the low-loss case to -5 db for the lossy case and the side lobes also disappear completely. Moreover, the 3-db bandwidth stays the same for the two cases while the Bragg wavelength shifts due to the change in the effective index of the ARROW due to varying its layer thickness. In these two figures, the horizontal and the vertical scales are kept the same so that an easy visual comparison can be made. This example shows that for very narrow pass-band optical filters, we should use shallow gratings with more periods to get substantial reflection.

If the groove depth is increased to 1.0%, the 3-db bandwidth of the low-loss ARROW grating is doubled and the side lobes become higher and more closely

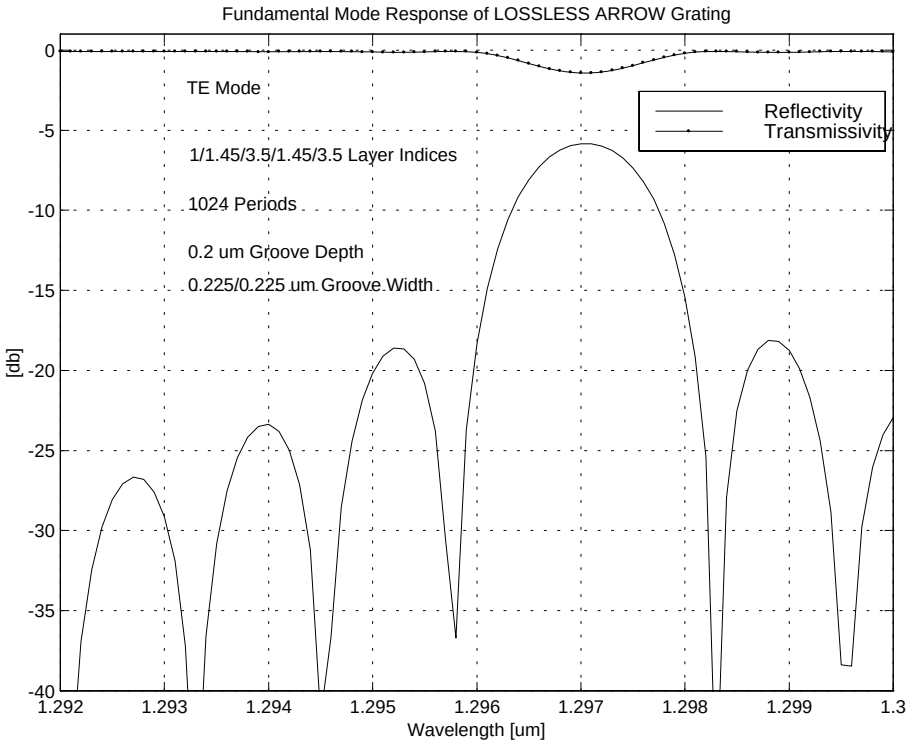

Figure 7.4: Low Loss ARROW Grating, 1024 Periods

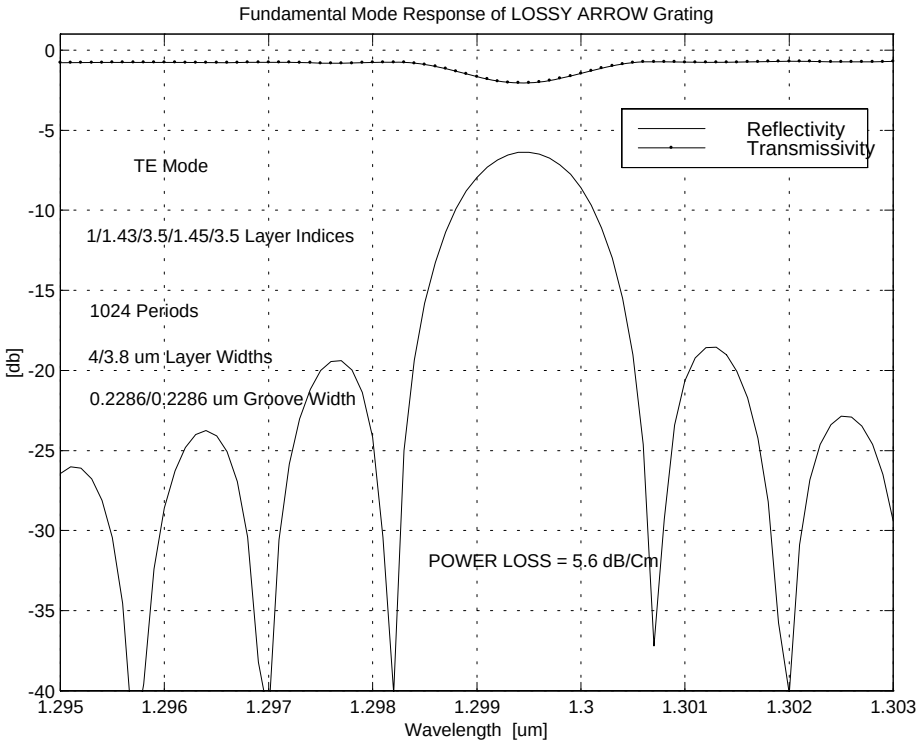

Figure 7.5: Lossy ARROW Grating, 1024 Periods

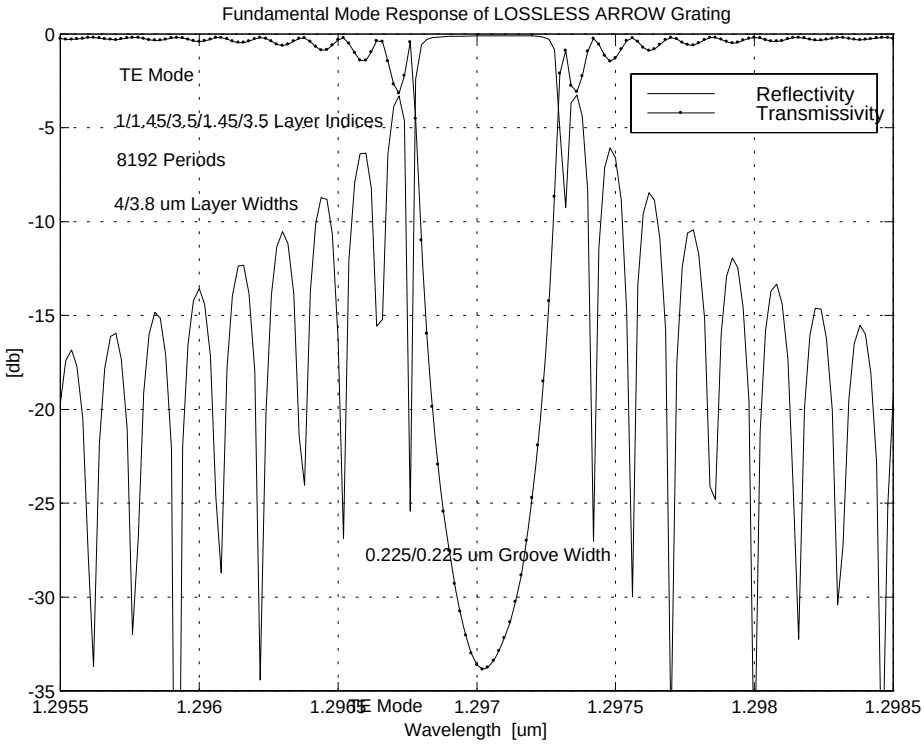

Figure 7.6: Low Loss ARROW Grating, 8192 Periods

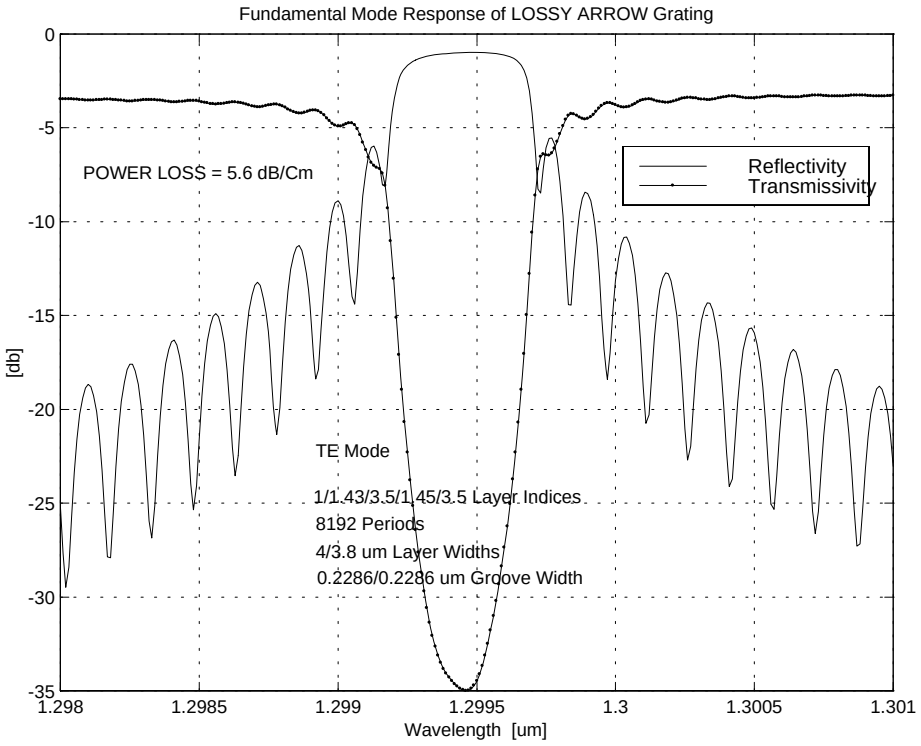

Figure 7.7: Lossy ARROW Grating, 8192 Periods

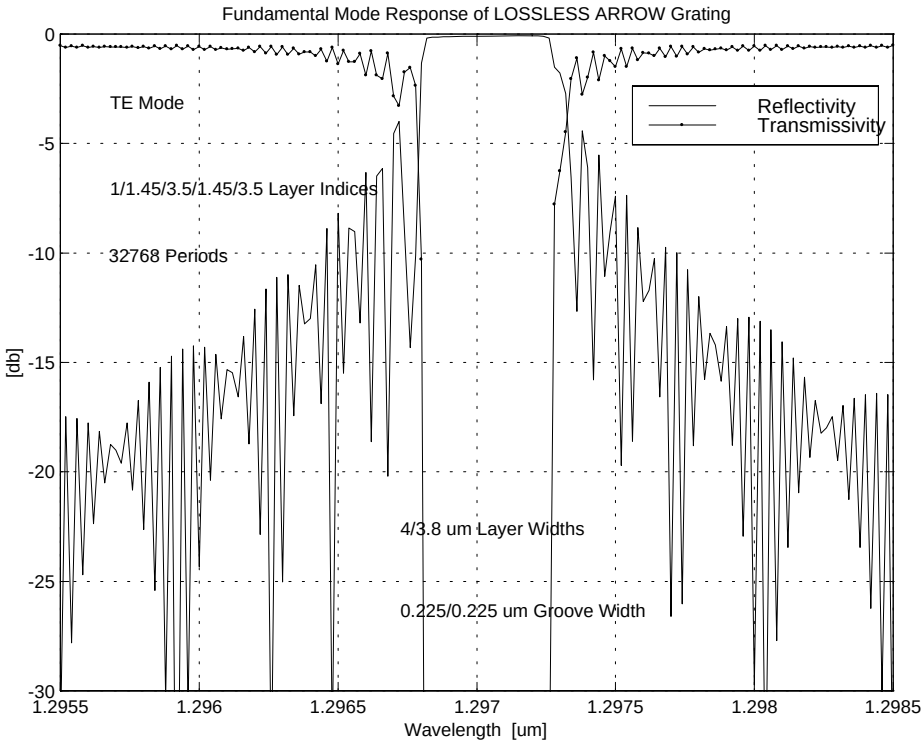

Figure 7.8: Low Loss ARROW Grating, 32768 Periods

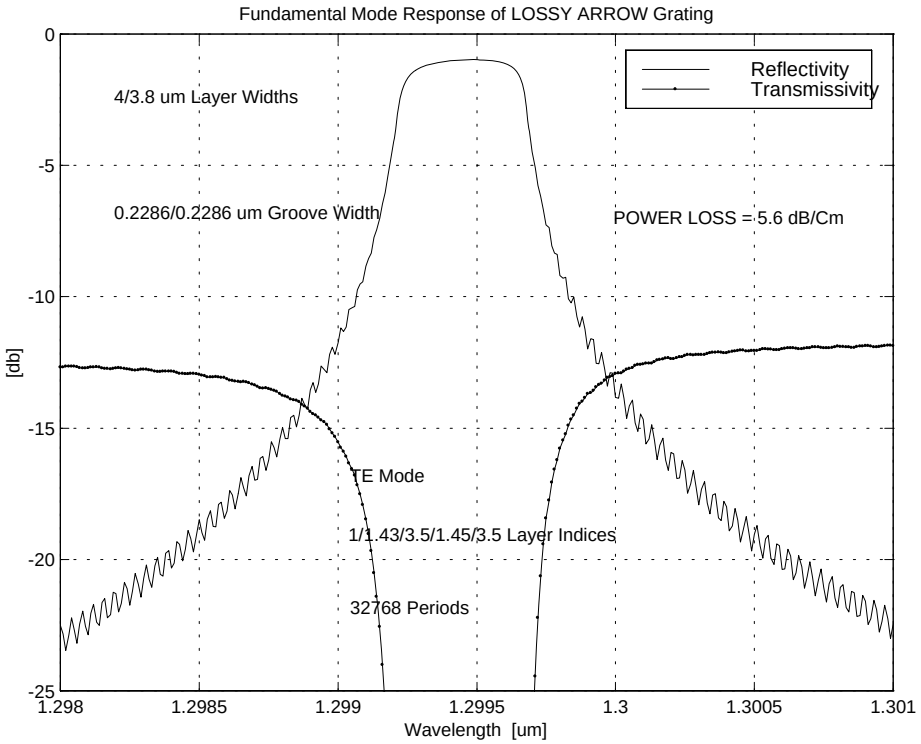

Figure 7.9: Lossy ARROW Grating, 32768 Periods

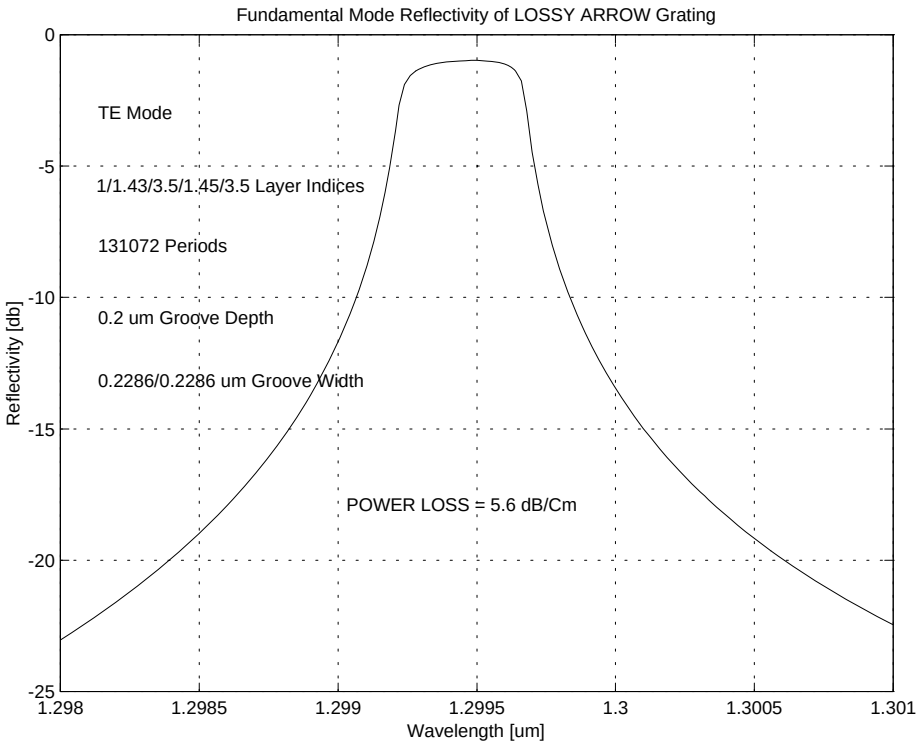

Figure 7.10: Lossy ARROW Grating, 131072 Periods, n_{guide} decreased

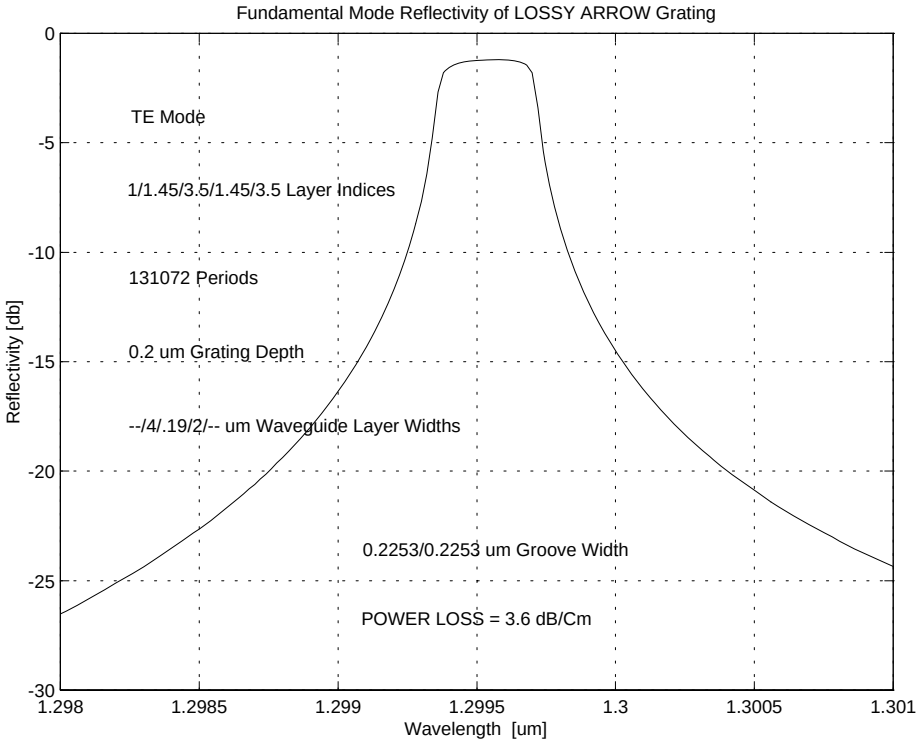

Figure 7.11: Lossy ARROW Grating, 131072 Periods, d_{ARROW} increased

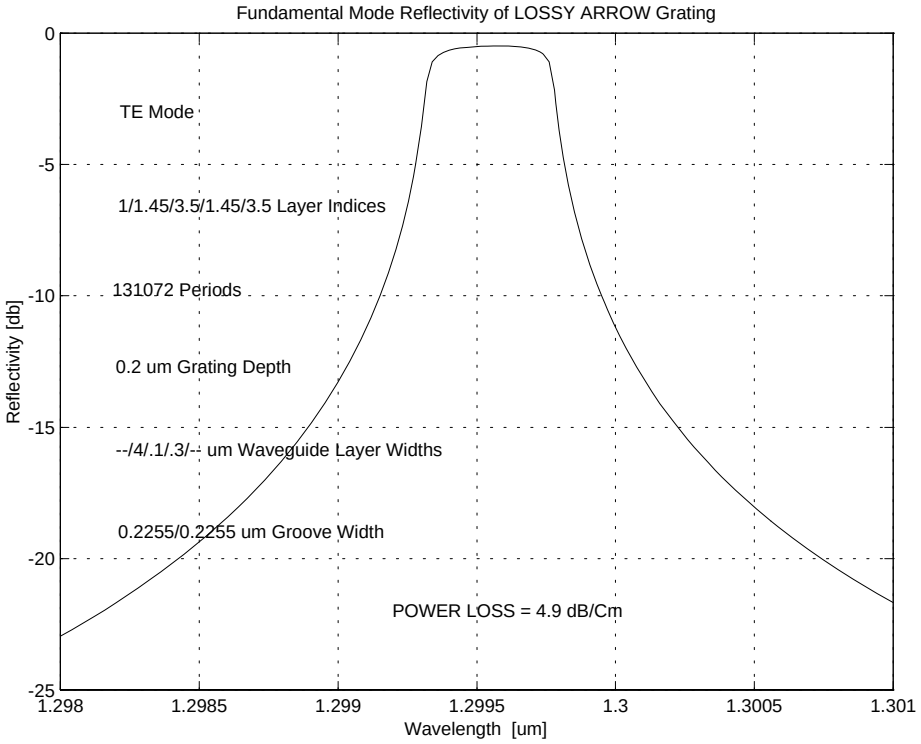

Figure 7.12: Lossy ARROW Grating, 131072 Periods, d_{Buffer} decreased

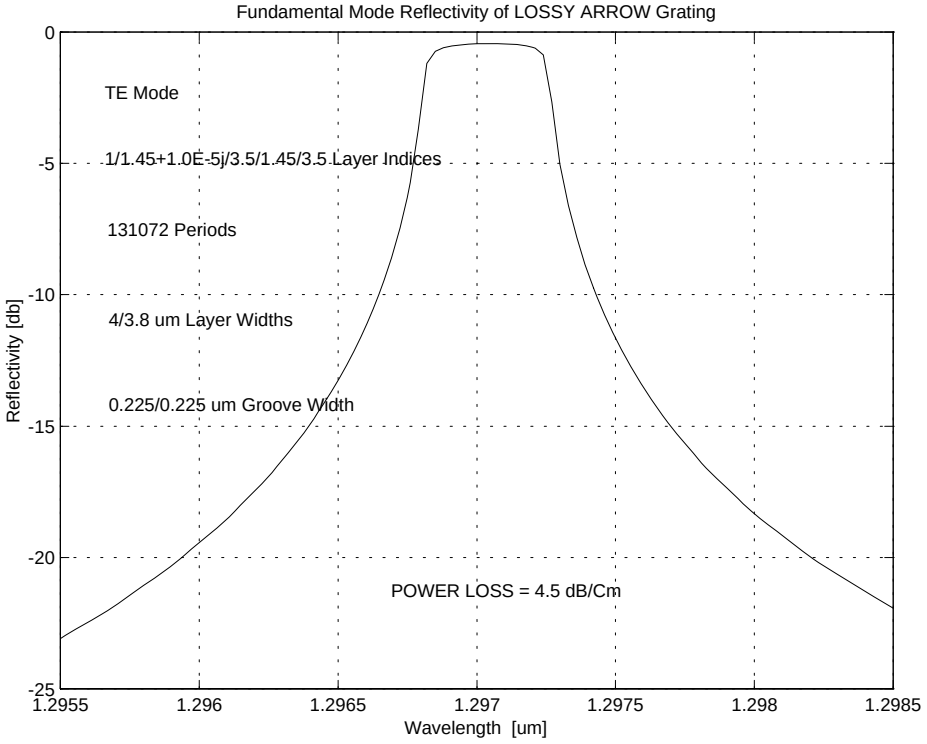

Figure 7.13: Lossy ARROW Grating, 131072 Periods, complex n_{guide}

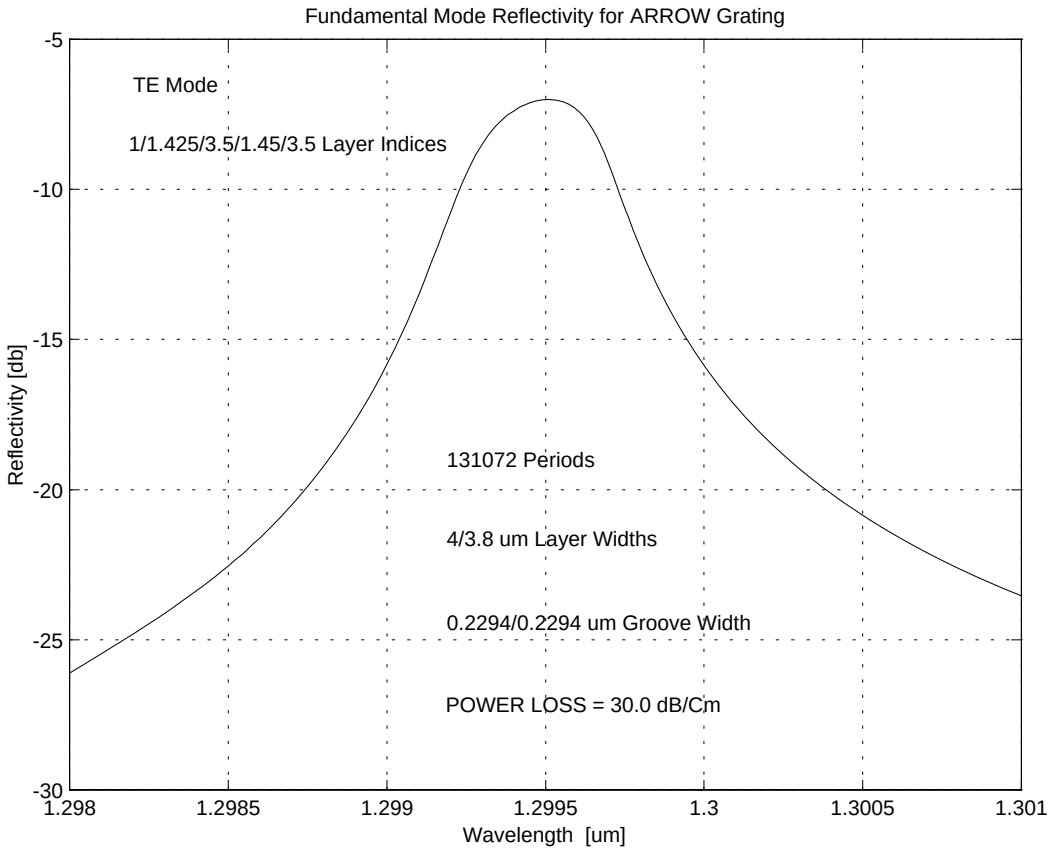

Figure 7.14: High Loss ARROW Grating, 131072 Periods

packed (see figure 7.17). In the companion figure 7.18, the ARROW is made lossy (power loss = 5.6 db/cm) by reducing the guide layer refractive-index from 1.45 to 1.43. The peak reflectivity for this lossy case decreases to -3 db and the side lobes are seen to smooth out while the 3-db bandwidth remains the same.

If the groove depth is still increased to 2.5%, the 3-db bandwidth of the low-loss ARROW increases to 0.25 nm (see figure 7.19 for 32768 periods). The side lobes are high and are very closely packed. The modal transmissivity curve is also plotted, and is seen to resemble a deep notch filter in the stop band. In the companion figure 7.20, a power loss of 5.6 dB/cm is introduced by lowering the guide layer index from 1.45 to 1.43. For the lossy ARROW, the side lobes disappear and peak reflectivity decreases from about 0 db to 2 db. The 3-db bandwidth remains the same. If the number of periods is further increased to 65536 for the same lossy ARROW, the ripples completely disappear and the transmissivity is further reduced as shown in figure 7.21.

7.2.4 Deep Gratings

If the grating depth is increased substantially, the modal spectral response becomes asymmetric and the main lobe bandwidth increases. In this section, the ARROW grating with 25% groove depth is analyzed for the low-loss and the lossy cases. In figure 7.22, the modal reflectivity and transmissivity of the low-loss ARROW grating with 1024 periods is plotted. The 3-db bandwidth is approximately 2 nm which is

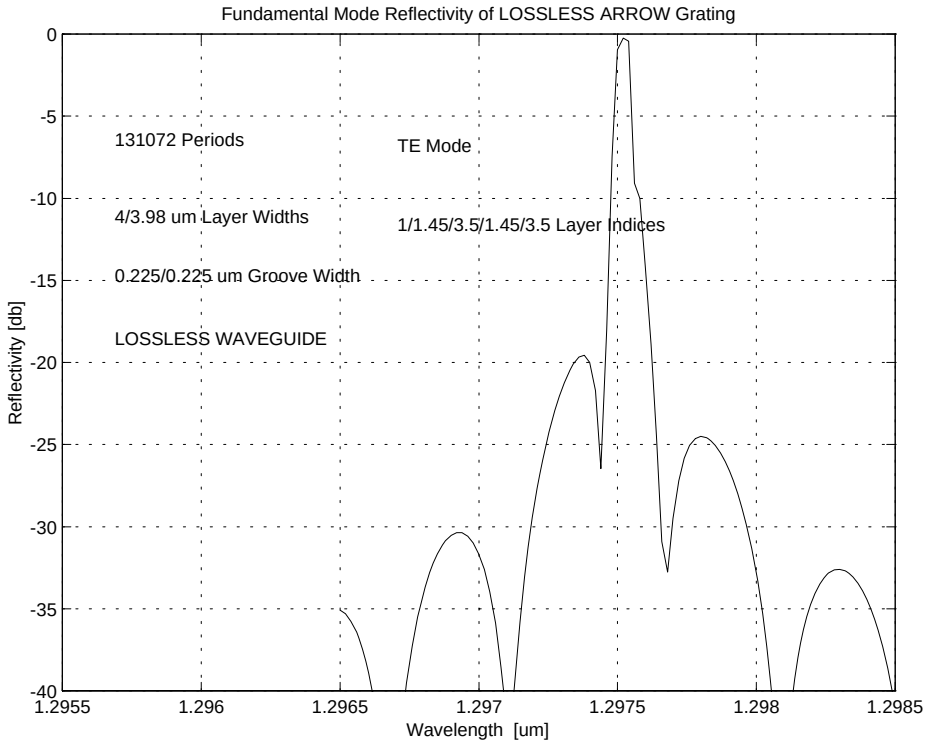

Figure 7.15: Low Loss ARROW Grating, 0.5% Groove Depth

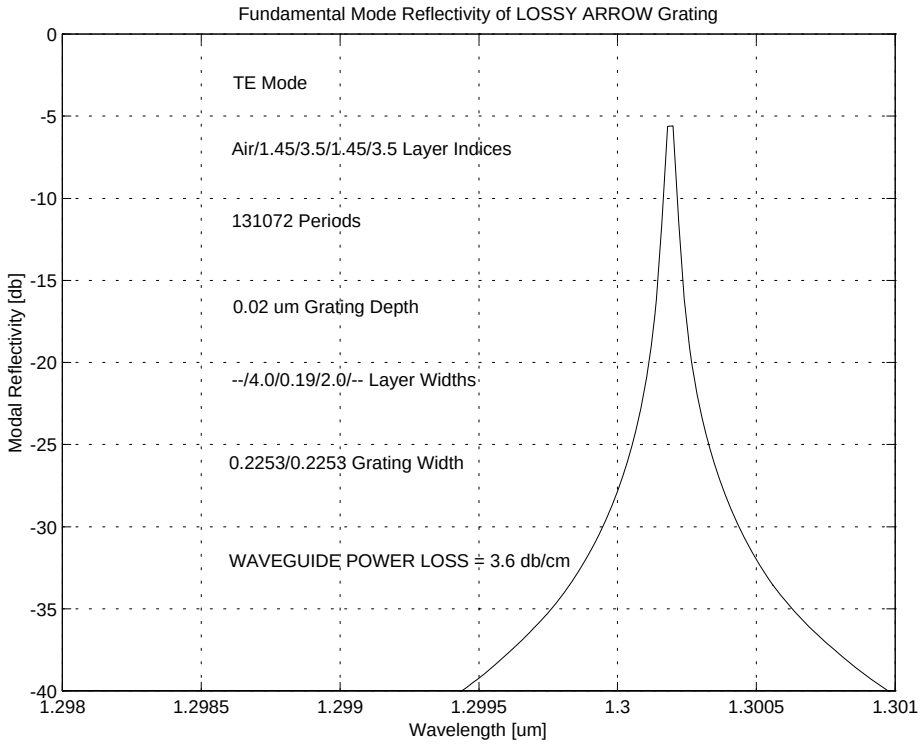

Figure 7.16: Lossy ARROW Grating, 0.5% Groove Depth

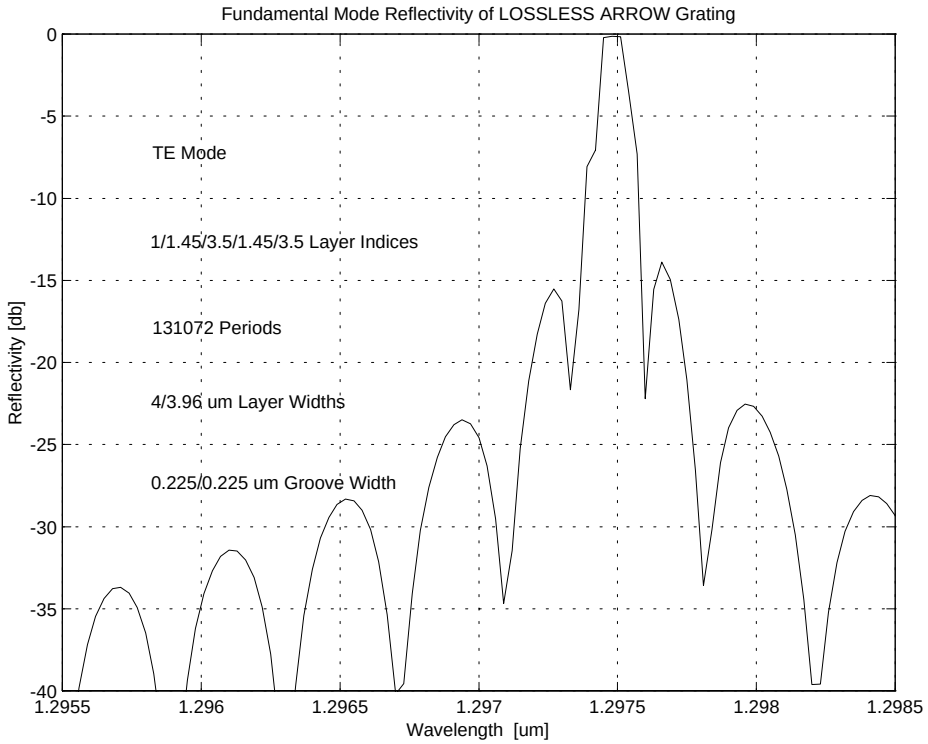

Figure 7.17: Low Loss ARROW Grating, 1.0% Groove Depth

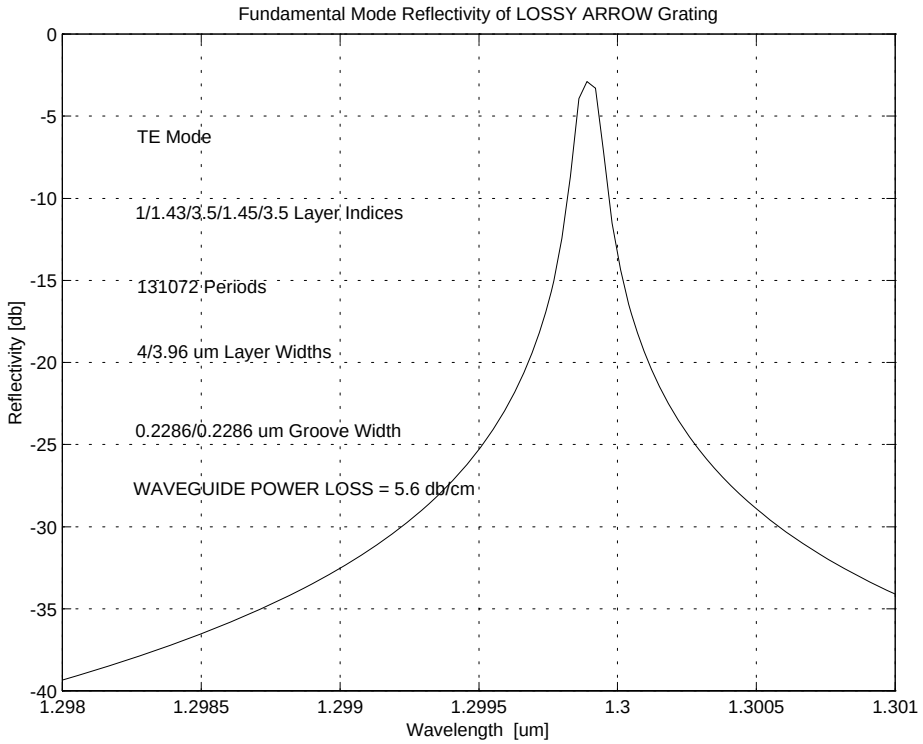

Figure 7.18: Lossy ARROW Grating, 1.0% Groove Depth

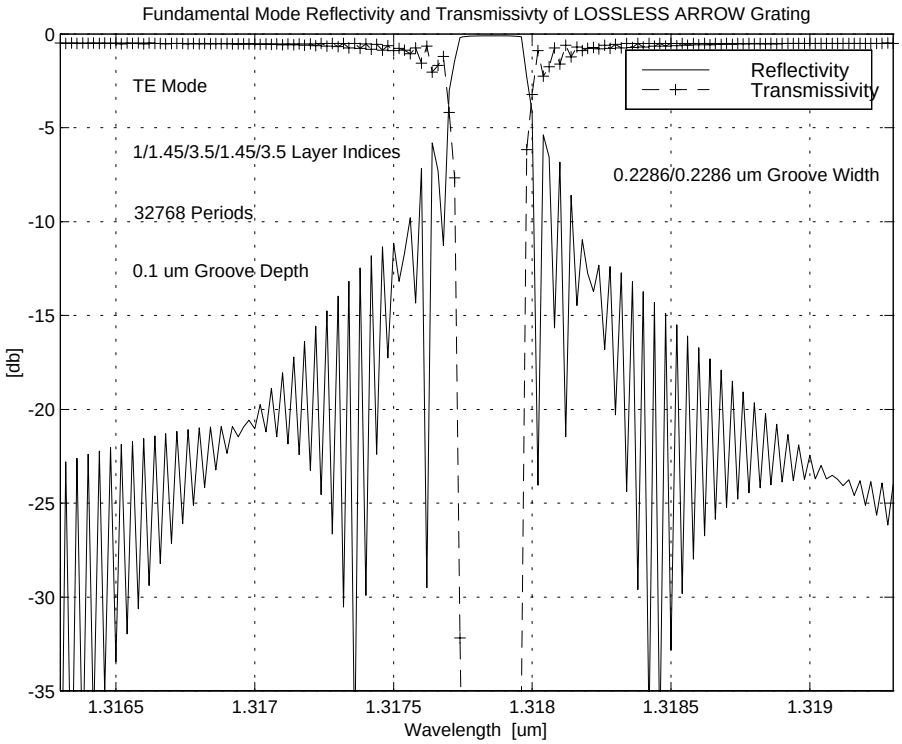

Figure 7.19: Low Loss ARROW Grating, 2.5% Groove Depth

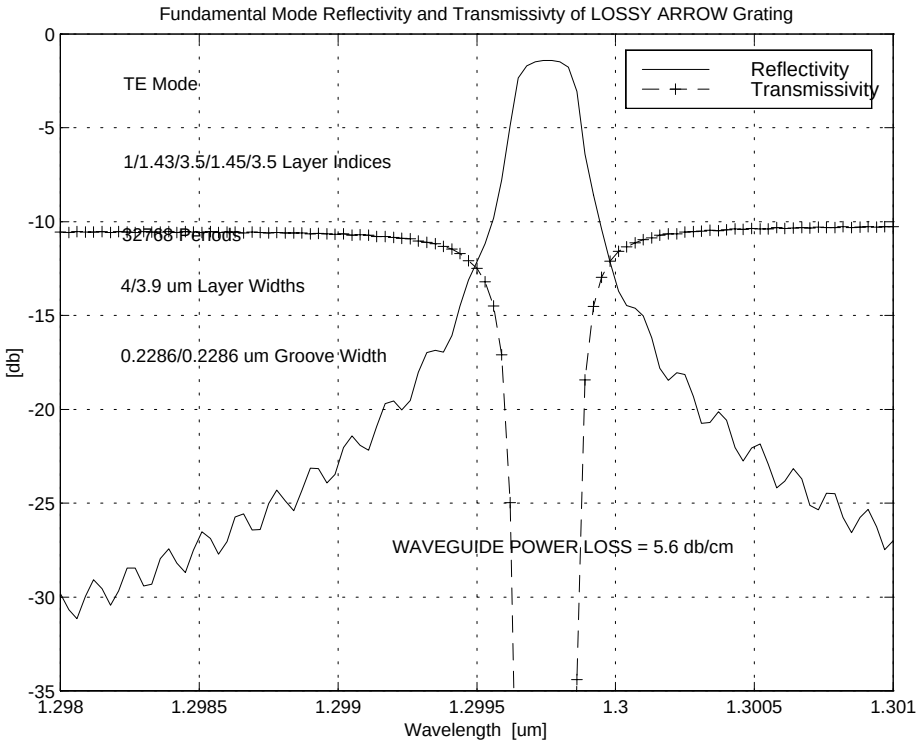

Figure 7.20: Lossy ARROW Grating, 2.5% Groove Depth, 32766 Periods

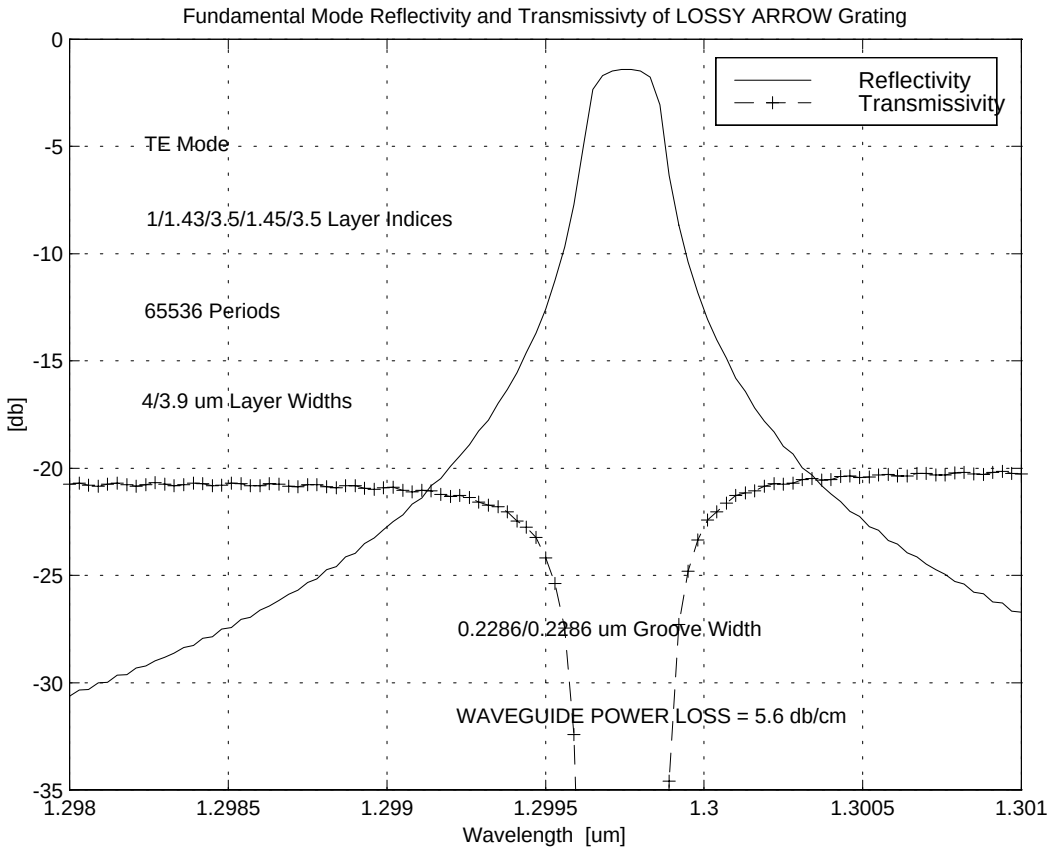

Figure 7.21: Lossy ARROW Grating, 2.5% Groove Depth, 65536 Periods

much broader than the previously discussed cases. Due to the asymmetric shape of the curve, it is unwise to characterize the performance of the grating by the usual 3-db bandwidth measure. If the waveguide is made lossy with a power loss of about 5.0 dB/cm, the peak reflectivity of the grating drops slightly and the side lobes are partially suppressed as shown in figure 7.23. The 3-db bandwidth is unchanged as compared to the low-loss case. If the number of periods is increased to 8192 for the same lossy waveguide, the side lobes are completely suppressed and peak reflectivity also increases (see figure 7.24). If the number of periods is increased further to 32768, there is no change in the response (see figure 7.25). This behaviour is similar to that observed in section 7.2.2. This shows that for a lossy grating, after a certain number of periods there is no field left to be reflected back from the grating discontinuities, and the reflectivity response will not change by adding more periods after that particular length. However, the transmission will drop by adding more length which is a result of waveguide loss.

7.3 Discussion of the ARROW Grating Behaviour

The modal spectral response of the low-loss ARROW grating (with corrugation on top) is very similar to that of the conventional waveguide grating. As the number of grating periods is increased, the peak reflectivity also increases as there are more discontinuities to reflect the incident field backwards. The side lobes become densely packed and the main lobe becomes flatter. There is not much effect on the side-lobe

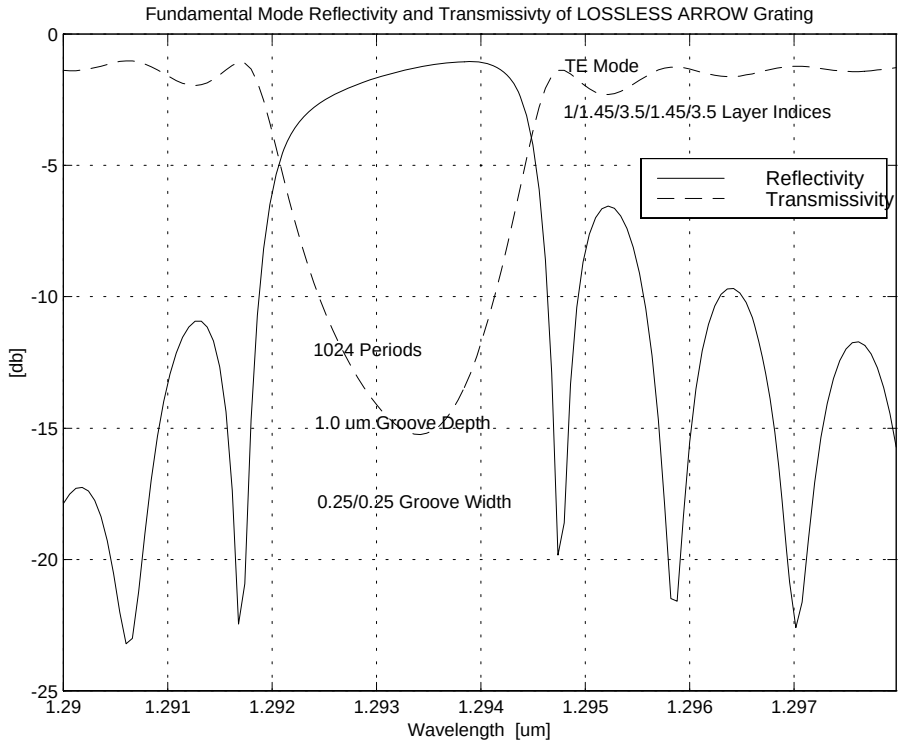

Figure 7.22: Low Loss ARROW Grating, 25% Groove Depth, 1024 Periods

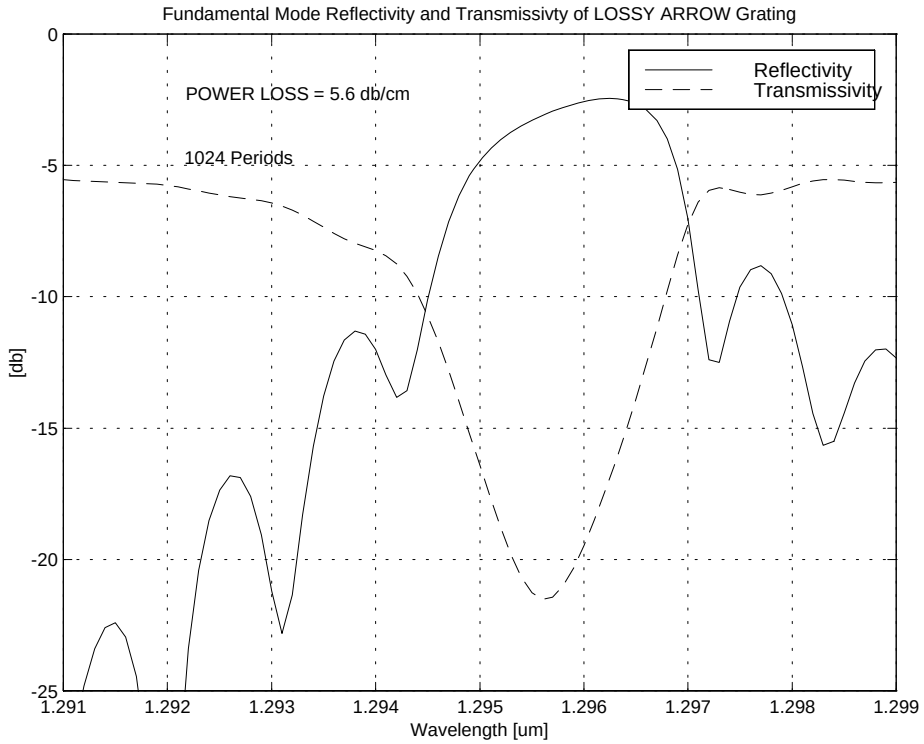

Figure 7.23: Lossy ARROW Grating, 25% Groove Depth, 1024 Periods

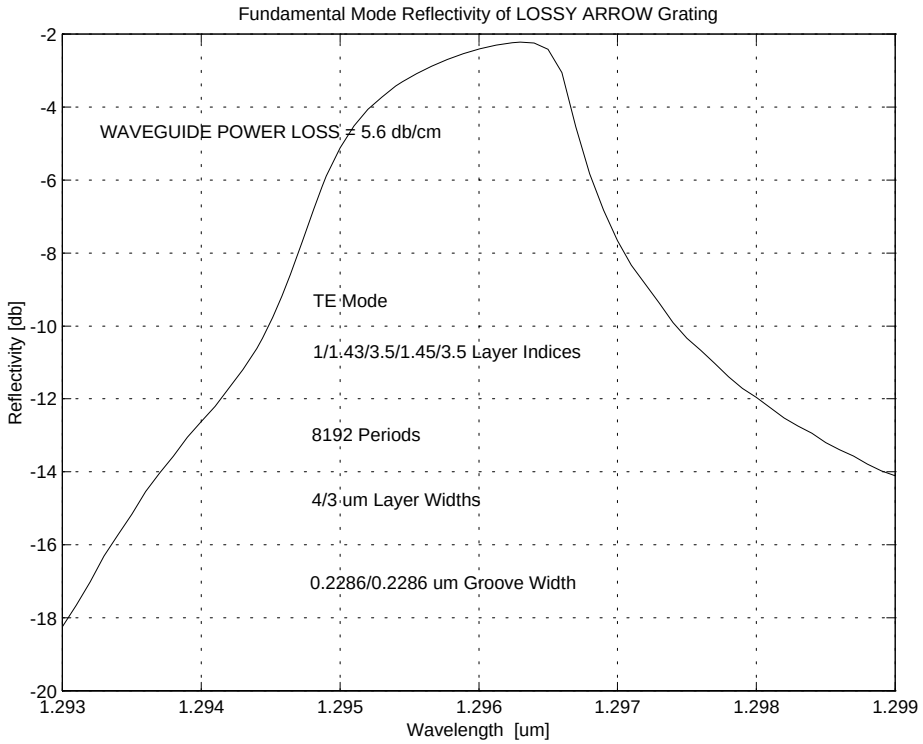

Figure 7.24: Lossy ARROW Grating, 25% Groove Depth, 8192 Periods

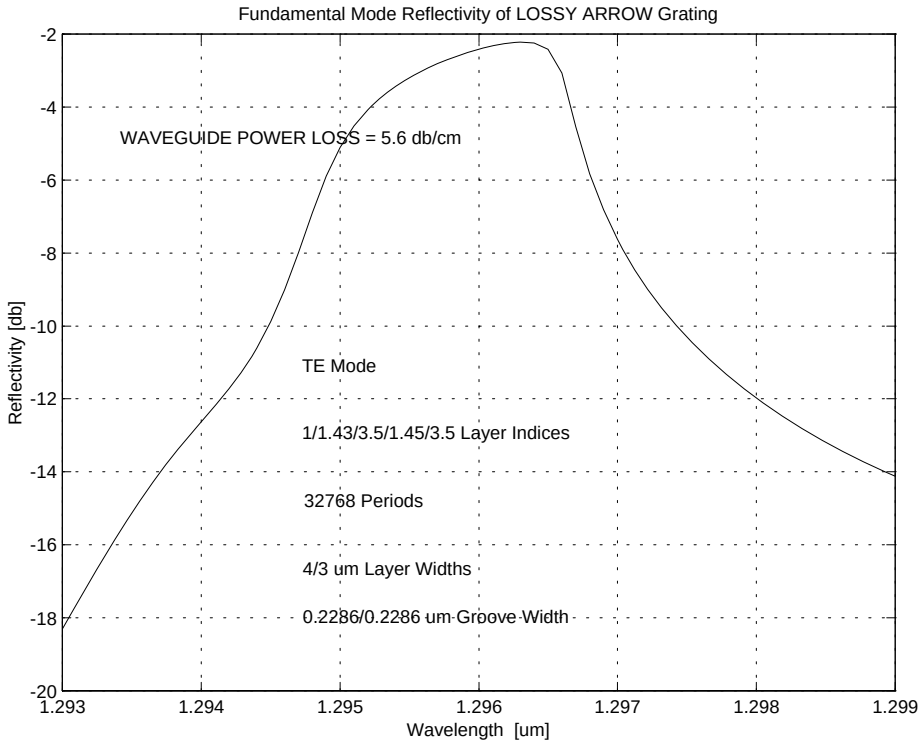

Figure 7.25: Lossy ARROW Grating, 25% Groove Depth, 32768 Periods

level and the 3-db reflectivity bandwidth.

For the shallow gratings, the response is symmetrical about the peak reflectivity wavelength. The main lobe has very narrow bandwidth and the side lobes are much lower. As the groove depth is increased, the response becomes asymmetric. The main lobe becomes broader and the side lobe level is increased.

For the lossy ARROW grating, the ripples in the side lobes are suppressed, but the side lobe level is not much reduced as compared to the low-loss case. The peak reflectivity also drops due to the presence of loss in the device. Thus, we need to use more periods to obtain substantial reflection at the resonance wavelength. However, the 3-db bandwidth does not change. The peak reflectivity wavelength also shifts due to the change in the effective index of the structure. The ARROW loss may be increased by reducing the guide layer index or by changing the layer thickness. The response of ARROW grating depends only upon the amount of power loss present. It does not depend on how this loss is introduced into the device, as we have seen that the leakage loss and the absorption loss influence the grating behaviour in about the same way. As the amount of loss is increased, the side lobe ripples are suppressed more and more until they vanish completely. If power loss is increased further, the response becomes broader and the 3-db bandwidth starts increasing. If more periods are added in a lossy grating, the ripples are suppressed more as the device length increases. However, after a certain number of grating periods, there is no effect of adding more periods on the spectral reflectivity curve. This is due to the fact that after a certain number of periods, all the field has been reflected back and

there is no field left to be reflected by the next set of discontinuities. Note that the added loss reduces the modal transmissivity of the ARROW grating and the device exhibits higher insertion loss. So it can be useful in the reflection mode only.

Chapter 8

Summary, Conclusions and Future Work

In this thesis, the Method of Lines (MoL) has been enhanced using higher-order approximations and applied effectively to find modal profiles and propagation constants of the eigen-modes of different multi-layer optical waveguide structures. It is also used to model field-propagation and scattering from waveguide discontinuities and gratings. A brief summary of the work done, followed by conclusions and some future extensions of this work is given below.

8.1 Summary

- The basic 3-point uniform-mesh MoL has been extended to the 5-point and the 7-point non-uniform formulation with the inclusion of appropriate interface

conditions (for both TE and TM polarization) at an abrupt transition of refractive-index or mesh discontinuity. As compared to other schemes, grid lines are *always* placed on an index or mesh discontinuity in this scheme.

- Perfectly Matched Layer (PML) absorbing boundary scheme has been used extensively in this research work. In chapter 4, single and multiple waveguide discontinuity problems are solved for different waveguide configurations. A recursive layer-by-layer algorithm is described to express the total field in a discontinuity region in terms of total field in the adjacent region.

- A Cascading and Doubling Algorithm is used to model long gratings with a large number of periods. It works by finding the *equivalent* reflection and transmission coefficient matrices of a discontinuity structure and then, duplicating it to find the equivalent reflection and transmission matrices of two such discontinuities attached together. So, the structure grows in a geometric progression in power of 2, like 1, 2, 4, 8, 16, 32 and so on. This algorithm is found to be stable and its accuracy is verified against published results. Different conventional waveguide gratings are modeled and their spectral responses are calculated.

- The MoL is used to find the modal fields and effective indices of the TE, TM and cladding modes of the ARROW device. The use of appropriately tuned PML gives correct open-space simulation for leaky modes of the ARROW, thus giving accurate estimation of the effective indices (real and imaginary part) of

different modes. These MoL predicted results are verified against published as well as analytical results. The effect of varying ARROW parameters, such as layer thickness and refractive indices, on the modal fields and power loss is also calculated.

- The MoL is applied to model an ARROW Grating structure and to find its modal spectral response for different configurations. Power loss is deliberately introduced into the ARROW by changing its parameters and the responses of the lossless and lossy ARROW gratings are analyzed and compared. The grating groove depth is varied from very shallow to very deep and the modal spectral reflectivity and transmissivity responses are calculated.

8.2 Conclusions

- As shown by modeling different waveguide structures in chapter 3, the higher-order approximations used in the MoL give much faster convergence to the analytical results. With this improved scheme, relatively few discretization lines are required to sample the problem space while obtaining an accurate estimation of the modal field and the effective-index. This results in a much reduced matrix size, faster computational speed and lower memory usage for stationary analysis as well as multiple discontinuity problems.

- As compared to Mur's ABC, the PML has been shown to give better absorption

of the radiative fields over a broader range of incident angles and frequencies. It is also easily incorporated into the MoL. To achieve better reflection characteristics, a non-uniform double layer PML is introduced in chapter 4. It can simulate a much *thicker* absorbing medium with relatively fewer sampling points, thus attenuating the radiative field substantially so that it does not get reflected back from the E/M wall of the computational window. Thus, the matrix size for the basic MoL is not much increased by the inclusion of the PML.

- The Cascading and Doubling Algorithm is found to be highly efficient and numerically stable in modeling long gratings. It can model 2^n grating periods in n calculational steps. For N discretiztion lines in the problem space, its memory usage is $N \times N$ while some other algorithms need $2N \times 2N$ matrices. It can easily and efficiently model periodic, aperiodic and quasi-periodic waveguide gratings.

- The excellent performance of the PML in simulating infinite space at the mesh boundary is evident from the ARROW waveguide modeling exercise in chapter 6. The MoL gives accurate prediction of the power loss factor (imaginary part of the effective index) for different ARROW modes. This shows that PML is effectively absorbing the leaky waves in the substrate layer of ARROW. As shown in chapter 6, the performance of the PML can be improved by decreasing the mesh size in the first PML layer and using a coarser mesh in

the second PML layer to simulate a relatively thicker absorber.

- The modal spectral response of the ARROW grating is found to be very similar to that of the conventional waveguide grating for the lossless case. As loss is introduced into the ARROW by increasing leakage or absorption, the response becomes smoother and ripples in the side lobes are reduced. This effect becomes more evident with the increase of the number of grating periods or increase in the amount of loss introduced. The peak reflectivity also drops due to the presence of loss. If more and more periods are added, the peak reflectivity gets close to 0 db for the lossy and lossless grating. However, the 3-db bandwidth is not much affected. The Bragg wavelength also changes due to the change in the effective index of the waveguide when loss is introduced.

8.3 Future Prospects

Scientific research is an ongoing process and there is always some room for improvement. The following is a brief list of suggestions for possible future work in this area.

- We have used a scalar approximation of the **E** or **H** field in this research work. This approximation is valid only for devices having planar geometry which is uniform along one transverse dimension. The Method of Lines can be extended in an efficient and stable way to model full-vectorial simulation of the **E** or **H** field, that is all six components $E_x, E_y, E_z, H_x, H_y, H_z$ of the field in a

waveguide are accounted for. The MoL can be extended to model 3-D geometries and devices. At present, this seems to be extremely memory hungry due to the large matrices involved. The eigen-vectors corresponding to evanescent and radiation modes can be discarded, thus reducing the matrix size. This will make the matrices non-square and pseudo-inverse or generalized-inverse may be used to solve the resulting equations.

- The MoL has been used to model active devices such as Distributed Bragg Reflector (DBR) lasers and Distributed Feedback (DFB) lasers using 2-D formulation [61]. It can be used to model complete 3-D active devices with appropriate 3-D modeling of thermal, optical and electronic sub-models. The *coupling* effects of these sub-models should also be included in the formulation.

- The MoL can be used to model electro-optical modulators, switches, multiplexers and de-multiplexers used in modern communication systems.

- The MoL can be used to model *inverse problems* in integrated optics and opto-electronics. This usually involves a fast *forward* analysis program which predicts the behaviour of a given device. The design or optimization program works in the *backwards* direction and changes the device design parameters to improve its performance as desired by the user. Both programs work in a feed-back loop and improvement of the device performance is done iteratively. The 1-D MoL [1] can be used as the fast analysis program with occasional switching back to the 2-D or 3-D MoL for accurate results. For the optimiza-

tion program, standard derivative-based methods (non-linear damped least squares), heuristic methods (genetic algorithms, simulated evolution) or probabilistic algorithms (simulated annealing) may be used.

- The MoL can be used to model photonic-bandgap structures. These are very fine structures of nano-meter dimensions which are etched over the surface of a substrate. They can guide, reflect and do other useful functions for short wavelengths.

- The MoL can be used to model Multi-Mode Interferrometric (MMI) devices. These devices are used as arbitrary-ratio power-splitters and mode filters in integrated optics. The device geometry is ideal for the MoL implementation as they have planar structures.

- The MoL may be used to model classical electro-magnetics (Maxwell's equation) and quantum mechanical effects (Schrodinger's equation) in a unified way. This will help in the design and analysis of nano-devices such as quantum well lasers, quantum dots and quantum wires.

- In this thesis, we have used MoL in the frequency-domain to model steady-state performance of the device assuming a monochromatic time-harmonic field. The MoL may also be used to model time-dependent phenomenon including the effects of transients.

Appendix A

MATLAB Program : Zero Finding Routine, Eigenvalue Finding Routine

```
%-----------------------------------------------------------------------
% Written By : Dr. H. A. Al-Jamid
% Associate Professor, Electrical Engineering Department,
% King Fahd University, Dhahran 31261, Saudi Arabia.
%-----------------------------------------------------------------------
% zero.m is a zero-finding program based on Muller's method.
% to use it, define the function whos zero is to be found as an M-file
% ( i.e ftest.m) , then run zero.m with the initial guess.
% the ftest.m file may for example be:
%
%    function y=ftest(x);
%    y=x^2-2.001*x+1.001;
%
%    zero('ftest',1.9);
%
% where ftest is the fuction name (must be the same as the M-file name)
```

```
% 1.9 is the initial guess.

function b=zero(FunFcn,x2)

nm=30; %input('number of iterations required = ');

low=10^(-8); h1=-1*10^(-6); h2=.5*10^(-6); x1=x2-h2; x0=x1-h1;
f0=feval(FunFcn,x0); f1=feval(FunFcn,x1); f2=feval(FunFcn,x2);
fu=(f2-f1)/h2; fd=(f1-f0)/h1;
%
%start loop
%
for m=1:nm;%
f3=(fu-fd)/(h1+h2);%
c=fu+h2*f3;h1=h2;%
pa=c-sqrt(c*c-4*f2*f3);%
ma=c+sqrt(c*c-4*f2*f3);%
paa=abs(pa);%
maa=abs(ma);%
if paa>maa, h2=-2*f2/pa; else h2=-2*f2/ma; end%
x1=x2; x2=x2+h2; f1=f2;%
f2=feval(FunFcn,x2);%
fd=fu;%
fu=(f2-f1)/h2;%
if abs(f2)<low zr=x2;%
end%
low=min(low,abs(f2));%
end b=zr;%

%                              STF1a
%
% This program computes the eigenvalues of guided
% TE and TM modes of a slab waveguide with an arbitrary number of
% layers.
% nps=superstrate refracive index squared. The superstrate is assumed
% to occupy the region x<0.
% nbs=substrate refractive index squared.
% ns=array containing the refractive index squared distribution of the
% layers between the superstrate and the substrate. The first entry
% corresponds to a layer next to the superstarate.
% d is similar to ns, but it contains the width distribution of the
% layers.
% Let TE=1 or any other non-zero number if TE modes are desired
```

```
% otherwise let TE=0 for TM modes.

function f=stf1a(ne);

TE=1; lambda=1.15; nps=3.4^2; nbs=3.4^2; ns=[3.44^2]; d=[1.0];

% Start calculation.

nes=ne*ne; k0=2*pi/lambda;%
asp=k0*sqrt(nes-nps);%
l1=k0*sqrt(ns(1)-nes);rho=1;%
if TE==0;rho=ns(1)/nps;end;%
a=1; b=rho*asp/l1; co=[a b]; m=length(ns);%

for s=2:m;
   l=k0*sqrt(ns(s-1)-nes);
   lp=k0*sqrt(ns(s)-nes);
   t=d(s-1);
   lt=l*t;
   rho=1;
   if TE==0;rho=ns(s)/ns(s-1);end;
   at=a*cos(lt)+b*sin(lt);
   b=rho*(-a*sin(lt)+b*cos(lt))*l/lp;
   a=at;
   co=[co a b];
   end;

   l=k0*sqrt(ns(m)-nes);
   asb=k0*sqrt(nes-nbs);
   t=d(m);  lt=l*t; rho=1;
   if TE==0;rho=nbs/ns(m);end;

   at=a*cos(lt)+b*sin(lt);
   a=-rho*(-a*sin(lt)+b*cos(lt))*l/asb;
   f=at-a;
```

Appendix B

MATLAB Program : 3-Point MoL

```
% Written By: Muhammad Nadeem, Research Assistant
% Method of Line Analysis of Slab Waveguide
% accurate discretization for core and cladding regions
% selects the index according to the 'side' of grid
% simulates correct thickness of the core
% Implements correct B.C.s at the layer interfaces
% General purpose program for TE, TM modes, Non-uniform Mesh
% 3 -point 2nd Derivative approximation

clear
Neff_Anal = 3.54396160934; % Analytical Value for TE Mode
TE = 1; % for TE mode, put TE = 1, otherwose TM mode is assumed
EQ = 1; % for uniform grid, put EQ = 1
lambda = 0.86; % Free sapce wavelength
ko = 2*pi/lambda; % Free space Wavenumber
n = [1 3.6 1]; % Refractive index, layer by layer
nlyr = length(n);
w = [1 0.6 1] ; % Layer widths
M = [20 20 20]; % Dicretization sections of the layers
% 1 ---> M(1) layer 1
% M(1)+1 ---> M(2) layer 2, and so on
MN = cumsum(M); % Interface locations

% Ordinary Regions, No interface
```

```
MS = [];
for i = 1:nlyr

   if i == 1
      s1=1;
      s2=MN(1)-1;
   elseif  i == nlyr
      s1=MN(nlyr-1)+1;
      s2=MN(nlyr);
   else
      s1=MN(i-1)+1;
      s2=MN(i)-1;
   end
   MS = [MS,s1,s2];
end
if EQ ~= 1
   h = w ./ M; % discretization distances
else
   h = w(2)/M(2);
   h = h*ones(1,nlyr);
   % New layer widths are
   w = M*h(1);
end

% The refractive index N matrix
N=[]; NN=[]; for i=1:nlyr
   N=n(i)^2*ones(1,M(i));
   NN=[NN,N];
end
N=diag(NN);

% The Derivative C matrix
MM=sum(M); C=zeros(MM);
% Regular 2nd derivative matrix
for i=2:MM-1
   C(i,i)=-2;
   C(i,i+1)=1;
   C(i,i-1)=1;
end C(1,1)=-2; C(1,2)=1; C(MM,MM)=-2; C(MM,MM-1)=1;

% Divide by denominator terms except at the interface
i=1; for k=1:nlyr
   C(MS(i):MS(i+1),:) = C(MS(i):MS(i+1),:)/h(k)^2;
```

```
   i=i+2;
end

% Modify the terms at the interface
for i=1:nlyr-1

   if TE == 1
      r21 = 1;
   else
      r21 = (n(i+1)/n(i))^2;
   end
   B = ko^2*(n(i)^2-n(i+1)^2);
   D = 0.5*(h(i)*h(i+1)*r21+h(i+1)^2);
   C(MN(i),MN(i))   = -(r21 * h(i+1)/h(i)+1+0.5*h(i+1)^2 * B)/D;
   C(MN(i),MN(i)-1) = h(i+1)/h(i) * r21/D;
   C(MN(i),MN(i)+1) = C(MN(i),MN(i)+1)/D;
end

% Q matrix
Q=C+ko^2*N;
% Diagonalize the Q matrix
[U,V]=eig(Q); % find the eigenvalues and eigenvectors

%Finding the Effective Indices and Propagation Constants for modes.
% TE/TM 0 mode has highest Propagation Constant (real).
% So search it in the Eigen Value matrix on the diagonal.
[a,b]=max(real(diag(V))); i=0 Tmode=i; ss=int2str(Tmode);%

if TE == 1
   s = 'TE';
else
   s = 'TM';
end

Neff=sqrt(V(b,b))/ko; figure;plot(U(:,b));grid;%
s=num2str(Neff,20); s = ['Neff = ' , s]; gtext(s); ax=axis;
axis([1 MM ax(3) ax(4)]);

% Transverse Coefficeints in Each Layer
g1=ko*sqrt(Neff_Anal^2 - n(1)^2); g2=ko*sqrt(n(2)^2-Neff_Anal^2);
g3=ko*sqrt(Neff_Anal^2 - n(3)^2);
% Field Amplitude
A=1; CC=A;
```

```
% Define X-axis
xo = M(1); % Origin of x-axis
xx=[]; x=[]; for i=1:nlyr
   xx=h(i)*ones(1,M(i));
   x=[x,xx];
end xo=sum(x(1:xo)); x=cumsum(x); x=x-xo;
% Define the Analytical Field
Field = []; for i=1:MN(1)
   Field(i,1) = A * exp(g1*x(i));
end
for i=MN(1)+1:MN(2)
   if TE ~= 1
      B = NN(MN(1)+1)/NN(MN(1)) * g1/g2;
   else
      B = g1/g2;
   end
   Field(i,1) = B * sin(g2*x(i)) + CC * cos(g2*x(i));
end
for i = MN(2)+1:MN(3)
      D = B*sin(g2*x(MN(2))) + CC*cos(g2*x(MN(2)));
      Field(i,1) = D * exp(-g3*(x(i)-x(MN(2))));
end
figure;plot(Field);grid;title('Analytical Field'); ax=axis;
axis([1 MM ax(3) ax(4)]);

figure;plot(Field/max(Field) - abs(U(:,c))/max(abs(U(:,c))));
grid;title('Error Between Analytical and Numerical Field');
ax=axis; axis([1 MM ax(3) ax(4)]);

% Propagate the Anaytical Field to +z
z=0; IU=inv(U); Vrt=V^0.5; s=int2str(z); s=['Z = ',s];
VV=diag(exp(diag(j*Vrt*z))); E=U*VV*IU*Field;
plot(abs(E));title(s);grid; ax=axis; axis([1 MM ax(3) ax(4)]);
```

Appendix C

MATLAB Program : 5-Point MoL

```
%-------------------------------------------------
%
%THE NECESSARY CHANGES IN THE 3-POINT MOL PROGRAM
%REST OF THE CODE REMAINS THE SAME
%-------------------------------------------------

% Ordinary Regions

MS = []; for i = 1:nlyr
   if i == 1
      s1=1;
      s2=MN(1)-2;
   elseif  i == nlyr
      s1=MN(nlyr-1)+2;
      s2=MN(nlyr);
   else
      s1=MN(i-1)+2;
      s2=MN(i)-2;
   end
   MS = [MS,s1,s2];
end

e = ones(MM,1);
```

```
% 5-point second derivative matrix, Sparse
C = spdiags([-e/12 16*e/12 -30*e/12 16*e/12 -e/12],-2:2,MM,MM);

% Divide by denominator terms except
% at the interface and two adjacent mesh points
i=1; for k=1:nlyr
   C(MS(i):MS(i+1),:) = C(MS(i):MS(i+1),:)/h(k)^2;
   i=i+2;
end

% Modify the terms at the interface for 5-Point

for i=1:nlyr-1
   if TE ~= 1
      % TM mode
      r21 = n(i+1)^2/n(i)^2;
   else
      % TE mode
      r21 = 1;
   end

   % On the Interface
   a0=1+0.5*h(i+1)^2*ko^2*(n(i)^2-n(i+1)^2)+...
       1/24*h(i+1)^4*ko^4*(n(i)^2-n(i+1)^2)^2;
   b0=1+2*h(i+1)^2*ko^2*(n(i)^2-n(i+1)^2)+...
        2/3*h(i+1)^4*ko^4*(n(i)^2-n(i+1)^2)^2;
   c0=1;
   d0=1;

   cof(1,1) = r21*(h(i+1)+1/6*h(i+1)^3*ko^2*(n(i)^2-n(i+1)^2));
   cof(1,2) = 0.5*h(i+1)^2+1/12*h(i+1)^4*ko^2*(n(i)^2-n(i+1)^2);
   cof(1,3) = r21*1/6*h(i+1)^3;
   cof(1,4) = 1/24*h(i+1)^4;

   cof(2,1) = r21*(2*h(i+1)+4/3*h(i+1)^3*ko^2*(n(i)^2-n(i+1)^2));
   cof(2,2) = 2*h(i+1)^2+ 4/3*h(i+1)^4*ko^2*(n(i)^2-n(i+1)^2);
   cof(2,3) = r21*4/3*h(i+1)^3;
   cof(2,4) = 2/3*h(i+1)^4;

   cof(3,1) = -h(i);
   cof(3,2) = 0.5*h(i)^2;
   cof(3,3) = -1/6*h(i)^3;
   cof(3,4) = 1/24*h(i)^4;
```

```
cof(4,1) = -2*h(i);
cof(4,2) = 2*h(i)^2;
cof(4,3) = -4/3*h(i)^3;
cof(4,4) = 2/3*h(i)^4;

icof = inv(cof);

tmp = -a0*icof(2,1)-b0*icof(2,2)-c0*icof(2,3)-d0*icof(2,4);

sd = [icof(2,2) icof(2,1) tmp icof(2,3) icof(2,4)];

C(MN(i),MN(i)+2) = sd(1);
C(MN(i),MN(i)+1) = sd(2);
C(MN(i),MN(i)) = sd(3);
C(MN(i),MN(i)-1) = sd(4);
C(MN(i),MN(i)-2) = sd(5);

% One point ahead of the Interface

cof(1,1) = h(i+1);
cof(1,2) = 0.5*h(i+1)^2;
cof(1,3) = 1/6*h(i+1)^3;
cof(1,4) = 1/24*h(i+1)^4;

cof(2,1) = 2*h(i+1);
cof(2,2) = 2*h(i+1)^2;
cof(2,3) = 4/3*h(i+1)^3;
cof(2,4) = 2/3*h(i+1)^4;

cof(3,1) = 3*h(i+1);
cof(3,2) = 9/2*h(i+1)^2;
cof(3,3) = 9/2*h(i+1)^3;
cof(3,4) = 27/8*h(i+1)^4;

cof(4,1) = -h(i)/r21 + 1/6*h(i)^3*ko^2*(n(i)^2-n(i+1)^2)/r21;
cof(4,2) = 0.5*h(i)^2 - 1/12*h(i)^4*ko^2*(n(i)^2-n(i+1)^2);
cof(4,3) = -1/6*h(i)^3/r21;
cof(4,4) = 1/24*h(i)^4;

a = 1-0.5*h(i)^2*ko^2*(n(i)^2-n(i+1)^2)+...
     1/24*h(i)^4*ko^4*(n(i)^2-n(i+1)^2)^2;
```

```
    icof = inv(cof);

    p1 = icof(2,1) + icof(2,2)+icof(2,3)+a*icof(2,4);
    p2 = icof(3,1) + icof(3,2)+icof(3,3)+a*icof(3,4);
    p3 = icof(4,1) + icof(4,2)+icof(4,3)+a*icof(4,4);

    sd(1) = icof(2,4)+h(i+1)*icof(3,4)+ 0.5*h(i+1)^2*icof(4,4);
    sd(2) = -p1 - h(i+1)*p2 - 0.5*h(i+1)^2*p3;
    sd(3) = icof(2,1)+h(i+1)*icof(3,1)+ 0.5*h(i+1)^2*icof(4,1);
    sd(4) = icof(2,2)+h(i+1)*icof(3,2)+ 0.5*h(i+1)^2*icof(4,2);
    sd(5) = icof(2,3)+h(i+1)*icof(3,3)+ 0.5*h(i+1)^2*icof(4,3);

    C(MN(i)+1,MN(i)+1-2) = sd(1);
    C(MN(i)+1,MN(i)+1-1) = sd(2);
    C(MN(i)+1,MN(i)+1) = sd(3);
    C(MN(i)+1,MN(i)+1+1) = sd(4);
    C(MN(i)+1,MN(i)+1+2) = sd(5);

% One point behind the interface

    cof(1,1) = -h(i);
    cof(1,2) = 0.5*h(i)^2;
    cof(1,3) = -1/6*h(i)^3;
    cof(1,4) = 1/24*h(i)^4;

    cof(2,1) = -2*h(i);
    cof(2,2) = 2*h(i)^2;
    cof(2,3) = -4/3*h(i)^3;
    cof(2,4) = 2/3*h(i)^4;

    cof(3,1) = -3*h(i);
    cof(3,2) = 9/2*h(i)^2;
    cof(3,3) = -9/2*h(i)^3;
    cof(3,4) = 27/8*h(i)^4;

    cof(4,1) = h(i+1)*r21 + 1/6*h(i+1)^3*ko^2*(n(i)^2-n(i+1)^2)*r21;
    cof(4,2) = 0.5*h(i+1)^2 + 1/12*h(i+1)^4*ko^2*(n(i)^2-n(i+1)^2);
    cof(4,3) = 1/6*h(i+1)^3*r21;
    cof(4,4) = 1/24*h(i+1)^4;

    a = 1+0.5*h(i+1)^2*ko^2*(n(i)^2-n(i+1)^2)+...
         1/24*h(i+1)^4*ko^4*(n(i)^2-n(i+1)^2)^2;
```

```
    icof = inv(cof);

    p1 = icof(2,1) + icof(2,2)+icof(2,3)+a*icof(2,4);
    p2 = icof(3,1) + icof(3,2)+icof(3,3)+a*icof(3,4);
    p3 = icof(4,1) + icof(4,2)+icof(4,3)+a*icof(4,4);

    sd(1) = icof(2,3)-h(i)*icof(3,3)+ 0.5*h(i)^2*icof(4,3);
    sd(2) = icof(2,2)-h(i)*icof(3,2)+ 0.5*h(i)^2*icof(4,2);
    sd(3) = icof(2,1)-h(i)*icof(3,1)+ 0.5*h(i)^2*icof(4,1);
    sd(4) = -p1 + h(i)*p2 - 0.5*h(i)^2*p3;
    sd(5) = icof(2,4)-h(i)*icof(3,4)+ 0.5*h(i)^2*icof(4,4);

    C(MN(i)-1,MN(i)-1-2) = sd(1);
    C(MN(i)-1,MN(i)-1-1) = sd(2);
    C(MN(i)-1,MN(i)-1) = sd(3);
    C(MN(i)-1,MN(i)-1+1) = sd(4);
    C(MN(i)-1,MN(i)-1+2) = sd(5);

end
```

Appendix D

MATLAB Program : 7-Point MoL

```
%-------------------------------------------------
%
%THE NECESSARY CHANGES IN THE 3-POINT MOL PROGRAM
%REST OF THE CODE REMAINS THE SAME
%-------------------------------------------------

% Ordinary Regions

MS = [];
for i = 1:nlyr
   if i == 1
      s1=1;
      s2=MN(1)-3;
   elseif  i == nlyr
      s1=MN(nlyr-1)+3;
      s2=MN(nlyr);
   else
      s1=MN(i-1)+3;
      s2=MN(i)-3;
   end
   MS = [MS,s1,s2];
end

MM=sum(M);
```

```
e = ones(MM,1);

% 7-point second derivative matrix, sparse
C = spdiags([2/180*e -27/180*e 270/180*e -490/180*e 270/180*e ...
      -27/180*e 2/180*e],-3:3,MM,MM);

% Divide by denominator terms except at the interface
% and two adjacent mesh points
i=1; for k=1:nlyr
   C(MS(i):MS(i+1),:) = C(MS(i):MS(i+1),:)/h(k)^2;
   i=i+2;
end

%%%%%%%%%%%%%%%%%%%%%%%%%%%%%%%%%%%%%%%%%%%%%%%%%%%%%%%%%%%%
% Modify the terms associated with the interface%
%%%%%%%%%%%%%%%%%%%%%%%%%%%%%%%%%%%%%%%%%%%%%%%%%%%%%%%%%%%%

for i=1:nlyr-1

   if TE ~= 1
      % TM mode
      r21 = n(i+1)^2/n(i)^2;
   else
      % TE mode
      r21 = 1;
   end

   % On the Interface

   n1 = n(i); n2 = n(i+1); h1 = h(i); h2 = h(i+1);

   B=ko^2*(n1^2-n2^2);
   a0=1+1/2*h2^2*B +1/24*h2^4*B^2+1/720*h2^6*B^3;
   b0=1+1/2*(2*h2)^2*B +1/24*(2*h2)^4*B^2+1/720*(2*h2)^6*B^3;
   c0=1+1/2*(3*h2)^2*B +1/24*(3*h2)^4*B^2+1/720*(3*h2)^6*B^3;

   cof(1,1) = r21*(h2+1/6*h2^3*B+1/120*h2^5*B^2);
   cof(1,2) = 1/2*h2^2+1/12*h2^4*B+1/240*h2^6*B^2;
   cof(1,3) = r21*(1/6*h2^3+1/60*h2^5*B);
   cof(1,4) = 1/24*h2^4+1/240*h2^6*B;
   cof(1,5) = r21*1/120*h2^5;
   cof(1,6) = 1/720*h2^6;
```

```
cof(2,1) = r21*(2*h2+1/6*(2*h2)^3*B+1/120*(2*h2)^5*B^2);
cof(2,2) = 1/2*(2*h2)^2+1/12*(2*h2)^4*B+1/240*(2*h2)^6*B^2;
cof(2,3) = r21*(1/6*(2*h2)^3+1/60*(2*h2)^5*B);
cof(2,4) = 1/24*(2*h2)^4+1/240*(2*h2)^6*B;
cof(2,5) = r21*1/120*(2*h2)^5;
cof(2,6) = 1/720*(2*h2)^6;

cof(3,1) = r21*(3*h2+1/6*(3*h2)^3*B+1/120*(3*h2)^5*B^2);
cof(3,2) = 1/2*(3*h2)^2+1/12*(3*h2)^4*B+1/240*(3*h2)^6*B^2;
cof(3,3) = r21*(1/6*(3*h2)^3+1/60*(3*h2)^5*B);
cof(3,4) = 1/24*(3*h2)^4+1/240*(3*h2)^6*B;
cof(3,5) = r21*1/120*(3*h2)^5;
cof(3,6) = 1/720*(3*h2)^6;

cof(4,1) = -h1;
cof(4,2) = 1/2*h1^2;
cof(4,3) = -1/6*h1^3;
cof(4,4) = 1/24*h1^4;
cof(4,5) = -1/120*h1^5;
cof(4,6) = 1/720*h1^6;

cof(5,1) = -2*h1;
cof(5,2) = 1/2*(2*h1)^2;
cof(5,3) = -1/6*(2*h1)^3;
cof(5,4) = 1/24*(2*h1)^4;
cof(5,5) = -1/120*(2*h1)^5;
cof(5,6) = 1/720*(2*h1)^6;

cof(6,1) = -3*h1;
cof(6,2) = 1/2*(3*h1)^2;
cof(6,3) = -1/6*(3*h1)^3;
cof(6,4) = 1/24*(3*h1)^4;
cof(6,5) = -1/120*(3*h1)^5;
cof(6,6) = 1/720*(3*h1)^6;

icof = inv(cof);

C(MN(i),MN(i)-3) = icof(2,6);
C(MN(i),MN(i)-2) = icof(2,5);
C(MN(i),MN(i)-1) = icof(2,4);
C(MN(i),MN(i)+0) = -(a0*icof(2,1)+b0*icof(2,2)+c0*icof(2,3)+...
                     icof(2,4)+icof(2,5)+icof(2,6));
```

```
   C(MN(i),MN(i)+1) = icof(2,1);
   C(MN(i),MN(i)+2) = icof(2,2);
   C(MN(i),MN(i)+3) = icof(2,3);

% One point behind the interface

   cof(3,:) = cof(4,:);
   cof(4,:) = cof(5,:);
   cof(5,:) = cof(6,:);

   cof(6,1) = -4*h1;
   cof(6,2) = 1/2*(4*h1)^2;
   cof(6,3) = -1/6*(4*h1)^3;
   cof(6,4) = 1/24*(4*h1)^4;
   cof(6,5) = -1/120*(4*h1)^5;
   cof(6,6) = 1/720*(4*h1)^6;


   icof = inv(cof);

p1=icof(2,1)*a0+icof(2,2)*b0+icof(2,3)+icof(2,4)+icof(2,5)+icof(2,6);
p2=icof(3,1)*a0+icof(3,2)*b0+icof(3,3)+icof(3,4)+icof(3,5)+icof(3,6);
p3=icof(4,1)*a0+icof(4,2)*b0+icof(4,3)+icof(4,4)+icof(4,5)+icof(4,6);
p4=icof(5,1)*a0+icof(5,2)*b0+icof(5,3)+icof(5,4)+icof(5,5)+icof(5,6);
p5=icof(6,1)*a0+icof(6,2)*b0+icof(6,3)+icof(6,4)+icof(6,5)+icof(6,6);


C(MN(i)-1,MN(i)-1-3) =
icof(2,6)-h1*icof(3,6)+1/2*h1^2*icof(4,6)-...
          1/6*h1^3*icof(5,6)+1/24*h1^4*icof(6,6);

C(MN(i)-1,MN(i)-1-2) =
icof(2,5)-h1*icof(3,5)+1/2*h1^2*icof(4,5)-...
          1/6*h1^3*icof(5,5)+1/24*h1^4*icof(6,5);

C(MN(i)-1,MN(i)-1-1) =
icof(2,4)-h1*icof(3,4)+1/2*h1^2*icof(4,4)-...
          1/6*h1^3*icof(5,4)+1/24*h1^4*icof(6,4);

C(MN(i)-1,MN(i)-1+0) =
icof(2,3)-h1*icof(3,3)+1/2*h1^2*icof(4,3)-...
          1/6*h1^3*icof(5,3)+1/24*h1^4*icof(6,3);
```

```
C(MN(i)-1,MN(i)-1+1) =
-p1+h1*p2-1/2*h1^2*p3+1/6*h1^3*p4-1/24*h1^4*p5;

C(MN(i)-1,MN(i)-1+2) =
icof(2,1)-h1*icof(3,1)+1/2*h1^2*icof(4,1)-...
          1/6*h1^3*icof(5,1)+1/24*h1^4*icof(6,1);

C(MN(i)-1,MN(i)-1+3) =
icof(2,2)-h1*icof(3,2)+1/2*h1^2*icof(4,2)-...
          1/6*h1^3*icof(5,2)+1/24*h1^4*icof(6,2);

% two point behind the interface

   cof(2,:) = cof(3,:);
   cof(3,:) = cof(4,:);
   cof(4,:) = cof(5,:);
   cof(5,:) = cof(6,:);

   cof(6,1) = -5*h1;
   cof(6,2) = 1/2*(5*h1)^2;
   cof(6,3) = -1/6*(5*h1)^3;
   cof(6,4) = 1/24*(5*h1)^4;
   cof(6,5) = -1/120*(5*h1)^5;
   cof(6,6) = 1/720*(5*h1)^6;

   icof = inv(cof);

p1=icof(2,1)*a0+icof(2,2)+icof(2,3)+icof(2,4)+icof(2,5)+icof(2,6);
p2=icof(3,1)*a0+icof(3,2)+icof(3,3)+icof(3,4)+icof(3,5)+icof(3,6);
p3=icof(4,1)*a0+icof(4,2)+icof(4,3)+icof(4,4)+icof(4,5)+icof(4,6);
p4=icof(5,1)*a0+icof(5,2)+icof(5,3)+icof(5,4)+icof(5,5)+icof(5,6);
p5=icof(6,1)*a0+icof(6,2)+icof(6,3)+icof(6,4)+icof(6,5)+icof(6,6);


C(MN(i)-2,MN(i)-2-3) =
icof(2,6)-2*h1*icof(3,6)+1/2*(2*h1)^2*icof(4,6)-...
      1/6*(2*h1)^3*icof(5,6)+1/24*(2*h1)^4*icof(6,6);

C(MN(i)-2,MN(i)-2-2) =
icof(2,5)-2*h1*icof(3,5)+1/2*(2*h1)^2*icof(4,5)-...
      1/6*(2*h1)^3*icof(5,5)+1/24*(2*h1)^4*icof(6,5);

C(MN(i)-2,MN(i)-2-1) =
```

```
icof(2,4)-2*h1*icof(3,4)+1/2*(2*h1)^2*icof(4,4)-...
      1/6*(2*h1)^3*icof(5,4)+1/24*(2*h1)^4*icof(6,4);

C(MN(i)-2,MN(i)-2+0) =
icof(2,3)-2*h1*icof(3,3)+1/2*(2*h1)^2*icof(4,3)-...
      1/6*(2*h1)^3*icof(5,3)+1/24*(2*h1)^4*icof(6,3);

C(MN(i)-2,MN(i)-2+1) =
icof(2,2)-2*h1*icof(3,2)+1/2*(2*h1)^2*icof(4,2)-...
      1/6*(2*h1)^3*icof(5,2)+1/24*(2*h1)^4*icof(6,2);

C(MN(i)-2,MN(i)-2+2) =
-p1+2*h1*p2-1/2*(2*h1)^2*p3+1/6*(2*h1)^3*p4-...
      1/24*(2*h1)^4*p5;

C(MN(i)-2,MN(i)-2+3) =
icof(2,1)-2*h1*icof(3,1)+1/2*(2*h1)^2*icof(4,1)-...
      1/6*(2*h1)^3*icof(5,1)+1/24*(2*h1)^4*icof(6,1);

% One point ahead of the Interface

   n1 = n(i+1); n2 = n(i); h1 = -h(i+1); h2 = -h(i); r21 = 1/r21;
   B=ko^2*(n1^2-n2^2);

   a0=1+1/2*h2^2*B +1/24*h2^4*B^2+1/720*h2^6*B^3;
   b0=1+1/2*(2*h2)^2*B +1/24*(2*h2)^4*B^2+1/720*(2*h2)^6*B^3;

   cof(1,1) = r21*(h2+1/6*h2^3*B+1/120*h2^5*B^2);
   cof(1,2) = 1/2*h2^2+1/12*h2^4*B+1/240*h2^6*B^2;
   cof(1,3) = r21*(1/6*h2^3+1/60*h2^5*B);
   cof(1,4) = 1/24*h2^4+1/240*h2^6*B;
   cof(1,5) = r21*1/120*h2^5;
   cof(1,6) = 1/720*h2^6;

   cof(2,1) = r21*(2*h2+1/6*(2*h2)^3*B+1/120*(2*h2)^5*B^2);
   cof(2,2) = 1/2*(2*h2)^2+1/12*(2*h2)^4*B+1/240*(2*h2)^6*B^2;
   cof(2,3) = r21*(1/6*(2*h2)^3+1/60*(2*h2)^5*B);
   cof(2,4) = 1/24*(2*h2)^4+1/240*(2*h2)^6*B;
   cof(2,5) = r21*1/120*(2*h2)^5;
   cof(2,6) = 1/720*(2*h2)^6;


   cof(3,1) = -h1;
```

```
   cof(3,2) = 1/2*h1^2;
   cof(3,3) = -1/6*h1^3;
   cof(3,4) = 1/24*h1^4;
   cof(3,5) = -1/120*h1^5;
   cof(3,6) = 1/720*h1^6;

   cof(4,1) = -2*h1;
   cof(4,2) = 1/2*(2*h1)^2;
   cof(4,3) = -1/6*(2*h1)^3;
   cof(4,4) = 1/24*(2*h1)^4;
   cof(4,5) = -1/120*(2*h1)^5;
   cof(4,6) = 1/720*(2*h1)^6;

   cof(5,1) = -3*h1;
   cof(5,2) = 1/2*(3*h1)^2;
   cof(5,3) = -1/6*(3*h1)^3;
   cof(5,4) = 1/24*(3*h1)^4;
   cof(5,5) = -1/120*(3*h1)^5;
   cof(5,6) = 1/720*(3*h1)^6;

   cof(6,1) = -4*h1;
   cof(6,2) = 1/2*(4*h1)^2;
   cof(6,3) = -1/6*(4*h1)^3;
   cof(6,4) = 1/24*(4*h1)^4;
   cof(6,5) = -1/120*(4*h1)^5;
   cof(6,6) = 1/720*(4*h1)^6;


icof = inv(cof);
p1=icof(2,1)*a0+icof(2,2)*b0+icof(2,3)+icof(2,4)+icof(2,5)+icof(2,6);
p2=icof(3,1)*a0+icof(3,2)*b0+icof(3,3)+icof(3,4)+icof(3,5)+icof(3,6);
p3=icof(4,1)*a0+icof(4,2)*b0+icof(4,3)+icof(4,4)+icof(4,5)+icof(4,6);
p4=icof(5,1)*a0+icof(5,2)*b0+icof(5,3)+icof(5,4)+icof(5,5)+icof(5,6);
p5=icof(6,1)*a0+icof(6,2)*b0+icof(6,3)+icof(6,4)+icof(6,5)+icof(6,6);


C(MN(i)+1,MN(i)+1+3) =
icof(2,6)-h1*icof(3,6)+1/2*h1^2*icof(4,6)-...
     1/6*h1^3*icof(5,6)+1/24*h1^4*icof(6,6);

C(MN(i)+1,MN(i)+1+2) =
icof(2,5)-h1*icof(3,5)+1/2*h1^2*icof(4,5)-...
     1/6*h1^3*icof(5,5)+1/24*h1^4*icof(6,5);
```

```
C(MN(i)+1,MN(i)+1+1) =
icof(2,4)-h1*icof(3,4)+1/2*h1^2*icof(4,4)-...
     1/6*h1^3*icof(5,4)+1/24*h1^4*icof(6,4);

C(MN(i)+1,MN(i)+1+0) =
icof(2,3)-h1*icof(3,3)+1/2*h1^2*icof(4,3)-...
     1/6*h1^3*icof(5,3)+1/24*h1^4*icof(6,3);

C(MN(i)+1,MN(i)+1-1) =
-p1+h1*p2-1/2*h1^2*p3+1/6*h1^3*p4-1/24*h1^4*p5;

C(MN(i)+1,MN(i)+1-2) =
icof(2,1)-h1*icof(3,1)+1/2*h1^2*icof(4,1)-...
     1/6*h1^3*icof(5,1)+1/24*h1^4*icof(6,1);

C(MN(i)+1,MN(i)+1-3) =
icof(2,2)-h1*icof(3,2)+1/2*h1^2*icof(4,2)-...
     1/6*h1^3*icof(5,2)+1/24*h1^4*icof(6,2);

   % Two point ahead of the Interface

   cof(2,:) = cof(3,:);
   cof(3,:) = cof(4,:);
   cof(4,:) = cof(5,:);
   cof(5,:) = cof(6,:);

   cof(6,1) = -5*h1;
   cof(6,2) = 1/2*(5*h1)^2;
   cof(6,3) = -1/6*(5*h1)^3;
   cof(6,4) = 1/24*(5*h1)^4;
   cof(6,5) = -1/120*(5*h1)^5;
   cof(6,6) = 1/720*(5*h1)^6;

   icof = inv(cof);

p1=icof(2,1)*a0+icof(2,2)+icof(2,3)+icof(2,4)+icof(2,5)+icof(2,6);
p2=icof(3,1)*a0+icof(3,2)+icof(3,3)+icof(3,4)+icof(3,5)+icof(3,6);
p3=icof(4,1)*a0+icof(4,2)+icof(4,3)+icof(4,4)+icof(4,5)+icof(4,6);
p4=icof(5,1)*a0+icof(5,2)+icof(5,3)+icof(5,4)+icof(5,5)+icof(5,6);
p5=icof(6,1)*a0+icof(6,2)+icof(6,3)+icof(6,4)+icof(6,5)+icof(6,6);
```

```
C(MN(i)+2,MN(i)+2+3) =
icof(2,6)-2*h1*icof(3,6)+1/2*(2*h1)^2*icof(4,6)-...
      1/6*(2*h1)^3*icof(5,6)+1/24*(2*h1)^4*icof(6,6);

C(MN(i)+2,MN(i)+2+2) =
icof(2,5)-2*h1*icof(3,5)+1/2*(2*h1)^2*icof(4,5)-...
      1/6*(2*h1)^3*icof(5,5)+1/24*(2*h1)^4*icof(6,5);

C(MN(i)+2,MN(i)+2+1) =
icof(2,4)-2*h1*icof(3,4)+1/2*(2*h1)^2*icof(4,4)-...
      1/6*(2*h1)^3*icof(5,4)+1/24*(2*h1)^4*icof(6,4);

C(MN(i)+2,MN(i)+2+0) =
icof(2,3)-2*h1*icof(3,3)+1/2*(2*h1)^2*icof(4,3)-...
      1/6*(2*h1)^3*icof(5,3)+1/24*(2*h1)^4*icof(6,3);

C(MN(i)+2,MN(i)+2-1) =
icof(2,2)-2*h1*icof(3,2)+1/2*(2*h1)^2*icof(4,2)-...
      1/6*(2*h1)^3*icof(5,2)+1/24*(2*h1)^4*icof(6,2);

C(MN(i)+2,MN(i)+2-2) =
-p1+2*h1*p2-1/2*(2*h1)^2*p3+1/6*(2*h1)^3*p4-...
      1/24*(2*h1)^4*p5;

C(MN(i)+2,MN(i)+2-3) =
icof(2,1)-2*h1*icof(3,1)+1/2*(2*h1)^2*icof(4,1)-...
      1/6*(2*h1)^3*icof(5,1)+1/24*(2*h1)^4*icof(6,1);


end
```

Appendix E

MATLAB Program :

ARROW-Grating

```
% Written By: Muhammad Nadeem, Research Assistant
%Method of Line Analysis of Slab Waveguide Gratings
%CASCADING AND DOUBLING ALGORITHM
%General Purpose Program for TE, TM modes, Non-uniform Mesh
%With PML absorber
%Using Sparse Matrices to Reduce Memory Requirement
%ARROW GRATING.

clear
TE = 1; % for TE mode, put TE = 1, otherwise TM mode is assumed
EQ = 0; % for uniform grid, put EQ = 1

% Refractive index, layer by layer
n = [1  1  1.45  3.5 1.45 3.5 3.5 3.5 3.5];
% First and Last layers are ABSORBING LAYERS
guidelayr=3;

% artificial conductivity of each layer
cond =[1 0 0 0 0 0 0 1 1];
```

```
nlyr = length(n);

w  = [1 1  4.0  0.1 2 2 0.03125 0.0625 0.125]; % Layer Widths

M = [8 8 32  6  10  10 5 10 10]; % Dicretization sections of the layers

MM=sum(M);
% 1 ---> M(1) layer 1
% M(1)+1 ---> M(2) layer 2, and so on

MN = cumsum(M); % Interface locations

% Ordinary Regions
MS = [];
for i = 1:nlyr
   if i == 1
      s1=1;
      s2=MN(1)-1;
   elseif  i == nlyr
      s1=MN(nlyr-1)+1;
      s2=MN(nlyr);
   else
      s1=MN(i-1)+1;
      s2=MN(i)-1;
   end
   MS = [MS,s1,s2];
end

if EQ ~= 1
   h = w ./ M; % discretization distances
else
   h = w(3)/M(3);
   h = h*ones(1,nlyr);
   % New layer widths are
   w = M*h(1);
end

% Introduce the Imaginary Distance for Absorber Layers
clear j; h(1:nlyr) = h(1:nlyr).*(1+j*cond(1:nlyr));

% The refractive index square N matrix

N=[]; NN=[]; Mesh=[]; for i=1:nlyr
```

```
   N=n(i)^2*ones(1,M(i));
   NN=[NN,N];
   N=(h(i))*ones(1,M(i));
   Mesh=[Mesh,N];
end

% Refractive index, layer by layer, Second waveguide
n1 = [1  1  1.45  3.5 1.45 3.5 3.5 3.5 3.5]; nlyr1 = length(n1);
w1  = [1 1  4.0  0.1  2.2 1.8 0.03125 0.0625 0.125]; % Second waveguide
M1  =  [8 8 32 6 11  9 5 10 10];   % Second waveguide
% 1 ---> M(1) layer 1
% M(1)+1 ---> M(2) layer 2, and so on
MN1 = cumsum(M1); % Interface locations
% Ordinary Regions
MS1 = [];
for i = 1:nlyr1
   if i == 1
      s1=1;
      s2=MN1(1)-1;
   elseif  i == nlyr1
      s1=MN1(nlyr1-1)+1;
      s2=MN1(nlyr1);
   else
      s1=MN1(i-1)+1;
      s2=MN1(i)-1;
   end
   MS1 = [MS1,s1,s2];
end

% The grid must be same
h1=h;

% The refractive index N1 matrix

N1=[]; NN1=[]; for i=1:nlyr1
   N1=n1(i)^2*ones(1,M1(i));
   NN1=[NN1,N1];
end

% X-axis
xo = MN(guidelayr-1); % Origin of x-axis
xx=[]; x=[]; for i=1:nlyr
   xx=real(h(i))*ones(1,M(i));
```

```
   x=[x,xx];
end xo=sum(x(1:xo)); x=cumsum(x); x=x-xo; clear xx;

% Grating Specifications
d2 = 0.4572; d0 = 0.5*d2; d1 = 0.5*d2; Effr=[];Efft=[];
NG = 2^15; % Number of Periods

e = ones(MM,1);

% 3-point second derivative matrix, sparse
C = spdiags([e -2*e e],-1:1,MM,MM);

C1 = C;

% Divide by denominator terms except at the interface
i=1; for k=1:nlyr
   C(MS(i):MS(i+1),:) = C(MS(i):MS(i+1),:)/h(k)^2;
   i=i+2;
end

% Divide by denominator terms except at the interface
i=1; for k=1:nlyr
   C1(MS1(i):MS1(i+1),:) = C1(MS1(i):MS1(i+1),:)/h1(k)^2;
   i=i+2;
end Ctmp = C; Ctmp1 = C1;


%*********************************************
% START THE LOOP FOR SPECTRAL RESPONSE
%*********************************************

for  lambda = 1.3163:0.00004:1.3193 % The Wavelength

ko=2*pi/lambda;

C = Ctmp;

% Modify the terms at the interface
for i=1:nlyr-1
   if TE == 1
      r21 = 1;
   else
      r21 = (n(i+1)/n(i))^2;
```

```
   end

   B = ko^2*(n(i)^2-n(i+1)^2);
   D = 0.5*(h(i)*h(i+1)*r21+h(i+1)^2);
   C(MN(i),MN(i))   = -(r21 * h(i+1)/h(i)+1+0.5*h(i+1)^2 * B)/D;
   C(MN(i),MN(i)-1) = h(i+1)/h(i) * r21/D;
   C(MN(i),MN(i)+1) = C(MN(i),MN(i)+1)/D;

end

% Now go for C1
C1 = Ctmp1;

% Modify the terms at the interface

for i=1:nlyr1-1
   if TE == 1
      r21 = 1;
   else
      r21 = (n1(i+1)/n1(i))^2;
   end

   B = ko^2*(n1(i)^2-n1(i+1)^2);
   D = 0.5*(h1(i)*h1(i+1)*r21+h1(i+1)^2);
   C1(MN1(i),MN1(i))   = -(r21 * h1(i+1)/h1(i)+1+0.5*h1(i+1)^2 * B)/D;
   C1(MN1(i),MN1(i)-1) = h1(i+1)/h1(i) * r21/D;
   C1(MN1(i),MN1(i)+1) = C1(MN1(i),MN1(i)+1)/D;

end

% Q matrix

Q=C+ko^2*diag(NN);

% Diagonalize the matrix
[U,V]=eig(Q); % find the eigenvalues and eigenvectors
V = sparse(V); Q = sparse(Q);

% Make the Imaginar Part of V matrix +ve so that the field does not GROW
%clear j;
for i=1:MM
   if imag(V(i,i)) < 0
      V(i,i) = conj(V(i,i)) ;
```

```
   end
end

% Find the ARROW Modes and Sort them according to LOSS.
% TE_0 Mode has highest Propagation Constant (real).

VR = []; VRn = []; for i=1:MM
   ne = sqrt(V(i,i))/ko;
   if imag(ne) < 1e-1 & real(ne) > n(guidelayr-1) & ...
         real(ne) < n(guidelayr);
         VR = [VR,V(i,i)];
         VRn =[VRn, i];
   end
end

% Sort the EigenValues according to the LOSS
if length(VR) > 1 for i = 1:length(VR)-1
   for k = i+1 :length(VR)
      if imag(VR(k)) < imag(VR(i))
         tmp = VR(i);
         VR(i) = VR(k);
         VR(k) = tmp;
         tmp = VRn(i);
         VRn(i) = VRn(k);
         VRn(k) = tmp;
      end
   end
end end

% Convert to Neff
VR = sqrt(VR)/ko;

% Plot the Numerical Mode and Effective Index

Tmode=0; % Select the Mode Number
Neff=VR(Tmode+1); Field=abs(U(:,VRn(Tmode+1)));

% Q1 matrix, for second waveguide

Q1=C1+ko^2* diag(NN1);

% Diagonalize the matrix
[U1,V1]=eig(Q1); % find the eigenvalues and eigenvectors
```

```
V1 = sparse(V1); Q1=sparse(Q1);

% Make the Imaginar Part of V matrix +ve so that the field does not GROW
for i=1:MM
   if imag(V1(i,i)) < 0
      V1(i,i) = conj(V1(i,i));
   end
end

QQ0p = U*diag(diag(V).^(0.5))*inv(U);

% Calculate the INCIDENT, TRANSMITTED and REFLECTED POWER for TE and TM
if TE==1 Pi = real(Field.' * (Mesh.' .* conj(QQ0p * Field))); else
Pi = real(Field' * (Mesh.' .* (diag(NN.^(-1)) * QQ0p * Field)));
end

% Calculate the common factors

Exp0 = U * diag(exp(j .* (diag(V)).^ 0.5 .* d0))*inv(U);%
Exp1 = U1* diag(exp(j .* (diag(V1)).^ 0.5 .* d1))*inv(U1);

% The Single Interface, R and T __|~~
if TE ~= 1
   T1 = U*diag((diag(V)).^(-0.5))*inv(U) * diag(NN)*diag(NN1.^-1)* ...
        U1*diag(diag(V1).^(0.5))*inv(U1);
else
   T1 = U*diag((diag(V)).^(-0.5))*inv(U) * U1*diag(diag(V1).^(0.5))*inv(U1);
end

Ra1 = (eye(MM)-T1)*inv(eye(MM)+T1);

% Double Interface, R and T __|~~|__
% The Complete Top Grove

VV = inv(eye(MM)-(Exp1*Ra1)^2)*Exp1*(eye(MM)+Ra1); R = Ra1
+(eye(MM)-Ra1)* Exp1*(-Ra1)*VV; T = (eye(MM)-Ra1)*VV;

% Now CASCADE to get the resultant, R and T Matrices
for i = 1:log2(NG)
   VV = inv(eye(MM)-(Exp0*R)^2)*Exp0*T;
   R = R + T*Exp0*R*VV;
   T = T * VV;
end
```

```
% Find the NET REFLECTED And TRANSMITTED FIELDS

AN = T*Field; B0 = R*Field;


% Calculate the Fundamental Mode Excitation Coefficient

if TE == 1

ModePower = Field' *  (Field .* Mesh.'); alpha = (B0'*  (Field .*
Mesh.'))/ModePower; betaa = (AN'*  (Field .* Mesh.'))/ModePower;

else

ModePower = Field' * (diag(NN)^(-1) * (Field .* Mesh.'));%
alpha = (B0'* diag(NN)^(-1)*(Field .* Mesh.'))/ModePower;%
betaa = (AN'* diag(NN)^(-1)*(Field .* Mesh.'))/ModePower;
end

% Calculate The Transmitted and Reflected Modal Power
if TE==1
   Prg = real(alpha  * Field.' * (Mesh.' .* conj(QQ0p * alpha * Field)));
   Ptg = real(betaa  * Field.' * (Mesh.' .* conj(QQ0p * betaa * Field)));

else Prg = real(alpha' * Field' * (Mesh.' .* (diag(NN.^(-1)) *
QQ0p * alpha * Field)));

Ptg = real(betaa' * Field' * (Mesh.' .* (diag(NN.^(-1)) * QQ0p *
betaa * Field)));

end

% Reflectivity and Transmissivity
Effr=[Effr,Prg/Pi]; Efft=[Efft,Ptg/Pi];

end

% SPECTRAL Plots
lambda = 1.3163:0.00004:1.3193;
figure;plot(lambda,10*log10(Effr));grid;%
xlabel('Wavelength[um]'); ylabel('Reflectivity [db]');
title('Fundamental Mode Reflectivity of ARROW Grating'); ax=axis;
```

```
axis([lambda(1) lambda(length(Effr)) ax(3) ax(4)]);

figure;plot(lambda,10*log10(Efft));grid; xlabel('Wavelength
[um]'); ylabel('Transmissivity [db]'); title('Fundamental Mode
Transmissivty of ARROW Grating'); ax=axis;%
axis([lambda(1) lambda(length(Effr)) ax(3) ax(4)]);
```

Bibliography

[1] Abiodun Ahmad Shittu. *Study of periodic waveguides by the finite-difference time-domain method and the Method of Lines.* PhD thesis, King Fahad University of Petroleum and Minerals, Dhahran 31261, Saudi Arabia, September 1994.

[2] J Ctyroky, S Helfert, and R Pregla. Analysis of deep waveguide bragg gratings. *Optical and Quantum Electronics*, pages 343–358, 1998.

[3] Qing-Huo Liu and Weng Cho Chew. Analysis of discontinuities in planar dielectric waveguides : An eigenmode propagation method. *IEEE Transactions on Microwave Theory and Techniques*, 39(3):422–430, March 1991.

[4] M A Duguay, Y Kokubun, T L Koch, and Loren Pfeiffer. Antiresonant reflecting optical waveuides in $SiO_2 - Si$ multilayer structures. *Applied Physics Letters*, 49(1):13–15, July 1986.

[5] Weiping Huang, Raed M Shubair, Arokia Nathan, and Y Leonard Chow. The modal characteristics or ARROW structures. *Journal of Lightwave Technology*, 10(8):1015–1022, August 1992.

[6] Jacek Kubica. Modal propagation within ARROW waveguides. *Optics Communications*, 78(2):133–136, August 1990.

[7] J M Kubica, A Malag, J Gazecki, M W Austin, and G K Reeves. AlGaAs/GaAs ARROW waveguides. *Electronics Letters*, 29(12):1058–1060, June 1993.

[8] J L Archambault, R J Black, S Lacroix, and J Bures. Loss calculations for antiresonant waveguides. *Journal of Lightwave Technology*, 11(3):416–423, March 1993.

[9] T Baba, Y Kokuban, T Sakaki, and K Iga. Loss reduction of an ARROW waveguide in shorter wavelength and its stack configuration. *Journal of Lightwave Technology*, 6(9):1440–1445, September 1988.

[10] C. L. Xu and W. P .Huang. *Finite-Difference Beam-Propagation Methods for Guided Wave optics.* Progress in Electromagnetics Research (PIER) 11. Elsevier Science Publishing Co., Inc., 1995.

[11] Husain M. Masoudi, Muhammad Al-Sunaidi, and John M. Arnold. Time-domain finite-difference beam propagation method. *IEEE Photonics Technology Letters*, 11(10):1274–1276, October 1999.

[12] S. T. Chu and S. K. Chaudhrui. *Finite-Difference-Time-Domain Methods for Optical Waveguide Analysis*. Progress in Electromagnetics Research (PIER) 11. Elsevier Science Publishing Co., Inc., 1995.

[13] Ashmeet Kaur Taneja and Anurag Sharma. Reflection characteristics of guided wave bragg gratings using the collocation method. *SPIE Proceedings, Internationl conference on fiber optics and photonics*, 3666:112–119, April 1999.

[14] J. Gerdes and R. Pregla. Beam-propagation algorithm based on the method of lines. *Optical Society of America (B)*, 8(2):389–394, February 1991.

[15] U. Rogge and R. Pregla. Method of lines for the analysis of strip-loaded optical waveguides. *Optical Society of America (B)*, 8(2):459–463, February 1991.

[16] K. S. Chiang. Review of numerical and approximate methods for the modal analysis of general optical dielectric waveguides. *Optical and Quantum Electronics*, 26:113–134, 1994.

[17] H. J. W. M. Hoekstra. On beam propagation methods for modelling in integrated optics. *Optical and Quantum Electronics*, 29:157–171, 1997.

[18] A. Sharma. *Collocation Method For Wave Propagation Through Optical Waveguiding Structures*. Progress in Electromagnetic Research, (PIER) 11. Elsevier Science Publishing Co., Inc., 1995.

[19] M. A. A. Pudensi and L. G. Ferreira. Method to calculate the reflection and transmission of guided modes. *Journal of Optical Society of America*, 72:126–130, 1982.

[20] Majid Jafar Al-Majid. Method of lines analysis of gaussian beam coupling to the dielectric slab waveguide. Master's thesis, King Fahad University of Petroleum and Minerals, Dhahran 31261, Saudi Arabia, February 1994.

[21] Yih Peng Chiou and Hung Chun Chang. Analysis of optical waveguide discontinuities using pade approximation. *IEEE Photonics Technology Letters*, 9:964–966, 1997.

[22] J Gerdes, B Lunitz, D Benish, and R Pregla. Analysis of slab waveguide discontinuities including radiation and absorption effects. *Electronics Letters*, 28(11):1013, May 1992.

[23] Wei Dong Yang and R. Pregla. Method of lines for analysis of waveguide structures with multidiscontinuities. *Electronics Letters*, 31(11):892, May 1995.

[24] R Pregla and W Yang. Method of lines for analysis of multilayered dielectric wavegides with bragg gratings. *Electronics Letters*, 29(22):1962, October 1993.

[25] R Pregla and E Ahlers. Method of lines for analysis of discontinuities in optical waveguides. *Electronics Letters*, 29(21):1845, October 1993.

[26] M. J. Adams. *An Introduction to Optical Waveguides.* John Wiley and Sons, 1981.

[27] Richard Syms and John Cozens. *Optical Guided Waves and Devices.* McGraw-Hill Book Company Europe, Shopenhangers Road, Maidenhead, Berkshire, SL6 2QL, England, 1992.

[28] V. Vemuri and Walter J. Karplus. *Digital Computer Treatment of Partial Differential Equations.* Prentice-Hall Series in Computational Mathematics. Prentice Hall, Inc., Englewood Cliffs, New Jersey 07632, 1981.

[29] Tatsuo Itoh, editor. *Numerical Techniques for Microwave and Millimeter-Wave Passive Structures.* John Wiley and Sons, 1989.

[30] Al-Bader S. J. and Jamid H. A. Method of lines applied to non-linear guided waves. *Electronics Letters*, 31(17):79–85, February 1995.

[31] M. Imtaar and S. J. Al-Bader. Analysis of diffraction from abruptly-terminated optical fibers by the method of lines. *Journal of Lightwave Technology*, 13(2):137–141, February 1995.

[32] E Ahlers and R Pregla. 3-D modeling of concatenations of straight and curved waveguides by MoL-BPM. *Optical and Quantum Electronics*, pages 151–156, 1997.

[33] Wei Dong Yand and Reinhold Pregla. The method of lines for analysis of integrated optical waveguide structures with arbitrary curved interfaces. *Journal of Lightwave Technology*, 14(5):879–884, May 1996.

[34] Ulrich Rogge. *Method of Lines for the Analysis of Dielectric Waveguides.* PhD thesis, Fern University, Hagen, Germany, 1991.

[35] Reinhold Pregla. High order approximation for the difference operators in the method of lines. *IEEE Microwave and Guided Wave Letters*, 5(2):53–55, February 1995.

[36] Shujun Xiao, Ruediger Vahldieck, Hang Jin, and Zhenglian Cai. A modified MoL algorithm with faster convergence and improved computational efficiency. *Microwave Symposium Digest, IEEE MTT-S International*, 1:357–360, 1991.

[37] R Stoffer. Efficient interface conditions based on a 5-point finite difference operator. *Optical and Quantum Electronics*, 30:375–383, 1998.

[38] O Conradi, S Helfert, and R Pregla. Modification of the finite-difference scheme for efficient analysis of thin film lossy metal layers in optical devices. *Optical and Quantum Electronics*, pages 369–373, 1998.

[39] Franz J. Schmuckle and Reinhold Pregla. The method of lines for the analysis of lossy planar waveguides. *IEEE Transactions on Microwave Theory and Techniques*, 38(10):1473–1479, October 1990.

[40] J J Gerdes. Bidirectional eigenmode propagation analysis of optical waveguides based on method of lines. *Electronics Letters*, 30(7):550, March 1994.

[41] S. T. Peng and T. Tamir. TM mode perturbation analysis of dielectric gratings. *Applied Physics*, 7(35):35–38, 1975.

[42] Jose Rodriguez, R. D. Crespo, and S. Fernandez. Radiation losses on discontinuities in integrated optical waveguides. *Optical Engineering*, 38(11):1896–1906, November 1999.

[43] Al-Bader S. J. and Jamid H. A. Mode scattering by a non-linear step-discontinuity in dielectric optical waveguides. *IEEE Transactions on Microwave theory and Techniques*, 44(2):218–224, February 1996.

[44] Jamid H. A. and Al-Bader S. J. Reflection and transmission of surface plasmon mode at a step discontinuity. *IEEE Photonics Technology Letters*, 9(2):220–222, February 1997.

[45] Jamid H. A. and Al-Bader S. J. Diffraction of surface plasmon-polaritons in an abruptly terminated dielectric-metal interface. *IEEE Photonics Technology Letters*, 7(3):321–323, March 1995.

[46] J. G. Blaschak and G. A. Kriegsmann. A comparative study of absorbing boundary conditions. *Journal of Computational Physics*, 77:109–139, 1988.

[47] S J Al-Bader and H A Jamid. Perfectly matched layer absorbing boundary conditions for the method of lines modeling scheme. *IEEE Microwave and Guided Waves Letters*, 8(11):357–359, November 1998.

[48] D. Marcuse. *Theory of Dielectric Optical Waveguides*. Academic Press Inc., 1974.

[49] D. C. Flanders and H. Kogelnick. Grating filters for thin-film optical waveguides. *Applied Physics Letters*, 24(4):194–196, February 1974.

[50] Kim A. Winick. Effective-index method and coupled-mode theory for almost-periodic waveguide gratings: a comparison. *Applied Optics*, 31(6):757–764, February 1992.

[51] Dr. H. A. Al-Jamid. Cascading and doubling algorithm to model long gratings. personal notes.

[52] Stefan F. Helfert and Reinhold Pregla. Efficient analysis of periodic structures. *Journal of Lightwave Technology*, 16(9):1694–1702, September 1998.

[53] Wenyan Jiang, J Chrostowski, and M Fontaine. Analysis of ARROW waveguides. *Optics Communications*, 72(3,4):180–186, July 1989.

[54] Jacek M Kubica, Jerzy Gazecki, and Geoffrey K Reeves. Multimode operation of ARROW waveguides. *Optics Communications*, 102(3,4):217–220, October 1993.

[55] Jacek M Kubica. A rigorous design method for antiresonant reflecting optical waveguides. *IEEE Photonics Technology Letters*, 6(12):1460–1462, December 1994.

[56] Z M Mao and W P Huang. An ARROW optical wavelength filter: Design and analysis. *Journal of Lightwave Technology*, 11(7):1183–1188, July 1993.

[57] J Gehler, A Brauer, W Karthe, U Trurschel, and M A Duguay. ARROW based optical wavelength filter in silica. *Electronics Letters*, 31(7):547–548, March 1995.

[58] V Delisle, U Trutschel, H Tremblay, M A Duguay, and F Lederer. High finesse wavelength selective coupler based on ARROW. *IEEE Photonics Technology Letters*, 8(6):791–793, June 1996.

[59] M Mann, U Trutschel, C Wachter, L Leine, and F Lederer. Directional coupler based on an antiresonant reflecting optical waveguide. *Optics Letters*, 16(11):805–807, June 1991.

[60] Essasm S Tony and Sujeet K Chaudhuri. An ARROW directional coupler acousto-optic filter. *Antennas and Propagation Society International Symposium, AP-S Digest*, 2:1362–1365, 1994.

[61] Weidong Yang. *Method of Lines for Analysis of Passisve and Active Integrated Optical Devices*. PhD thesis, Fern University, Hagen, Germany, 1996.

Vita

1971/12 : Born in Faisal-Abad, Islamic Republic of Pakistan.

1986 : Matriculation with Science Major.

1988 : F.Sc. (with distinction) Pre-Engineering, second position in Multan District.

1989-1994 : B.Sc. (with Honors) Electrical Engineering, University of Engineering and Technology, Lahore, Pakistan, Major : Communication, Microwave and Digital Systems.

1993-1994 : Apprenticeship, Zelin Medical Systems (Pvt.) Ltd. Designed and implemented PC based patient-monitoring system to record Electro-cardiogram (ECG) data. Designed front-end differential amplifier, analog filters, A/D conversion and PC slot interface. Written control software in PASCAL and ASSEMBLY Language.

1994-1995 : R & D Engineer, Carrier Telephone Industries, Islamabad, Pakistan. Designed analog/digital circuits for telcommunication. Worked on microprocessors, micro-controllers and Field-Programmable-Gate-Arrays (FPGA) for custom logic deign. Used softwares from ALTERA and CYPRESS Semiconductors.

1995-1998 : Assistant-Manager Electro-Optics, Advanced Engineering Research Organization, Wah Cantt, Pakistan. Designed digital-scan-converter for analog camera to convert 'xyz' video into CCIR compatible video. Worked on Infra-Red optical design. Designed single and multiple field-of-view IR telescopes, Kaplerian and Galilean telescopes, two-step zoom telescopes, continuous zoom telescopes, zoom extender, multi-spectral objectives, FPA objectives for starring arrays. Used lens design softwares SYNOPSYS and ZEMAX.

1998-2000 : M.Sc. Electrical Engineering, King Fahd University of Engineering and Technology, Dhahran, Saudi Arabia. Worked on integrated optics modeling, waveguide discontinuities, gratings and ARROW waveguide using numerical Method of Lines (MoL). Worked on Finite-Difference Time-Domain (FDTD) method to model electro-magnetic wave propagation. Worked as a Research/Teaching Assistant in the Electrical Engineering department.
Thesis Advisor : Dr. Hussain A. Al-Jamid.